ELECTRONIC STRUCTURE OF DEFECTS IN SOME OXIDES

By

SISTER JEANETTE M. FELDOTT

Bachelor of Science
Notre Dame College
St. Louis, Missouri
1964

Master of Science
Emporia State University
Emporia, Kansas
1972

Submitted to the Faculty of the Graduate College
of the Oklahoma State University
in partial fulfillment of the requirements
for the Degree of
DOCTOR OF PHILOSOPHY
July, 1977

TO

MY MOTHER

AND

SISTERS PHYLLIS AND LORAN

ELECTRONIC STRUCTURE OF DEFECTS IN SOME OXIDES

Thesis Approved:

Geo. J. P. Summa
Thesis Adviser

Joel J. Martin

Paul Westhaus

Horacio A. Mottola

Norman N. Durham
Dean of the Graduate College

ACKNOWLEDGMENT

The author wishes to express her appreciation to her major adviser, Dr. Geoffrey P. Summers, for his professional guidance and assistance throughout this study. For the personal encouragement he gave, the example he set, and the stimulating and friendly atmosphere he provided, I am deeply grateful.

Appreciation is also expressed to the other committee members, Dr. Joel J. Martin, Dr. Paul Westhaus and Dr. Horacio Mottola, for their assistance in the preparation of the final manuscript. Special mention must be given to Dr. Paul Westhaus for many valuable discussions, for his patience in answering questions and helping me to a greater understanding of Physics and for his faithful encouragement.

Thanks are also extended to Dr. T. M. Wilson for his advice and for many pertinent discussions concerning the theoretical aspects of this study. Appreciation is also extended to Dr. Y. Chen of Oak Ridge National Laboratory who supplied some of the crystals used in this study and who, together with Dr. William A. Sibley of this department, helped during several valuable discussions. A note of thanks is given to Dr. James Lange for the loan of equipment used for fluorescence lifetime measurements. A great deal of credit must also be given to Mr. Heinz Hall and the other members of the Physics-Chemistry Machine Shop Staff, for without their excellent work this research project could not have proceeded as smoothly as it did. Sincere thanks are also extended to Mrs. Janet Sallee for her excellent assistance in typing both the final

draft and the final copy of the manuscript.

Special thanks are also extended to all members of the Physics Faculty for their availability and willingness to be of assistance and who, together with the Graduate Students and Staff, have in so many ways provided an atmosphere of warmth, interest and encouragement, thus making my residence at Oklahoma State University very enjoyable.

Special gratitude is expressed to my Mother and family, to my Religious Community, the School Sisters of Notre Dame, especially Sister Phyllis and Sister Loran, to the staff at St. John's University Parish, Stillwater, and to all my friends who have continually supported me with their prayers, sacrifices and encouragement.

Finally appreciation is extended to the United States' Energy Research and Development Administration for the financial support provided during the past two and one-half years which has enabled me to more effectively concentrate my efforts on my research.

TABLE OF CONTENTS

LIST OF TABLES

LIST OF FIGURES

CHAPTER I

DEFINING THE PROBLEM

I. Introduction

The study of point defects in crystalline materials has become an important branch of solid state physics since the presence of such defects frequently directly affects the electronic and physical properties of a material. Point defects can be generally divided into two classes: (a) impurity defects and (b) radiation-induced defects. This study is concerned principally with point defects of the latter type.

The term color center refers to a particular type of point defect involving electrons or holes which gives rise to optical absorption bands in the visible and ultraviolet and near infrared region of the spectrum in otherwise transparent crystals.

Color centers can be introduced into the material by several methods (1), including exposure to ionizing radiation, such as x-ray, γ-ray and ultraviolet radiation and by fast particle irradiation with electrons, protons or neutrons. Some types of defects can also be produced by heating the material in an excess of the metallic vapor. This process is known as additive coloration (2).

General review books describing work on color centers in alkali halides and other materials include those by Schulmann and Compton (3), Fowler (4), and Crawford and Slifkin (5). Comprehensive review articles on radiation-induced defects in the alkaline earth oxides include those

by Henderson and Wertz (6) and Hughes and Henderson (7).

Color centers have been a subject of investigation over a considerable span of years. The darkening of an alkali halide and the characteristic color produced by bombardment with cathode rays was noted by Goldstein (8) as early as 1894. The discovery, in 1895, of x-rays by Roentgen and natural radioactivity by Becquerel brought increased interest. Efforts to control color center properties were made in Pohl's laboratory in Göttingen (9), starting in 1925 as experiments dealing with electronic conductivity and luminescence were carried out. Interest in radiation damage was further heightened by the advent of the nuclear reactor in 1943. Since reactor components could be adversely affected by the high energy radiation products, new emphasis was given to the importance of understanding how material properties are altered by inadvertent or deliberate irradiation. It is essential that materials to be used in space or near nuclear reactors be tested to determine how seriously the hostile environments will affect important properties.

Two questions of primary concern in the study of radiation damage are: 1) What are the physical and electronic properties of the radiation-induced defects? and 2) What are the processes and mechanisms that lead to the creation of such defects? This study will be primarily concerned with the first of these questions, although there will be some discussion of the second question, as related to the oxides, later in this chapter.

A large part of the past research on radiation-induced defects has been performed on alkali halide crystals. These crystals have the face-centered-cubic structure and are comparatively easily grown. Various types of point defects can be created in the alkali halides quite

readily by either ionizing or particle irradiation and additive coloration. The simplest anion vacancy defect is an F-center which in an alkali halide consists of a single electron trapped at a halide ion vacancy. The F-center therefore holds a central position in the area of defects in solids which is similar to that held by the hydrogen atom in Atomic Physics.

II. Alkaline Earth Oxides: Physical Properties

More recently the alkaline earth oxides, and in particular simple defects in these materials, have been the subject of many studies (6,7). The alkaline earth oxides are the divalent structural analogues of the alkali halides and therefore present a logical extension of the alkali halide studies (Figure 1). They are highly ionic having larger lattice energies than the alkali halides. Table I compares the percent ionic character of the bonds, the lattice energies (cohesive energies) and the bond strengths for the alkaline earth oxides and some of the alkali halides.

Some of the physical properties of these materials are shown in Table II. Band gaps of 4-8 eV and dielectric constants ranging from 10 to 34 serve to make these materials good insulators. These materials also have high melting points ranging between 1900 and nearly 3000^{o}C. Consequently, they are comparatively difficult to grow as single crystals. It is only recently that reasonably high quality samples of the alkaline earth oxides have become available. The crystals are usually grown by the arc fusion method (7) and the most common impurities are Fe, Si, Al, Zn and other alkaline earth metals.

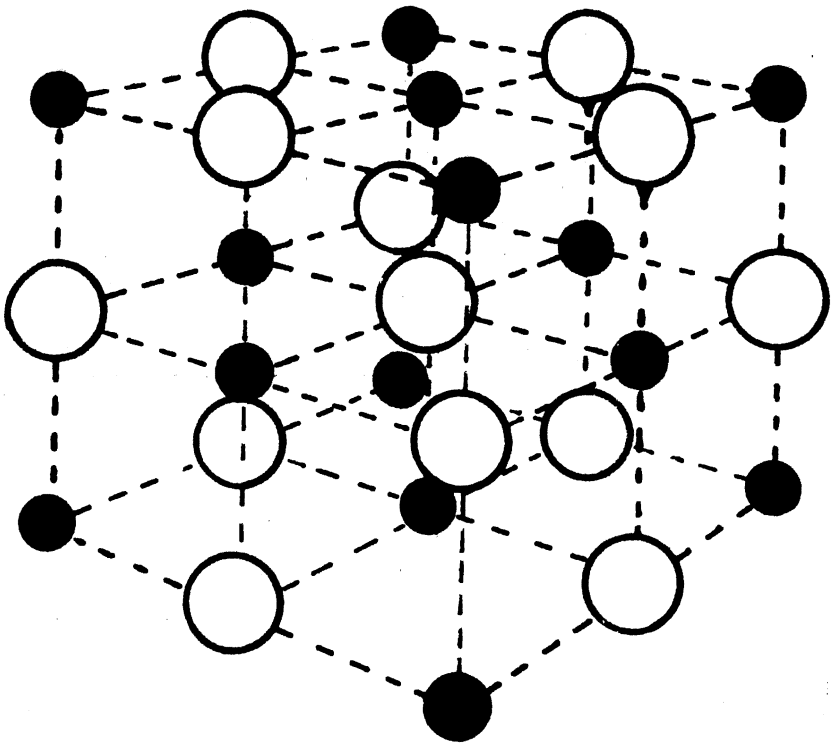

Figure 1. Crystal Structure for the Alkaline Earth Oxides

TABLE I

COMPARISON OF SOME ALKALI HALIDES AND ALKALINE EARTH OXIDES

Material	Lattice Constant[a] a_o (Å)	% Ionic Character[b] for Bond	(Lattice Energy) Cohesive Energy for Crystal (kcal/mole)	25°C Bond Strength[c] (kcal/mole)
LiF	4.02	79.5	240.1[c]	137.5
NaF	4.62	83.2	213.4[c]	114
KF	5.34	87.0	189.7[c]	118.9
RbF		87.0	181.6[c]	116.1
LiCl	5.14	46.0	199.2[c]	111.9
NaCl	5.62	49.0	183.1[c]	97.5
KCl	6.28	52.1	165.4[c]	101.3
RbCl	6.1	52.1	160.7[c]	100.7
MgO	4.2112	55.3	905[d] 914[e]	96
CaO	4.8105	61.9	815[d] 814[e]	88
SrO	5.1602	61.9	767[d] 765[e]	96
BaO	5.523	65.3	736[d] 735[e]	125.9

[a]Reference 10; [b]Calculated from: % ionic character = $16(X_B - X_A) + 3.5 (X_B - X_A)^2$, X_B the larger electronegativity, reference 11: electronegativity values from reference 12.

[c]Reference 13; [d]Reference 14; [e]Reference 15.

Lattice energy: The energy required to separate the ions of a crystal to an infinite distance from each other.

Strength of a chemical bond (bond dissociation energy): the heat of the reaction RX → R + X in kcal/mole.

TABLE II

PHYSICAL PROPERTIES OF ALKALINE EARTH OXIDES

Materials	Band Gap (eV)	ε_o	Lattice Constant a_o (Å)	Melting Point (°C)
MgO	7.8[a], 8.7[b]	9.65[e]	4.2112[f]	2800[e]
CaO	7.0[c], 7.7[d]	11.8[e]	4.8105[f]	2600[e]
SrO	6[e]	13.3[e]	5.1605[f]	2415[e]
BaO	4.8[e]	34[e]	5.523[f]	1928[e]

[a]Reference 16; [b]Reference 17; [c]Reference 18; [d]Reference 19; [e]Reference 20; [f]Reference 10

In order to create vacancies or interstitials in these materials, it is necessary to use particle irradiation or additive coloration because ionizing radiation alone is ineffective. During particle irradiation numerous changes can occur in the lattice and in the impurities which are present. These may be categorized as: (1) electronic defects involving changes in valence states; (2) ionic defects consisting of displaced lattice ions; and (3) gross imperfections or aggregates.

III. Radiation Damage Processes

Radiation damage processes in a polar crystal may be classified according to the following scheme: (1) electronic processes; (2) elastic collisions; and (3) radiolysis. Processes in which an electronic state is changed or charge is moved about, but which do not involve the formation of an ionic or atomic defect, are classified as electronic

processes. Elastic collisions result in the displacement of an ion or atom due to momentum and energy transfer from the irradiating particles. Radiolysis processes involve the production of ionic or atomic defects by a series of reactions beginning with an electronic excitation.

The anion vacancy defects with which we will be concerned are produced in the oxides during particle irradiation by knock-on collisions. Therefore we will limit our discussion, for the most part, to radiation damage produced by elastic collisions.

An energetic charged particle, such as an electron or proton, is scattered by the crystal's electrons and nuclei by means of a Coulomb interaction as it traverses the material and passes close to atoms. The Coulomb scattering produces two principle effects on the incident particle that are of importance: energy loss by ionization and multiple deflections (21). The electrons in the crystal are excited by the Coulomb interactions with the incident particle and may occasionally gain sufficient energy to escape from the ions to which they were bound. The energy gained by the crystal electrons is acquired at the expense of the fast-moving incident particle, with the result that the incident particle is decelerated and may eventually be brought to rest. Since accelerating charged particles radiate energy, the decelerating fast-moving charged particle also loses some energy to the radiation field as the creation of electromagnetic waves or bremsstrahlung (22). Most of the energy loss of the incident particle results from electronic encounters while most of the deflection results from interactions with the nuclei.

The energy loss per centimeter of path for heavy irradiation particles due to the interactions with the crystal electrons is given by the

expression

$$\frac{dE}{dx} = \frac{(2\pi\, e^4 z^2 N_o ZM)}{m_e E} \log\left(\frac{4m_e E}{I M}\right); \quad \frac{2E}{M} = v^2 \qquad (1)$$

where e and m_e are the electronic charge and mass, respectively, ze, v, E and M are the charge, velocity, kinetic energy and mass, respectively, of the irradiating particle, N_o is the atomic density of the crystal, Z is the number of electrons per atom and I is the average excitation potential of the crystal electrons. Equation (1) is valid for nonrelativistic velocities. For heavy particles moving with velocities approaching the speed of light, the log term in Equation (1) is replaced by $\log (4m_e E/IM) - \log (1 - \beta^2) - \beta^2$, where $\beta = v/c = \frac{1}{c}\sqrt{\frac{2E}{M}}$, c being the speed of light.

When fast electrons are used as the irradiating particle, the formula for dE/dx differs slightly from Equation (1) because the incident electrons are indistinguishable from the crystal electrons. Further, since they have the same e/m as the crystal electrons, they can lose an appreciable fraction of their energy during a single collision. However, qualitatively the electron gives up energy in a manner similar to that of the heavier particles and the initial factor in Equation (1) may also be used for electrons if the correction is made for velocities approaching the speed of light.

The penetration depth of a particle in a crystal is very important in radiation damage, in deciding what is the best kind of radiation to use for a given solid and in determining the uniformity of radiation damage. By considering only the initial factor in Equation (1) it is

seen that for a given energy E, the energy absorbed per unit length from the irradiating particle is proportional to the mass, M, of the incident particle. Consequently, the energy absorbed per unit length from a proton (z=1) is very much greater than that absorbed from an electron (z=1). The distance the particle penetrates into the material depends inversely on its average energy loss per unit length. The penetration depth can be found from the range-energy relation for a given irradiation particle and absorbing material. An approximate form for this function can be found by integrating Equation (1) neglecting the slowly varying logarithmic term after using the relations $N_o = N_A \frac{\rho}{A}$ and $\rho dx = dR$ where N_A is Avogadro's number, ρ is the density and A the atomic weight in cgs units. The range, R, is expressed in units of grams per square centimeter. When R is expressed in these units, the range-energy relation is roughly independent of the stopping material (21). The penetration depth, x, in the absorbing material for an irradiation particle of energy E can, therefore, be estimated from the known range-energy relation for another material by dividing the known range for the particle with energy E by the density of the absorbing material. Table III gives some numbers that show how far particles that are often used in radiation damage experiments can be expected to penetrate in the materials dealt with in this thesis. It can thus be seen that fast electrons will penetrate deep into the crystal producing uniform damage throughout fairly thick samples, whereas heavier charged particles, such as protons, are stopped near the surface.

Neutrons, since they are electrically neutral particles and experience no Coulomb interaction, do not excite the crystal electrons directly or experience deflections due to Coulomb interactions with the nuclei.

The neutron can, therefore, penetrate deep into the crystal before colliding with a nucleus. If the neutron displaces a crystal ion, the recoiling ion gives up some of its kinetic energy to the electronic structure of the crystal in the manner just described above. Since displacement is caused by nuclear collisions and the mass of the neutron is quite large, a large amount of structural damage is done by neutrons.

TABLE III

PENETRATION OF IRRADIATING PARTICLES[a]

Particle	Energy Mev	Approximate Penetration Depth (cm) CaO	SrO	β^2
Electron	1.5	.212	.15	.94
Proton	1.5	2.4×10^{-3}	1.7×10^{-3}	3.2×10^{-3}

[a]Calculated from data assembled in Ref. 13 and 23 using the ranges (given in grams/cm^2) of electrons and protons in aluminum.

The effectiveness of the incident particle in creating ionic vacancy defects depends on the maximum amount of kinetic energy, T_m, it can transfer to the ion. By means of momentum and energy transfer during elastic collisions, the irradiating particle must impart sufficient energy to the lattice ion to displace it through the energy barrier presented by its nearest neighbors into an interstitial site. For nonrelativistic head-on collisions, the maximum kinetic energy transferred is given by

$$T_m = \frac{4M_1M_2E}{(M_1 + M_2)^2} \tag{2}$$

or for relativistic particles by

$$T_m = \frac{2(E + 2\,M_1c^2)E}{M_2\,c^2} \tag{3}$$

where M_1 and E are the mass of the incident particle and its corresponding energy at the time of collision, M_2 is the mass of the lattice ion and c is the speed of light.

The displacement energy, T_d, required to displace a lattice ion through the saddle point between its nearest neighbors is about 30 eV. If the radiation transfers less energy than the displacement energy, $T < T_d$, then no elastic collision radiation damage will result.

In general, five types of radiation may produce displaced atoms or ions by elastic collisions. These include: (1) gamma rays, (2) energetic electrons, (3) thermal neutrons, (4) fast neutrons, and (5) energetic atoms or ions. Gamma rays produce defects in two steps. First, they generate fast electrons through the photoelectric or Compton effects; then these electrons in turn transfer energy and momentum to lattice ions.

Table IV lists the maximum amount of energy, T_m, that can be transferred to oxide lattice ions by several types of irradiating particles that will be used in the work described in this thesis. T_m has been determined using the initial energy E of the irradiating particle and is therefore the very maximum energy that could be transferred to the crystal ion provided the incident particle has not undergone previous

collisions or lost energy through scattering. The amount of energy actually transferred is considerably less than the maximum T_m because the overwhelming majority of collisions are not head-on elastic collisions. Moreover, the particle's energy E is continually decreasing as the projectile penetrates deeper into the crystal. The optimum condition for producing single ionic vacancy defects is that the energy, T, transferred to the lattice ion be between T_d and $2T_d$ (less than approximately 100 eV).

TABLE IV

ENERGY TRANSFER BETWEEN VARIOUS IRRADIATING PARTICLES AND LATTICE IONS

Particle	Energy, MeV	T_m (eV)		
		Ca^{++}	Sr^{++}	O^{--}
Electron	1.5	202	93	507
Proton	1.5	143,000	67,400	334,000
Neutron	1.5	143,000	67,400	334,000

From Table IV it can be seen that heavier particles, such as protons and neutrons, are much more effective than the lighter electron in displacing lattice ions. But recalling the mass dependence of dE/dx as well as the results in Tables III and IV, one is reminded that the damage done by protons is at or near the surface of the material. Heavy particles, such as neutrons, are sometimes so effective in displacing crystal ions that they produce "cascades" which result when a large

amount of kinetic energy is transferred from the incident radiation to one lattice ion and that lattice ion, in moving through the lattice, transfers by elastic collisions sufficient kinetic energy to other lattice ions to dislodge them from their normal positions. It can thus be seen that proton and electron irradiations have the advantage of more controlled energy at collisions due to energy loss from scattering via the Coulomb interactions with the electrons and nuclei of the crystal lattice.

IV. F-type Defects in the Alkaline Earth Oxides

In the alkaline earth oxides, because of the divalent nature of the ions, two types of simple anion vacancy defects are found, the F- and F^+-centers. The nomenclature used in this study is that suggested by Sonder and Sibley (1). A single electron trapped at an oxygen ion vacancy is an F^+-center, whereas the F-center consists of two electrons trapped at the oxygen ion vacancy. The F-center is effectively a neutral defect whereas the F^+-center is a singly ionized F-center and has a positive charge with respect to the rest of the lattice. There are several variations of F-type centers found in the alkaline earth oxides. These include the F_A- and F_A^+-centers, F- or F^+-centers, respectively, in which one of the six nearest neighbor ions of the defect has been replaced by an impurity cation. These F-type defects have been produced in the oxides by electron irradiation (24,25,26,27), proton irradiation (26,27,29) and by neutron irradiation (6,29). In proton and neutron irradiated samples, F^+-centers are more prevalent than F-centers, whereas in electron irradiated samples for sufficiently high concentrations, F-centers are more numerous than F^+-centers (1). Further discussion

regarding this point will be presented in Chapter IV, Experimental Results. F-type defects have also been produced in some of these oxides by additive coloration (30) with the formation of F-centers being dominant. Additive coloration produces F-type defects by heating in an excess of the metallic vapor. High temperatures, typically 1500^{o}C, are required for additive coloration, which makes the technique more difficult than in the alkali halides. Arc-fusion growth itself sometimes produces "accidentally" colored portions of the melt, particularly in CaO.

The study of color centers in the alkaline earth oxides has been done, for the most part, in the following ordering: MgO, CaO, SrO and BaO. The order was determined primarily by the availability of good samples. CaO, SrO and BaO are also hygroscopic, thereby making handling of these materials difficult.

In the same sense that the F-center in the alkali halides is analogous to the hydrogen atom, the F^{+}-center in the alkaline earth oxides is analogous to the He^{+} ion. The ground state and excited states can be referred to as "1s-", "2s-" and "2p-" like, respectively, in further analogy to the He^{+} ion. The F-center in the oxides is analogous to the helium atom and the ground and first excited states are correspondingly referred to as ^{1}S and ^{3}S, ^{1}P or ^{3}P.

Optical absorption arises because of excitation of these trapped electrons. Figure 2 shows, for example, the optical density measured at 77 K on proton irradiated samples of SrO and CaO. The main features introduced by the irradiation are the asymmetric bands centered at 3.1 and 3.65 eV which arise from the F^{+}-centers in SrO and CaO, respectively. The background absorption increases as the energy of the incident photons approaches that of the band gap of the respective materials.

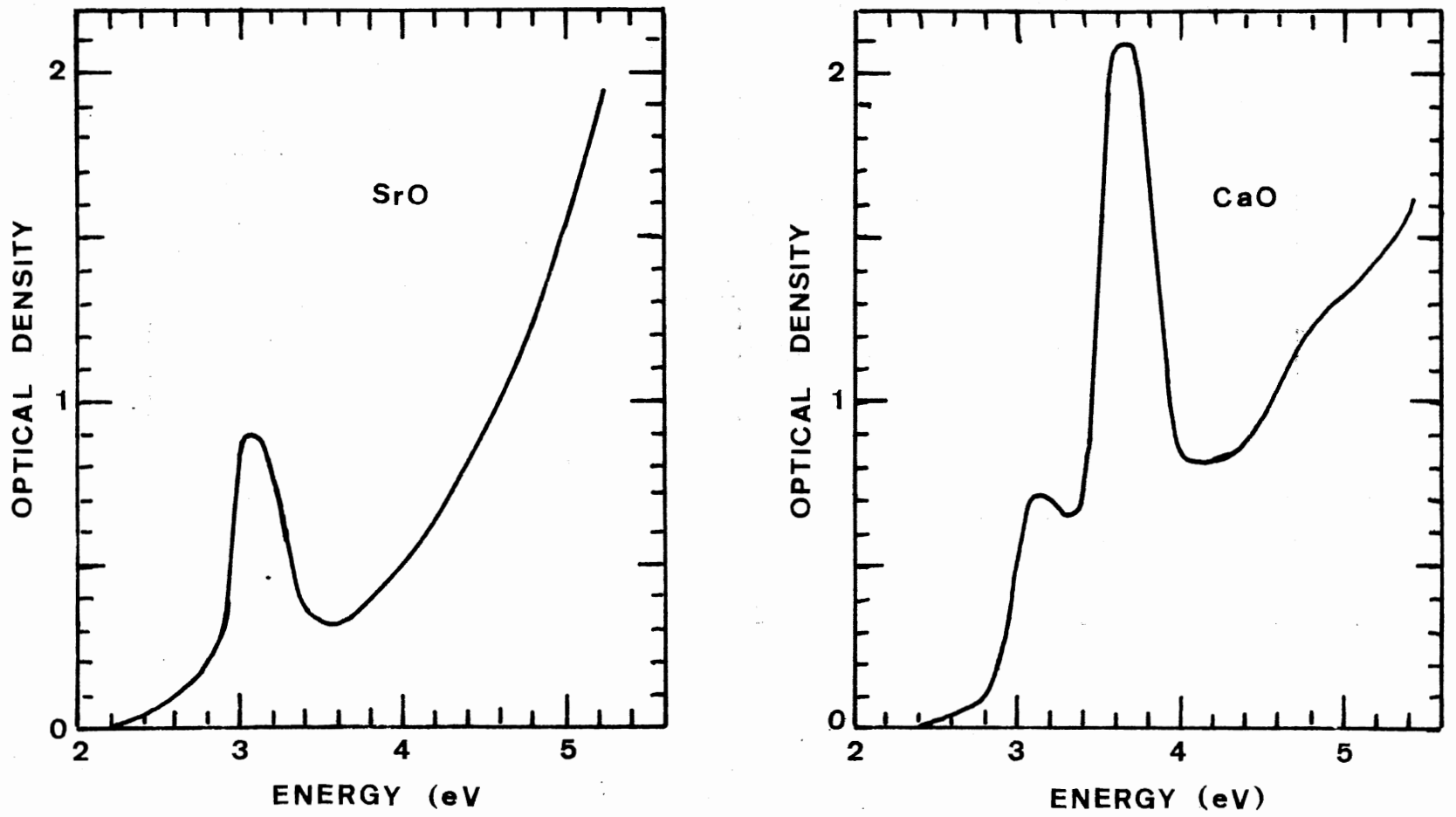

Figure 2. Optical Absorption Spectra at 77 K of Proton Irradiated SrO (a) and CaO (b). The SrO was irradiated at 195 K with 1.5 MeV protons to a dose of about 2 x 10^{17} protons/cm^2 and the CaO was irradiated at 77 K to a dose of about 5.6 x 10^{16} protons/cm^2

V. Survey of Experimental Studies

Positive optical identification of the F- and F^+-centers and their corresponding emissions in the alkaline earth oxides has been fairly recent. An optical band, correlating to the F^+-center ESR (electron spin resonance) signal was identified as the F^+ absorption band in MgO by Wertz et al. (31) and by Henderson and King (32) on neutron irradiated samples. Chen et al. (33) observed an absorption band, attributed to the F-center, in additively colored and electron irradiated MgO at the same energy which did not have an associated ESR signal. Chen et al. (34,35) also reported that only the one intense absorption band resulted from additive coloration or electron or neutron irradiation of MgO. Consequently, it has been determined that the F and F^+ optical absorption bands in MgO nearly coincide.

Magneto-optical studies of F^+-centers in the alkaline earth oxides have been instrumental in identifying the optical bands of the centers. In conjunction with ESR, optically detected ESR, Faraday rotation (FR) or magnetic circular dichroism (MCD) spectra have substantiated the identification of the F^+-center optical bands for MgO (36,37), CaO (29, 37,38,39), SrO (29,37) and BaO (29,37).

The F-center absorption band in CaO was observed in additively colored crystals by Ward and Hensley (40) and in crystals colored accidentally during growth by Henderson, Stokowski and Ensign (41). The magnetic circular dichroism of the CaO F-band was reported by Modine (42). The absorption band for the F-center in SrO was reported by Johnson and Hensley (43) and in BaO by Rose and Hensley (44).

Luminescence from the F- and F^+-centers in MgO has been reported by Chen, Kolopus and Sibley (35) and Kappers, Kroes and Hensley (45) and

from the F- and F^+-centers in CaO by Evans, Cheng and Kemp (46), Henderson, Stokowski and Ensign (41), Henderson, Chen and Sibley (25), Bates and Wood (47) and Feldott and Summers (26). Luminescence from the F^+-center in SrO has been suggested by Evans and Kemp (48) and Hughes and Webb (49) and reported by Feldott et al. (28).

The peak absorption and emission energies for the F- and F^+-centers in the alkaline earth oxides are listed in Table V. For both MgO and BaO, the F and F^+ absorption bands coincide. In CaO and SrO, however, the two bands are distinct which enables one to determine more readily which center is producing a particular phenomenon. The peak absorption energies for both F-type centers in the alkaline earth oxides decrease as the size of the cation and as the corresponding lattice constant decreases.

VI. Magnetic and Optical Properties of F-type Centers in the Oxides

In the oxides the F^+-center has a single electron in the ground state which gives rise to paramagnetism. The structure of the ground state can be studied by various techniques such as ESR and ENDOR (electron-nuclear double resonance). This "s-like" ground state has spin quantum number $s = \frac{1}{2}$. The state of the system depends on the interactions of the electron and the magnetic moments of the neighboring nuclei and can be described by quantum numbers which include "spin up and spin down" states for the electron. In addition both the electron and the neighboring nuclei can interact with an external dc-magnetic field which further splits the energies of these states. The actual number of energy levels depends on the spin state of the neighboring

TABLE V

ABSORPTION AND EMISSION ENERGIES FOR F AND F^+-CENTERS IN THE ALKALINE EARTH OXIDES

Material	F-Center		F^+-Center	
	Absorption (eV)	Emission (eV)	Absorption (eV)	Emission (eV)
MgO	5.01[a,b,c]	2.4[i]	4.92[m,n,o,p]	3.13[a,i]
CaO	3.1[d,e,f]	2.0[e,j,k,l]	3.65[o,q,r,s]	3.3[e,j,l,t]
SrO	2.49[g]		3.1[o,q]	2.5[u,v,w]
BaO	2.3[h]		2.0[o,q]	

[a]Reference 35; [b]Reference 33; [c]Reference 34; [d]Reference 40;

[e]Reference 41; [f]Reference 42; [g]Reference 43; [h]Reference 44;

[i]Reference 45; [j]Reference 25; [k]Reference 47; [l]Reference 26;

[m]Reference 32; [n]Reference 31; [o]Reference 37; [p]Reference 36;

[q]Reference 29; [r]Reference 38; [s]Reference 39; [t]Reference 46;

[u]Reference 48; [v]Reference 49; [w]Reference 28.

nuclei and the probability that the electron will be found at these neighboring nuclei (i.e., the extent of the electronic wave function). Transitions can be induced between various "spin up" and "spin down" states by applying a microwave radiation field of appropriate frequency. The electron undergoes mutual magnetic interactions with the neighboring nuclei which have nonzero spin. The hyperfine structure which may result on the ESR spectrum can yield information concerning the symmetry of the center, the number and identification of nearest neighbor ions and the orientation of the center in the crystal.

In the preceding discussion, attention was focused on the ground state of the center. In order to study an excited state of a center, a transition from the ground to the excited state must occur. This transition occurs when the resonance condition, $\Delta E = h\nu$, is met. The energy absorbed by the system is provided by radiation of frequency ν usually in the visible or ultraviolet region of the spectrum.

ESR-FR (Faraday Rotation) (29,36) and ESR-MCD (Magnetic Circular Dichroism) (37) Double Resonance experiments have been instrumental in identifying the optical bands of the F^+-centers in the oxides. These experiments measure properties of the F-type centers in absorption and reveal the character of the excited state before lattice relaxation.

As illustrated in Figure 3, the spin-orbit splitting of the excited state is accompanied by further Zemann splitting of the degenerate spin states when placed in an external magnetic field. If plane-polarized light is then allowed to traverse the sample in the direction of a longitudinal external magnetic field, the left- and right-circularly polarized components of the plane-polarized light wave are absorbed in different transitions, as depicted in Figure 3. The absorption coefficient at

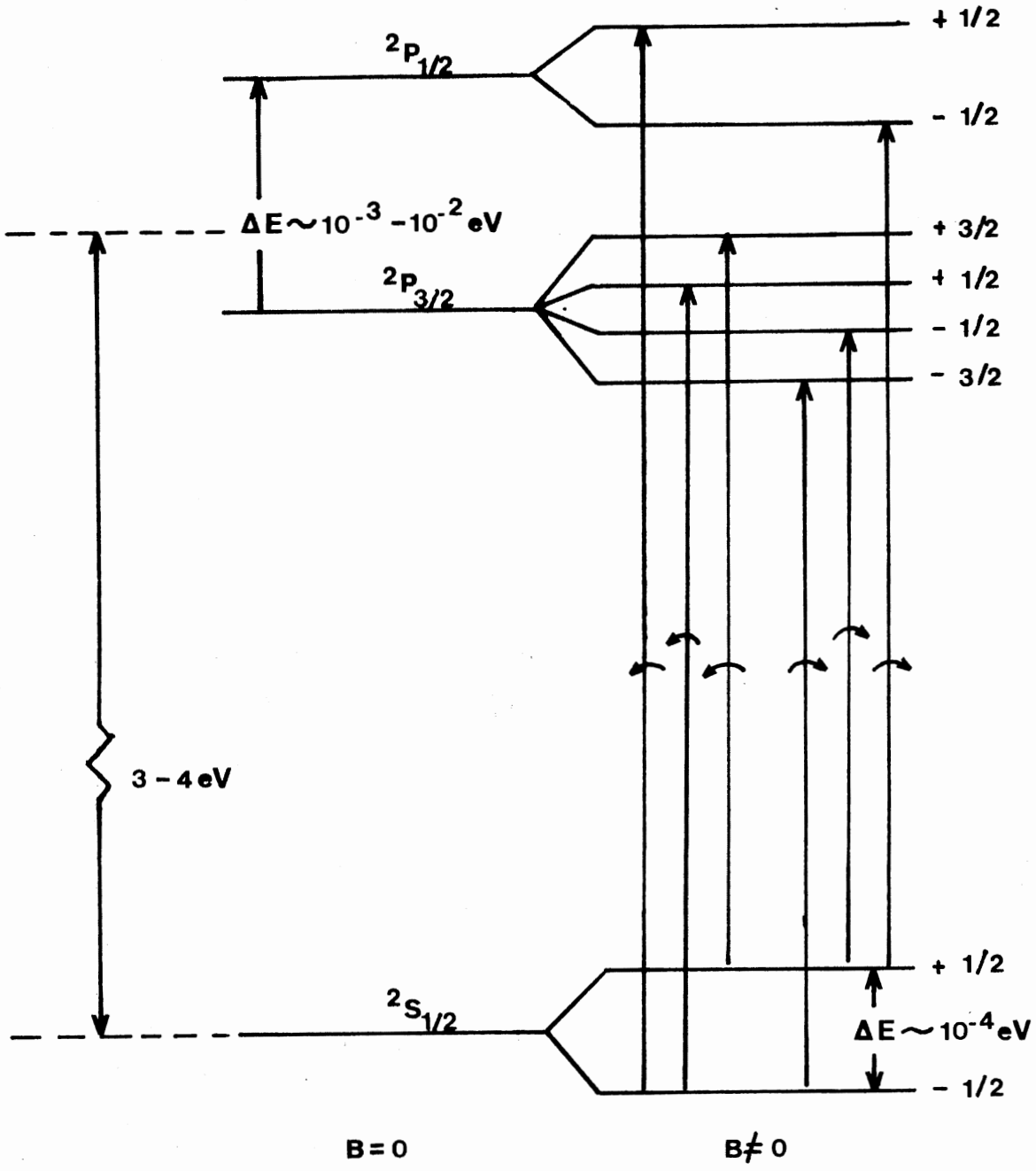

Figure 3. Energy Level Diagram of F^+-center Showing the Negative Spin-orbit Splitting and the Approximate Effect of a Magnetic Field B

a given wavelength is therefore slightly different for the two circularly polarized components of the plane-polarized light wave. The difference between these two slightly shifted absorption curves leads to the magnetic circular dichroism (50).

Faraday rotation (7,50) is closely related to the measurement of circular dichroism. Faraday rotation is the rotation of the plane of polarization of a plane-polarized light wave upon traversing an optical medium in the direction of a longitudinal magnetic field. The amount of rotation depends upon the phase difference of the two circularly polarized components of the plane-polarized wave after traversing the medium. The difference in phase results from different indices of refraction for the left- and right-circularly polarized components. Faraday rotation therefore measures the difference in refractive indices rather than absorption coefficients measured in MCD. The two are related through the Kramers-Kronig relations.

From such measurements values can be determined for the magnetic and spin-orbit splittings (26,29,34,37). The spin-orbit energy is found to be negative, essentially because an F-type center is an inside-out atom, an electron in a cage of surrounding nuclei rather than an electron surrounding a nucleus. Since the optical band width for an F-type center in the oxides is on the order of several tenths of an eV, the spin-orbit splittings of approximately 10^{-2} eV cannot be resolved and must therefore be obtained by the techniques just described.

Again, it should be noted that ESR and FR permit some description of the unrelaxed excited state of the center. To gain information about the relaxed excited state, one can observe, for example, fluorescence and/or photoconductivity. Optical detection of paramagnetic resonance

(51,52) in the excited states of F-centers, which is related to fluorescence, is also possible.

VII. Statement of the Problem

The electron, in the relaxed excited state of the center, is considered to have predominantly two competing modes of escape: 1) radiative decay to the ground state--luminescence; or 2) thermal release into the conduction band across a small energy gap, E_a--photoconductivity. A third possibility is non-radiative decay to a nearby excited state with the emission of phonons followed by radiative decay to the ground state or non-radiative decay directly to the ground state. The detailed study of these two competing processes will be the subject of the remainder of this thesis with emphasis on the photoconductivity studies.

The objective of this study is to investigate the electronic structure of F-type defects in CaO and SrO by means of dc-photoconductivity in association with optical measurements and related techniques such as luminescence and fluorescence lifetime measurements. These techniques provide a sensitive tool for investigating the electronic structure of these defects, particularly the proximity of the relaxed excited state to the conduction band. Trapping mechanisms in the crystal will also be investigated.

Configuration coordinate diagrams will be presented in the following chapter which will also contain an in-depth discussion of photoconductivity, luminescence and fluorescence lifetime along with the probability of the occurrence of these two competing processes. The complete experimental procedure, as well as the apparatus employed in this study, will be presented in Chapter III. Chapters IV and V will

be presentations of experimental results on SrO and CaO, respectively, followed by discussion and analysis. Chapter VI will consist of a summary of the results contained in this thesis, conclusions resulting from the measurements and suggestions for further study.

CHAPTER II

THEORY: ELECTRONIC STRUCTURE OF DEFECTS THROUGH PHOTOCONDUCTIVITY AND LUMINESCENCE

I. Introduction

Before advancing to the experimental techniques used and the results obtained in this dissertation, it is first necessary to build a theoretical framework in which the results of experimentation can be interpreted. The review which follows includes a discussion of configuration coordinate diagrams, optical properties and transition probabilities, absorption band shapes and vibronics, and the study of photoconductivity and luminescence originating from F-type defects in crystals.

II. Configuration Coordinate Diagrams

In finding the stationary states of a crystal, one must solve the exact eigenvalue equation

$$H\psi_\Lambda = E_\Lambda\psi_\Lambda \qquad (1)$$

where H is the Hamiltonian operator describing the kinetic energy of all the particles, electrons and nuclei, and their potential energy of interaction. Since the nuclei are much more massive and, in a sense, would move much more slowly than the electrons, the Born-Oppenheimer approximation allows the nuclei, so to speak, to follow the motion of the elec-

trons; i.e., the electronic state of motion is responsible for governing the motion of the nuclei. Translated into mathematical terms, the Born-Oppenheimer approximation (4) allows us to write the state function ψ_Λ for the entire crystal as the product $\phi_i(r,R)X_{i\nu}(R)$ where $\phi(r,R)$ is the electronic wave function obtained with the nuclei fixed at position R and X(R) is the wavefunction for the nuclei (53). The electronic Hamiltonian, H_{el}, of which $\phi(r,R)$ is an eigenfunction, may be obtained from the full Hamiltonian, H, by setting the masses of the nuclei equal to infinity in the kinetic energy terms and by fixing the nuclear positions (R) in the potential energy terms. We then have for the total electronic eigenvalue problem

$$H_{el}\phi_i = E_i\phi_i \tag{2}$$

where the total electronic Hamiltonian, H_{el}, and its resulting total electronic eigenfunctions, ϕ_i, and eigenvalues, E_i, are parameterized by the position of the nuclei, R. In practice one has the option of including the nuclear-nuclear (ion core-ion core) repulsion in the electronic Hamiltonian or adding on their contribution later as the lattice contribution, E_L, to get the total energy of the crystal for a fixed configuration of the nuclei. The total energy of the crystal for a fixed configuration of the nuclei is then given by

$$U_i(R) = E_i(R) + E_L(R), \tag{3}$$

the sum of the total electronic energy and the lattice energy. The term, lattice energy, shall be used here to refer to the energy due to electrostatic interactions among all the charged particles that are not explicitly considered in the electronic Hamiltonian. In either case $U_i(R)$

serves as the potential energy in finding the subsequent motion of the nuclei.

One then has

$$H_n \, X_{i\nu}(R) = E_{i\nu} \, X_{i\nu}(R) \tag{4}$$

where H_n is the Hamiltonian for the nuclear motion such that the potential energy operator $V(R)$ is the total energy $U(R)$, (total electronic energy $E_i(R)$ and lattice energy $E_L(R)$). Since each $U_i(R)$ depends on the electronic state i, H_n will be different for different electronic states and the vibrational frequency of the normal modes will thus depend on the electronic state of the crystal. The eigenvalues $E_{i\nu}$ of H_n measure both the kinetic energy of the nuclei and the potential energy of interaction for these nuclei and thus corresponds to the total energy E for a particular state of the crystal.

Even if the approximation of writing the stationary state wavefunction $\psi_\Lambda = \phi_i(r,R) \, X_{i\nu}(R)$ proves to be insufficient, one can show that the exact stationary states can be written as a linear combination of such product wave functions,

$$\psi_\Lambda = \sum_j \sum_\nu C_{j\nu} \, \phi_j \, X_{j\nu} \, . \tag{5}$$

The Born-Oppenheimer Approximation is a way of recognizing that one term in such an expansion usually predominates. Significant contributions from two or more terms is an indication of the Jahn-Teller effect (53), which will be discussed further in Section IV.

Even to solve for the total electronic states would involve a many-body problem of great difficulty. The independent electronic model, in

which each electron is assigned to its own orbital in keeping with the Pauli Exclusion Principle, shall therefore be adopted for the electronic states of the crystal. The spatial orbitals are solutions to a single electron Hamiltonian eigenvalue problem

$$h\Phi_{\mu} = \varepsilon_{\mu}\Phi_{\mu} \tag{6}$$

where h contains a single electron potential energy operator describing the effective potential seen by an electron. For the crystal containing a defect, one has a very complicated single electron Hamiltonian, h, which describes, in principle, not only the orbitals of the defect electron but the remaining single particle electronic states of the crystal as well.

Before focusing on the defect, a look at the perfect crystal is in order. For simplicity, consider a monatomic linear solid of lattice constant, a, with the ion cores (nucleus and inner shell electrons) fixed in position. The variation of the electrostatic potential energy of a conduction electron in the field of the positive ion cores of the monatomic linear lattice can be represented schematically by Figure 4. Using the single-electron approximation, we can write

$$h\Phi_{kn} = \left[-\frac{\hbar^2}{2m} + V(x)\right]\Phi_{kn} = \varepsilon_{kn}\Phi_{kn} \tag{7}$$

where h is the single electron Hamiltonian and Φ and ε are the corresponding eigenfunctions (orbitals) and energy eigenvalues. V(x) denotes the potential energy of an electron in the linear lattice. The electron, in the independent electron model, sees a periodic potential due to the ion cores and an average potential due to its interaction with the other electrons. In contrast to the free electron gas model, these

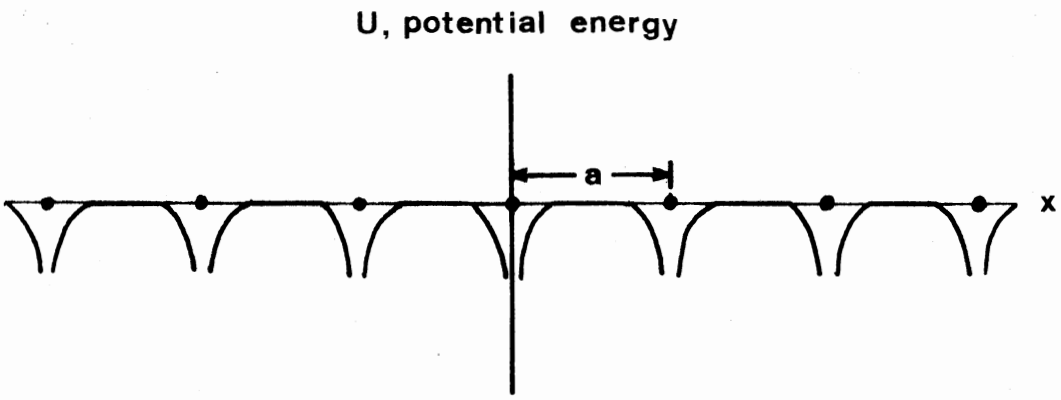

Figure 4. Variation of the Potential Energy of a Conduction Electron in the Field of the Ions of a Linear Lattice

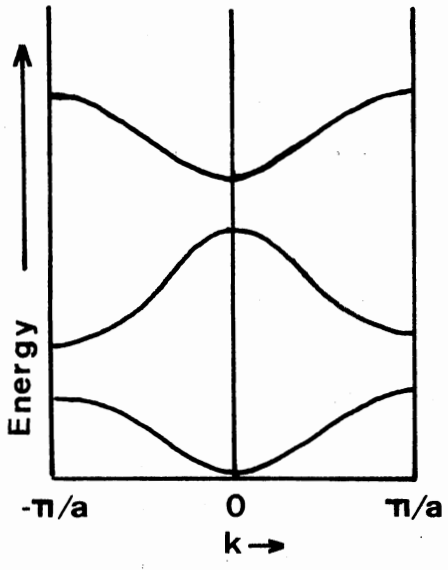

Figure 5. Three Energy Bands of a Linear Lattice Plotted in the Reduced Zone Scheme

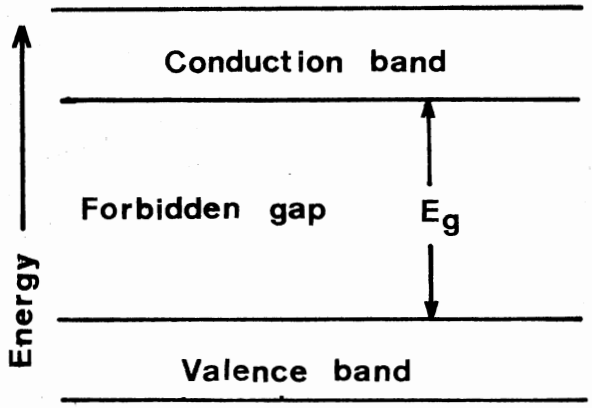

Figure 6. Band Scheme for an Insulator. All states in the valence band are filled and all states in the conduction band are vacant

effects do not cancel. The solution to this problem can be found in any solid state text, such as Kittel's (54). The spatial orbitals, Φ, can be doubly occupied with electrons having spin quantum number $m_s = \pm 1/2$. Typically the single electron energy levels fall into continuous bands with gaps between the various bands. This is illustrated in Figure 5 using the reduced zone scheme in which each value of k in the First Brillouin zone corresponds to an infinite but discrete energy eigenvalue spectrum, with each energy eigenvalue belonging to a different energy band. The concepts of energy bands and gaps carry over to the 3-dimensional lattice. The mathematics becomes more complicated and the symmetry of the 3-dimensional lattice plays an important role in calculating the energy bands.

The ground electronic state of the crystal is formed by filling in the orbitals, beginning with the lowest energy according to the density of states for each energy band. The extent to which the valence electrons of the atoms fill in, partially, or completely, the energy bands of the crystal, determines whether the material is a metal, insulator or semiconductor. The electronic band scheme for an insulator can be represented as indicated in Figure 6. All states in the valence band are filled and all states in the conduction band are vacant. The conduction band is separated by an energy gap E_g from the filled valence band. The band gap is the difference between the lowest energy point of the conduction band and the highest energy point of the valence band (see Figure 7).

In ionic crystals, such as the alkali halides and the alkaline earth oxides, the metal ions have the closed electronic shells of the noble gas structure. The most loosely bound electrons which remain on the

metal ions are in such deep energy levels that they generally play no part in any phenomena other than x-rays. It is thus the electrons in the negative ions which fill the levels of the filled (valence) band with which we are concerned (3,55).

The best values of band gap energies are obtained by optical absorption. The threshold of continuous optical absorption at frequency ω_g determines the band gap $E_g = \hbar\omega_g$ in Figure 7a. In the direct absorption process (Figure 7a) a photon is absorbed by the crystal with the creation of an electron in the conduction band and a hole in the valence band. In the indirect absorption process (Figure 7b) a photon of energy $\hbar\omega$ is absorbed with the creation of three particles: a free electron in the conduction band, a hole in the valence band and a phonon such that $\hbar\omega = E_g + \hbar\Omega$. Both processes conserve energy and momentum (54). The increasing broad background absorption observed in SrO (Chapter IV, Figure 22) and CaO (Chapter V, Figure 40) as the energy of the incident photons approach the band gap energy can possibly be explained in part as a consequence of the indirect absorption process. Both absorption processes give rise to intrinsic photoconductivity.

If the photon absorbed is not sufficiently energetic to separate completely the electron and the positive hole, they remain bound to each other by Coulomb attraction. The electrically neutral entity thus formed is an excited state of the crystal and may be viewed as a "particle" free to wander through the crystal, transporting energy but no net electrical charge. The mobile "particle" consisting of an electron bound to a positive hole is often referred to as an "exciton" (3) and the energy states corresponding to this entity are called exciton states. Excitons may be considered to arise from excitation of a valence elec-

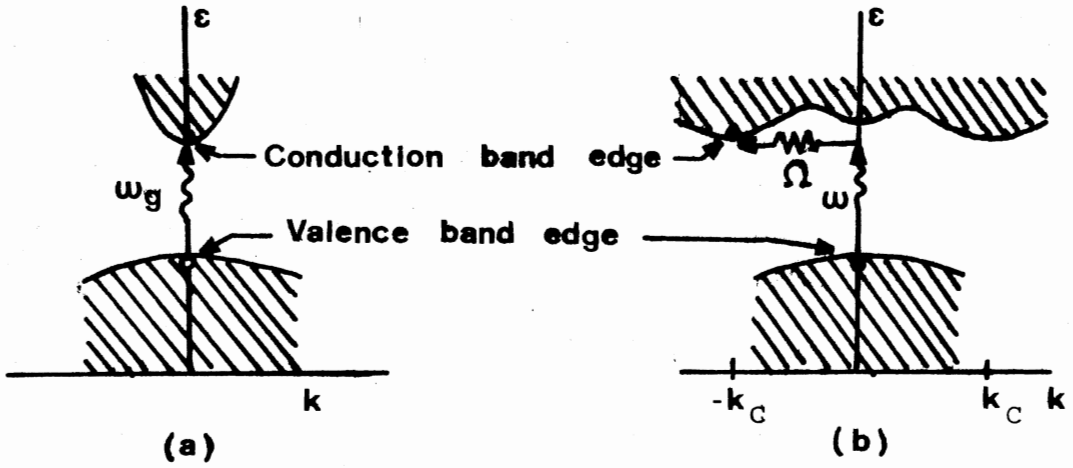

Source: Kittel (54)

Figure 7. Direct Absorption Process (a) and Indirect Absorption Process (b). A photon is absorbed with the creation of a free electron and a hole: $E_g = \hbar\omega_g$ (a) and with the creation of a free electron, a hole and a phonon: $\hbar\omega = E_g + \hbar\Omega$ (b)

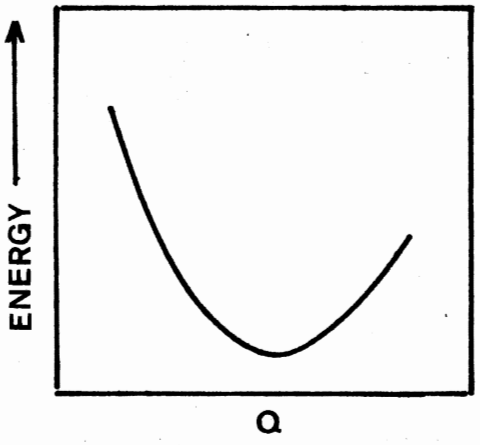

Figure 8. Diagram of the Total Energy U of the Crystal as Function of Fixed Configurations of the Ion Cores

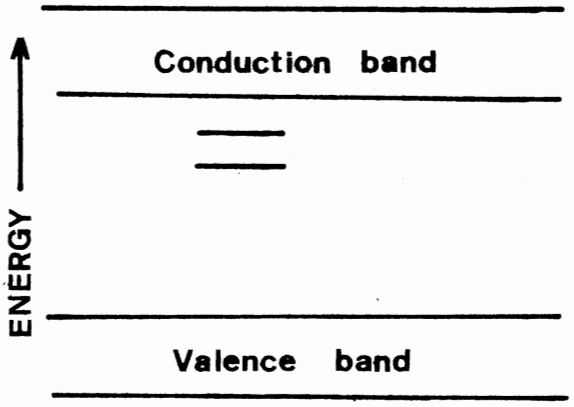

Figure 9. Schematic Diagram Showing the Relative Energies of the Valence and Conduction Band of the Crystal and the Energy Levels for the Defect Electron Trapped at the Anion Vacancy

tron of the negative ion, such as Cl^- in KCl by the absorption of light, $X^- \xrightarrow{\hbar\omega} X^{-*}$. The excited halogen ion X^{-*} can transfer its energy to a nearby halogen ion X^- and the energy can thus migrate through the crystal without any of the atoms themselves moving. The motion of the exciton does not give rise to an electric current.

In solving the energy eigenvalue problem above (Equation 7), using the single electron approximation, the ion cores were fixed in position with lattice constant, a. The total electronic energy of the crystal in the ground state is given by the sum of the single electron energies for that particular configuration, Q, of the ion cores. Q is a single variable used to represent and calculate the positions of the ion cores as they vibrate in a particular normal mode. Usually the breathing mode is assumed for simplicity. The total energy, U, of the crystal for a given configuration of the ion cores is equal to the sum of the total electronic energy and the electrostatic repulsion of the cores (the lattice energy). The energy U is a function of the configuration of the cores since the single electron energy eigenvalues, and consequently the total electronic energy of the crystal, as well as the electrostatic repulsion of the ion cores will take on different values for various configuration of the ion cores. This could be represented schematically by Figure 8 where <u>each</u> point on the curve represents the total energy, U_i, of the crystal correspoinding to the ion cores frozen into a particular configuration, Q_i. There is a configuration, Q, of the ion cores for which U is minimum. For the actual vibrating crystal, this curve then serves as the potential energy for the vibratory motion of the ion cores. This will be further illustrated below.

Keeping this background in mind, consider now the crystal containing

defects consisting of a single electron trapped at an anion vacancy.

In describing the electronic state of such a crystal, for a given configuration of the nuclei, attention is focused on the possible states of the electron trapped in the vacancy. In principle the calculation should be done "self-consistently" in that not only the effects of the other electrons on the defect electron, but also the effects of the defect electron in changing the orbitals of the other electrons, especially those on the neighboring ions, should be taken into account. In practice, however, one is concerned only with the electronic states of the defect electron as it moves in a potential which is constructed by knowing the orbitals, and thus the charge distributions, on the ions surrounding the defect and by mimicking the effects of the rest of the crystal on the defect electron. The resulting effective potential energy experienced by the defect electron is very complicated and further approximations are necessary to solve the Schrodinger equation $h'\Phi = \varepsilon\Phi$ for the orbitals Φ of the defect electron. The electronic Hamiltonian has the symmetry of the defect and therefore its eigenfunctions, i.e., the orbitals of the defect electron, transform as the irreducible representations of the symmetry group corresponding to the site in which the defect electron finds itself.

Since the vacancy appears to have a double positive charge with the removal of an O^{-2} in the alkaline earth oxides, if the crystal anisotropy is ignored, the electron can be imagined to be trapped by a spherically symmetric Coulomb potential of charge +2. The orbitals would then be the He^{+} orbitals labeled in part by the irreducible representation of the rotation symmetry group, i.e., by the angular momentum quantum number l=0, s; l=1, p). In reality we do not have rotational symmetry

because of the anisotropies introduced by the ions surrounding the defect. The point group symmetry for these F-type defects in the alkaline earth oxides is O_h. The S states correspond to A_{1g} and the P states correspond to T_{1u} and higher angular momentum states can be reduced into two or more irreducible representations of O_h. Since the defect, as pictured above, looks like the He^+ ion, the atomic notation is often used for convenience and the actual symmetry orbitals are referred to as s-like and p-like.

In the case of the 2-electron defects, attention is once again focused on the electronic states of the defect for a given configuration of the nuclei. Here, in addition to each electron moving in an effective potential, there is the coulomb interaction between the two electrons. The electronic states of the defect are found by solving for the two-electron eigenstates of the two-particle Hamiltonian which includes not only the effective interactions experienced by each electron but also their mutual electrostatic repulsion. The two-electron state can also be classified according to group theory irreducible representations, but in addition the Pauli Principle and the fact that the electrons have an intrinsic spin must also be taken into account. Thus the electronic wave functions are either singlets (antisymmetric spin function multiplied by symmetric spatial functions) or triplets (symmetric spin function multiplied by antisymmetric spatial function).

The remainder of the development leading to the configuration coordinate diagram shall be applicable to both the singly or doubly electron-occupied anion vacancy defects. The configuration coordinate diagram is a simple model used to represent information about the electronic structure of the defect. The one- or two-electron eigenfunctions

obtained for the defect electrons are more localized than are the single electron orbitals obtained for the perfect crystal. The ground and excited states of the defect electron will differ, however, from those of an electron in a vacuum in that the wavefunctions usually spread out over a larger volume, such as that occupied by the neighboring ions in the crystal (55). As regards the single electron orbitals for the remaining electrons in the crystal, the energy scheme would be essentially the same as that of the perfect crystal since the structure of the two crystals is essentially the same except for an oxygen ion vacancy occupied by one or two electrons. The energy scheme for the crystal containing such defects could be represented by Figure 9, where the bound levels below the conduction band are associated with the defect electron (3,55) and the levels in the filled valence band are associated with the other electrons in the crystal. When the defect electron has been raised to its lowest excited state it may require only a small additional energy, which can often be supplied by the thermal vibrations of the lattice, to be freed into the conduction band (55).

Just as for the perfect crystal, the electronic calculations for the defect electron are repeated for different fixed positions of the nuclei and the total energy of the electronic system along with the lattice energy is then taken as the potential energy for the vibratory motion of the nuclei. The total energy, U_i, of the crystal for a particular configuration, Q, of the nuclei is given by the sum of the total electronic energy (defect electron and other electrons in the crystal) and the lattice energy. In Figure 10 each point on the curves, corresponding to the ground state (lower curve) and first excited state, represents the total energy, U_i, of the crystal corresponding to the

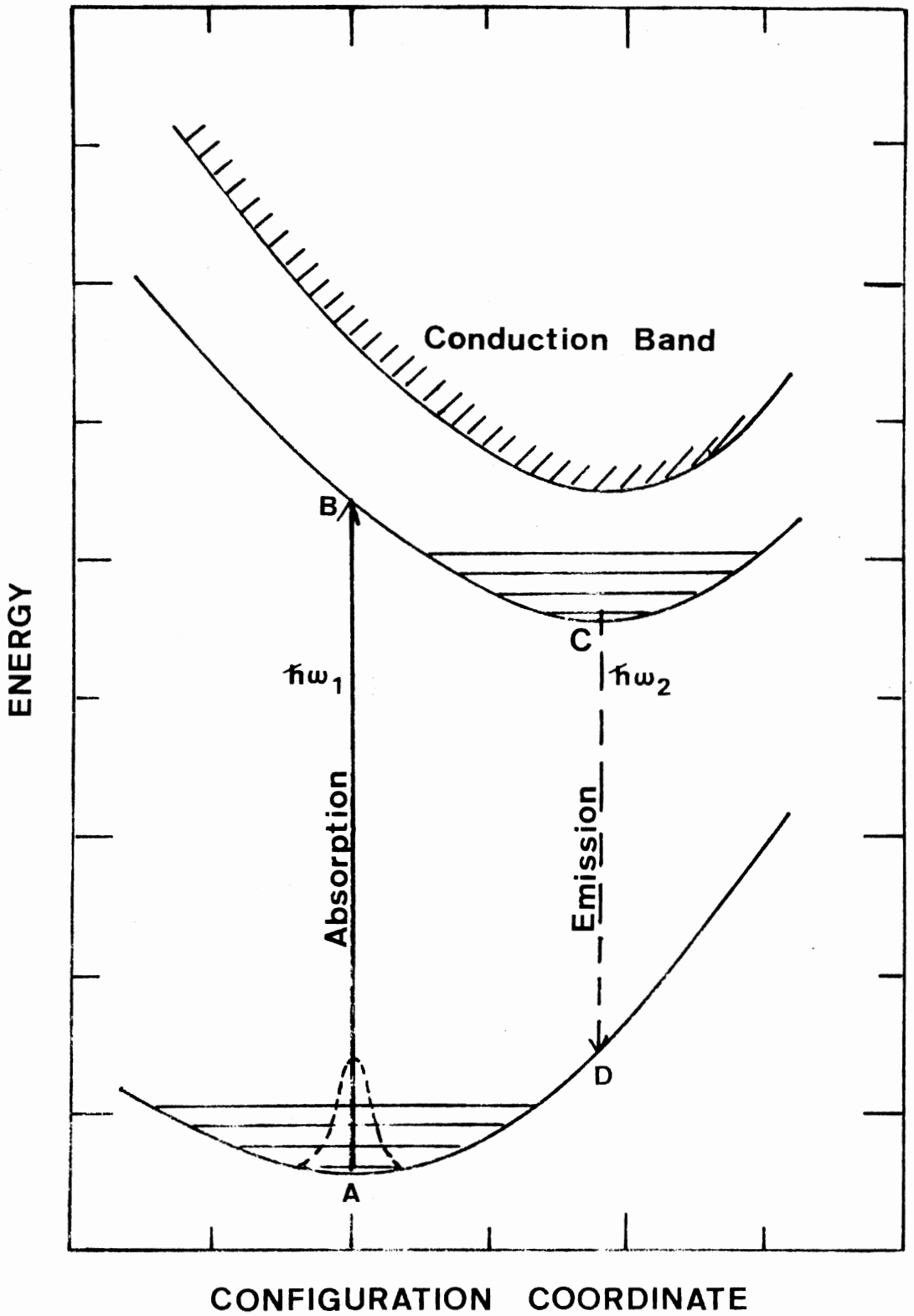

Figure 10. Configuration Coordinate Diagram

nuclei frozen into a particular configuration, Q. These curves, though representing the total energy, U_i, are given the label corresponding to the state for the defect electron. The energy, U_i, changes as the configuration coordinate, Q, changes. As stated above, the energy, U, serves as the potential energy for the motion of the nuclei. To the extent that these curves are parabolic in the configuration coordinate Q the stationary state wave functions for the nuclear vibrations are those of a simple harmonic oscillator and the typical energy spectrum is given by $(n + 1/2)\hbar\omega$ where ω is the frequency for a single normal mode of vibration, usually assumed to be a "breathing mode" of the defect's nearest neighbors. ω is determined by the mass of the vibrating ions and the curvature of the potential energy curve. Since the electronic energy is already included in defining the potential energy operator for these vibrations, the eigenvalues $(n + 1/2)\hbar\omega$ represent the total energy of the crystal. The energy of a given state--electronic and vibrational--can be represented as a horizontal line on the configuration coordinate diagram. Adjacent states associated with an electronic energy curve differ in energy by $\hbar\omega$. The energy difference between two states on two different electronic curves is the difference between the energy eigenvalues of each represented by the horizontal lines. Since the curvature of different electronic states may be quite different, the vibrational frequency, and hence the vibrational energy spacings within any one electronic energy curve can be quite different than those corresponding to another electronic energy state.

In this dissertation the F- and F^+-center in CaO and the F^+-center in SrO are of particular interest. Calculations of the electronic energy for these centers, as a function of the % distortion of the lattice for

various normal modes of vibration have been performed by Mills (56) and Wood and Wilson (57,58,59,60). Their model emphasizes the importance of 1) electronic structure on the ions neighboring the defect, 2) electronic and ionic polarization of the lattice and 3) lattice distortion and its effect on the energy levels and wavefunctions of the defect (59). Figure 11a and b, show the configuration coordinate diagrams obtained by Wood and Wilson for the F-center in CaO (59) and the F^+-center in SrO (60). Wood and Wilson (57) have found that different configuration coordinate diagrams are necessary for absorption and emission for the F-centers in these materials. In the $^1A_{1g}$ ground state of the center, the charge density of the two electrons is almost entirely confined to the vacancy, but in the $^1T_{1u}$ excited state, the excited electron is almost completely outside of the vacancy. The ions are unable to respond to the change in the effective charge of the vacancy during the optical transition, but once in the excited state, the ions can adjust to this change, and the diffuse excited states are therefore shifted in energy relative to the more compact states before absorption. Therefore the configuration coordinate diagram for the F-center in CaO in emission is shown in Figure 11a, since this is the one that will be pertinent later for comparison to experimental results.

III. Optical Properties

Since electronic excitation of the defect electron takes places through the absorption of light and the excited electron may radiatively decay back to the ground state, a review of some of the theory pertaining to optical transitions in color centers (F and F^+) is presented below.

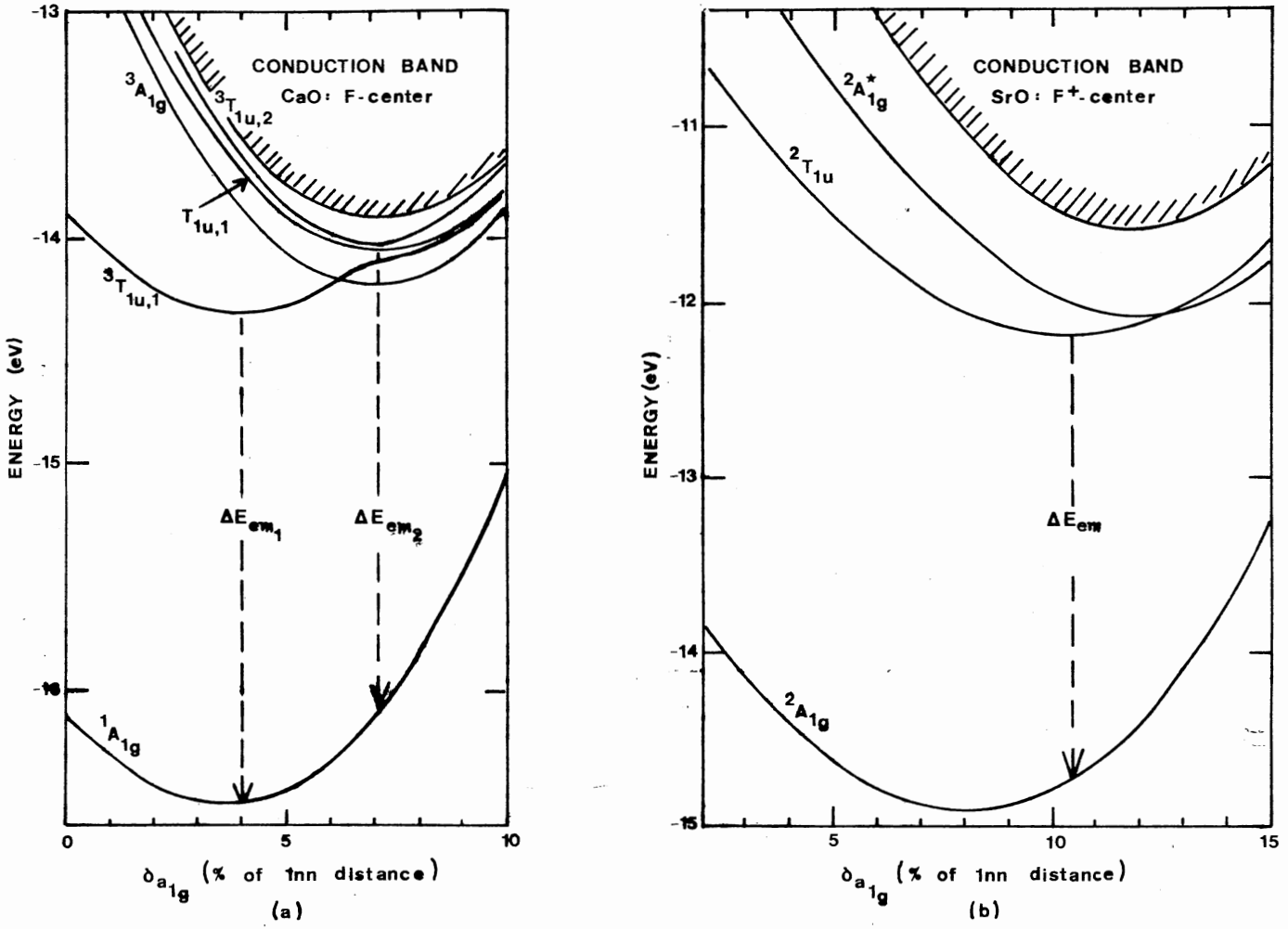

Source: a) Wood and Wilson (59) and b) Wilson et al. (60).

Figure 11. Configuration Coordinate Diagrams for CaO F-center (a) and SrO F^+-center (b), Both in Emission. δ = relaxation parameter and 1nn = first nearest neighbor distance

The electronic state of the center can be changed by the absorption or emission of photons. If the crystal is initially in the ground state at time t=O, then the other states will be occupied with certain probabilities at later times if light of sufficient energy is permitted to fall on the sample. Correspondingly the probability that the system will be found in the initial state at time t > o, will be less than one. If, on the other hand, the system is initially in an excited state it will spontaneously radiate photons and decay to a lower energy level. The probability that after time t, the initial state is still occupied is

$$P(t) = e^{-t/\tau} .$$

The time constant, τ, describing the transition depends on the states involved and measures the transition rate from one state to another in that $\frac{1}{\tau_{i\nu \to i'\nu'}}$ is the probability per unit time that a transition from the state $i\nu$ to the state $i'\nu'$ will take place. The change in the probability that the state is occupied with time is given by

$$\frac{dP(t)}{dt} = - \left(\frac{1}{\tau}\right) \left(e^{-t/\tau}\right),$$

i.e., the transition rate times the probability that the system is still in the initial state at time t.

According to quantum theory, the probability per unit time, $1/\tau_{i\nu \to i'\nu'}$ is proportional to the absolute square of the matrix element between the states $\psi_{i\nu} = \phi_i \, X_{i\nu}$ and $\psi_{i'\nu'} = \phi_{i'} \, X_{i'\nu'}$ of the operator which describes the coupling of the photons (electromagnetic field) with the crystal. Many approximations are necessary to evaluate these matrix

elements. The fact that we are interested in light with wavelength between 6000-3000 Å permits the use of the so-called electric dipole approximation for the transition operator (61). Based on the assumption that the wavefunctions for each state can be written as a product of an electronic wavefunction times a vibrational wavefunction it turns out that the matrix element itself can be approximated by (62,4)

$$R_{i\nu,i'\nu'} = \int dQ \int dr\, X^{*}_{i\nu}(Q)\, \phi^{*}_{i}(r,Q)\, M_e\, \phi_{i'}(r,Q)\, X_{i'\nu'}(Q)$$

$$= \int dQ\, X^{*}_{i\nu}(Q) \int dr\, \Phi^{*}_{i}(r,Q)\, M_e\, \phi_{i'}(r,Q)\, X_{i'\nu'}(Q)$$

$$= \int dQ\, X^{*}_{i\nu}(Q)\, R_e(Q)\, X_{i'\nu'}(Q) \qquad (8)$$

where M_e is the electric dipole operator and the electronic transition moment

$$R_e(Q) = \int dr\, \Phi^{*}_{i}(r,Q)\, M_e\, \phi_{i'}(r,Q) \qquad (9)$$

is in principle a function of the configuration coordinate Q.

The Franck-Condon Principle states that during an electronic transition the electronic state changes so fast that (1) the nuclei do not move and (2) the nuclei do not change their momenta (63). The transition is therefore shown as a vertical line (see Figures 10 and 11) indicating that the positions of the neighboring nuclei in the lattice do not have time to change appreciably during the nearly instantaneous electronic transition. The quantum mechanical formulation of the Franck-Condon Principle (62) rests on the assumption that the variation of the electronic transition moment with Q is slow, thereby allowing it to be replaced by an average value determined for $Q = Q_e$

$$\overline{R_e} = \int dr\ \phi_i^*(r,Q_e)\ M_e\ \phi_i'(r,Q_e) \qquad (10)$$

Using this result, Equation 8 becomes

$$R_{i\nu,i'\nu'} = \overline{R_e} \int X_{i\nu}^*(Q)\ X_{i'\nu'}(Q)\ dQ \qquad (11)$$

the product of an integral involving only the electronic coordinates and wavefunctions and an integral involving the vibrational wavefunctions and coordinates. The latter integral is just an overlap integral between two vibrational wave functions. Consequently the most likely transitions will be those between vibrational levels for which the overlap integral is relatively large, thus giving essentially the same results as those from the classical Franck-Condon Principle given above.

The fact that the electronic wave functions can be classified according to the irreducible representations of the spatial symmetry group gives rise to certain selection rules, i.e., the integrals of the transition operator sandwiched between initial and final wave functions will be zero except for selected cases. For O_h symmetry, the symmetry of the F-type centers in the alkaline earth oxides, the electric dipole transition takes place between the ground state A_{1g} and T_{1u}. Since the electric dipole transition operator does not contain spin operators, there is the additional restriction that the spin quantum number does not change, i.e., $\Delta S = 0$. Thus for the two electron center only singlet → singlet or triplet → triplet transitions are allowed in the electric dipole approximation. If for a given transition the matrix elements of the electric dipole moment are zero, the matrix elements formed with higher order terms in the transition operator (magnetic dipole and electric quadrapole moments) may be nonzero. Thus transitions

which are disallowed because of the electric dipole transition selection rules may take place by these higher order processes but the transition rates are generally much smaller than for electric dipole transitions. Magnetic dipole transition probabilities are only 10^{-5} and quadrapole transition probabilities only 10^{-8} of dipole transition probabilities (62). Transitions that cannot occur in the electric dipole approximation are considered forbidden transitions.

One particular transition between a given initial and a given final state occurs at a very particular wavelength. However, the absorption or emission spectrum of a defect center is spread out into a broad band due to the proximity of the vibrational levels associated with the various electronic states. To illustrate this consider Figure 10. The dotted curve represents the probability density for the n=0 vibrational level, that is the probability of the neighboring nuclei appearing at various distances from the center of the defect--the total energy of the system remaining the same for these different values of Q. For centers, with the neighboring nuclei displaced from the equilibrium position, the transition will be to points displaced from B on the excited electronic curve. Therefore the lattice vibrations at A lead to a spread in energies due to the steepness of the curve at B, thereby giving rise to a broad absorption band. Immediately after the transition to the excited state the lattice relaxes (10^{-12} - 10^{-13} sec), emitting phonons, as a new equilibrium position of the nearest neighbor ions is reached.

Since one phase of the experimental work included in this dissertation is optical absorption measurements, the relation between absorption bands, oscillator strengths and the number of centers involved should be reviewed briefly. These concepts will be useful later in the

interpretation of the experimental results obtained in this dissertation.

Assuming that the centers giving rise to the absorption band do not interact with each other, the area under the absorption curve is directly proportional to the concentration of absorbing centers. For Lorentzian bands, Smakula's equation (3) is

$$Nf = \frac{9mc}{2e^2} \frac{n}{(n^2+2)^2} \alpha_{max} W = 1.29 \times 10^{17} \frac{n}{(n^2+2)^2} \alpha_{max} W \qquad (12)$$

where

N = the number of F-centers/cm^3;

f = the oscillator strength for a particular electronic transition;

n = the refractive index of the crystal for the wavelength at the peak of the absorption;

α_{max} = the absorption coefficient in cm^{-1} at the peak of the absorption band;

W = the half-width of the absorption band in electron volts;

m = mass of the electron;

e = charge of the electron;

c = velocity of light.

The oscillator strength, f, is a dimensionless quantity which is related to the probability per unit time of the optical transition producing absorption (3). The oscillator strength can be written (4) as

$$f_{i\nu,i'\nu'} = \left(\frac{2m}{3\hbar}\right)\left(\frac{E_{i'\nu'}-E_{i\nu}}{\hbar}\right)\left|R_{i\nu,i'\nu'}\right|^2 . \qquad (13)$$

However, for imperfections in crystals transitions between such discrete states are not often observed. Rather a broad band is observed repre-

senting the sum of many such transitions. The electronic oscillator strength of the transition $i \rightarrow i'$, summed over the final vibrational states and averaged over the initial vibrational states is given by (4)

$$f_{i,i'} = \frac{2m}{3\hbar} \left(\frac{E_{i'}-E_i}{\hbar}\right) \left|\overline{R_e}\right|^2 . \qquad (14)$$

The total oscillator strength for a transition from a given state is the sum of the oscillator strengths for all possible transitions from that state and this sum is the number of electrons associated with the center. (For an F center in the alkaline earth oxides, $f_{total} = 2$). The larger one particular "$f_{i,i'}$" is the more likely will be that particular transition relative to the other transitions. So if one measures the optical density as a function of wavelength on a crystal containing a given type of defect, the optical density will be largest for that electronic transition having the greatest oscillator strength. Similarly, if the optical absorption measured on a crystal shows two bands corresponding to two different types of centers (e.g., F and F^+), one cannot by comparison of the bands conclude anything about the relative number of each type of defect unless the oscillator strengths are known.

IV. Absorption Band Shapes and Vibronic Properties

In the configuration coordinate diagram in Figure 10, the defect was imagined coupled to a single vibrational mode Q--usually assumed to be the "breathing mode" of the defect nearest neighbors, although, in principle, it could be more complex, as indeed is the case for the F^+-center in CaO and SrO. At T = 0 K the probability of a transition from

the n = 0 vibrational level of the ground state to the n = m vibrational level of the excited state can be given as (7)

$$P_{Om} = e^{-S} \frac{S^m}{m!} \tag{15}$$

where S, the Huang-Rhys factor, is a dimensionless measure of the linear coupling. The most probable transition at a temperature of 0 K is from the n=0 vibrational level of the ground state to the m=S level in the excited state. For large values of S, P_{Om} approximates a Gaussian shape which is consistent with absorption spectra obtained for F-centers in alkali halides.

For Gaussian curves (or P_{Om} for large S) the half-width W is related to its second moment M_2 by

$$W^2 = (8 \ln 2) M_2 \tag{16}$$

where

$$M_2 = S \hbar^2 \omega^2 \coth (\hbar\omega/2kT), \tag{17}$$

Consequently,

$$\left(\frac{W}{\hbar\omega}\right)^2 = (8 \ln 2)\ S \coth (\hbar\omega/2kT) \tag{18}$$

and it follows that

$$\frac{W^2(T)}{W^2(O)} = \coth (\hbar\omega/2kT), \tag{19}$$

W(O) is relatively simple to measure since in practice it is constant up

to 30 - 40 K when temperature broadening usually begins (64). By measuring W as a function of T, one can derive the effective frequency ω and the Huang-Rhys factor S. ω tends to lie in the acoustic branches of the phonon spectrum. Since the excited electronic state of the F^+-center interacts with a whole spectrum of normal modes of the defect lattice, ω is in practice only an effective mean frequency.

The Stokes shift (the shift between the energy of the absorption and emission bands), see Figure 10, can be predicted from values of S and the effective frequency ω, where the Stoke's shift $E_{ab} - E_{em} = 2 S \hbar\omega$ (7).

Reference to the F^+ band in SrO (Chapter IV, Figure 23) and CaO (Chapter V, Figures 41 and 42) immediately draws attention to the asymmetric shape of the bands which is in direct contrast to the symmetric Gaussian shape bands which have been assumed up to this point. A clearly resolved zero-phonon line at 355.7 nm is also noted on the CaO F^+ absorption band indicating that the coupling of the p state to the phonons is not very strong. From Equation 15, it is seen that at a temperature of 0 K the intensity of the zero-phonon transition (P_{oo}) is only a fraction e^{-S} of the whole band, and is usually undetectable unless $S \lesssim 6$. The Huang-Rhys factor, S, is crucial in determining the appearance of the zero-phonon line. In addition to determining S from the temperature dependence of the band half-width, W, one should also, according to the ideas presented above, be able to determine S from the separation of the band centroid and the zero-phonon line according to $\delta = S\hbar\omega$. However, the value of S for the CaO F^+-center determined from $\delta = S\hbar\omega$ ($S \sim 4$) (46) is much smaller than that determined from the half-width ($S \sim 13$-16) (7).

The asymmetric absorption band for the F^+-center in CaO and SrO, as well as the discrepancy in values of S determined by the two methods above for the F^+-center in CaO, are both explained as consequences of the dynamic Jahn-Teller effect in these defects. The Jahn-Teller effect is the intrinsic instability of an orbitally degenerate state of a crystalline defect with respect to asymmetric distortions of its surroundings which lowers the energy and removes some of the degeneracy (53,65). The Jahn-Teller effect for a T_{1u} orbital state comes about because of coupling to noncubic vibrational modes of E_g and T_{2g} symmetry. For the F^+-center in CaO, it has been shown (67,68,69) that the Jahn-Teller couplings of the $^2T_{1u}$ electronic state to the noncubic E_g and T_{2g} vibrational modes are approximately equal in strength, and dominate the coupling to the symmetrical A_{1g} (breathing) mode. Similar calculations are currently being performed by Wood and Wilson (60) for the F^+-center in SrO. This situation is in contrast to that for F-centers in alkali halides, where coupling to A_{1g} modes usually dominates (70).

The Jahn-Teller effect is a manifestation of the break down of the approximation inherent in the Born-Oppenheimer picture. The "vibronic" (i.e., combined electronic-vibrational) wavefunction in the Born-Oppenheimer approximation is written as a single product

$$\psi = \phi_i(r,R)\, X_{i\nu}(R)$$

and the electronic and nuclear hamiltonians were considered as if separate entities. In considering the Jahn-Teller effect it is seen that they are in fact inseparable. Though the conditions for validity for the Born-Oppenheimer approximation begin to break down, the vibronic wavefunction can still be written as a linear combination of usually a small

number of Born-Oppenheimer products, i.e., (53)

$$\psi = \sum_j \sum_\nu C_{j\nu} \phi_j X_{j\nu}.$$

With the occurrence of a complicated Jahn-Teller effect, one defines a Huang-Rhys factor and an effective frequency for each type of mode, i.e., $S_{A_{1g}}$, S_{E_g}, $S_{T_{2g}}$. For the equal coupling case, $S_{E_G} = S_{T_{2g}} = S'$ and the separation of the band centroid and the zero-phonon line is now given by $\delta = S'\hbar\omega$ (7). Since a zero-phonon transition by definition takes the system to one of the energy minima, it "feels" the Jahn-Teller effect. The "effective" Huang-Rhys factor, S, determined from the temperature dependence of the absorption band half-width, W, is now given by

$$S = S_{A_{1g}} + S_{E_g} + \frac{3}{2} S_{T_{2g}}$$

for the equal coupling case (68) if the assumption is made that the vibrational frequencies for the various modes are equal. Thus the Jahn-Teller effect can be used to explain the discrepancy in the experimental determination of S as pointed out above. The discussion which follows is concerned with photoconductivity and luminescence--the two phenomena of primary interest in this dissertation.

V. Photoconductivity and Luminescence

All the considerations above must be brought to bear on our understanding of how the crystal, and in particular the defect electron, is excited by the absorption of light and also on the various modes of escape open to the defect electron once it is in an excited state.

The system, in absorbing light, has undergone an electronic transition to an optically accessible excited state (A → B in Figure 10). Since in the excited electronic state the wavefunction (and the charge density) are more diffuse (less confined to the vacancy and spread out over more surrounding ions) a polarization effect occurs which gives rise to lattice relaxation. This is indicated by B → C in Figure 10, corresponding to a different equilibrium separation of the neighboring ions from the center of the defect. Since the lattice relaxes the crystal potential, used to calculate the electronic states before absorption, changes. Consequently the electronic wave function for the excited state, following lattice relaxation, at C, may be quite different from that involved in absorption at B (although they may be labeled by the same quantum numbers). In addition, the ordering of the excited electronic states may have changed. Thus one speaks of two sets of electronic wave functions, one set for absorption and one for emission (57,71). The excited state after lattice relaxation in this "emission picture" shall be referred to as the relaxed excited state of the center.

The electron, now in the relaxed excited state of the center, is considered to have two possible, competing modes of escape:

1) radiative decay to the ground state--luminescence--with the emission occurring at a lower energy, higher wavelength, than that of the absorption, or

2) thermal release into the conduction band across a small energy gap E_a--photoconductivity.

It is with the study of these two processes, as they relate to F-type centers in CaO and SrO that this dissertation is concerned. Measurements of these processes, together with associated optical measurements, provide a sensitive tool for investigating the electronic structure of these defects.

The probability per unit time for spontaneous radiative decay to the ground state, with the emission of photons, is given by $\frac{1}{\tau_R}$ (the Einstein A coefficient) where τ_R is the radiative lifetime. The transition takes place from an excited electronic state, i', to a lower electronic state, i, and $\tau^{-1}_{R_{i'\to i}}$ is the weighted average of all $\tau^{-1}_{i'\nu'\to i\nu}$ over initial states ν', summed over all final states ν

$$\frac{1}{\tau_{R_{i'\to i}}} = <\tau^{-1}_{R_{i'\nu'\to i\nu}}> = \sum_{\nu} \frac{\sum_{\nu'} \tau^{-1}_{R_{i'\nu'\to i\nu}} e^{-E_{i'\nu'}/kT}}{\sum_{\nu'} e^{-E_{i'\nu'}/kT}} . \qquad (20)$$

Previous experimental investigations (72,73) indicate that τ_R is, to a good approximation, independent of temperature. This can also be shown to follow from the Born-Oppenheimer approximation and the slow variation of the electronic transition moment R_e (Equation 9,10) with the configuration coordinate. (See DiBartolo and Powell (63), Section 10.10.) For our purposes here $\frac{1}{\tau_{R_{i'\to i}}}$ will be assumed to be temperature independent.

The second mode of escape for the electron in the relaxed excited state of the center is governed by a temperature dependent probability per unit time for thermal ionization of the electron across an energy gap E_a into the conduction band

$$\frac{1}{\tau_T} = \frac{1}{\tau_o} e^{-E_a/kT} , \qquad (21)$$

The probability per unit time for thermal ionization is given by a frequency factor, $\frac{1}{\tau_o}$, times the Boltzmann statistics factor, $e^{-E_a/kT}$, which

gives the probability that sufficiently energetic phonons are available. The frequency factor $1/\tau_o$ consists of the probability per unit time that, given sufficiently energetic phonons, the electron in the excited state will absorb the phonons undergoing a transition to higher vibrational levels (10^{13}/sec) times the probability that it will undergo a further transition to a state in the conduction band degenerate with the excited state vibrational level. The latter may be quite a small quantity and consequently $\frac{1}{\tau_o}$ is considerably less than the frequency of the lattice vibrations (10^{13}/sec) (55).

In terms of a simple model, the lifetime of the excited state may be written as

$$\frac{1}{\tau} = \frac{1}{\tau_R} + \frac{1}{\tau_o} e^{-E_a/kT} + \frac{1}{\tau_Q} \tag{22}$$

the sum of the probabilities per unit time for radiative decay, thermal ionization and $1/\tau_Q$ the probability per unit time of any other process occurring (4). Assuming a simple two level model and neglecting other processes such as nonradiative recombination with the ground state (50, 72,73), the lifetime of the excited state is then given by:

$$\tau = \frac{\tau_R}{1 + (\frac{\tau_R}{\tau_o}) e^{-E_a/kT}} . \tag{23}$$

The fraction of optically excited electrons which are thermally assisted into the conduction band is given by

$$\eta_T = \frac{\frac{1}{\tau_T}}{\frac{1}{\tau}} = \frac{1}{1 + \left(\frac{\tau_o}{\tau_R}\right) e^{+ E_a/kT}} \tag{24}$$

where η_T is the quantum efficiency for thermal ionization or the yield of free electrons. Similarly the quantum efficiency for radiative decay, η_R, the fluorescence yield, is given by:

$$\eta_R = \frac{\frac{1}{\tau_R}}{\frac{1}{\tau}} = \frac{1}{1 + \left(\frac{\tau_R}{\tau_o}\right) e^{- E_a/kT}} . \tag{25}$$

In this model

$$\eta_T + \eta_R = 1 . \tag{26}$$

Equations (23) and (25) predict identical temperature dependence for the fluorescence yield and the lifetime of the excited state and such results were obtained by Swank and Brown (72,73) for the F-center in KCl. (See Figure 12a and 12b).

Swank and Brown (72,73) likewise found that the excited state lifetimes, whether determined from the decay of photoconductivity or the decay of luminescence, were identical. This is to be expected since the lifetime measured in either case is the effective lifetime of the excited state as given in Equation (23). $1/\tau$ gives the probability per unit time that the electron will leave the excited state, but gives no indication as to which process--radiative decay or thermal ionization--will occur with the greatest probability. Since the two processes are competing modes of escape for the electron in the relaxed excited state of

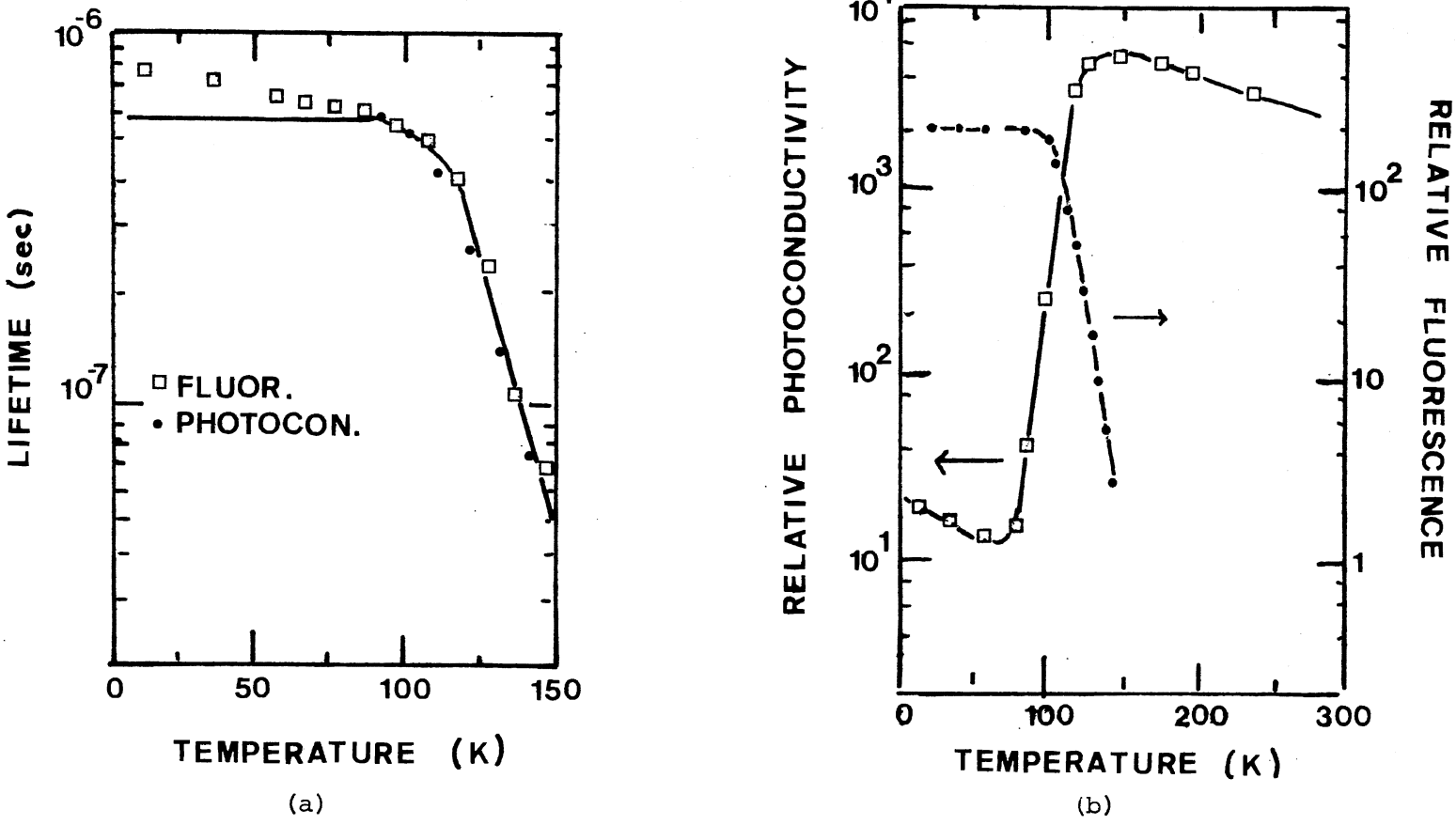

Source: R. F. Swank and F. C. Brown (72,73)

Figure 12. Lifetime of the Excited State From Fluorescence and Photoconductivity Measurements (a); the Relative Fluorescence Yield and Photoconductivity Yield for Illumination in the F Band of KCl (b)

the center, the quantum efficiency for fluorescence should decrease as that for photoconductivity increases with changing temperature. Such results were likewise obtained by Swank and Brown for F-centers in KCl (72,73). (See Figure 12b.) At low temperatures, near 0 K, $\tau \sim \tau_R$. For allowed (electric dipole) transitions in atoms τ is of the order 10^{-8} sec. If no allowed transitions can occur the mean lifetime is much larger; of the order 10^{-3} sec if magnetic dipole transitions are possible and of the order of 1 sec if only electric quadrapole transitions are possible (62). If the probability for thermal ionization is small but the lifetime of the excited state is reasonably long, then the electron has a better chance of getting to the conduction band.

Before beginning the discussion of transient dc-photocurrents, such as that originating from F-centers in alkali halides, a distinction is to be made between primary and secondary photocurrents. An insulator placed between metal electrodes has no current flowing in the dark because the electrons do not have sufficient energy to pass into the conduction levels. If such a crystal is illuminated with light of suitable wavelength, electrons in the crystal are raised to the conduction level, and drawn toward the anode giving rise to a primary photocurrent. In some crystals, the continued passage of the primary photocurrent appears to break down the resistance of the crystal so that electrons can enter the crystal from the cathode and pass through it. The resulting current is known as a secondary photocurrent (55). The photocurrents measured in this work are of the former type.

The crystal is mounted between plane parallel electrodes and illuminated with light in the F-type band. The current is measured with an electrometer. When a "slice" of the crystal is illuminated, the elec-

trons released into the conduction band are drawn by the field into the unilluminated portion where they are trapped after drifting a certain distance. In the absence of an electric field the electron will execute a kind of Brownian motion before getting trapped. Though the point where the electron is trapped may lie, for example, about 10^{-3} cm from the point where it was released, the total length of the Brownian path covered by the electron may be more than a centimeter (55). In the absence of an electric field, summing over all the random displacements would produce no net displacement of charge in any one direction. With an applied electric field the number of electrons which are trapped at points lying towards the anode from the point where they were released is greater than the number of electrons which are trapped at points lying toward the cathode from where they were released. Consequently an effect is observed on the electrometer. The current detected by the electrometer is the same as it would be if all the photoelectrons had drifted down the field a certain small distance ω, the same for all. The distance ω is known as the mean range of the photoelectrons in that field (55).

For the released electron which travels across the crystal, the charge measured by the electrometer would be the electronic charge, e. If the electron travels only a distance x, the charge measured will be

$$q = e\frac{x}{d} \tag{27}$$

where d is the distance between the electrodes. The electrometer detects a current, even if no charge flows from the crystal to the electrode, i.e., if all the electrons are trapped in the crystal. It is not necessary that the electrodes be in contact with the crystal (55).

(It shall be seen in the following chapter that, for the experimental results reported in this dissertation, sapphire plates were placed between the crystal and the electrodes to prevent charge from entering or leaving the crystal.)

The mean range ω is proportional to the electric field. For weak fields the mean distance x traveled by the electron is equal to ω and the current is proportional to the field. For strong fields, ω increases and the photocurrent saturates as shown in Figure 13. In strong fields, the actual track traveled by an electron is no longer than usual; it is just less coiled back on itself. In a crystal containing 10^{15} F-centers/cm^3 the length of the actual track before capture is of the order of a centimeter, regardless of the field (55). Wild and Brown (74) found saturation effects for the photocurrent from F-centers in KCl at a temperature of 10 K when an electric field of about 180 kV/cm was applied across a thin crystal (d ~ 0.06 cm) and determined that $\omega_o = \omega/E \sim 6 \times 10^{-7}$ cm^2/V or $\omega \sim 0.1$ cm for these conditions.

Assuming that the electron remains in the free state for a time T before it is captured, and that T is independent of the field E, the range ω is then given by

$$\omega = \mu E T \tag{28}$$

where μ is the mobility (velocity of drift/unit field). If an electron is in the free state, the probability that it is captured in time dt is $\frac{dt}{T}$. If at a given instant of time, n_o electrons are freed, the number remaining free at time t is given by

$$n = n_o e^{-t/T} .$$

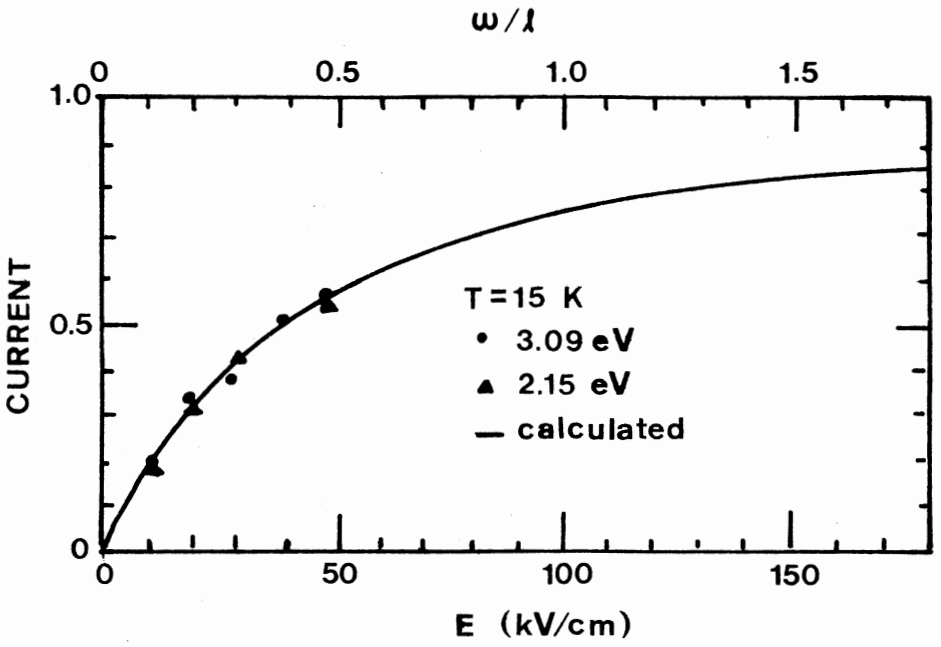

Source: R. L. Wild and F. C. Brown (74)

Figure 13. Saturation Curve for F-centers in KCl for Large Electric Fields

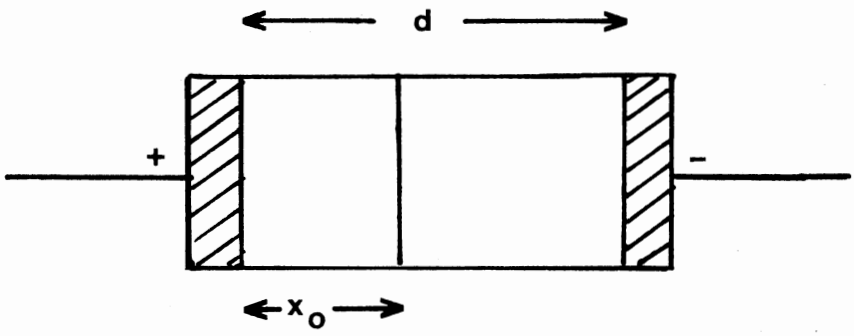

Figure 14. n_o Electrons are Released in the Crystal a Distance x_o From the Anode

Following an analysis given in Mott and Gurney, (55) consider first the situation in which the n_o electrons are released at a distance x_o from the anode (Figure 14). After traveling a distance x in the direction of the field there will be n left, where

$$n = n_o e^{-x/\mu ET}$$

or, by (28) where ω is the mean range

$$n = n_o e^{-x/\omega} . \tag{29}$$

The number which end their path in the range dx is

$$-\frac{dn}{dx} dx = \frac{n_o}{\omega} e^{-x/\omega} dx . \tag{30}$$

The total distance traveled by the n_o particles is the sum of two terms; the first term giving the distance drifted by the particles which do not reach the anode and the second giving the distance drifted by the particles which do reach the anode. The total distance drifted by the particles which are trapped before reaching the anode is given by

$$-\int_o^{x_o} x \frac{dn}{dx} dx = \int_o^{x_o} x \frac{n_o}{\omega} e^{-x/\omega} dx$$

$$= \frac{n_o}{\omega} \left[\frac{e^{-x/\omega}}{(-\frac{1}{\omega})^2} (-\frac{x}{\omega} - 1) \right]_o^{x_o}$$

which reduces to

$$n_o \{\omega(1 - e^{-x_o/\omega}) - x_o e^{-x_o/\omega}\} . \tag{31}$$

The total distance drifted by the $n_o e^{-x_o/\omega}$ (from Equation (29)) particles which do reach the anode is given by

$$x_o n_o e^{-x_o/\omega} . \tag{32}$$

Taking the sum of (31) and (32) and dividing by n_o particles, the mean distance drifted by an electron is given by

$$\bar{x} = \omega(1 - e^{-x_o/\omega}) . \tag{33}$$

If d is the length of the crystal, the ratio ψ of the charge passing through the electrometer, $n_o e \frac{\bar{x}}{d}$, to the charge released, $n_o e$, is given by

$$\psi = \frac{\omega}{d}(1 - e^{-x_o/\omega}) \tag{34}$$

a formula due to Hecht (75).

The above considerations can be used to derive the net charge flow in the external circuit for the simple case described above. However, in reality the relation between measured charge and the charge released is complicated by the penetration of light into the crystal. The discussion which follows is based on one given by Van Heyningtonand Brown (76). For light pulses of N_o total photons incident upon the crystal, the number actually entering the crystal is $N_o(1-R)$ where R is the reflection coefficient. The light intensity at a depth x in terms of the incident intensity is given by

$$I = I_o e^{-\alpha x} = N_o(1-R)e^{-\alpha x}$$

where α is the absorption coefficient for a given wavelength. Using this relationship, the number of photons actually absorbed within the crystal in the interval x to x + dx is

$$dN = \alpha N_o (1-R) e^{-\alpha x} dx.$$

We, however, are interested only in those absorptions which produce free electrons. The quantum efficiency, η_T, or the number of free electrons, dn, produced per absorbed photon for the interval dx can therefore be written as the ratio

$$\eta_T = \frac{dn}{dN}$$

and

$$dn = \eta_T \alpha N_o (1-R) e^{-\alpha x} dx. \tag{35}$$

Using the result above and integrating from 0 to d over the thickness of the crystal, gives

$$n = \eta_T N_o (1-R)(1-e^{-\alpha d}) \tag{36}$$

where n is now the total number of electrons released within the crystal. Since the electrometer records a charge q = ex/d (Equation 27) for each electron which drifts a distance x in the crystal, the charge which flows in the external circuit is analogously given by

$$Q = nq = e\eta_T N_o (1-R)(1-e^{-\alpha d})\psi \tag{37}$$

where ψ is a saturation factor defined as $\bar{x}/d$ such that $\bar{x}$ is the average

electron displacement, equal to the total displacement X of all the electrons divided by n electrons. The factor ψ takes into account the mean range of the electron and the finite depth of optical absorption.

To derive ψ, one proceeds in a manner similar to that used above (Equation 29-34) for the simpler case in which n_o electrons were released a distance x_o from the anode. The problem encountered here is somewhat more complicated since the electrons are, in reality, released at all depths throughout the crystal. The total displacement X consists of two parts: X_1 due to electrons trapped in the crystal volume and X_2 due to electrons collected at the anode. Of the Δn electrons released within the interval x to x+dx a number $d(\Delta n')$ will be trapped in the interval x' to x'+dx'. (Figure 15). Following from Equation (30),

$$d(\Delta n') = -\frac{\Delta n}{\omega} e^{-(\frac{x'-x}{\omega})} dx';\ x'>x.$$

Integrating the following expression over all values of x' gives

$$\Delta X_1 = \int_x^d (x'-x)\ d(\Delta n')$$

$$= \int_x^d (x'-x)\ \frac{\Delta n}{\omega} e^{-(\frac{x'-x}{\omega})} dx';\ x'>x$$

$$\Delta X_1 = \omega\ \Delta n\left[1 - \frac{d-x+\omega}{\omega} \exp\left[-\frac{(d-x)}{\omega}\right]\right], \qquad (38)$$

the contribution to X_1 coming from electrons released in the interval x to x+dx which are subsequently trapped in the crystal volume. Analogous to Equation (32), for the simple case above, the contribution ΔX_2 to X_2 which comes from the electrons released between x and x+dx which are collected at the anode is

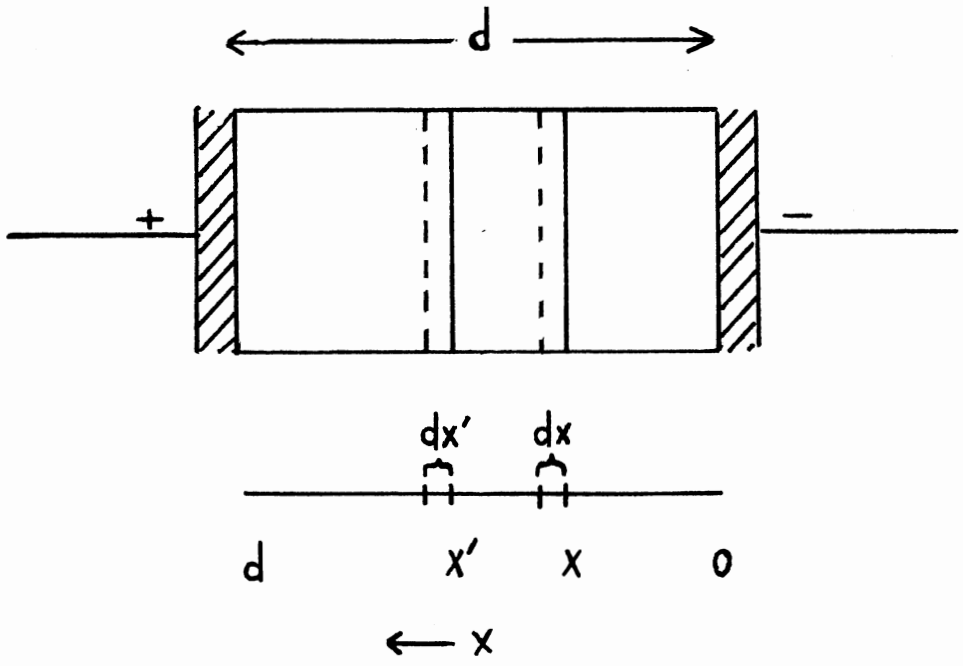

Figure 15. A Crystal Exposed to Light. Electrons released in the interval from x to x+dx are trapped between x' and x'+dx'. Electrons are released and trapped throughout the crystal

$$\Delta X_2 = \Delta n(d-x)\ \exp\left[-\frac{(d-x)}{\omega}\right] . \qquad (39)$$

Equations 38 and 39 were obtained assuming all the electrons (Δn) were released in the interval x to x+dx. However, x can take on all values between O and d. Replacing the Δ's by differentials, using Equation (35) for dn and integrating over $O \leq x \leq d$ gives

$$X_1 = \int \omega\left[1 - \frac{d-x+\omega}{\omega} \exp\left[-\frac{(d-x)}{\omega}\right]\right]dn$$

$$= \omega\eta_T\ \alpha\ N_o(1-R) \int_O^d (e^{-\alpha x})\left[1 - \frac{d-x+\omega}{\omega} \exp\left[-\frac{(d-x)}{\omega}\right]\right]dx . \qquad (40)$$

Similarly

$$X_2 = \eta_T\ \alpha\ N_o(1-R) \int_O^d e^{-\alpha x}\ (d-x)\ \exp\left[-\frac{(d-x)}{\omega}\right]dx . \qquad (41)$$

Obtaining the total displacement $X = X_1 + X_2$ is simplified by taking the sum of Equation (40) and (41) before the integration is carried out, thereby giving

$$X = \omega\eta_T\ \alpha\ N_o(1-R) \int_O^d e^{-\alpha x}\ dx - \omega\eta_T\ \alpha\ N_o \int_O^d e^{-\alpha x}\ e^{-\left[-\left(\frac{d-x}{\omega}\right)\right]}\ dx$$

and

$$X = \eta_T\ N_o(1-R)\left[\omega\left[1-e^{-\alpha d}\right] - \frac{\omega^2\alpha e^{-\alpha d}}{1-\alpha\omega} + \frac{\omega^2\alpha e^{-d/\omega}}{1-\alpha\omega}\right]$$

which upon division by n, the total number of electrons released (Equation 36) gives

$$\bar{x} = \frac{X}{n} = \frac{\omega}{1-e^{-\alpha d}} \left[(1-e^{-\alpha d}) - \frac{\omega\alpha e^{-\alpha d}}{1-\alpha\omega} + \frac{\omega\alpha e^{-d/\omega}}{1-\alpha\omega} \right]$$

$$= \frac{\omega}{1-e^{-\alpha d}} \left[1 - \frac{e^{-\alpha d}}{1-\alpha\omega} + \frac{\alpha\omega e^{-d/\omega}}{1-\alpha\omega} \right]$$

and consequently,

$$\psi = \frac{\bar{x}}{d} = \frac{1}{1-e^{-\alpha d}} \left(\frac{\omega}{d}\right) \left[1 - \frac{e^{-\alpha d}}{1-\alpha\omega} + \frac{\alpha\omega e^{-d/\omega}}{1-\alpha\omega} \right] . \qquad (42)$$

Taking the limit of ψ as $\alpha \to \infty$ which corresponds to all the light being absorbed at $x = 0$ gives

$$\psi = \frac{\omega}{d} (1-e^{-d/\omega}) \qquad (43)$$

which is in agreement with Equation (34) obtained for the simpler case above.

Taking the limit as $\alpha \to 0$ corresponds to uniform absorption. Finding a common denominator and factoring the last factor of Equation (42) gives

$$\psi = \frac{1}{1-e^{-\alpha d}} \frac{\omega}{d} \left[\frac{(1-e^{-\alpha d}) - \alpha\omega(1-e^{-d/\omega})}{1-\alpha\omega} \right]$$

$$= \frac{\omega}{d} \left[\frac{1 - \alpha\omega \dfrac{(1-e^{-d/\omega})}{(1-e^{-\alpha d})}}{1 - \alpha\omega} \right]$$

which upon expansion of $e^{-\alpha d}$ for small α gives

$$\psi = \frac{\omega}{d}\left[\frac{1 - \frac{\omega}{d}\left(1 - e^{-d/\omega}\right)}{1 - \alpha\omega}\right]$$

which in the limit as $\alpha \to 0$ yields

$$\psi = \frac{\omega}{d}\left[1 - \frac{\omega}{d}\left(1 - e^{-d/\omega}\right)\right] . \tag{44}$$

This case is of particular interest in this study since the experimental measurements were made on samples having small optical densities and thus correspondingly small optical absorption coefficients. In addition, for small electric fields, since $\omega << d$, the saturation factor ψ (Equation (44)) is further approximated by

$$\psi = \frac{\bar{x}}{d} \sim \frac{\omega}{d} . \tag{45}$$

The photocurrent is therefore given by the following expression:

$$I = e\eta_T N_o (1-R)(1-e^{-\alpha d}) \frac{\omega}{d} , \tag{46}$$

where N_o is now the number of photons incident upon the crystal per unit time. This can be rearranged to give

$$\eta\omega_o = \frac{I}{N_o}\frac{d^2}{eV} \tag{47}$$

where

$$\eta = \eta_T (1-R)(1-e^{-\alpha d})$$

$$\omega_o = \omega \frac{d}{V} .$$

In this form all of the measurable quantities are on one side of the equation and $\eta\omega_o$, the photoresponse of the crystal for a given wavelength is on the other. It should be noted that the magnitude of the photoresponse from a center is expressed as the product $\eta\omega_o$ where η is the quantum efficiency per incident photon and ω_o is the mean range of the free electron per unit applied electric field.

It should be emphasized that the above analysis was based on several assumptions. It was assumed that only electrons contribute to the photocurrent (76) and that these electrons originated from one type of defect and that a single trapping mechanism was involved. In addition all the photoelectrons were considered to have drifted down the field a certain small distance, ω, the same for all (55). This picture, though an over-simplication, nonetheless does the job of providing a picture in terms of which the photoconductivity observed from F-centers in alkali halides (55,73) and related materials (76) can be understood. Rather than being concerned with an in-depth study of photoconductivity for its own sake, this study is interested principally in the study of the photoconductivity originating from F-type centers as a meaningful way to investigate the electronic structure of such defects. For these purposes the above development (Equation 28-47) proves quite satisfactory, especially for low concentrations of defects and low light intensities. However, for high concentrations of centers, more complex trapping mechanisms are involved as evidenced in Appendixes A and B of this work, and some modifications may be required in our simple development.

One would like to measure ω separately but the Hall effect is difficult because of low mobilities and the small number of charge carriers.

From Equation (28), ω is inversely proportional to the concentration of trapping centers since as the density of traps increases, the time T before the free electron is captured decreases. The range depends on the temperature through the mobility and the density of deep traps (76). In general, the mobility is low in the vicinity of room temperature. Brown and Inchauspe (77), working with additively colored KCl, found the mobility at room temperature to be in the vicinity of 5-10 cm^2/volt-sec. They also found that the mobility increased steeply by about three orders of magnitude as the temperature was lowered below 80 K due to freezing out of the optical modes of lattice vibrations (77). A residual mobility near 4000 cm^2/volt-sec was found below 30 K. The photoconductivity measurements in this same temperature range (74) did not reflect the rise in mobility apparently because of the existence of shallow traps in the crystals. Swank and Brown (73) have shown that for additively colored KCl the mobility, and hence ω_o, may decrease slightly but does not vary much or rapidly with temperature increases in the region between 80 K and 300 K. Noticeable increases in the photoresponse with changing temperature are usually attributed to a change in the quantum efficiency, η.

If an alkali halide crystal is illuminated in its F-band, every wavelength in this band shows equal quantum efficiency for providing photoconductivity (55). The spectral dependence of the photocurrent, and hence $\eta\omega_o$, should follow the optical absorption for the same center, measured on the same crystal, since both then are proportional to $(1-e^{-\alpha d})$ (see Equations (46-47).) For small absorption coefficients the spectral dependence of the photoresponse has the same shape as that of the optical density since for small α, $(1-e^{-\alpha d}) \sim \alpha d$ and O.D. = $\log_{10}$

$I_o/I = \alpha\, d/2.3$.

Measuring the temperature dependence of the photoresponse can yield information about the electronic structure of the relaxed F- and F^+-center and the proximity of the relaxed excited state to the bottom of the conduction band. A sharp increase in the photoresponse for a given center (see Figure 12b) as the temperature is varied, is characteristic of a thermally assisted ionization. Using this temperature dependent data and by rearranging Equation (24) to give

$$\left(\frac{1}{\eta_T} - 1\right) = \frac{\tau_o}{\tau_R} \exp\,(E_a/kT)\ , \tag{48}$$

the thermal activation energy, E_a, can be determined. In the approximation that ω_o and the oscillator strength, f, of the particular F-type band under study remains independent of temperature over the interval corresponding to the sharp increase in the photoresponse, it is thus assumed that the temperature dependence of $\eta\omega_o$ is due to the change in η. Assuming that the centers are fully ionized at the temperature corresponding to the maximum photoresponse, η_T is taken as unity at that temperature. By plotting $\ln\left(\frac{1}{\eta_T} - 1\right)$ vs. 1/T over the temperature interval corresponding to the sharp increase in photoresponse, one can determine the activation energy E_a and the ratio τ_o/τ_R. For further details and applications to our study, see Chapters IV and V.

Keeping the theoretical background provided above in mind, a description of the experimental techniques and apparatus used in this study to investigate the electronic structure of the F-type defects in SrO and CaO will be given in the following chapter before moving into a discussion of the actual experimental results.

CHAPTER III

EXPERIMENTAL APPARATUS AND PROCEDURE

I. Introduction

In this study we are concerned primarily with CaO and SrO and, more specifically, with the study of F- and F^+- centers in these materials. The techniques used in this study, namely photoconductivity, luminescence and fluorescence lifetime measurements used in conjunction with optical absorption measurements, provide a sensitive method of investigating the electronic structure of defects in solids.

Most of the experiments performed in this study involved electron or proton irradiated samples. Electron irradiated samples, having a small density of single defects distributed throughout the bulk of the crystal were the most satisfactory for photoconductivity measurements. Proton and neutron irradiated samples, containing a large concentration of centers near the surface or throughout the sample, respectively, were more effective for the luminescence and fluorescence lifetime measurements.

In this chapter, the preparation of samples will be treated first. The various experimental techniques used in this study will then be described thoroughly.

II. Sample Preparation

Crystals of nominally 99.5% pure SrO and CaO were obtained from W.

and C. Spicer, Ltd., and were approximately 10 x 5 x 2 mm in dimensions. CaO crystals, which had been grown in a reducing atmosphere, containing a high concentration of F-centers were also obtained from W. and C. Spicer, Ltd. Dr. Y. Chen of Oak Ridge National Laboratory provided a boule (S/N 120-021172) of CaO from which samples about 10 x 5 x 2 mm in dimensions were cleaved. Samples of CaO grown with color centers were also provided by Dr. Chen. CaO samples, doped with Mg to 1% concentration, were obtained from A. E. Hughes of the Atomic Energy Research Establishment at Harwell (78).

Since CaO and SrO are hygroscopic, the samples were usually stored in paraffin oil at room temperature. Just prior to irradiation or making optical, photoconductivity, or fluorescence measurements the crystals were polished on alumina impregnated lapping discs, which removed surface contamination and gave the surfaces a good optical polish. In some cases the crystals were cleaved, but our measurements were not noticeably changed by cleaving.

The samples could be irradiated with gamma rays from a ^{60}Co gamma source, 1.5 MeV electrons or 1.5 MeV protons using a Van de Graaff accelerator. The electron and proton irradiations were performed at 77, 195 or 300 K.

Electron and proton irradiations (79) were performed with the sample attached to the copper cold finger of a small cryostat located in the Van de Graaff extension tube. Irradiations were carried out at 77 K or 195 K. Irradiations at 77 K seemed to introduce the F^+ band at about twice the rate of irradiations at 195 K. The sample was secured to the copper tail with silicon high vacuum grease and then covered with aluminum foil to prevent bombardment by heavier particles. The align-

ment of the beam was checked at this position in a separate experiment prior to irradiation of the samples and was necessary to insure that the electrons or protons were hitting the sample. Blue print paper, placed at the sample position, was developed in ammonia fumes following a very short irradiation at low beam current to determine the position and size of the beam at this position.

The current striking the crystal was monitored during irradiation. Low incident current densities were always used to prevent the samples being overheated during irradiation. The samples were irradiated for several hours, with currents of 2-3 μamp being used for SrO and average currents of about 5 μamp being used for CaO. Irradiations of several hours were performed in 3-4 minute intervals to further prevent overheating of the samples and to permit refilling of the small cryostat cold reservoir. Because of the hygroscopic nature of the samples, it was necessary to warm them to room temperatures before removing them from the Van de Graaff extension tube and transferring them to the optical cryostat. This method was also used because it was necessary to transfer the irradiated sample to the photoconductivity cryostat at room temperature.

Electron irradiated samples were used for most photoconductivity measurements since, as explained in Chapter I, the incident electrons produce mainly individual vacancies throughout the bulk of the crystal, whereas incident protons produce a high density of damage near the surface.

The samples could also be irradiated at room temperature with a ^{60}Co gamma source with a strength of about 5×10^4 R/hr. This ionizing irradiation used alone was found to be ineffective in producing F- and F^+-

centers in our samples. Gamma irradiation was used, however, on samples containing F- and F^+-centers produced by previous electron or proton irradiations to re-populate the centers between successive experiments (see Chapters IV and V for further details).

Samples of SrO and CaO which contained a high concentration of F^+-centers produced by neutron irradiation at room temperature were provided by Y. Chen of ORNL.

III. Optical Absorption Measurements

Optical absorption measurements over a photon energy range from 1.8 eV to 6.2 eV (7000 - 2000Å) were made with a Cary 14 Spectrophotometer. The Cary 14 records optical density as a function of wavelength. The optical density is given by: $O.D. = \log_{10} \frac{I_o}{I}$ where I and I_o are the intensity of the light transmitted through the sample and the intensity of the reference beam, respectively. The intensity of the light transmitted through the sample is given by $I = I_o e^{-\alpha d}$ where I_o is the intensity of the incident beam (reference beam), α is the absorption coefficient and d, the thickness of the sample. The optical density, O.D., is related to the absorption coefficient by $\alpha = 2.303 \left(\frac{O.D.}{d}\right)$ cm^{-1}. Optical absorption measurements were usually performed at 77 K.

IV. Photoconductivity Measurements

A block diagram of the apparatus used in photoconductivity measurements is shown in Figure 16. Photoconductivity measurements were made with incident photon energies ranging from 2-6 eV and at temperatures ranging from 77 K to about 350 K. Light from a source such as a xenon or deuterium lamp is dispersed by a monochromator. After emerging from

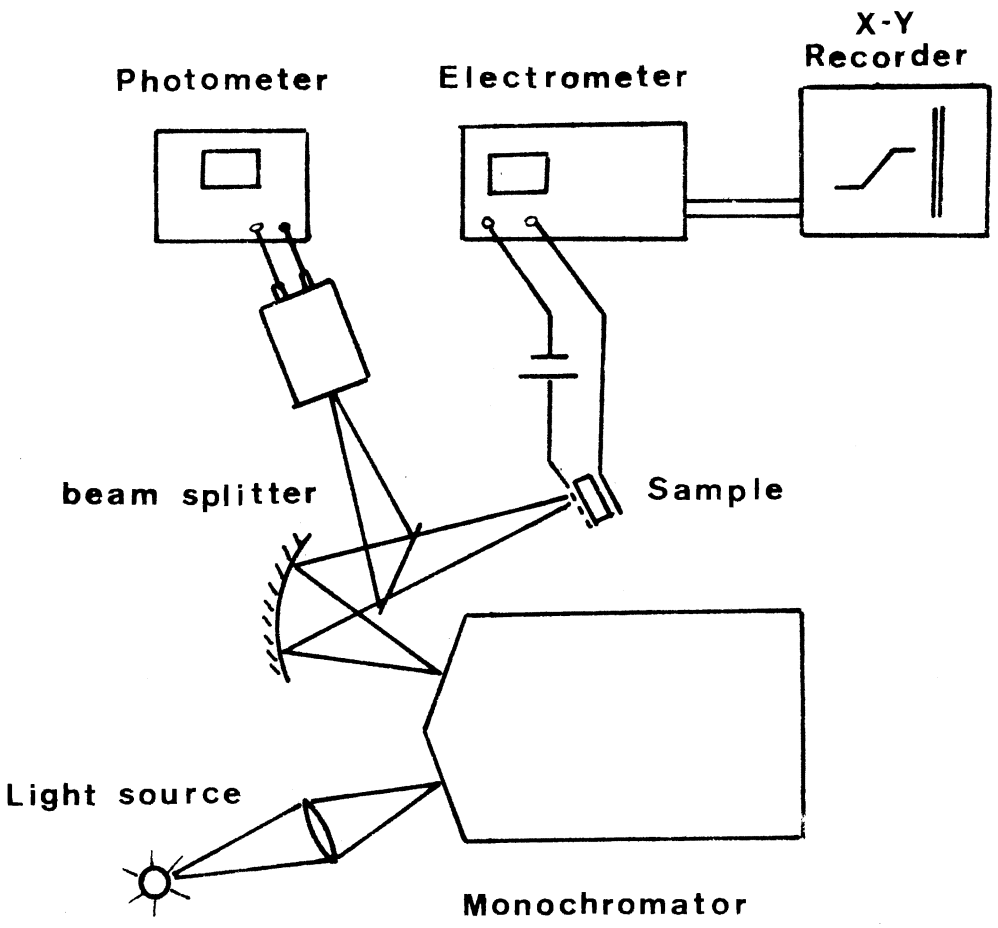

Figure 16. Apparatus for Photoconductivity Measurements

the monochromator the light is focused on the crystal through a beam splitter which reflects a small fraction of the light onto a photomultiplier tube. The photomultiplier can be used during each measurement to monitor the light falling on the crystal. The incident light falls on the crystal, of thickness d, between plane parallel electrodes. The crystal is located in a cryostat and an electric field, $E = V/d$, is established across the crystal in a direction parallel to that of the incident light. This field is set up by a battery in the external circuit in series with the electrometer, used in the "rate of charge" mode. The output of the electrometer was fed to a potentiometric recorder. With this overall picture of the apparatus in mind, we now proceed to a more detailed discussion of the individual components.

The light source was a 75 watt xenon lamp or, for ultraviolet measurements, a 60 watt deuterium lamp. The light was dispersed by a McPherson 218 monochromator which had a linear dispersion of 2.65 nm/mm. The reflection grating used was blazed at 3000Å and had 1200 grooves/mm. With both slits set 2 mm wide, the bandwidth was a constant 5.3 nm. After emerging from the monochromator, a front silvered mirror focused the light on the crystal. A magnesium fluoride beam splitter reflected a small fraction of the incident light onto a 6256S EMI photomultiplier tube having a maximum and fairly constant quantum efficiency from about 2000-5000Å. Corning glass filters with sharp optical cut off were used following the light source to eliminate higher orders from the incident light striking the sample.

The light source was calibrated in a separate experiment by placing a Molectron 100 pyroelectric radiometer at the sample position in Figure 16. The radiometer was used to determine the power, in μ watts, of the

incident light falling on the front surface of the sample holder as a function of wavelength. The radiometer had a calibration traceable to the N.B.S. For a given wavelength, λ, of the incident light, the number of photons/sec, n_{λ_o}, striking the front surface of the sample assembly is given by $n_{\lambda_o} = P\lambda/hc$ where P is power in μ watts, h is Planck's constant, and c is the speed of light. The number of photons/sec, N_{λ_o}, incident on the crystal at a given wavelength is given by (n_{λ_o})(% optical transmission of the front electrode) where the second factor is necessary to insure that only the photons actually incident on the crystal are considered. Figure 17 illustrates in curve a) a typical graph for the power falling on the radiometer, and therefore on the front electrode of the sample holder, and in curve b) the number of photons/sec incident on the sample, N_{λ_o}, both as functions of wavelength. The number of photons falling on the sample varied from about 10^{13}/sec at 2 eV to about 10^{11}/sec at 6 eV. Simultaneous measurements, during the calibration experiment, of the photomultiplier current and the power on the radiometer corresponding to a given wavelength made it possible to determine N_λ in subsequent experiments by use of a simple correction factor. By determining the photomultiplier current at a standard wavelength λ_s, such as 3000Å, in each experiment, the values of N_λ as a function of wavelength, in any subsequent experiment are given by $N_\lambda = N_{\lambda_o}$ $(PMI_{\lambda_s})/(PMI_{\lambda_o})$ where N_{λ_o} is the number of photons/sec incident on the sample in the calibration experiment, PMI_{λ_o} is the photomultiplier current at the reference wavelength in the calibration experiment and PMI_{λ_s} is the photomultiplier current at the reference wavelength in subsequent experiments. It is estimated that the absolute measurement of light intensity falling on a sample could be made to within about 8%.

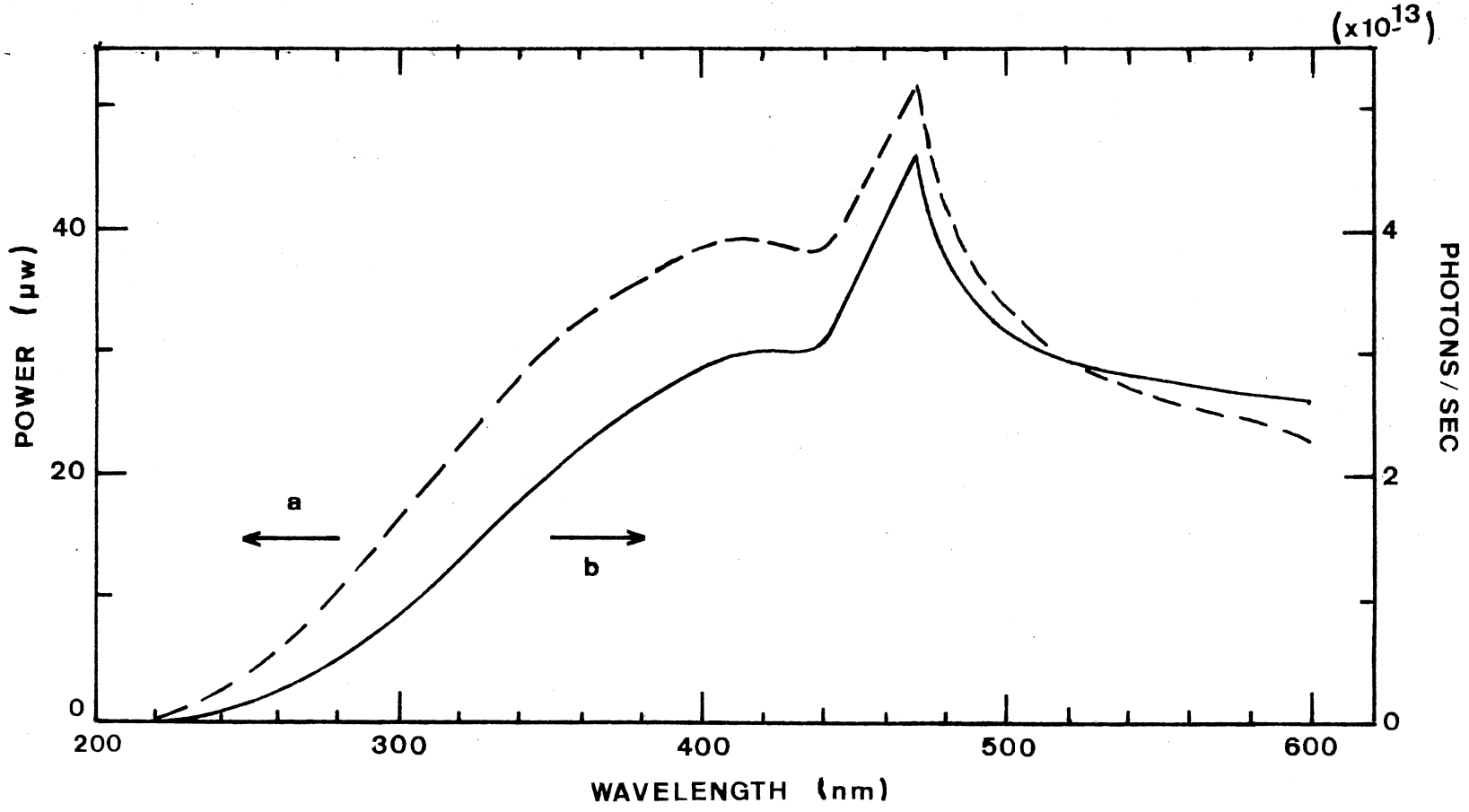

Figure 17. Spectral Output of 75 Watt Xenon Lamp. The power falling on the front electrode of the sample holder, curve a; the number of photons/sec, N_{λ_o}, incident on the sample, curve b. The McPherson monochromator grating was blazed at 3000 Å

The photoconductivity measurements were made with the sample holder shown in Figure 18. The sensitive electrode, g, made of copper foil 0.05 mm thick, 3 mm wide and 8 mm long, was connected to the electrometer. This electrode was electrically insulated from the copper tail of the cryostat, a, by a sapphire plate, h, 0.25 mm thick. The incident light passes into the crystal, e, through the front electrode, d, a phosphor-bronze screen of 0.55 mm diameter wire and 100 mesh. The screen was held against the crystal by a quartz plate, c, which was supported by phosphor-bronze springs. Sapphire plates, f, 0.25 mm thick were placed on either side of the crystal between the crystal and the corresponding electrode to prevent charge from entering or leaving the sample. The screen electrode assembly transmitted about 35% of the incident light. The sample was located in a copper chamber bolted to the tail of the cryostat. Dry helium exchange gas could be admitted to the chamber to produce good thermal contact. The cryostat could be used at liquid nitrogen or liquid helium temperatures.

A shielded lead connected the phosphor-bronze screen electrode to a battery in the external circuit which produced an electric field, typically about 500 V/cm, in a direction parallel to that of the incident light. The direction of the applied electric field could be easily reversed after individual measurements to prevent polarization effects in the sample.

The sensitive electrode was connected, by a shielded lead, to the input of a Cary 401 vibrating reed electrometer which could be used in either the "rate of charge" or current mode. However, the small photocurrents of interest here ($\sim 10^{-14}$ amp) necessitated the use of the "rate of charge" mode. The output of the electrometer was fed to an

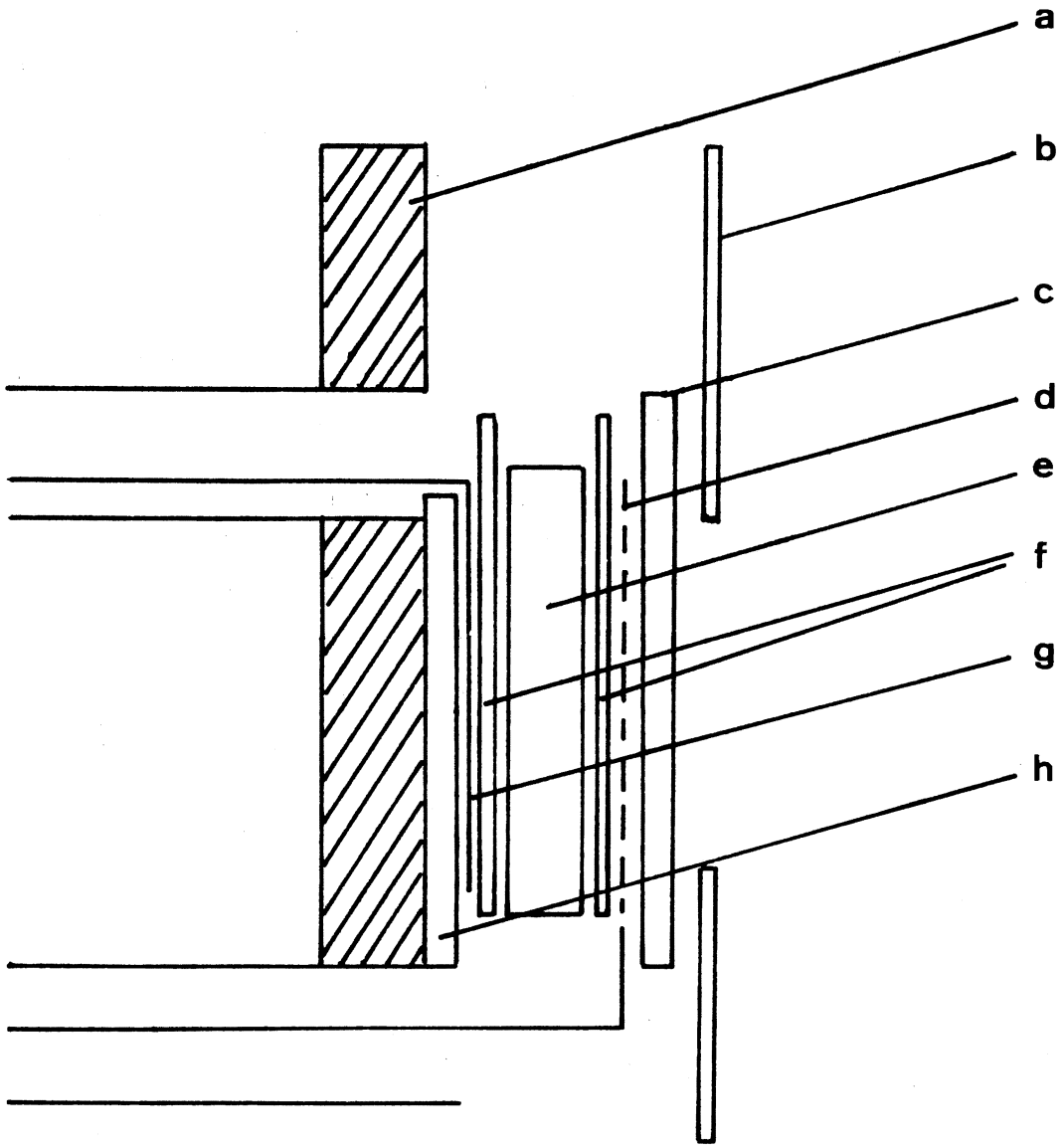

Figure 18. Sample Holder. a, cryostat tail; b, mask; c, quartz plate; d, phosphor-bronze screen; e, sample; f, sapphire plates; g, copper electrode; h, sapphire plate

Omnigraphic 2000 t-y potentiometric recorder. During a typical measurement a pulse of light of about 5 seconds duration fell on the crystal, with the monochromator set at a specific wavelength. Under these conditions, the photocurrent corresponding to incident light of a given wavelength was given by the following expression: $I_\lambda = dQ/dt \doteq C_c' \Delta E_r / \Delta t$, where Q is the charge in coulombs, C_c is the charge collecting capacitance (2×10^{-11} farad) of the electrometer, ΔE_r is the change in the recorder reading as a fraction of the full scale times the electrometer range in volts, Δt is the time interval in seconds. The photocurrents measured were typically on the order of 10^{-14} amps.

With liquid nitrogen in the cryostat, the background noise was below 10^{-16} amps. The minimum current detectable was $\sim 5 \times 10^{-17}$ amps. The sensitivity of the apparatus fell off, however, as the incident light approached 2000Å due to the fact that the output of the light source fell off rapidly in this region of the spectrum. The resolution of the apparatus at 6.0 eV was about 0.1 eV.

V. Photoluminescence

The apparatus used for photoluminescence measurements is illustrated in Figure 19. Exciting light from either a 75 watt xenon or a 100 watt mercury lamp was dispersed by a Jarrell-Ash 82-410 25 cm monochromator with a linear dispersion of 1.65 nm/mm and blazed at 5000Å or 3000Å. The grating blazed at 5000Å was used in our measurements. The exciting light was chopped at a frequency of 169 Hz with a PAR 125A Mechanical light chopper. The sample, located in the optical cryostat, was rotated slightly off of a 45° angle to minimize reflection of the exciting light into the detector and to maximize the emitted light into

FLUORESCENCE

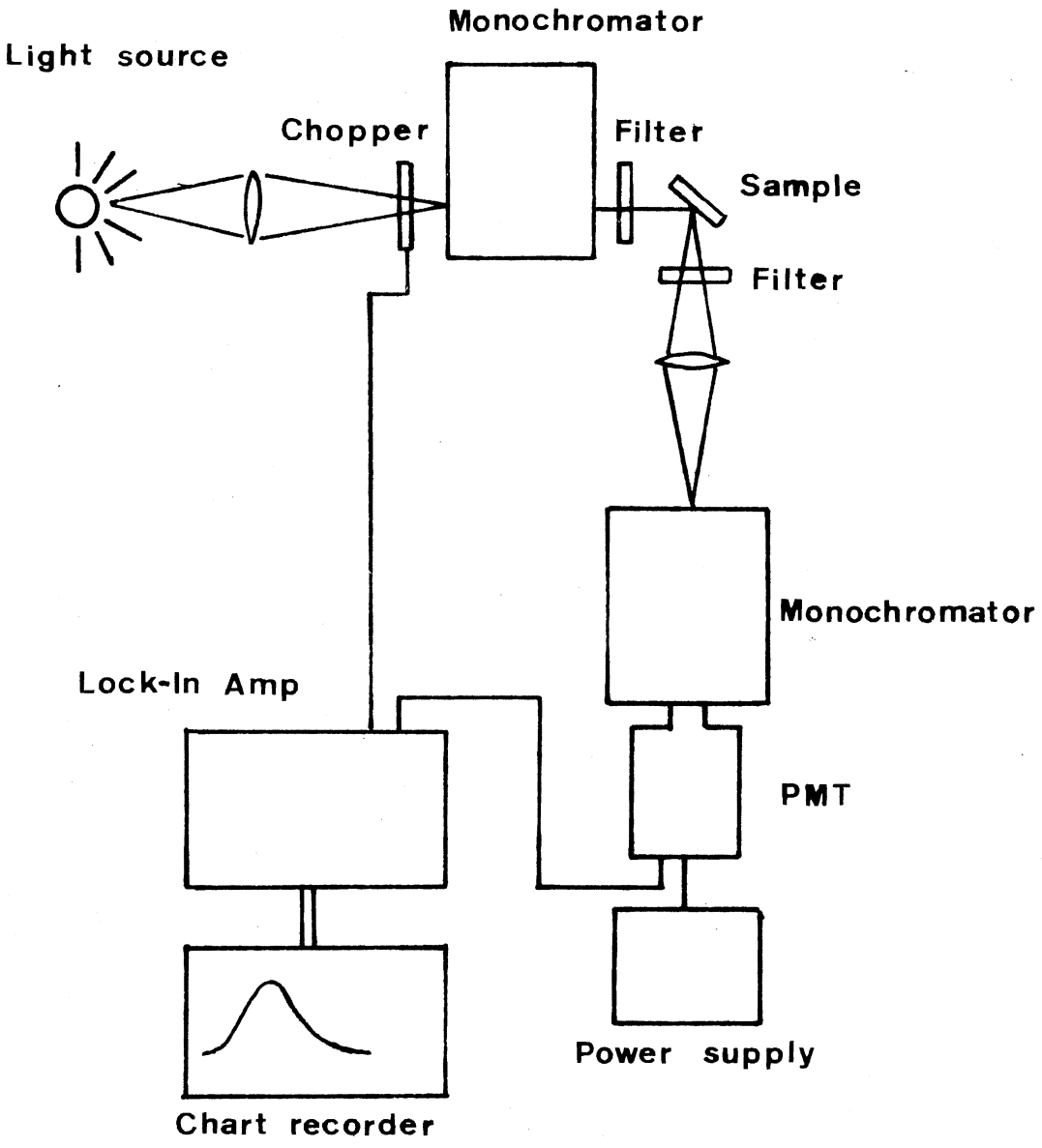

Figure 19. Apparatus for Fluorescence Measurements

the detection system. Appropriate sharp cut off and interference filters were used to define a narrow band for the exciting light. To eliminate the exciting light reflected by the crystal, as well as higher orders, from reaching the detection system, a sharp cut off filter was placed between the sample and detector as the emitted light left the sample. The emitted light was dispersed by the McPherson monochromator described above. After dispersion, the emitted light was detected with a thermoelectrically cooled RCA C31034 photomultiplier which was usually operated at about 1000 V. The output from the photomultiplier was connected to the input of a PAR 181 current sensitive preamplifier and the output of this to a PAR 128A lock-in amplifier. The frequency of the light chopper was used as the reference signal for the lock-in amplifier which converts only that part of the input signal which is synchronous with the reference signal into a dc level which is proportional to the input signal. The detected luminescence intensity was plotted as a function of wavelength with a Heath SR-205 chart recorder. Photoluminescence was measured over the temperature range from about 10 K to 350 K.

The response of the various components in the detection system varies as a function of wavelength. For instance, the grating used in the McPherson monochromator was blazed at 3000Å and the response of the photomultiplier, which is nearly constant between 3000-8000Å, begins to fall off rapidly on either side of this range. Therefore, the response of the luminescence detection system, as a unit, must be determined to see if it is fairly constant in the wavelength range of interest or if the emission curves must be corrected for the varying response of the detection system.

The response of the detection system was determined using the same

arrangement as in Figure 19, but with the sample by-passed. After dispersion by the Jarrell-Ash monochromator, blazed at 5000Å, the light from the xenon lamp was immediately dispersed by the McPherson monochromator. The appropriate sharp cut off filter was used after the light source to eliminate higher orders. Both monochromators were set at the same wavelength reading. The response of the detection system, proportional to the intensity of the light of a known wavelength falling on the photomultiplier, was then determined using conventional lock-in techniques. The power of the light emerging from the Jarrell-Ash monochromator, as a function of wavelength, was determined in a separate experiment. The number of photons/sec, for a known wavelength of light entering the McPherson monochromator (and hence the detection system) could then be determined as described in the previous section. The response of the detection system/(photons/sec) as a function of wavelength was determined and the results normalized to unity. One such response curve is shown in Figure 20. The response of the luminescence detection system thus obtained was corrected by multiplying the emission intensity at a given wavelength by the corresponding reciprocal of the numbers just obtained.

The excitation spectrum for a corresponding luminescence band was determined using the apparatus described in Figure 19. The McPherson monochromator was set at λ_{em}, corresponding to the peak of the emission band, and the exciting wavelength was automatically scanned with the Jarrell-Ash monochromator. The intensity of the emission at λ_{em} was then obtained as the wavelength of the exciting light was varied.

Since the intensity of the emission was measured at a set wavelength, λ_{em}, the only changing factor was the power and the correspond-

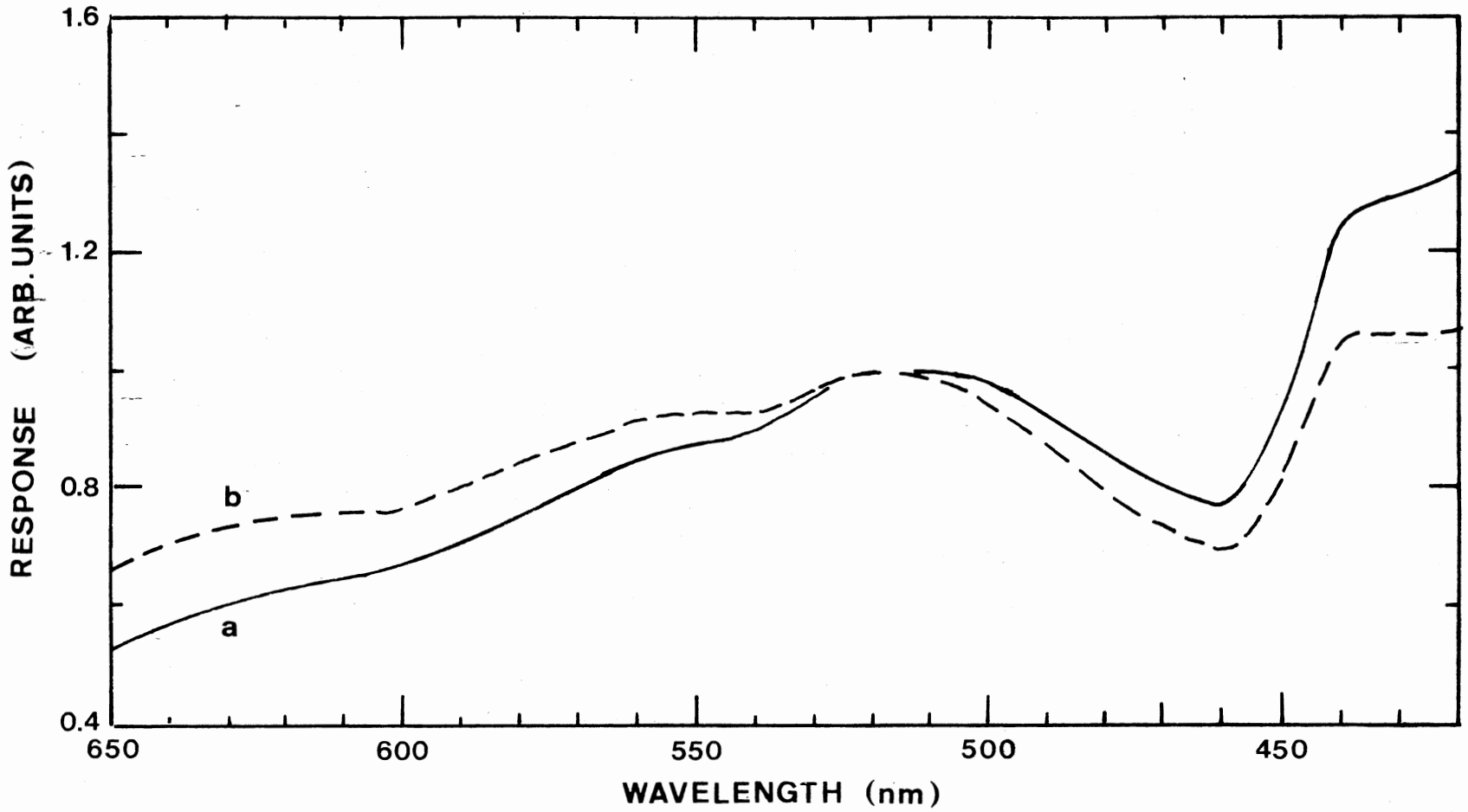

Figure 20. Response of Luminescence Detection System as a Function of Wavelength. Response of detection system/(photons/sec), curve a; response of detection system/μw, curve b. Both curves were normalized to unity at 5200 Å. The McPherson monochromator grating was blazed at 2000 Å

ing number of photons/sec incident upon the sample for a given wavelength, λ_{ex}, of exciting light. The exciting light from the xenon lamp was dispersed by the Jarrell-Ash monochromator. The power of the dispersed light was determined as a function of wavelength, with the radiometer at the sample position. The corresponding number of photons/sec incident on the sample was determined and normalized to unity at the wavelength corresponding to the peak of the excitation spectrum. The corrected excitation spectrum was then obtained by multiplying excitation intensities by the corresponding reciprocal of the above numbers.

VI. Radiative Lifetime Measurements

Fluorescence lifetime measurements were made with an optical arrangement similar to that used for photoluminescence measurements (Figure 21). Pulses of exciting light with a half-width of about 25 nsec were produced by a Xenon Corporation air spark discharge lamp. The pulses were repeated at a frequency of about 10/sec. The emitted fluorescence decay was photographed from the screen of a Tektronics 535A oscilloscope. The resolution of the apparatus was about 30 nsec. Fluorescence lifetime measurements were made in the temperature range of 10-300 K.

VII. Temperature Measurement

Standard potentiometric techniques were employed for monitoring temperatures. The optical and photoconductivity cryostats were equipped with copper vs. constantum thermocouples attached to the tail piece near the sample. The reference junction was maintained at $0^{o}C$.

Temperatures higher than 10 K or 77 K, ranging to room temperature,

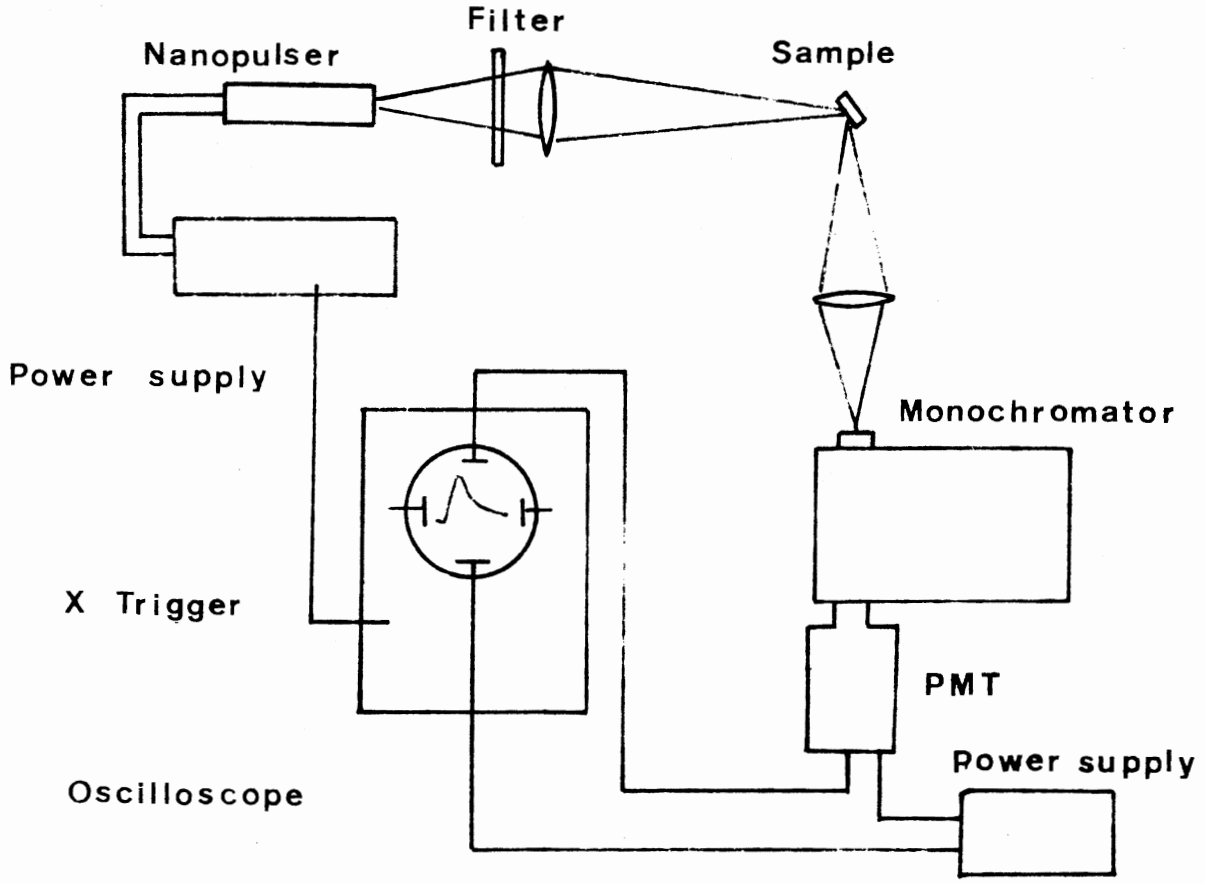

Figure 21. Apparatus for Radiative Lifetime Measurements

were achieved by slowly blowing air into the bottom of the liquid nitrogen reservoir after removing the liquid nitrogen. Temperatures above 300 K were achieved by a constantum heating coil wound around the copper cold finger of the cryostat above and below the sample. The temperatures were maintained for a few minutes to allow the system to come to thermal equilibrium before the various measurements were recorded when temperature dependent data was collected.

CHAPTER IV

EXPERIMENTAL RESULTS AND DISCUSSION:

STRONTIUM OXIDE

I. Introduction

The alkaline earth oxides, characterized by the face-centered cubic crystalline structure, have large band gaps (4-8 eV) which give rise to a wide transparent spectral region in which the effects of impurities, vacancies and other defects can be studied (4). The F^+-center in the alkaline earth oxides consists of a single electron trapped at an oxygen ion vacancy whereas the F-center consists of a pair of electrons trapped at the anion vacancy. Experimental studies of F-type centers, particularly in MgO and CaO have recently been done in some detail (7). However, less work has been done on F-type defects in SrO.

The doubly charged oxygen vacancies which are produced when currently available SrO is irradiated with either protons or neutrons each trap, in general, only a single electron to form F^+-centers (29). The vibronic properties of the non-gaussian and asymmetric F^+ absorption band, which is located at 3.1 eV, have been investigated by Hughes and Webb (49). Hughes and Webb (49) reported three luminescence bands at 77 K in neutron or proton irradiated SrO peaking at approximately 458, 500, and 554 nm. Of these three emission bands which were excited by light in the F^+ absorption band or at shorter wavelengths, only the 500 nm band

was significantly temperature dependent between 77 K and 300 K, and it was tentatively assigned to the F^+-center. An emission band near 510 nm was also reported in neutron irradiated SrO by Evans and Kemp (48). The two electron center, the F-center, has been produced by additive coloration of SrO with excess strontium (43). The F absorption band is reported near 2.5 eV.

On the basis of charge consideration alone it might be expected that F-centers in alkaline earth oxides would produce photoconductivity in a manner similar to F-centers in alkali halides but that F^+-centers, being positively charged, would not produce photoconductivity at ordinary temperatures. The experimental results reported in this study indicate, however, that the situation is not as straight forward as this viewpoint suggests. In MgO the F and F^+ band overlap at 5.0 eV. Roberts and Crawford (80) reported that gamma-irradiation just prior to mounting a sample in the cryostat was necessary to detect photoconductivity in MgO which had been irradiated with electrons or neutrons. It was tentatively concluded from these measurements and others made on additively colored samples that the photocurrent originated from F-centers. The experimental results reported in this study indicate, however, that photocurrent originating from F^+-centers in MgO cannot yet be ruled out although it is likely that the photocurrent observed by Roberts and Crawford did originate mainly from F-centers. A similar uncertainty exists for BaO. Rose and Hensley (44) have shown recently that the F band and F^+ band overlap in this material also, so that the origin of a photoconductivity band observed by Dash (81) at 2.0 eV in x-irradiated BaO is still uncertain. On the other hand in both CaO and SrO the F band and the F^+ band are separated in energy and it is possible to in-

vestigate each band separately. Electron irradiation, even at liquid nitrogen temperature, has so far been ineffective in producing F-type centers in SrO (27,82). In fact, the two electron center, the F-center, cannot be introduced into currently available SrO by particle irradiation so that the F^+ absorption band is not overlapped by the F band as it is in the other alkaline earth oxides. Consequently, we can focus our attention on the band associated with the F^+-center in SrO. The results of photoconductivity measurements made on F-type centers in electron irradiated CaO (26,83), which will be presented in the following chapter, show that both F-centers and F^+-centers produce photoconductivity in this material.

II. Irradiation and Optical Absorption

The optical density of a typical unirradiated SrO crystal at 77 K was similar to that previously reported by Bessent et al. (29). The optical density, shown in Figure 22, increased from about 0.1 at 2 eV to over 3 at 5.5 eV. There were no obvious absorption peaks in the spectrum except for a small band which could be sometimes detected at about 5.7 eV and which seemed to correspond to an exciton band (84). As the energy of the incident photons approaches the band gap energy the absorption of these photons gives rise to intrinsic photoconductivity (4).

Gamma-irradiation alone, for up to 75 hours, was ineffective in producing F-type defects in SrO and the optical density measured on these samples was the same as that of the unirradiated crystal.

Figure 23 shows the absorption spectrum at 77 K of a crystal which had been irradiated at about 195 K with 1.5 MeV protons to a dose of

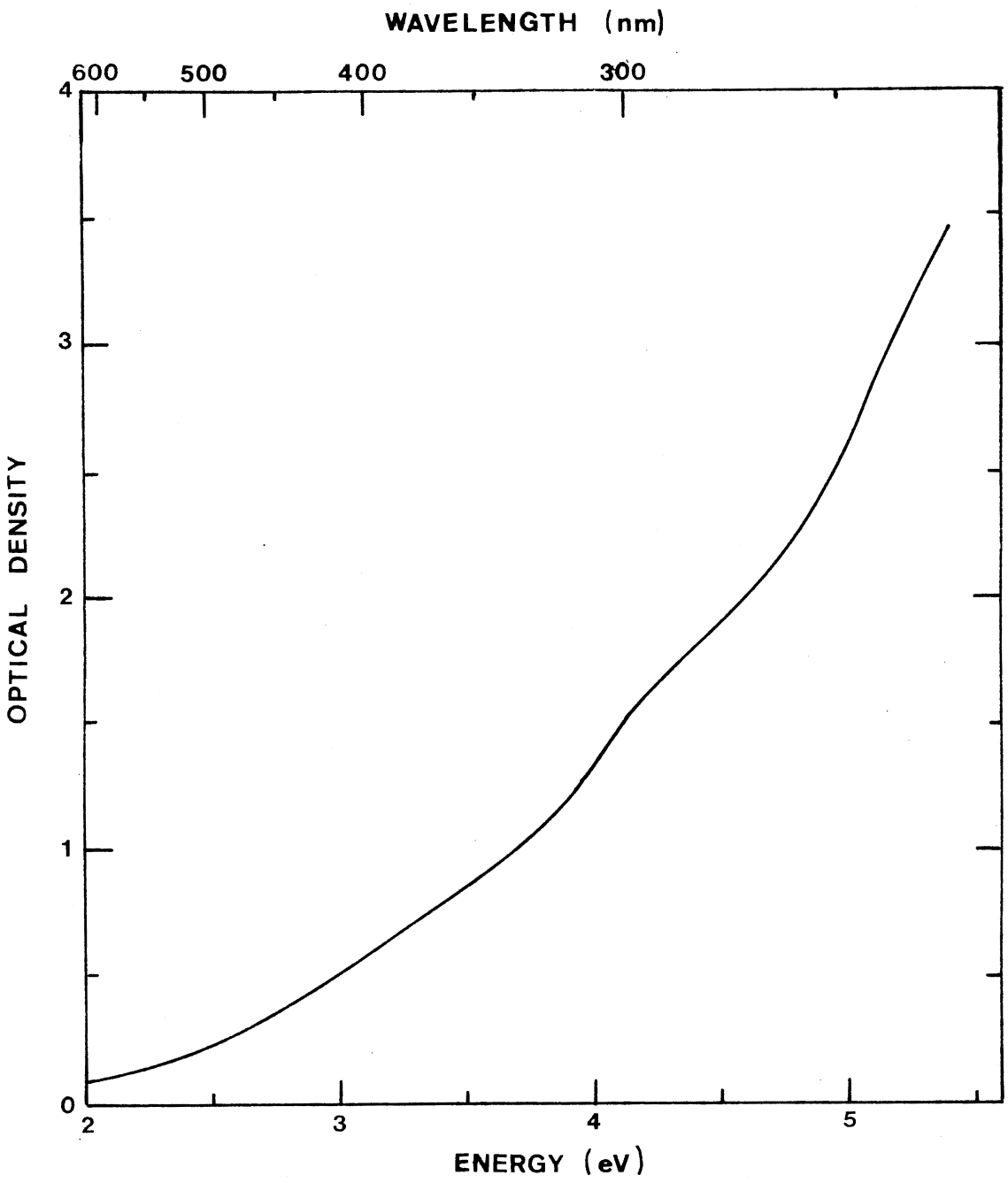

Figure 22. Optical Absorption Spectrum at 77 K of SrO Which Has Received No Irradiation

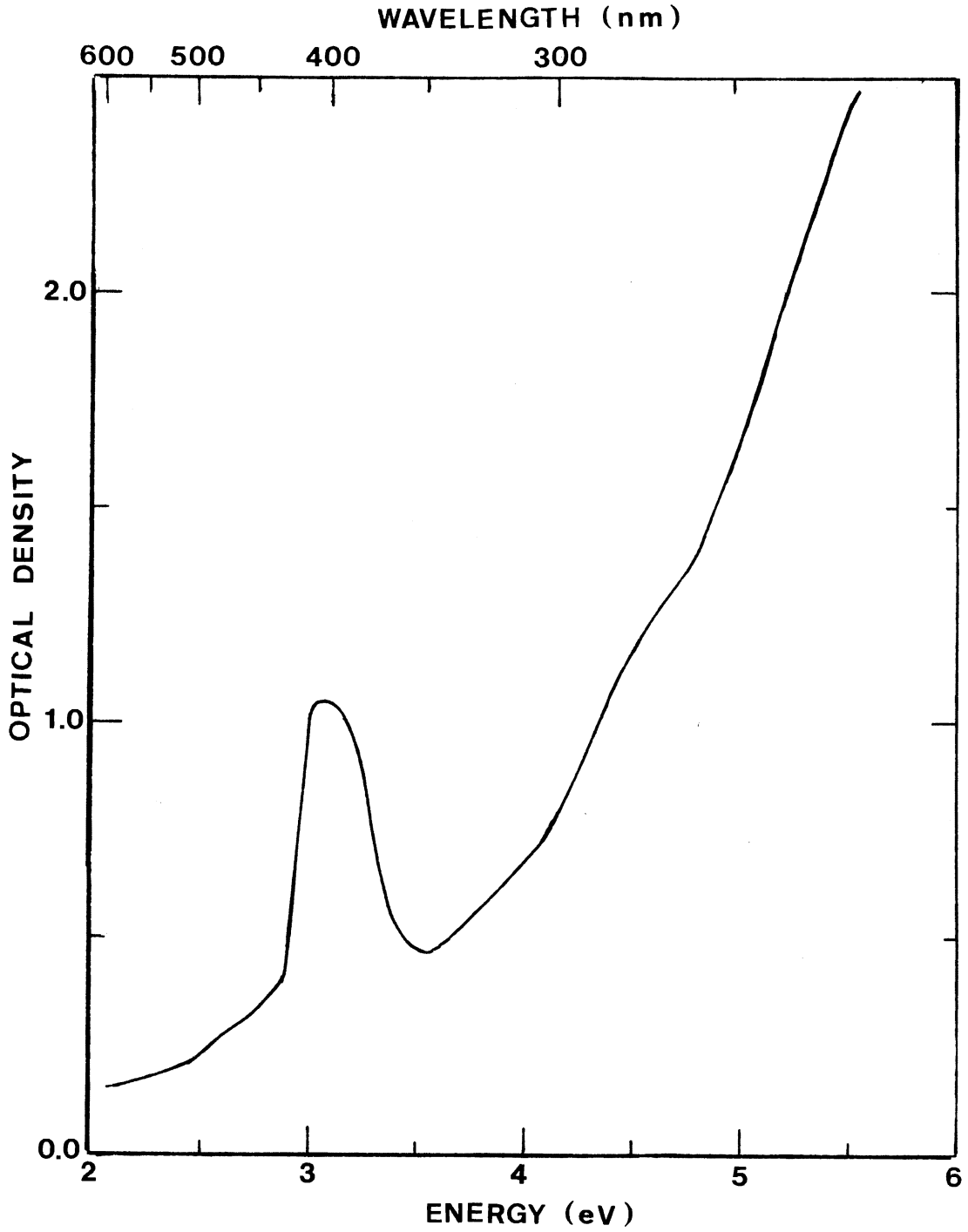

Figure 23. Optical Absorption Spectrum at 77 K of SrO Which Has Been Irradiated at 195 K With 1.5 MeV Protons to a Dose of Approximately 2 x 10^{17} Protons/cm^2. The main feature introduced by irradiation is the asymmetric F^+ band located near 3.1 eV

about 2 x 10^{17} protons/cm^2. The irradiation produced the asymmetric F^+ band with a peak at 3.1 eV, which has been seen previously (29,49). It can be seen that although the optical density at the peak of the F^+ band is about 0.7 there is no evidence of the F band at 2.5 eV. This behavior is in contrast to that observed in CaO (see Chapter V) where the F band would be easily observed at this stage of irradiation. Proton irradiation at 77 K seemed to introduce the F^+ band at about twice the rate of irradiation at 195 K, although detailed studies of the defect production rate as a function of temperature were not made.

It was not found possible, however, to produce a measurable F^+ absorption band in samples irradiated with 1.5 MeV electrons at 77 K even up to doses of 5 x 10^{17} electrons/cm^2. Low incident current densities were always used to prevent the samples being heated during irradiation. Nevertheless, we shall see in the following section that F^+-centers introduced by electron irradiation, though too few to produce a measurable optical absorption band using a Cary 14 spectrophotometer, did produce an easily measurable photocurrent because of the sensitivity of the photoconductivity technique. The reason for using electron irradiated samples in our photoconductivity experiments was that incident electrons produce mainly individual vacancies throughout the bulk of the crystal, whereas incident protons produce a high density of damage near the surface. For this reason, it was not found possible to make completely satisfactory photoconductivity measurements on proton irradiated samples. Proton and neutron irradiated samples were, however, used for fluorescence lifetime and luminescence experiments. The optical density measured at 77 K for a SrO sample grown at Oak Ridge National Laboratory and neutron irradiated at room temperature is shown in Figure 24. It

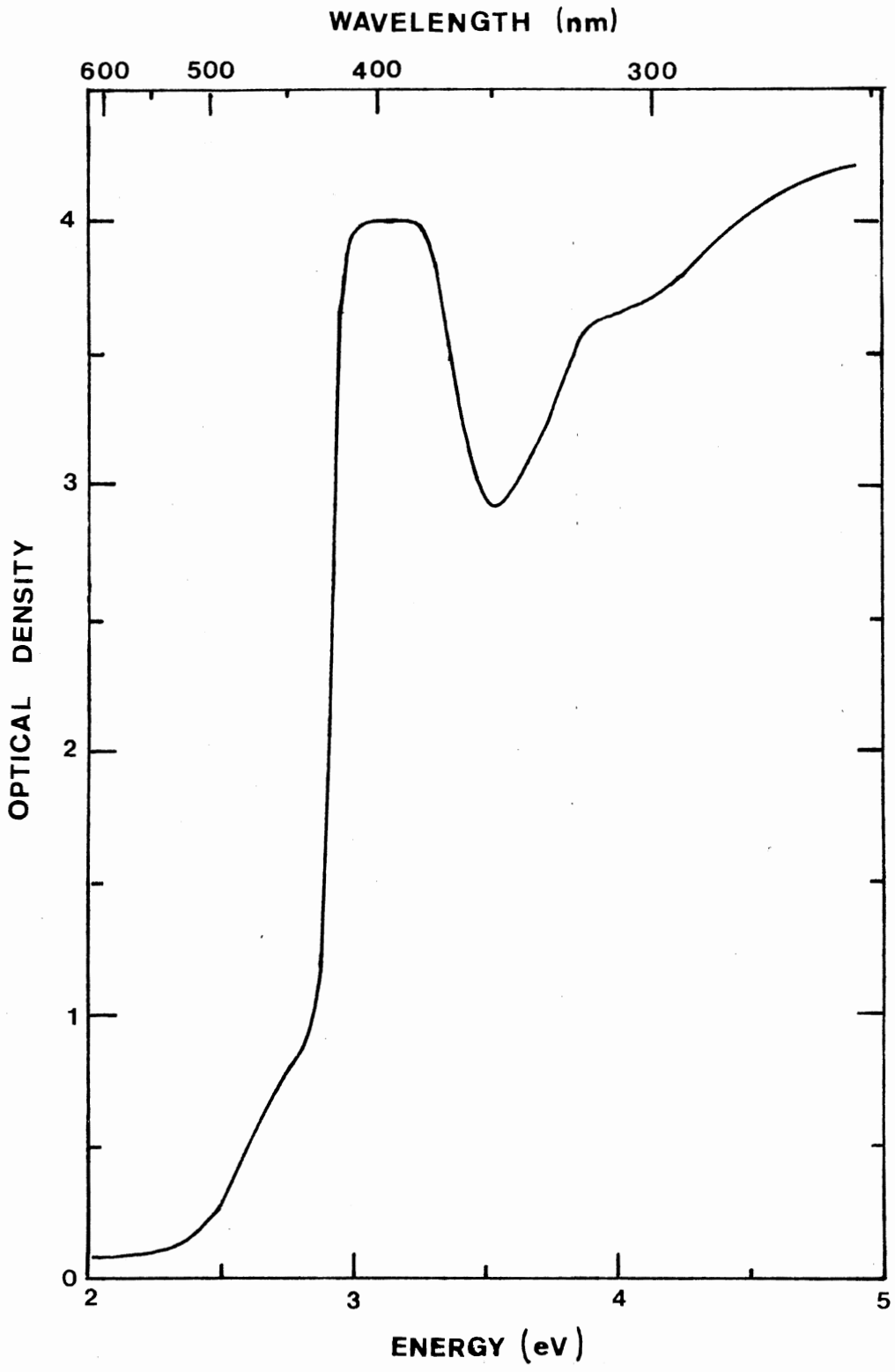

Figure 24. Optical Absorption Spectrum at 77 K of ORNL-SrO Which Had Been Neutron Irradiated at Room Temperature

is readily seen that neutron irradiation has done massive damage to the crystal as indicated by the broader than normal absorption at 3.1 eV and by the high background optical density for higher incident photon energies. Neutron irradiation (Chapter I), especially at high specimen temperatures, can give rise to the formation of F-aggregate or small cluster defects. These may have optical transitions underlying the F^+ band, thus contributing an additional apparent width to the true F^+ band (7).

III. Photoconductivity

In this section a brief description of the spectral dependence of the photoresponse obtained from γ-irradiated, proton irradiated, or electron irradiated samples will be followed by a thorough presentation of the photoresponse results obtained from electron irradiated samples. The temperature dependence of the luminescence intensity and the lifetime of the fluorescence from the F^+ center, as they relate to the photoconductivity, will be presented in the following section.

In Figure 25, curve a, we show the photoresponse of an untreated SrO sample at 77 K over the spectral range from 2 eV to 6 eV. It can be seen that the photoresponse was immeasurably small until the incident photon energy was at least 4 eV. Then as the photon energy increased further the photoresponse increased sharply by more than three orders of magnitude until the photon energy was about 5.4 eV. The photoresponse then decreased abruptly by two orders of magnitude and became immeasurably small again at 5.8 eV. Although the apparatus could detect photoconductivity for photon energies out to about 6.2 eV no photoconductivity could be detected in SrO above 5.8 eV. Since the photoresponse $\eta\omega_o$,

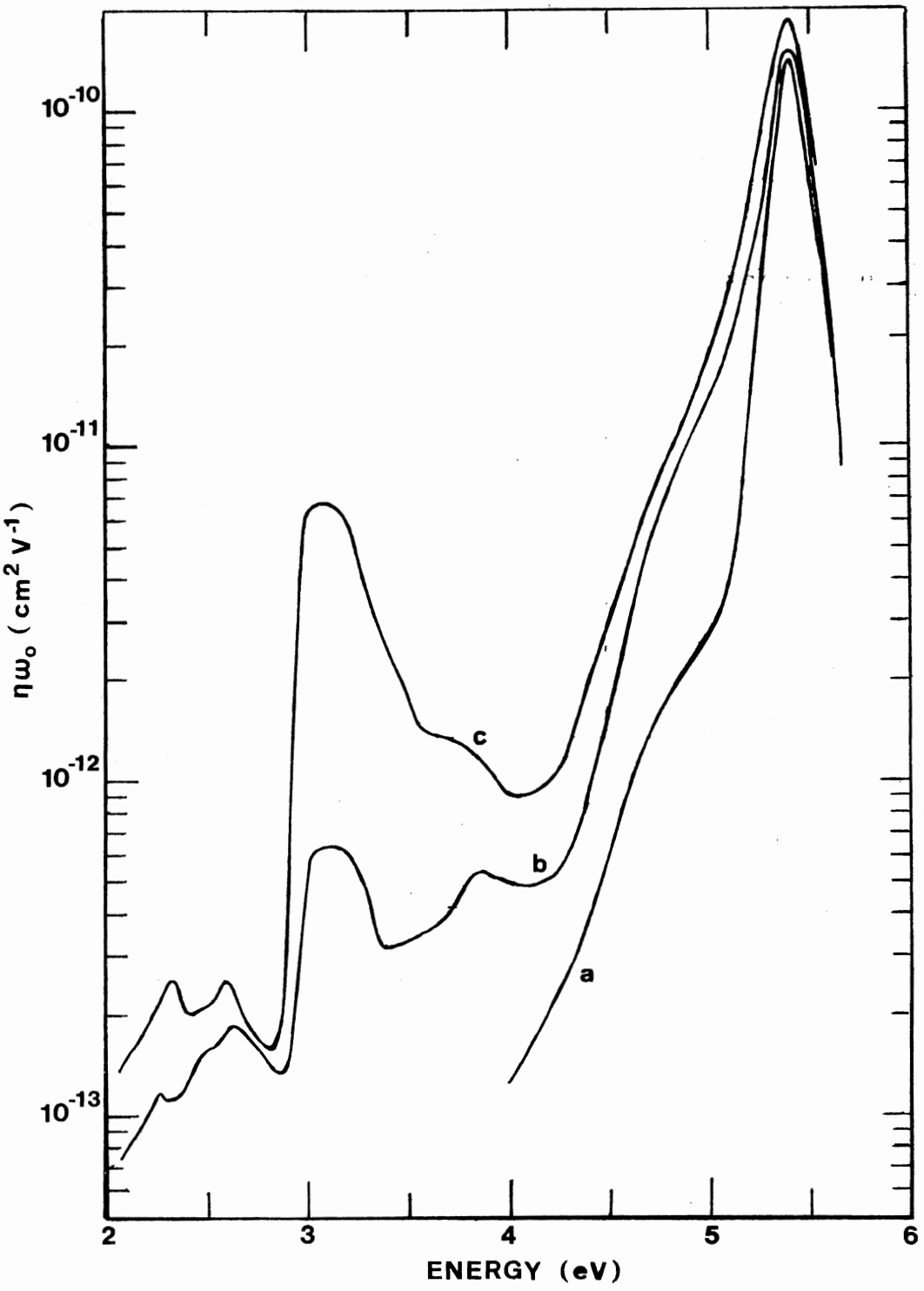

Figure 25. Spectral Dependence of the Photoresponse, $\eta\omega_o$, for SrO. An unirradiated sample measured at 77 K, curve a; a sample which had been irradiated at 195 K with 1.5 MeV electrons to a dose of about 1 x 10^{17} electrons/cm^2 and measured at 77 K and 105 K, curves b and c, respectively

given by $\eta\omega_o = \frac{I_\lambda}{N_\lambda}\left(\frac{d^2}{eV}\right)$, is inversely proportional to N_λ, the quanta/sec incident on the sample, the minimum detectable photoresponse was comparatively large at 6.0 eV because the output of the light source and monochromator fell rapidly at energies above 5.0 eV. The photocurrent at 5.4 eV was the same for either direction of the applied electric field and was constant in time for constant illumination. The photocurrent was directly proportional to the applied electric field up to 1500 V/cm and also to the incident light intensity to within an experimental error of a few per cent. The abrupt increase in photoresponse observed at about 5.3 eV indicated that the incident photon energy was approaching the band gap of the sample thus giving rise to intrinsic photoconductivity. These results will be discussed in more detail in Section V.

In Figure 25, curves b and c, the photoresponse is shown over the spectral range from 2 eV to 6 eV for a sample of SrO which had been irradiated at 195 K with 1.5 MeV electrons to a dose of approximately 1×10^{17} electrons/cm^2. Curve b shows the photoresponse at 77 K and curve c at 105 K. The most prominent feature introduced by electron irradiation was the temperature dependent asymmetric band located at 3.1 eV. According to the model described in Chapter II the photoconductivity from the F^+-center involves a two step process, namely optical absorption for the optical transition from the ground to an optically accessible excited state of the center followed by thermal ionization of the charge carrier. Therefore the photoresponse band centered at 3.1 eV in curves b and c of Figure 25 can be shown to be due to F^+-centers by comparing it to the spectral dependence of the F^+ optical absorption band, as is demonstrated in Figure 26. In Figure 26, curve a, is shown the

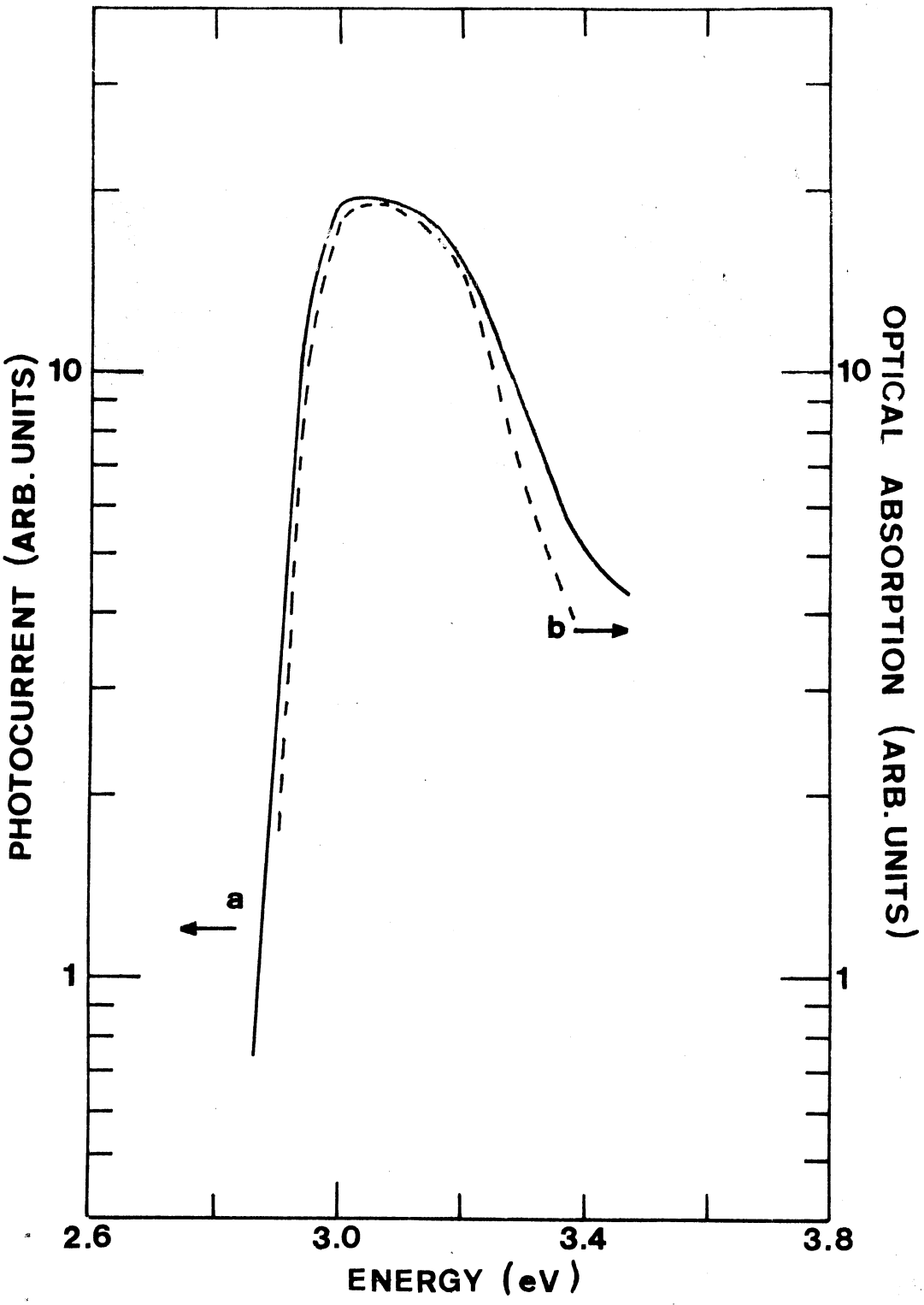

Figure 26. Comparison of the Spectral Dependence of the Photocurrent in Electron Irradiated SrO, Curve a, and the Optical Absorption of the F^+ Band in Proton Irradiated SrO, Curve b. Both sets of measurements were made at 110 K

photoresponse of an electron irradiated sample in the vicinity of 3.1 eV. In Figure 26, curve b, is shown the F^+ absorption band measured on a proton irradiated sample. Curve b is proportional to $[1 - \exp(-\alpha d)]$ where α is the absorption coefficient of the F^+ band. For small optical density, the absorbed light is proportional to α and therefore to the optical density. Both curves, which were measured at 110 K, were normalized at 3.1 eV. It can be seen that these curves coincide over the whole F^+ band except near the high energy tail, where the photoresponse from a band located at 3.9 eV, which can be seen in Figure 25, overlaps the F^+ band. We conclude, therefore, that the photoresponse band centered at 3.1 eV is indeed due to F^+-centers in SrO.

We show in Figure 27, curve a, the photoresponse at 77 K of a crystal which was gamma-irradiated at room temperature for about 30 minutes and measured with no further treatment. Gamma-irradiation increased the photoresponse generally between 2 eV and 5 eV and introduced a band at 2.65 eV, which is also observed in electron irradiated crystals (see Figure 25). The inflection in the photoresponse at about 4.8 eV which is observed in unirradiated crystals is further enhanced by the gamma-irradiation. Gamma-irradiation alone was ineffective in producing any F^+ photoresponse.

Figure 27, curve b, shows the photoresponse at 77 K of a crystal which was proton irradiated at 77 K to a dose of about 2×10^{16} protons/cm^2. It can be seen that the most prominent feature introduced by the irradiation is again the asymmetric F^+ band located at 3.1 eV. The irradiation also introduced photoresponse bands centered at 2.65 eV and 3.9 eV as well as an inflection at 2.5 eV. The 2.65 eV band was introduced by electron irradiation as well as by gamma-irradiation and is

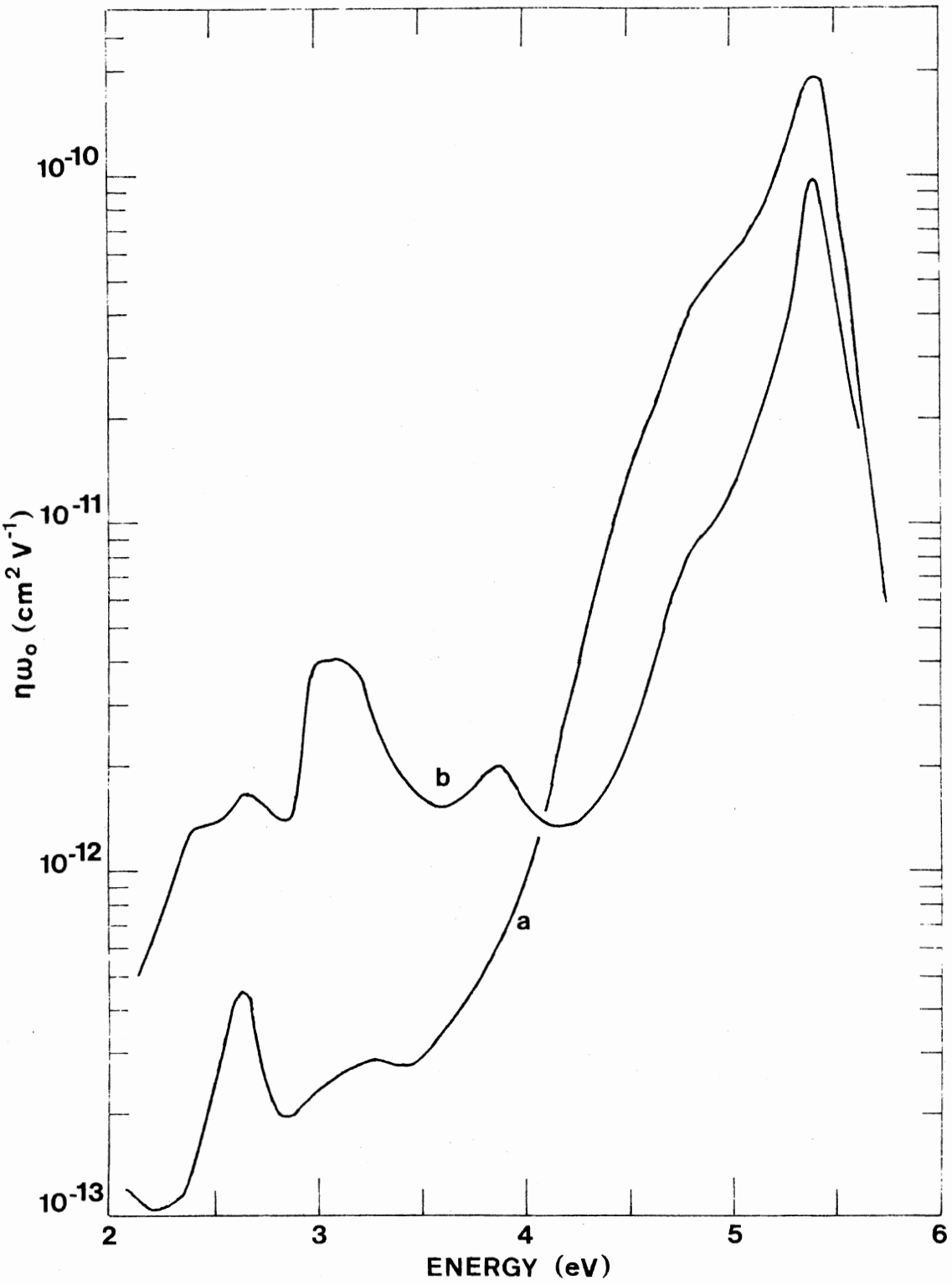

Figure 27. Spectral Dependence of the Photoresponse, $\eta\omega_o$, for SrO at 77 K After γ-irradiation at Room Temperature, Curve a; After Irradiation With 1.5 MeV Protons to a Dose of About 2×10^{16} Protons/cm^2, Curve b

presumably due to an impurity in the crystal. The band at 3.9 eV, which was also produced by electron irradiation, may be associated with the same type of center which is produced when SrO is plastically deformed (85).

The photocurrent at 3.1 eV was directly proportional to the applied electric field up to 1500 V/cm within an experimental error of a few percent (Figure 28). Typically an applied electric field of 500 V/cm was used during the measurements. In addition the photocurrent at 3.1 eV was also directly proportional to the incident light intensity, within a few percent, as the intensity varied by a factor of about fifty (Figure 28).

It can be seen in Figure 25 that as the temperature increased from 77 K to 105 K the photoresponse of the F^+ band grew by over an order of magnitude, whereas the photoresponse away from the F^+ band was almost independent of temperature over the same range. The detailed temperature dependence of the F^+ photoresponse over the range from 63 K to 180 K is shown in Figure 29. At 63 K the F^+ band was almost indistinguishable from the background photoconductivity and above 180 K the dark current became so large that accurate photocurrent measurements could not be made. The insert in Figure 29 shows how the thermally stimulated current, or dark current, increased with temperature. The thermally stimulated current was obtained by first filling available traps by illuminating the sample for about 90 minutes at 77 K with ultraviolet light in the absence of an externally applied electric field. With an electric field across the crystal, the dark current was then measured as the traps emptied due to the gradual warming of the sample from 77 K to 200 K. It can be seen that none of these traps empties in the region of

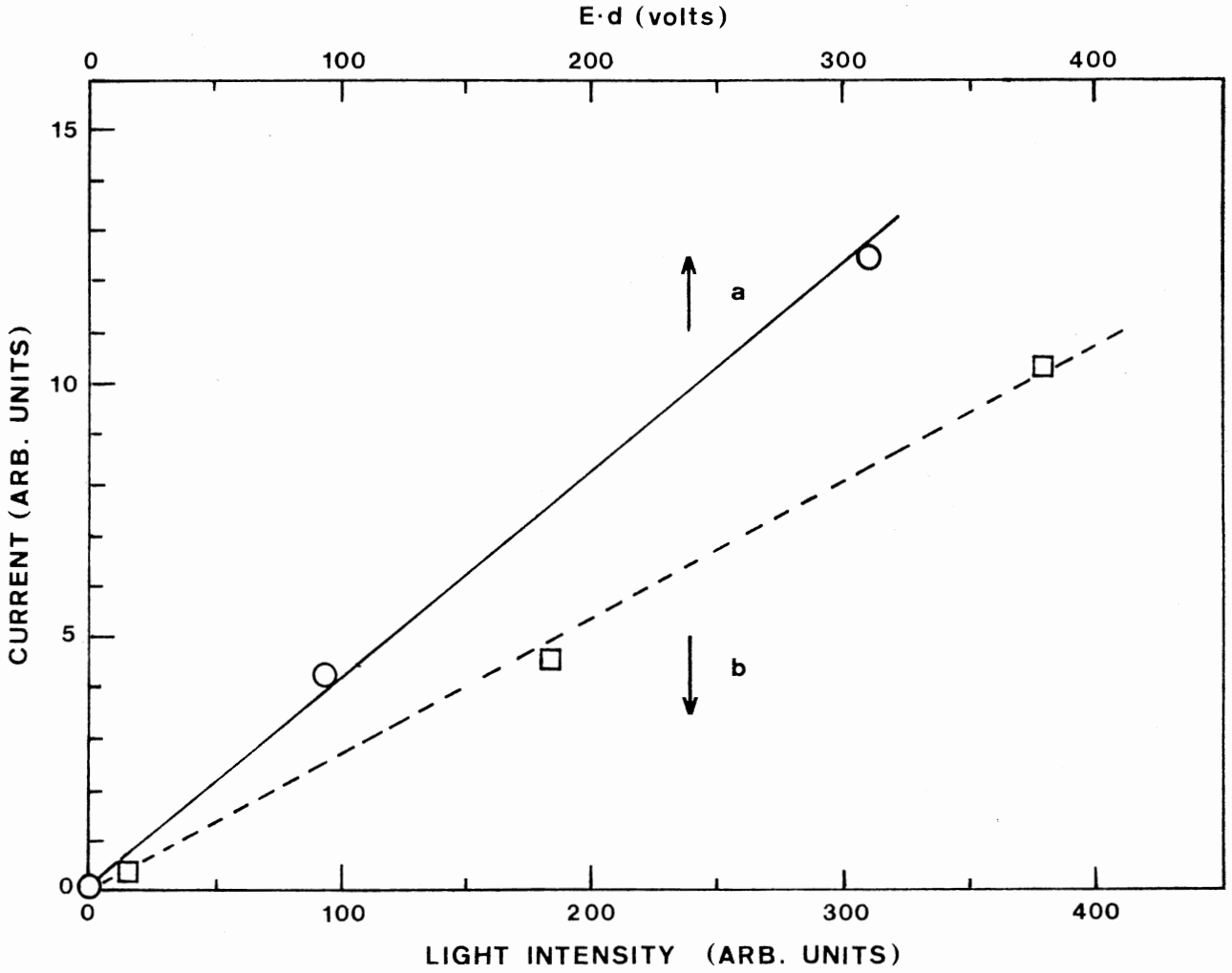

Figure 28. Photocurrent as a Function of Applied Electric Field (E=V/d), Curve a; and as a Function of Incident Light Intensity, Curve b. Measurements were taken at 120 K with 3.1 eV light incident on an electron irradiated sample of SrO

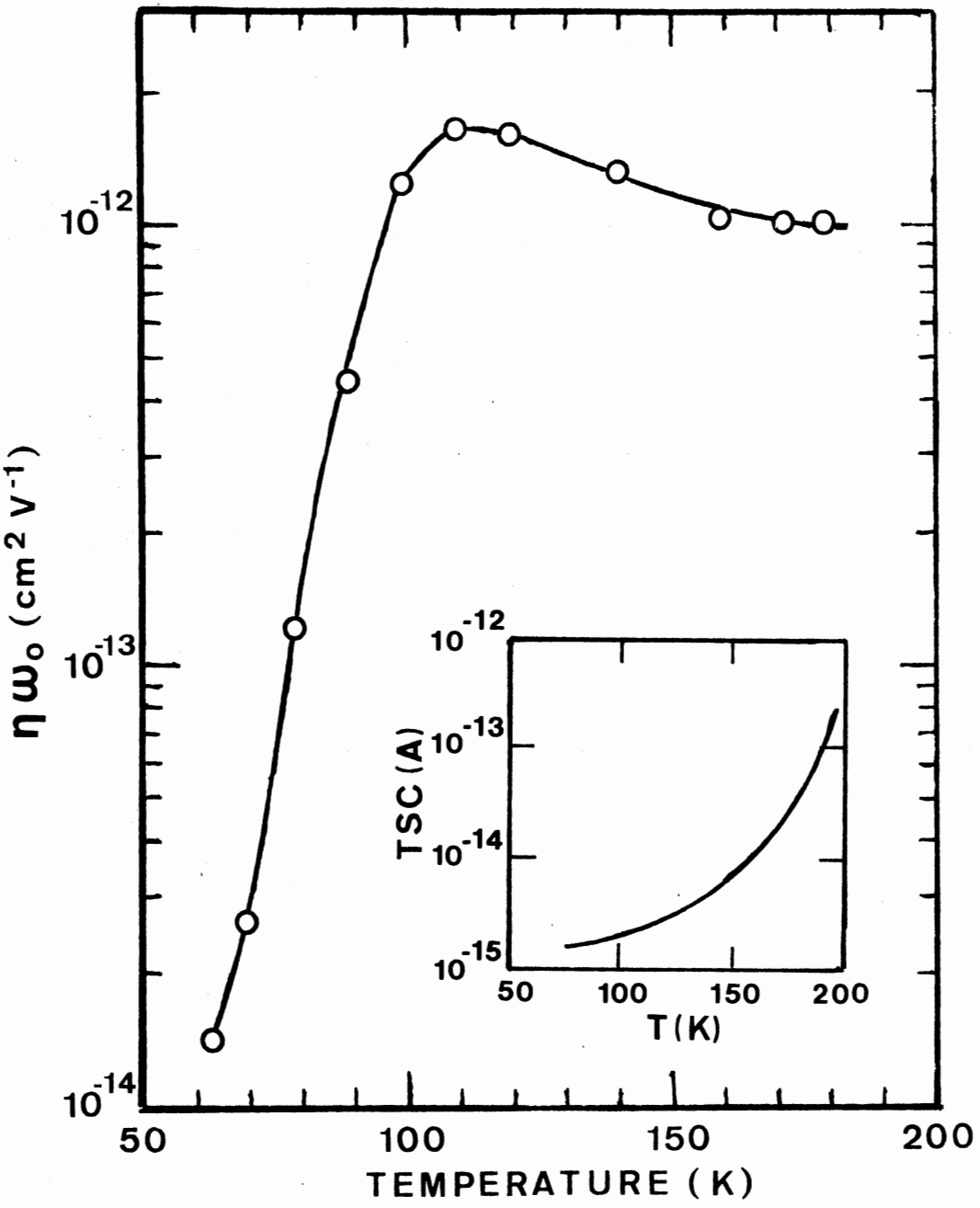

Figure 29. Temperature Dependence of the F^+ Band Photoresponse in Electron Irradiated SrO. The measurements were made with an incident photon energy of 3.1 eV. The insert shows the thermally stimulated current in an electron irradiated crystal which had been illuminated with ultraviolet light at 77 K

the abrupt increase in F^+ photoresponse at about 80 K. The sharp increase in photoresponse between 63 K and 100 K is characteristic of a thermally assisted ionization such as occurs, for example, for the F-center in KCl at about 120 K (55). Above 110 K an F^+-center in SrO which has absorbed a photon, frees a charge carrier with essentially unit probability and the temperature dependence of the photoresponse is due mainly to the temperature dependence of the mean range of the carriers. The significance of the data in Figure 29 will be discussed more fully in Section V.

It was found that prolonged illumination in the F^+ band region at temperatures above about 90 K partially destroyed the photoresponse. It took about a minute to reduce the photoresponse to half its initial value. However, the photoresponse could be restored by illuminating the sample with light of energy greater than 3.7 eV. Low energy photons were not effective in restoring the photoresponse. Consequently photoconductivity measurements above 90 K, such as those presented in Figures 25, 26 and 29, were made by illuminating the crystal for several seconds with ultraviolet light following each measurement made in the region of the F^+ band. This bleaching effect is similar to experimental results found by Dash (81) in BaO. He found that the photoresponse of the 2.0 eV band could be enhanced if the crystal was simultaneously irradiated with ultraviolet light. One possible explanation of these results is that the ultraviolet light released charge carriers from comparatively deep traps and that these carriers repopulated bleached F^+-centers.

Kemp and Neeley (86) have suggested that the $^2A_{1g}$ ground state of the F^+-center lies several eV below the top of the valence band of the host crystal. Following from this suggestion, once the F^+-center ab-

sorbed a photon it might, then, be energetically possible for an electron on one of the surrounding oxygen ions to jump into the vacancy. This sort of charge transfer process, would leave a hole on the oxygen ion and photoconductivity could occur if this hole were released and sufficiently mobile. This explanation, therefore, requires that the charge carriers be positive. However, using a technique suggested by Peria (87), we determined the sign of the charge carriers to be negative, as we now describe. A sample was supported such that the electric field was parallel to the 5 mm dimension and perpendicular to the direction of the incident light. A section at the center of the sample, 1 mm wide and the height of the sample, was illuminated, while the right hand electrode was held positive with respect to the left hand electrode by an external battery. Although the mean range of the charge carriers in the direction of the applied electric field is much less than the thickness of the crystal, the net result of illuminating the crystal is that a space charge electric field is established in the crystal going from left to right across the illuminated region if we assume at this point that the charge carriers are electrons for purposes of explanation. An important fact here is that the electron excess lies outside the illuminated region while the electron deficiency lies within this region. The external electric field was then removed and the photocurrent was measured as a function of the position of a thin band of light as the band scanned the crystal. The data shown in Figure 30, curve a, was obtained. Notice that the photocurrent was a maximum when the light was falling on the region of the crystal which had been illuminated with 3.1 eV light and which is delineated by the vertical arrows, and that the photocurrent fell rapidly to zero outside this region.

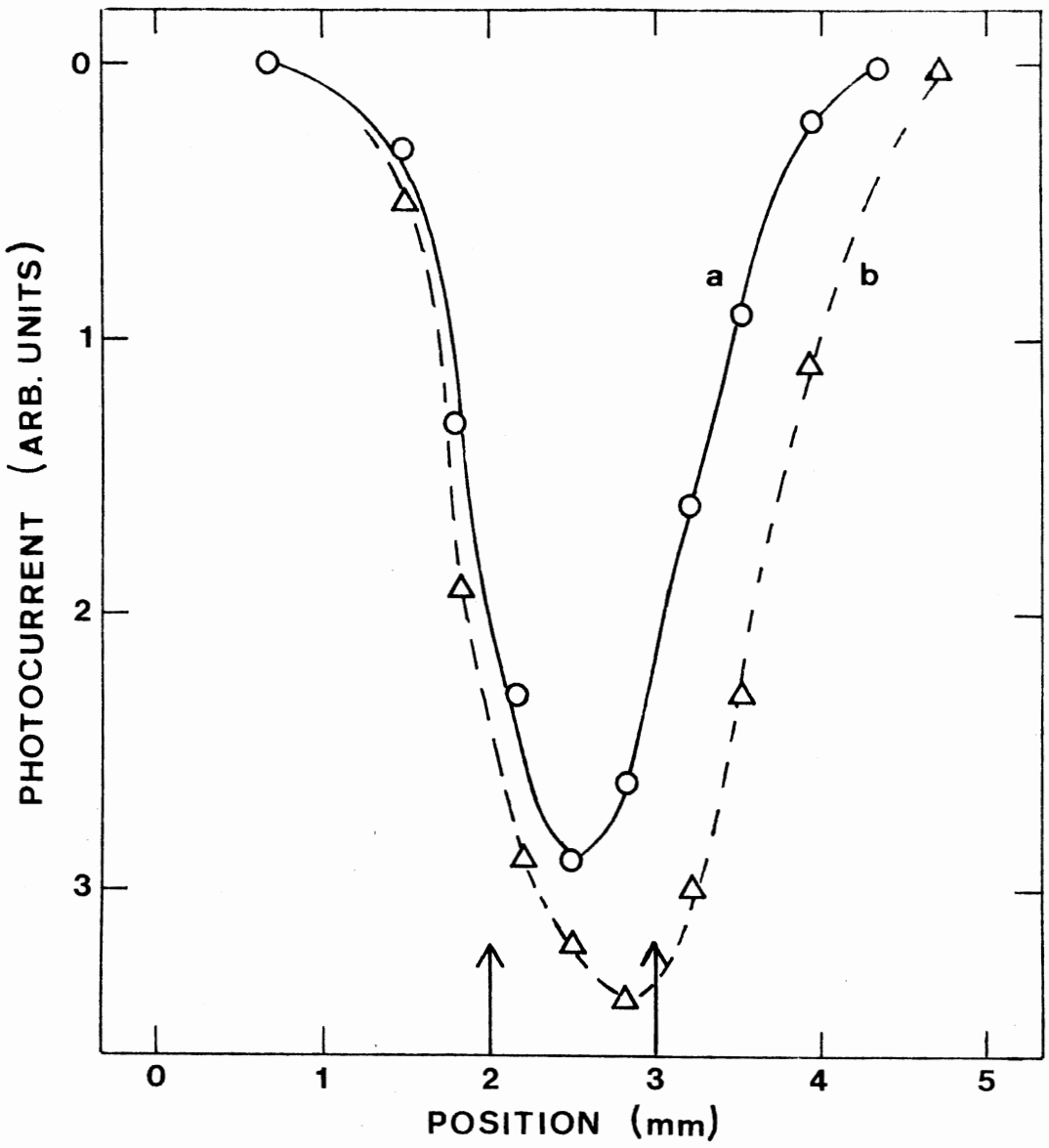

Figure 30. Electric Field Distribution Obtained in the Determination of the Sign of the Charge Carriers Excited by 3.1 eV Light in Electron Irradiated SrO. The measurements were made with both electrodes held at the same potential after illumination with an externally applied electric field going from right to left, curve a, and after subsequent illumination with no applied electric field, curve b. Curve a has been reduced a factor of 10 to accommodate it on the figure. The vertical arrows indicate the region of the crystal which was illuminated

The central region of the crystal, the same volume as previously illuminated, was then illuminated with 3.1 eV light again, with no externally applied electric field. During the first illumination period the charge carriers (assumed to be electrons in this explanation) move just beyond the right hand edge of the illuminated region. During the second illumination period these carriers remain trapped but electrons originating from centers just inside the right hand edge of the illuminated region move towards the left under the influence of the polarization field, with the result that a dipolar space charge region is established at the right hand edge of the illuminated region of the crystal.

The sign of the charge carriers can be determined if this dipole layer can be located. This can be done experimentally by moving a narrow beam of light across the crystal and measuring the photocurrent as a function of the beam position. According to the above explanation, if the charge carriers are electrons, the space-charge distribution and its corresponding electric field would have an appreciable value only at the right hand edge of the illuminated region. The photocurrent was thus determined as the crystal was scanned again with a narrow band of light and the charge carriers moved under the influence of the electric field set up by the dipolar space-charge which had been established at the edge of the illuminated section of the crystal, and Figure 30, curve b, was obtained. The photocurrent data of curve a has been reduced by a factor of ten to accommodate it on the figure. The maximum in the photocurrent, curve b, can be seen to have occurred at the right hand edge of the region which had been illuminated with 3.1 eV light. This measurement located the dipole layer and indicated that the charge

carriers were negative, i.e., electrons. If the carriers had been positive holes an analysis similar to that above shows that the dipole layer would have been located at the left hand edge of the region which had been illuminated with 3.1 eV light (87). The experiment was repeated with the initial externally applied electric field in the opposite direction, in order to determine whether any geometrical effects in the apparatus were affecting the result. The sign of the carriers was again determined to be negative.

The performance and interpretation of the type of experiments described above are somewhat difficult and more direct confirmation of the result will be required, such as would come, for example, from Hall effect measurements. It is worth noting, however, that similar experiments performed, in this study, on the 400 nm F band in CaO indicated that the charge carriers were electrons in this case too, as expected.

The photocurrent originating from F^+-centers in SrO was found to go to zero within a fraction of a second of the incident light being removed. There was no evidence of the long lived dark current found by Roberts and Crawford (80) after illuminating the 5.0 eV band in MgO. We also found that the F^+ absorption band in proton irradiated SrO could not be optically bleached at 120 K, although from the temperature dependence of the photoresponse, Figure 29, F^+-centers which have absorbed a photon are expected to be thermally ionized with almost unit probability at this temperature. If we assume that F^+-centers produced in proton irradiated SrO are mutually independent, these results suggest that in high concentrations the oxygen vacancy is an efficient trap in SrO. Furthermore, the fact that there is no sign of F-centers being formed in SrO which has been heavily irradiated and which contains a comparatively

large concentration of F^+-centers, Figure 23, suggests that F^+-centers, on the other hand, are not effective electron traps in our material, since an F^+-center which traps a second electron becomes an F-center.

When an electron irradiated sample was subsequently γ-irradiated for 30 minutes at room temperature just prior to being mounted in the cryostat, the photoresponse was found to have increased uniformly by a factor of about two across the spectral range from 2 eV to 4 eV. The F^+ photoresponse was unchanged relative to the background and no band was introduced in the region of 2.5 eV, where the F absorption has been reported (43). This result again suggests that the F^+-center is not an efficient electron trap compared to other traps in the crystal.

Additional experimental results pertaining to photoconductivity measurements on proton irradiated and neutron irradiated SrO can be found in Appendix A.

Having described in detail the results from our photoconductivity measurements, we now turn our attention to the second competing mode of escape for the optically excited F^+-center electron, that is, radiative decay to the ground state.

IV. Luminescence and Fluorescence Lifetime Measurements

Luminescence and fluorescence lifetime measurements were made on samples which were obtained from two sources. Samples from W. and C. Spicer, Ltd. were irradiated at 77 K with 1.5 MeV protons. Another sample, grown at Oak Ridge National Laboratory (ORNL), which had been neutron irradiated at room temperature, was given to us by Dr. Y. Chen.

The luminescence and fluorescence lifetime measurements were made

as described in Chapter III. The luminescence spectra were obtained using 402 nm light from a xenon lamp as the exciting source for F^+-center emission. The luminescence spectrum emitted at 10 K by a Spicer sample which had been irradiated at 77 K to a dose of approximately 1 x 10^{17} protons/cm^2 is shown in Figure 31, curve a. The sample had an optical density of about 0.3 and was 2 mm thick. The peak of the emission spectrum occurs at 2.5 eV and the emission spectrum has a half-width of 0.34 eV. Similar results were obtained for the luminescence spectrum of the ORNL-neutron irradiated sample at 10 K, as illustrated in Figure 34.

The excitation spectrum for the 2.5 eV emission band, measured at 10 K, is shown in curve a of Figure 32. The excitation spectrum was obtained by measuring the intensity of the emission at 500 nm as the wavelength of the exciting light was varied. That is, with the detection system set at 500 nm, the peak of the emission band, the intensity of the emission at 500 nm was measured as the wavelength of the exciting light which pumps the emission was varied. The excitation spectrum was obtained on the same sample as that used in Figure 31, curve a. The excitation spectrum can be compared to the spectral dependence of the intensity of the light absorbed into the F^+ band measured on the same crystal. The absorption spectrum measured on the same sample, at 77 K, is shown in Figure 32, curve b. It has been displaced vertically to avoid overlap. Hughes and Webb (49) have reported that the F^+ optical absorption does not change significantly between 10 K and 77 K. Inspection shows a close similarity between the two bands. The near coincidence of the two curves in Figure 32 leads us to conclude that the 2.5 eV emission results from absorption of light by the F^+-center, with the

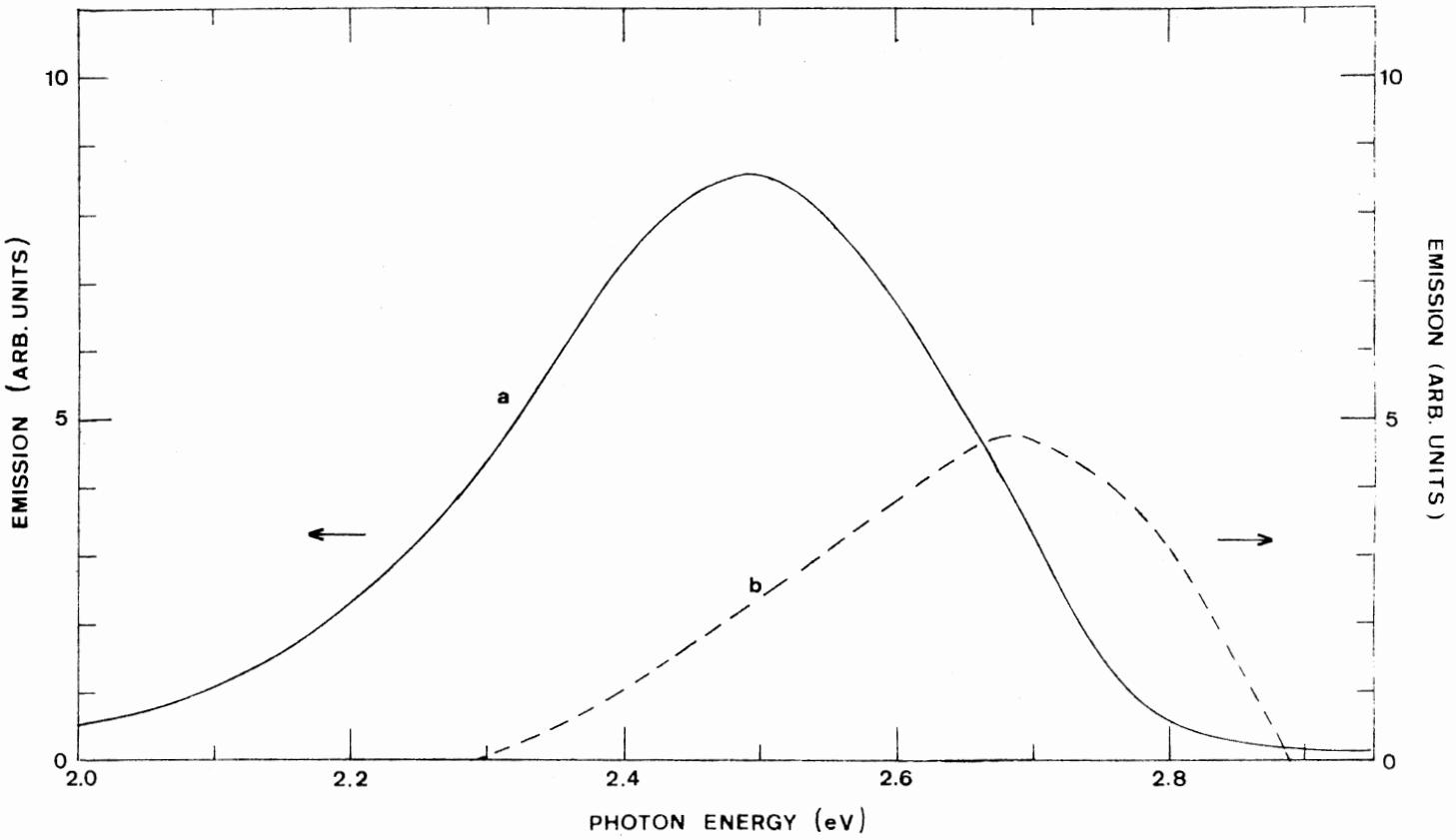

Figure 31. Luminescence Spectrum Emitted at 10 K by a Spicer Sample of SrO Which Had Been Irradiated at 77 K to a Dose of About 1 x 10^{17} Protons/cm^2, Curve a; Luminescence Spectrum in Unirradiated Spicer Sample at 112 K, Curve b. The luminescence was excited with 402 nm light

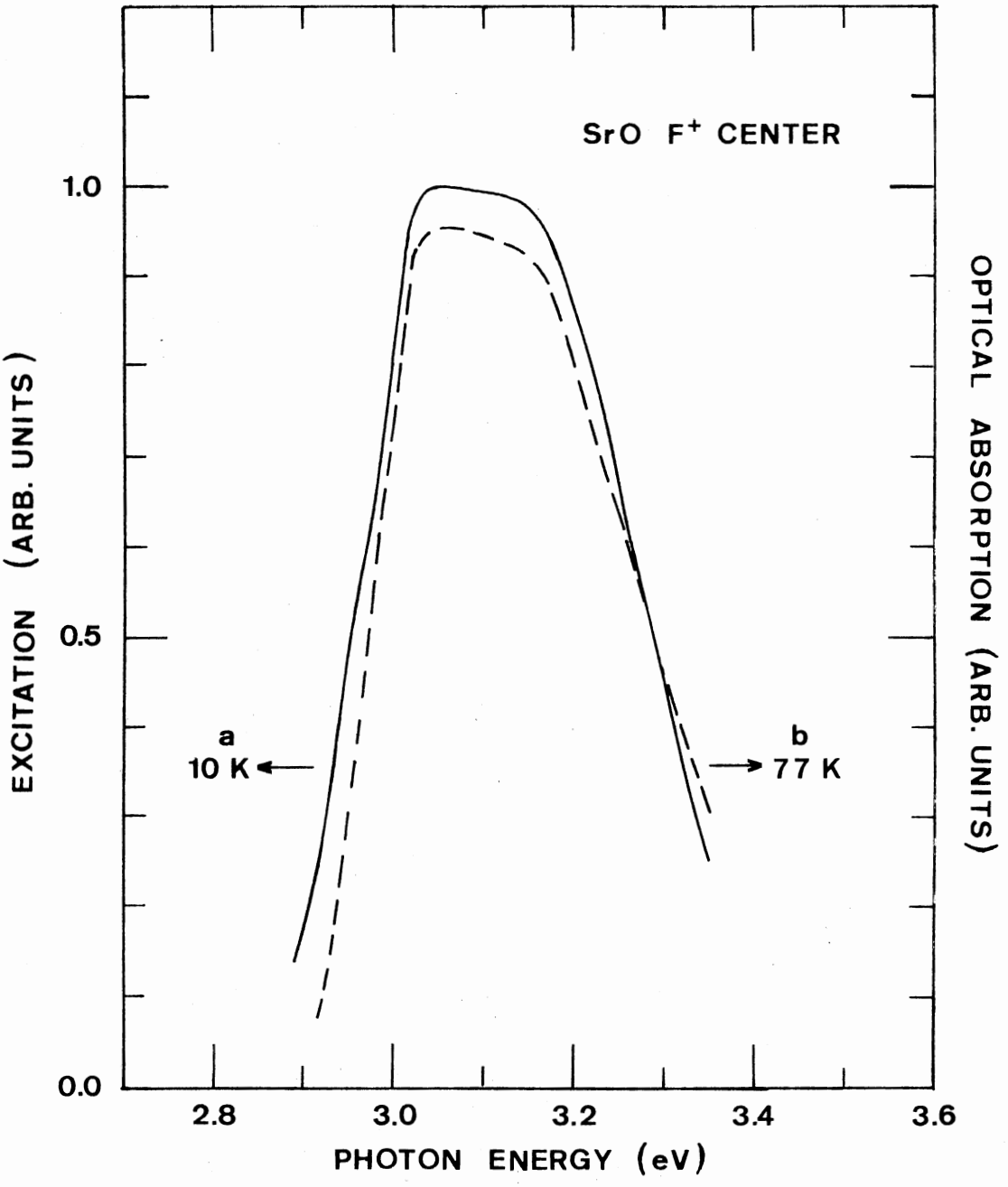

Figure 32. Comparison of the Spectral Dependence of the Excitation Spectrum at 10 K for F^+-center Emission in Proton Irradiated SrO, Curve a, and the Optical Absorption of the F^+ Band Measured at 77 K on the Same Sample, Curve b

photoluminescence occurring as the optically excited F^+-center electron radiatively decays from an excited state to the ground state of the center.

The samples also show a weak, but easily detectable, luminescence band, which peaks near 2.7 eV, in the unirradiated Spicer samples. This emission is indicated in Figure 31 as the broken curve. The emission intensity axes for the two curves in Figure 31 are approximately the same but an absolute comparison should not be made since the two curves were obtained in separate experiments with different samples. The excitation spectrum obtained for the 2.7 eV emission was quite complicated, extending out to at least 4 eV and showed no resemblance to the F^+ absorption band. The 2.7 eV emission band is, therefore, thought to be associated with an unidentified impurity in the crystals.

Figure 33 illustrates the F^+ emission spectrum, measured as a function of temperature. These measurements were made on the sample used for Figures 31 and 32. One readily observes that the intensity of the F^+ emission band, which peaks at 2.5 eV, decreases with increasing temperature. Similar measurements are shown in Figure 34 for the luminescence spectrum emitted by the ORNL-neutron irradiated sample at 10 K, 73 K and 117 K. The intensity of the F^+ emission in the neutron irradiated sample, likewise, decreased with increasing temperature. For these measurements the luminescence was excited with 402 nm light. The zeroth moment, M_o, is proportional to the area under the emission curve and measures directly the number of centers involved in absorption and emission. M_o is expected to be temperature insensitive provided the quantum efficiency for fluorescence remains constant. Upon inspection of Figures 33 and 34, it is obvious that the F^+ emission intensity and

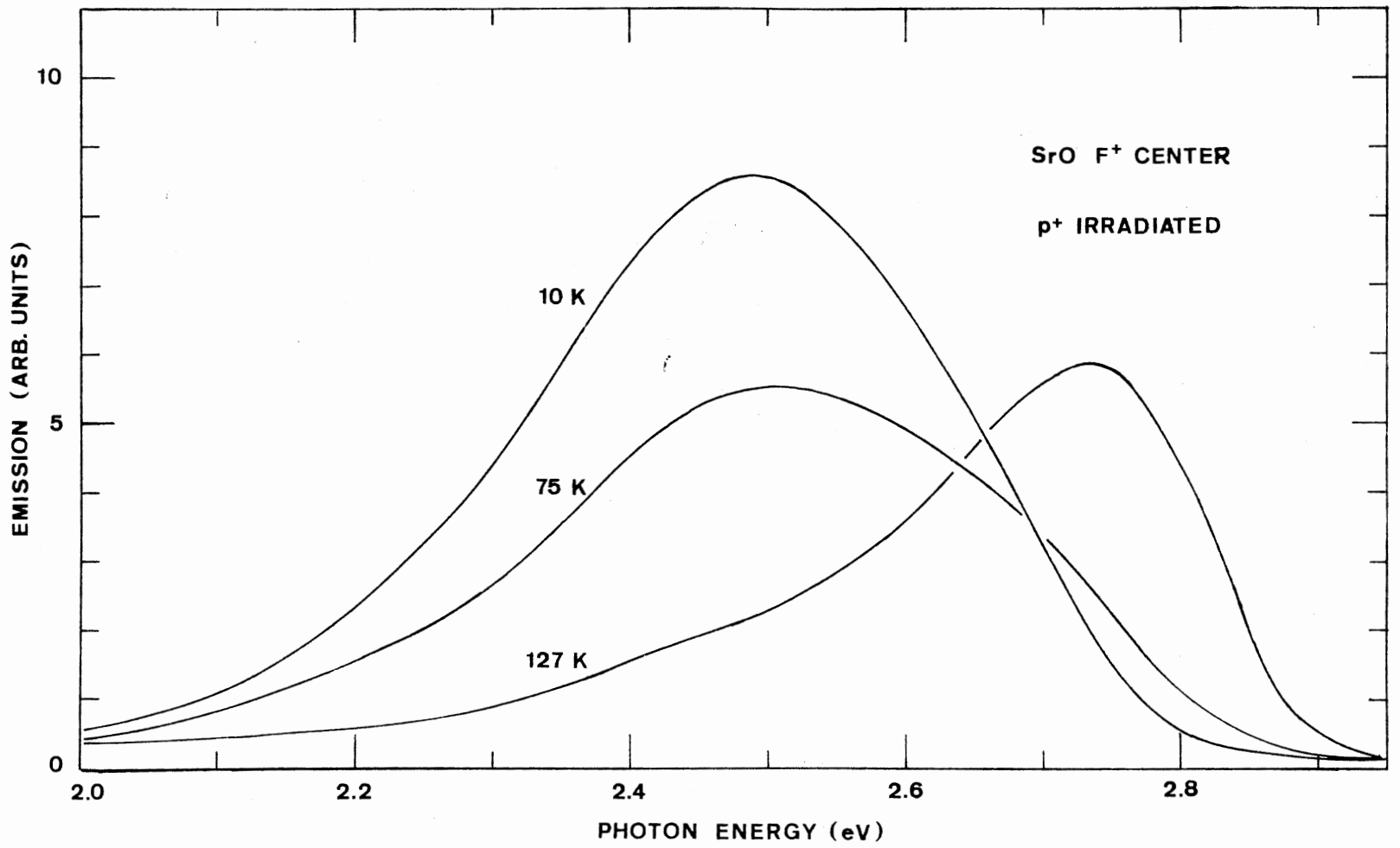

Figure 33. Emission Spectra, Measured at Various Temperatures, on a Spicer Sample of SrO Which Had Been Irradiated at 77 K to a Dose of About 1 x 10^{17} Protons/cm^2. The luminescence was excited with 402 nm light

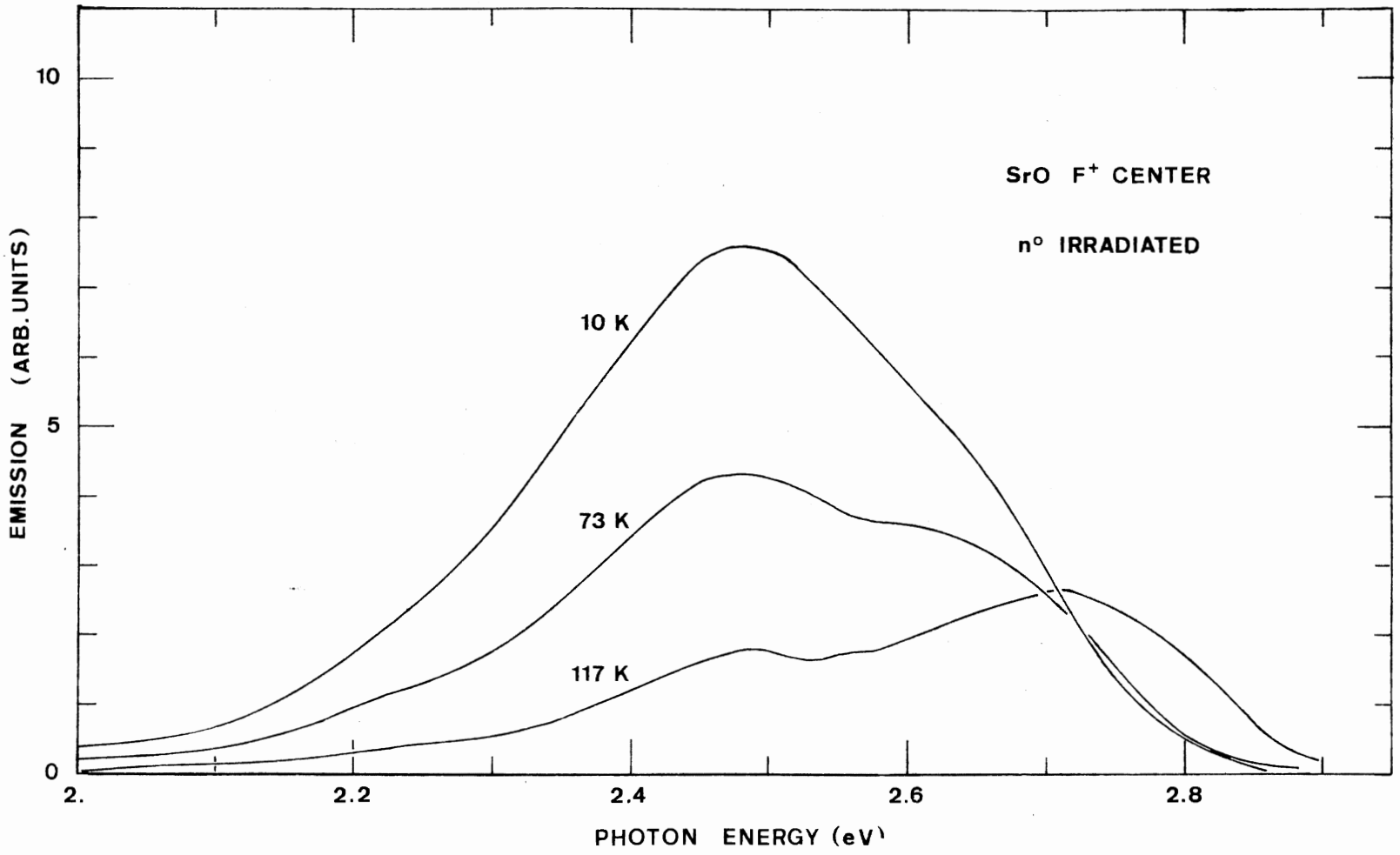

Figure 34. Emission Spectra, Measured at Various Temperatures, of ORNL-SrO Which Had Been Neutron Irradiated at Room Temperature. The luminescence was excited with 402 nm light

the corresponding zeroth moment are decreasing with increasing temperature. The zeroth moment is decreasing in the temperature region where we expect the quantum efficiency for fluorescence to decrease since the quantum efficiency for photoconductivity is increasing in this same temperature region. In Section III we reported an increase in the F^+ photoresponse of nearly two orders of magnitude between 60 K and 100 K. If we assume that ω_o and the oscillator strength, f, remain independent of temperature over the interval of interest, the increase in the photoresponse between 63 K and 100 K is then due to an increasing quantum efficiency for thermal ionization. According to the two level model described in Chapter II, the electron in the relaxed excited state of the center has two competing modes of escape: radiative decay to the ground state (luminescence) and thermal release of the charge carrier (photoconductivity). Since these phenomena are competing modes of escape for the optically excited F^+-center electron, one would expect one process to occur at the expense of the other. As shown for the simple model developed in Chapter II, the fraction of excited centers which decay by luminescence is given by η_R (Equation II-25) and the fraction which decay by thermal ionization is given by η_T (Equation II-24), such that $\eta_R + \eta_T = 1$, where only one excited state is considered and other modes of escape are neglected. When taken in conjunction with Figure 29 which represents an increase in the quantum efficiency for thermal ionization, we see that the decrease in the emission intensity, illustrated in Figures 33 and 34, and the corresponding decrease in the zeroth moment, M_o, represent a decrease in the quantum efficiency for the F^+ fluorescence. The second emission band which peaks at 2.7 eV and which becomes more apparent with increasing temperature is thought

to be due to the impurity discussed in the preceding paragraph.

The F^+-center fluorescence lifetime was measured as described in Chapter III. The fluorescence, excited by the air spark filtered with a Corning CS7-51 filter in combination with an interference filter with peak transmission at 402 nm, was detected over the spectral range from 490 nm to 550 nm using a combination of Corning filters CS3-70 and CS4-96. The fluorescence decay curves were photographed from the screen of an oscilloscope. Figure 35 shows the semilogarithmic plot of the emission decay curves measured at 10 K, 77 K and 106 K on the same proton irradiated sample used to obtain the results in Figures 31, 32, and 33. The decay of the excitation is also shown for comparison. The intensity of the emission at time t, for a simple exponential decay, is given by:

$$I = I_o \exp(-t/\tau)$$

where τ is the fluorescence lifetime, the time it takes for the emission intensity to decay to 1/e of the initial value. τ can also be determined from the slope of the semilogarithmic plot of the exponential decay. τ is expected to be temperature dependent (73). We see that at very low temperatures, such as 10 K, the F^+ emission decays exponentially with a lifetime $\tau \sim \tau_R$ of about 0.46 μsec, where τ_R is the radiative lifetime. This value is considerably longer than would be expected for the F^+-center in the alkaline earth oxides and suggests that the fluorescence is partially forbidden. This will be discussed further in Section V. The radiative lifetime measured on the neutron irradiated sample was slightly shorter as may be expected considering the massive damage done by neutron irradiation. The electron would, in general, leave the ex-

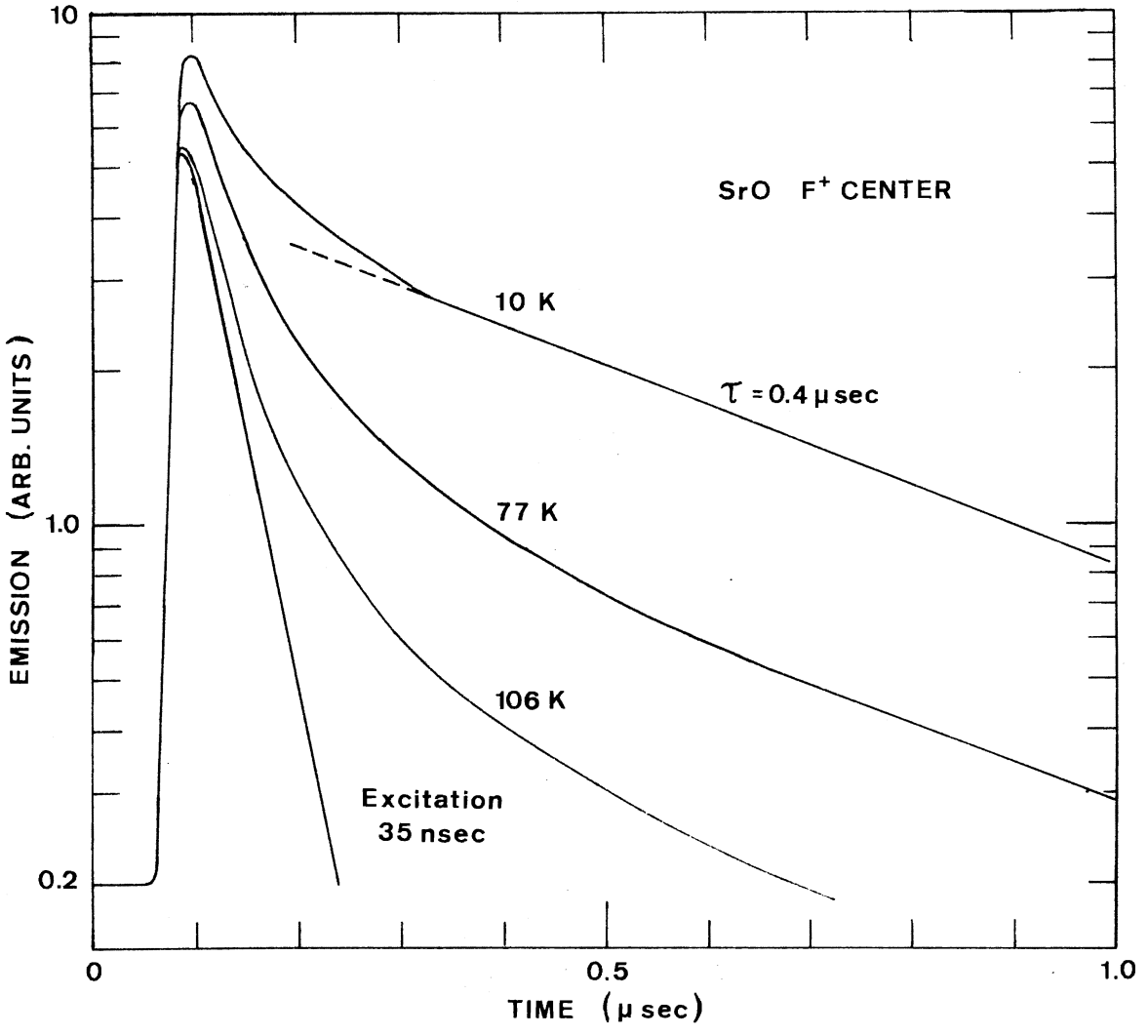

Figure 35. Emission Decay Curves, Measured at Various Temperatures, for F^+ Fluorescence in Proton Irradiated SrO. The sample had been irradiated at 77 K to a dose of about 1 x 10^{17} protons/cm^2. The decay of the excitation is also shown for comparison

cited state by the fastest mode of escape resulting in a slightly shorter lifetime for the excited state of the F^+-center.

As the temperature increases it is apparent that the lifetime continues to show the 0.4 μsec component. It is also apparent that there is a faster component which becomes more dominant with increasing temperature. In order to determine the faster component, the emission decay curve obtained at 106 K (Figure 35) has been redrawn in Figure 36. If we assume that the emission intensity decay curve measured is the sum of two exponential decay curves, one (C) which decays rapidly and a second (B) which decays with a much longer lifetime, we can determine the shorter lifetime component. The fast component would make no significant contribution in the region of A for $t > 0.5$ μsec, and the lifetime measured would essentially be that of the exponential decay shown in B, i.e., the 0.4 μsec component which was dominant at low temperatures. However, in the region of A for $0.1\ \mu\text{sec} < t < 0.2\ \mu\text{sec}$, the measured exponential decay would have significant contributions from both the short-lived component (C) and the longer-lived component (B). Therefore, the rapidly decaying exponential, C, can be found by subtracting the exponential decay, B, from the measured decay curve, A. The time needed for C to decay to 1/e of its initial value is $\tau_2 \sim 35$ nsec which is as fast as could be measured. The values for the two lifetime components remained nearly constant with changing temperature.

Possible explanations of these two lifetime components will be discussed in the following section along with other results obtained from photoconductivity and luminescence measurements.

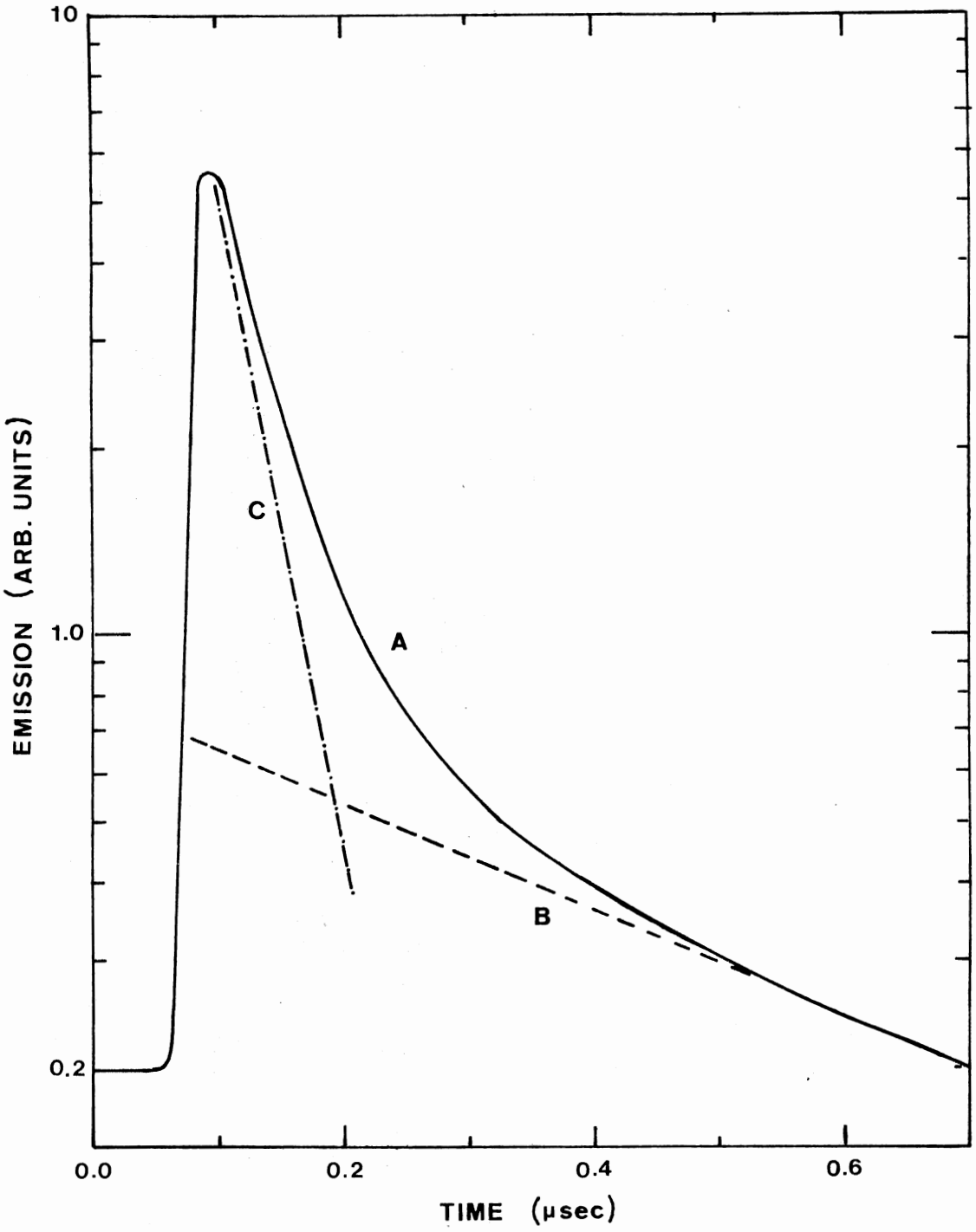

Figure 36. Emission Decay Curve for F^+ Fluorescence in SrO at 106 K, Curve A; Exponential Decay, $I = I_o \exp(-t/\tau_i)$ where $\tau_1 \sim 0.4$ μsec, Curve B, and $\tau_2 \sim 35$ nsec, Curve C. $A \sim I_o \exp(-t/\tau_1) + I_a \exp(-t/\tau_2)$

V. Analysis and Discussion

The temperature dependence of the photoresponse between 70 K and 110 K, shown in Figure 29, can be explained quite well by a two level model (55). As described in Chapter II, an electron in the relaxed excited state of the center has a temperature dependent probability $\frac{1}{\tau_T} = \frac{1}{\tau_o} e^{-E_a/kT}$ of being thermally ionized across an energy gap E_a. There is also a temperature independent probability, $1/\tau_R$, of radiative decay to a lower energy level. The yield of free carriers per absorbed photon, η_T, from Equation II-48 is given by

$$(\frac{1}{\eta_T} - 1) = (\frac{\tau_o}{\tau_R}) e^{E_a/kT} .$$

In order to compare this equation with our experimental results, Figure 29, which give directly the product $\eta\omega_o$ as a function of temperature, we make the approximations that ω_o and the oscillator strength of the F^+ band remain independent of temperature between 70 K and 110 K. The temperature dependence of $\eta\omega_o$ is thus assumed to be due entirely to the change in η_T over this temperature interval. Since it appears that F^+-centers are effectively fully ionized at 115 K, η_T is taken as unity at this temperature and we can plot $\ln(\frac{1}{\eta_T} - 1)$ against 1/T using the data of Figure 29. The resulting curve is shown in Figure 37, where it can be seen that over several orders of magnitude a straight line is obtained. The thermal activation energy, E_a, and the ratio τ_R/τ_o were determined from the slope of the line and values for E_a of 0.12 ± .01 eV and τ_R/τ_o of 5×10^6 were obtained. Since photoconductivity originating from F^+-centers was unexpected due to the net positive charge on

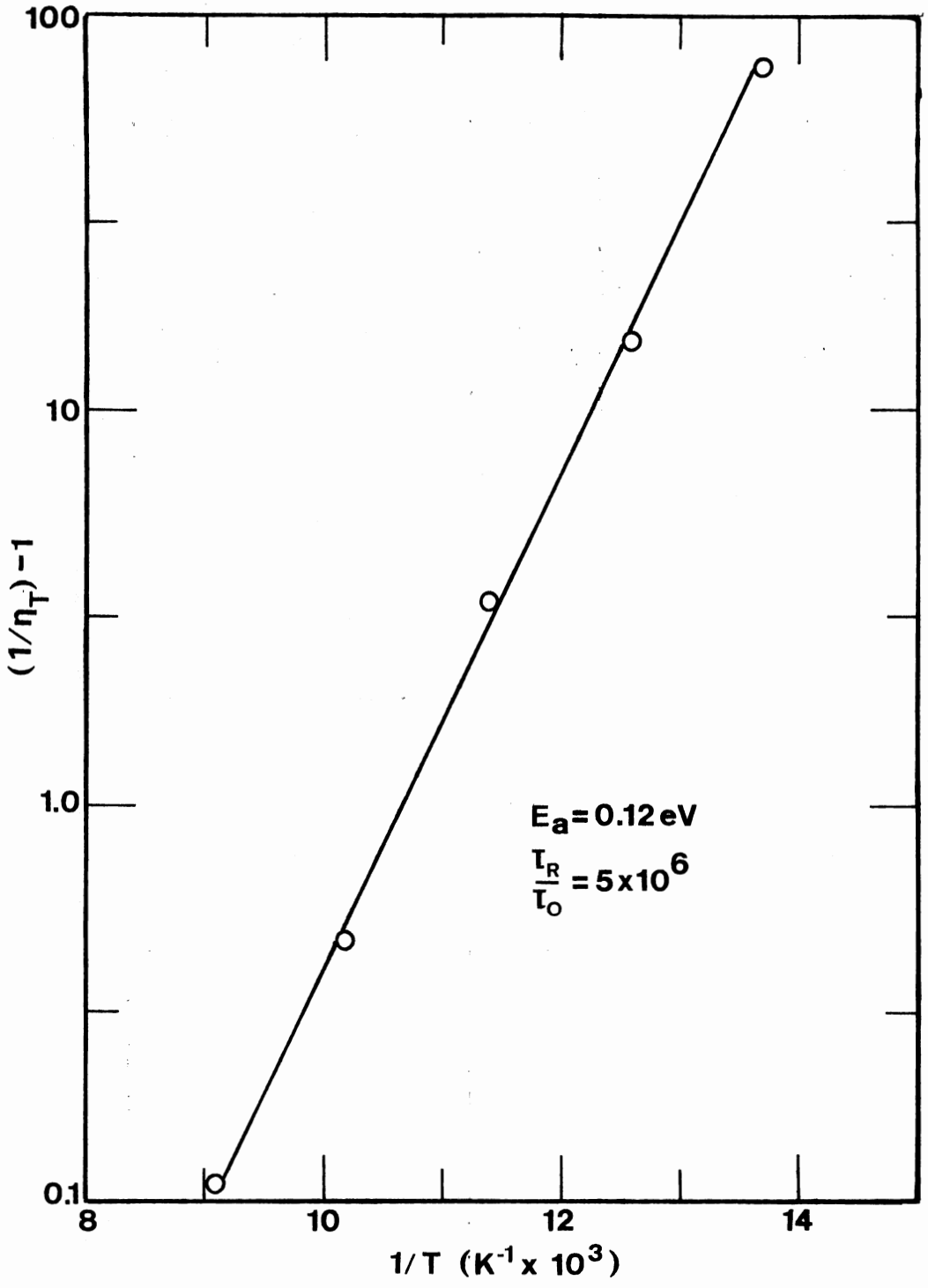

Figure 37. Semi-logarithmic Plot of $(1/\eta_T)-1$ Versus Inverse Temperature, 1/T. Data points were obtained from the experimental results shown in Figure 29 as described in the text

the center which would lead one to believe it would be harder to free the F^+ electron, it is interesting that these values are close to those found for F-centers in alkali halides (88). In the alkali halides (73) τ_o was found to be within an order of magnitude of 10^{-12} sec. If τ_o has a similar value in the alkaline earth oxides, and the results of Henderson et al. (25) suggest that this is probably the case, our value of $\tau_R/\tau_o = 5 \times 10^6$ suggests a value for τ_R of the order of a microsecond. This value is in good agreement with the longer lifetime component (0.46 μsec) reported in Section IV determined by fluorescence lifetime measurements. As suggested in Section IV, if this were the radiative lifetime for an allowed decay from the $^2T_{lu}$ excited state to the $^2A_{lg}$ ground state, it is considerably longer than would be expected for the F^+-center. As mentioned in Chapter II, Section V, the mean lifetime, τ, for allowed (electric dipole) transitions in atoms is of the order of 10^{-8} sec. For strong allowed transitions of F-type centers in absorption, it would be expected that the emission would be similarly allowed, with a lifetime of about 10^{-8} sec and a low temperature quantum efficiency near unity (64). The oscillator strengths for the alkali halides ($f_{KCl} = 0.9$; $f_{KBr} = 0.8$; $f_{NaCl} = 0.81$) (3) indicate strong allowed transitions in absorptions and the quantum efficiency for luminescence of the F-center at low temperatures has been found to be nearly unity as expected. The lifetime for F-center luminescence in KCl (73) has, however, been found to be on the order of 10^{-6} sec at low temperature, much longer than would be expected. Similarly, Wood and Wilson have calculated an oscillator strength of about 0.82 (60) for the $^2A_{lg} \rightarrow {}^2T_{lu}$ absorption in the SrO F^+-center. Since a decrease in free electron yield (Figure 29) with decreasing temperature is expected to be accom-

panied by an increase in the fluorescence yield (73) (Equation II-26), it appears that the quantum efficiency for radiative decay is nearly unity at low temperature. But, analogous to the alkali halides above, the radiative lifetime for the SrO F^+-center, reported above, $\tau_R \sim 0.46$ μsec is likewise larger than would be expected for the $^2T_{1u} \rightarrow {}^2A_{1g}$ transition and suggests that the fluorescence is partially forbidden. We will first consider some proposed explanations as to how these long lifetimes may arise in the alkali halides and then consider the possibility of these same effects increasing the radiative lifetime for the F^+-center in SrO.

One such possibility, studied by Fowler (71) for alkali halides, is that the F-center excited state wavefunction is very diffuse in emission in comparison with the ground-state wavefunction. As mentioned in Chapter II, Section V, the excited-state wavefunction for emission is more diffuse than that for absorption, while the ground-state wavefunction changes only slightly. The squared dipole matrix element (proportional to the transition probability) for emission is considerably smaller than that for absorption (Fowler (71) calculated $|\langle z\rangle|^2_{em}/|\langle z\rangle|^2_{abs} \sim 0.13$) because of the relatively small configuration space overlap between the excited- and ground-state wavefunctions for emission as compared with that for absorption. This would lead to a reduced transition probability and a longer lifetime.

We now consider a second proposed explanation for the relatively long lifetime of the excited state of the F-center in alkali halides. Absorption in the F-center arises from the 1s → 2p-like electronic transition. Absorption measurements give information about the F-center in its unrelaxed excited state. For the F-center in KCl in absorption the

2s-state lies about 0.11 eV about the 2p-state (89). However, the excited state involved in emission is the relaxed excited state of the center. Bogan and Fitchen (90) concluded that the two excited states are actually admixtures of s and p states and that these two mixed states are about 0.017 eV apart with the lower state having a predominantly s-character wave function. At low temperature, the emission transition would be from the lower excited state of predominantly s-like character to the 1s-ground state, giving rise to a smaller transition probability than that for the pure 2p → 1s transition and consequently a longer lifetime.

Both of these proposed explanations of the long lifetime of the excited state for the F-center seem plausible and in KCl it appears that both make significant contributions (64).

According to calculations presently being performed by Wood and Wilson for the F^+-center in SrO (60,91) the excited state wavefunction for emission has been found only slightly more diffuse than that for absorption, but not nearly so much as for the F-center in alkali halides (71) or the F-center in alkaline earth oxides (57,58,59). The relaxed excited state of the F^+-center in SrO is more localized and compact than that for the F-center in the alkali halides or alkaline earth oxides. This fact is further evidenced by the strong Jahn-Teller effect for the F^+-center in SrO. The calculated transition probability for emission (~ 0.5-0.6 for $^2T_{1u} \rightarrow {}^2A_{1g}$) (91) is only slightly smaller than for absorption, $^1A_{1g} \rightarrow {}^2T_{1u}$. It would thus appear that this effect does not have as significant a role in increasing the length of the lifetime of the excited state of the F^+-center in SrO as it perhaps does in the alkali halides.

In absorption the $^2T_{1u}$ and $^2A^*_{1g}$ excited states of the F^+-center in SrO are well separated in energy, as indicated in the configuration coordinate diagram for absorption in Figure 38. Although present theory (60) predicts that the $^2T_{1u}$ state minimum is slightly lower than the $^2A^*_{1g}$ state minimum in emission (Figure 38), the results are only semi-quantitative and are not reliable enough to make definite claims about the ordering (91). If spin orbit interactions are taken into account there may well be a mixing of the $^2A^*_{1g}$ and $^2T_{1u}$ states with the excited states being admixtures of $^2A^*_{1g}$ and $^2T_{1u}$. This coupled with the small energy separation at the minimum for the $^2A^*_{1g}$ and $^2T_{1u}$ states as shown may result in the lower state having a predominantly A_{1g} (s-like) character wavefunction. The transition from such an excited state to the ground $^2A_{1g}$ state is a "spin orbit allowed electric dipole transition". The transition from the predominantly s-like excited state to the s-like ground state is only "partially allowed" due to the small admixture of p-like character in the excited state. Consequently, the excited state lifetime would be longer than expected for an allowed electric dipole transition. Such an ordering of the excited states in emission could possibly also explain the presence of the approximately 35 nsec lifetime component observed in emission (Section IV) which becomes more dominant with increasing temperature. In fact our interpretation of the appearance of the shorter lifetime component in the luminescence at higher temperatures suggests that the state of predominantly A_{1g} character (which we subsequently refer to as the $^2A^*_{1g}$ state) is indeed the lower of the two states. According to this interpretation, at low temperatures the transition would be predominantly $^2A^*_{1g} \rightarrow {}^2A_{1g}$, partially forbidden and correspond to the 0.46 μsec lifetime component. The slightly higher

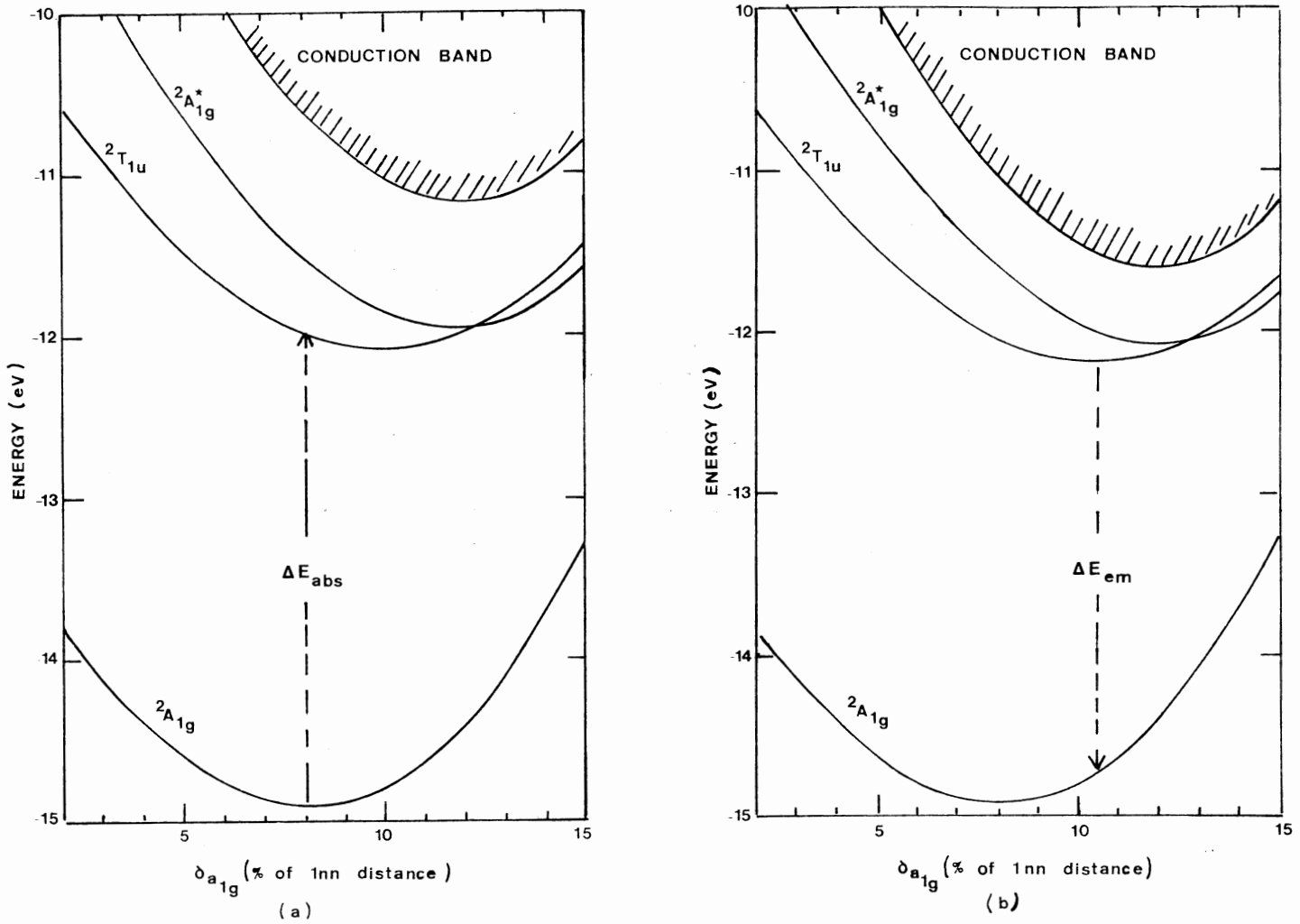

Source: Wilson et al. (60)

Figure 38. Configuration Coordinate Diagram for the F^+-center in SrO. δ = relaxation parameter and 1nn = first nearest neighbor distance

state of predominantly $^2T_{1u}$ character (which we call the $^2T_{1u}$ state) becomes increasingly populated at somewhat higher temperatures, thus giving rise to the $^2T_{1u} \rightarrow {}^2A_{1g}$ allowed electric dipole transition which would then be associated with the nanosecond lifetime component observed.

Since the $^2T_{1u}$ and $^2A^*_{1g}$ relaxed excited states are so close in energy, the $^2T_{1u} \rightarrow {}^2A_{1g}$ and $^2A^*_{1g} \rightarrow {}^2A_{1g}$ transitions would, for all practical purposes, give rise to a single emission band which is also in agreement with the experimental results reported in Section IV.

The fast lifetime component (τ < 35 nsec) may alternatively be associated with the impurity that is responsible for the 2.7 eV emission band (Figure 31) since the tail of the 2.7 eV band would also be detected at 5000 $\mathring{A}$.

As discussed in Section IV, the zeroth moment, M_o, for emission generally decreased with increasing temperature. The actual plot of M_o as a function of temperature is shown in Figure 39 for the proton irradiated sample. M_o here, is proportional to the total area under the emission band excited by 402 nm light. As such it includes the 2.5 eV F^+ emission band as well as the 2.7 eV impurity band which was always present. Using this data, in conjunction with Figure 29, it was concluded in Section IV that the decrease in the zeroth moment represented a decrease in the quantum efficiency for F^+ fluorescence. The fluorescence lifetime of an F-type center is expected to decrease with increasing temperature if the free carrier yield is increasing and the fluorescence yield is decreasing (73) based on the similar temperature dependence for the lifetime of the excited state (Equation II-23) and the fluorescence yield (Equation II-25). Reference to the lifetime data in Section IV shows, however that as the temperature increased up to

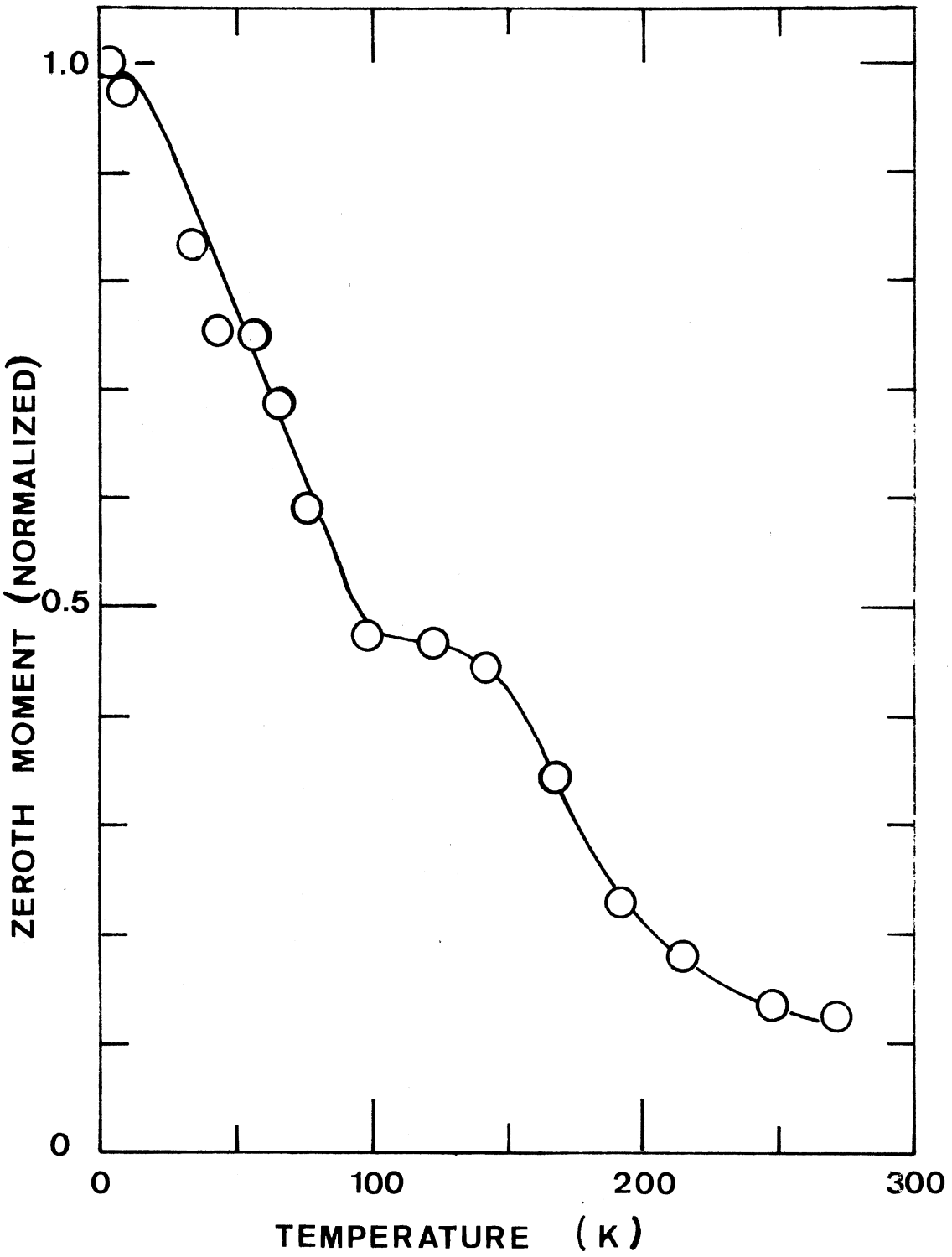

Figure 39. Temperature Dependence of the Zeroth Moment, M_o, of the F^+ Luminescence Band in Proton Irradiated SrO

77 K, the quantum efficiency for the 2.5 eV F^+ emission decreases without an apparent change in the lifetime although there was some evidence that above 77 K the lifetime decreases. At present we have no explanation for this except that the above prediction is based on a simple two-level model, which from these anomalies may be too restrictive an assumption for the F^+-center in SrO.

Since the 2.7 eV impurity band was noticeably visible above 77 K and, though hidden beneath the broad emission band below this temperature nevertheless contributed to the width of the observed emission band, it was not possible to determine the half-width of the emission band originating from the F^+-center alone. In spite of this, an attempt was made to determine the effective frequency, ω, and the Huang-Rhys factor, S, for the F^+-center by choosing to ignore the presence of the 2.7 eV impurity band below 77 K and assuming the entire emission band observed in this temperature range to be due to the F^+-center. The plot of $\coth^{-1}\left[\frac{W(T)}{W(O)}\right]^2$ as a function of 1/T (see Equation II-19), however, did not yield a straight line for either the proton or the neutron irradiated sample, and thus the attempt was abandoned.

Even if it were possible to determine the half-width of the F^+ emission band as a function of temperature, additional problems may be encountered in efforts to determine the effective frequency, ω, and the Huang-Rhys factor for this defect. The relationships described in Chapter II-Section IV were developed, in general, for Gaussian absorption bands and systems for which the Jahn-Teller effect was not significant. These again are not valid assumptions for the SrO F^+-center. The F^+-center in SrO is a Jahn-Teller coupled system in absorption (49,60) with the Jahn-Teller effect contributing significantly to the

asymmetric shape of the absorption band.

The main feature of the photoresponse of SrO at high photon energies, Figures 25 and 27, is the relatively abrupt increase in the vicinity of 5.3 eV. A steep rise in the photoresponse is expected when the incident photon has an energy equal to the band gap of the crystal (92). A threshold for intrinsic photoconductivity then occurs. Photons of higher energy do not penetrate far into the surface because of the strong absorption of the crystal and the photoresponse usually decreases (55). Our results indicate, therefore, a value for the photoconducting band gap of SrO of 5.3 eV, which is somewhat lower than has been given previously (20). It appears that the exciton bands at 5.7 eV and 5.8 eV (84) are about 0.5 eV above the bottom of the conduction band.

In conclusion, we see that the F^+-center in SrO produces photoconductivity in a manner very similar to that of the F-center in the alkali halides, which in light of the net positive charge on the defect is in some ways surprising. It also appears that the theoretical model being used by Wood and Wilson to calculate the electronic structure of this defect is a good approximation of the system since their results are in substantial agreement with our experimental results. We now move on to the experimental results obtained for the F- and F^+-centers in CaO which will be presented in the following chapter.

CHAPTER V

EXPERIMENTAL RESULTS AND DISCUSSION: CALCIUM OXIDE

I. Introduction

In the preceding chapter, it was shown that F^+-centers in electron irradiated SrO (27,82) produce photoconductivity in a way reminiscent of F-centers in alkali halides (55). In this chapter the results of experimental investigations of the electronic structure of both F and F^+-centers in CaO (26,83) will be presented. CaO is the most convenient alkaline earth oxide to use for this type of investigation because it can be obtained comparatively pure and because the F and F^+ optical bands are well separated in energy (7). Photoconductivity measurements on MgO (80,87) and BaO (81) containing F-type centers are more difficult to interpret because the F and F^+ bands overlap in these materials. The F^+ band in CaO has been observed in samples which had been neutron irradiated (29,38,93), proton irradiated (83), electron irradiated (25,26,83) or additively colored (38,93). In CaO the asymmetric F^+ absorption band is located at 3.65 eV (340 nm) with a corresponding luminescence band centered at 3.35 eV (370 nm) (25). The F band has been observed in additively colored crystals (40) and in crystals colored accidentally during growth (41) as well as in electron or proton irradiated samples (26,83). The F absorption band is located at 3.1 eV (400 nm) with luminescence bands at about 2.05 eV (605 nm) (41,47).

Detailed measurements which yield information about the vibronic properties of the F^+-center have been made on MgO and CaO (7). Similar absorption studies have been made on the F^+-center in SrO (49). The F^+ band in CaO shows a clearly resolved zero-phonon line at 355.7 nm and associated vibronic structure (46,48,68). None of the other oxide F-type bands have yet been found to show vibronic details.

Detailed calculations of the electronic structure of the F-center in alkaline earth oxides have been presented recently (57,58,59) including an account of lattice relaxation effects. These results can be compared satisfactorily with the results presented here. No such detailed calculations for F^+-centers are currently in the literature. It shall be seen below, however, that F^+-centers in CaO appear to behave, so far as our experiments were concerned, similarly to F^+-centers in SrO and F-centers in alkali halides.

II. Irradiation and Optical Absorption

Samples of CaO about 10 x 5 x 2 mm in dimensions were cleaved from a boule (S/N 120-021172) which was supplied to us by Dr. Y. Chen of Oak Ridge National Laboratory. Crystals of nominally 99.5% pure CaO about 10 x 5 x 2 mm in dimensions were also obtained from W. & C. Spicer, Ltd. For reasons which will be explained in Section III, the Spicer samples did not prove satisfactory for our work. Unless specifically indicated otherwise, all experiments described in this chapter were performed on CaO samples from ORNL.

The optical density of the unirradiated CaO crystals at 77 K, illustrated in Figure 40, increased from approximately 0.1 at 2.0 eV to nearly 2 at 6.0 eV with no obvious absorption peaks in the spectrum.

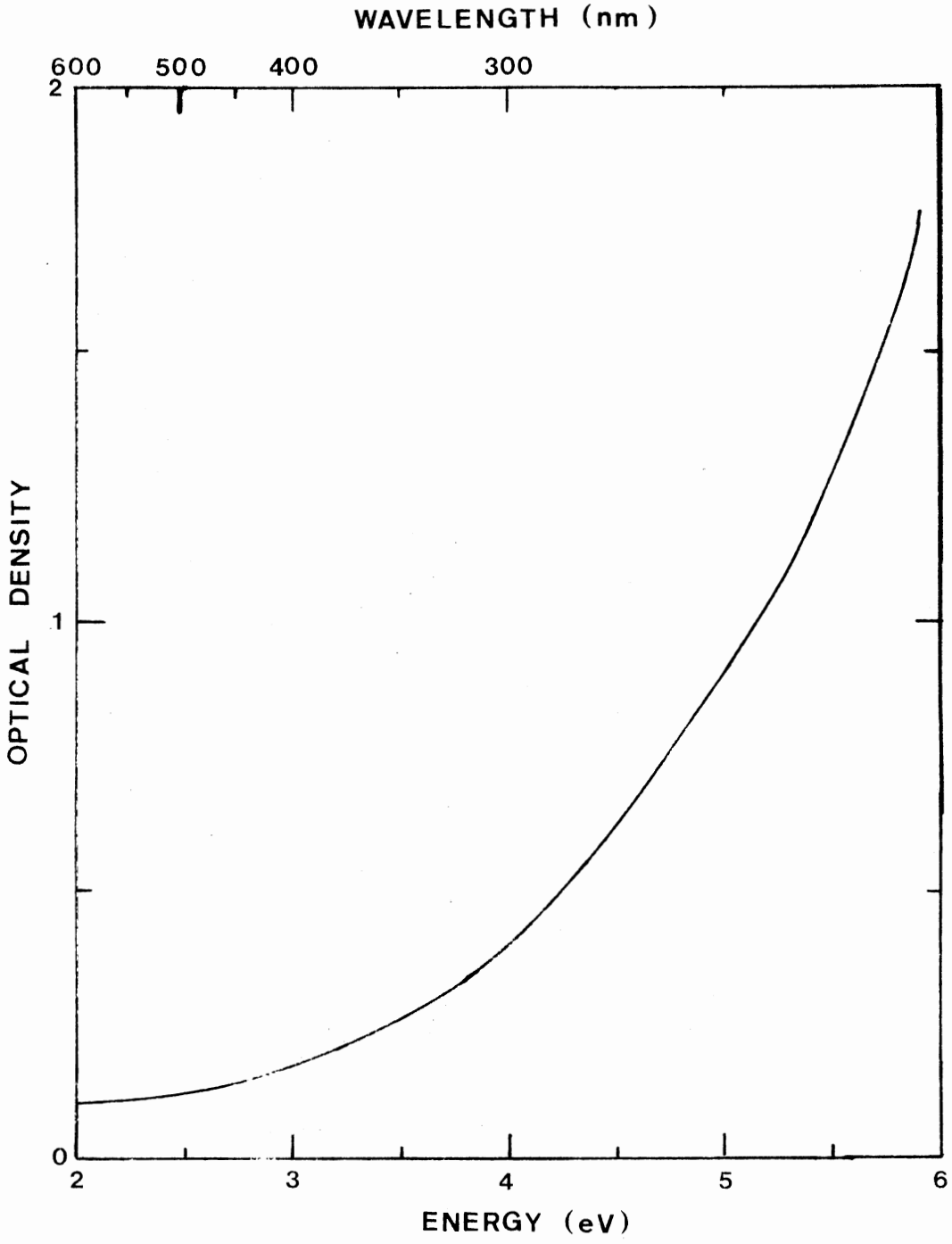

Figure 40. Optical Density of Unirradiated ORNL-CaO at 77 K

This is similar to results reported by Bessent et al. (29) and the optical density of the unirradiated sample shows the familiar increase as the incident photon energy approaches the band gap energy of CaO (~7 eV) (18).

The optical density of CaO which had been irradiated at room temperature with a ^{60}Co gamma source showed no differences when compared to that of the untreated crystal. As was the case for SrO in the preceding chapter, gamma-irradiation alone proved ineffective in producing F-type defects in CaO.

The absorption spectrum measured at 77 K of an electron irradiated sample is shown in Figure 41. The crystal was irradiated at 77 K with 1.5 MeV electrons to a dose of approximately 5×10^{17} electrons/cm^2. The irradiation produced the asymmetric F^+ band located at 3.65 eV and a small F band at 3.1 eV. The F^+ band has an optical density of about 0.26 compared to an optical density of about 0.02 for the F band. Note also the presence of a resolved zero-phonon line at 355.7 nm on the F^+ band. As mentioned above, CaO stands alone among the oxides in showing such vibronic structure although the F^+ band in SrO does have the asymmetric shape.

In Chapter IV we showed that electron irradiation of SrO, although generally ineffective in producing enough F-type defects to give rise to an F or F^+ absorption band, actually did yield F^+-centers as evidenced by our photoconductivity measurements. This information, in conjunction with the above absorption spectrum for electron irradiated CaO, seems to indicate that, for at least some initial period, electron irradiation of the alkaline earth oxides produces predominantly F^+-centers rather than F-centers. After sufficient electron irradiation, F-centers are expected

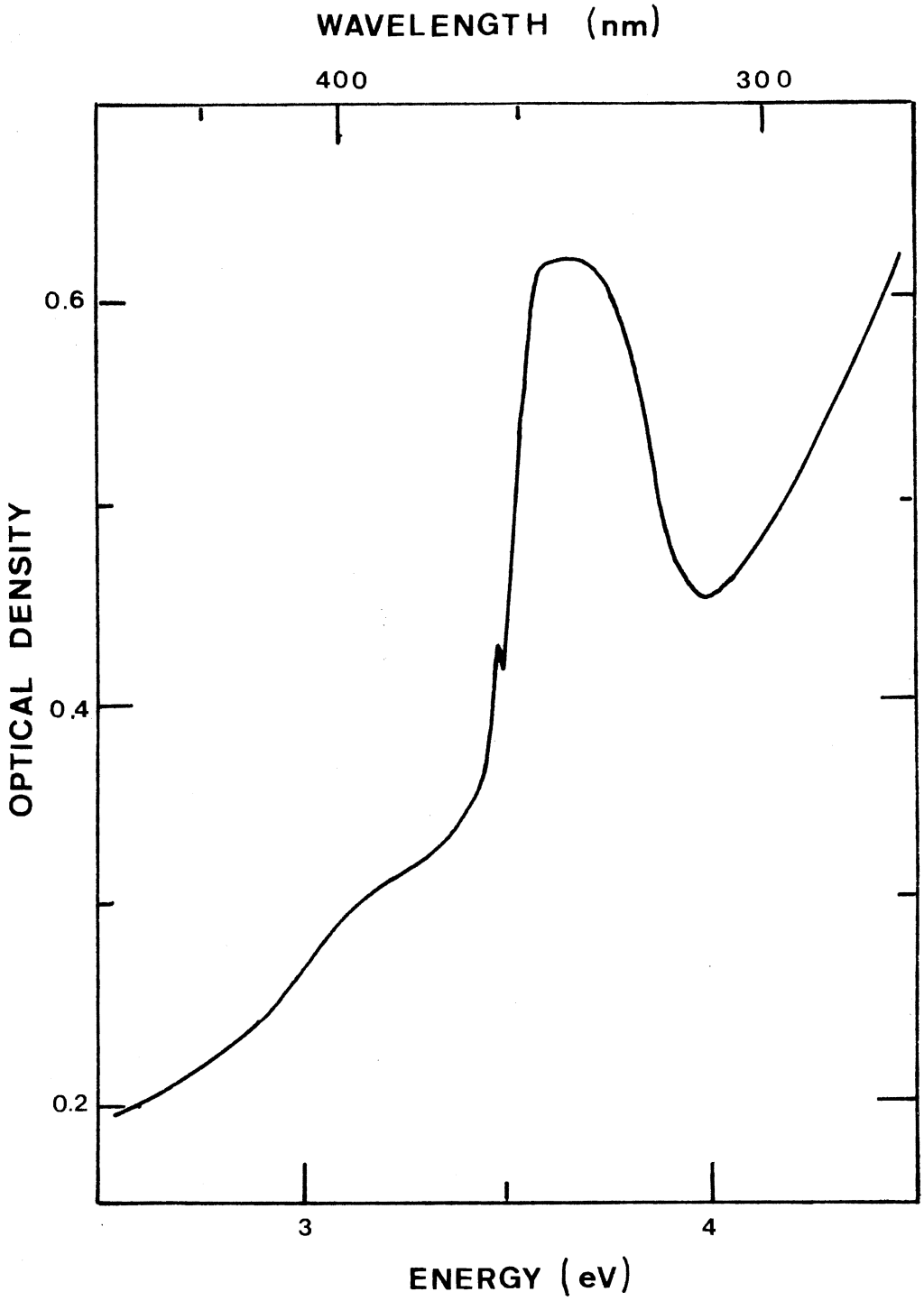

Figure 41. Optical Density Measured at 77 K on a CaO Sample Which Had Been Irradiated at 77 K With 1.5 MeV Electrons to a Dose of about 5 x 10^{17} Electrons/cm^2

to be more numerous than F^+-centers (1). Apparently, even though the F^+-center is a deep trap, and should therefore attract a second electron, there must be other deep traps in the crystal which compete for the electron. As these traps are filled, the second electron begins to occupy the F^+-center. The formation of F^+-centers should then saturate accompanied by a corresponding increase in the formation of F-centers with the final result that F-centers would be more numerous than F^+-centers. In our electron irradiations, however, we were never able to reach or even approach the point at which F-centers were more prevalent than F^+-centers. A study of F- and F^+-center concentration versus irradiation dose could bear further investigation.

Figure 42 illustrates the optical density of the F^+ band in an electron irradiated sample of CaO measured at four different temperatures. Note the zero-phonon line at 355.7 nm and the asymmetric shape of the band. The integrated absorption of the F^+ band is nearly independent of temperature and the peak of the F^+ band shifts to slightly lower energies with increasing temperature. The thermal expansion of the lattice contributes in part to this shift.

Figure 43 shows the optical density measured at 77 K for a CaO sample irradiated at 77 K to a dose of approximately 5.6×10^{16} protons/cm^2. The main features introduced by the irradiation are the asymmetric F^+ band located at 3.65 eV having an optical density of about 1.7 and the F band, located at 3.1 eV with an optical density of about 0.5. This behavior is in contrast to that described in the previous chapter for SrO in which only the F^+ band was measurable following a dose of 2×10^{17} protons/cm^2 at 195 K. Proton irradiation at 77 K seemed to introduce the F-type bands in CaO at about 2-3 times the rate of irradiation at

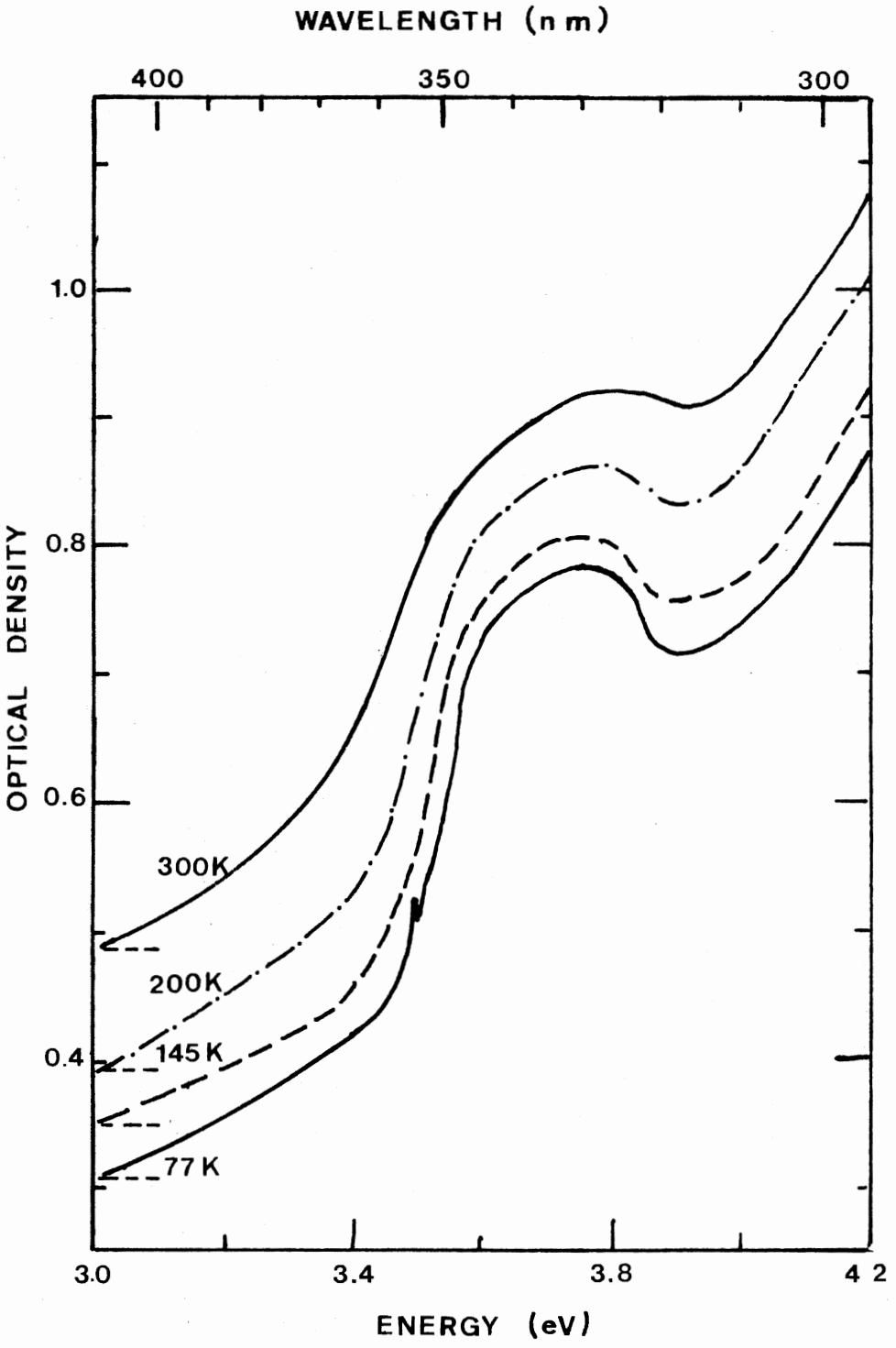

Figure 42. The Optical Density of the F^+ Band in an Electron Irradiated Sample of CaO Measured at Various Temperatures. The curves have been shifted upward to avoid overlap

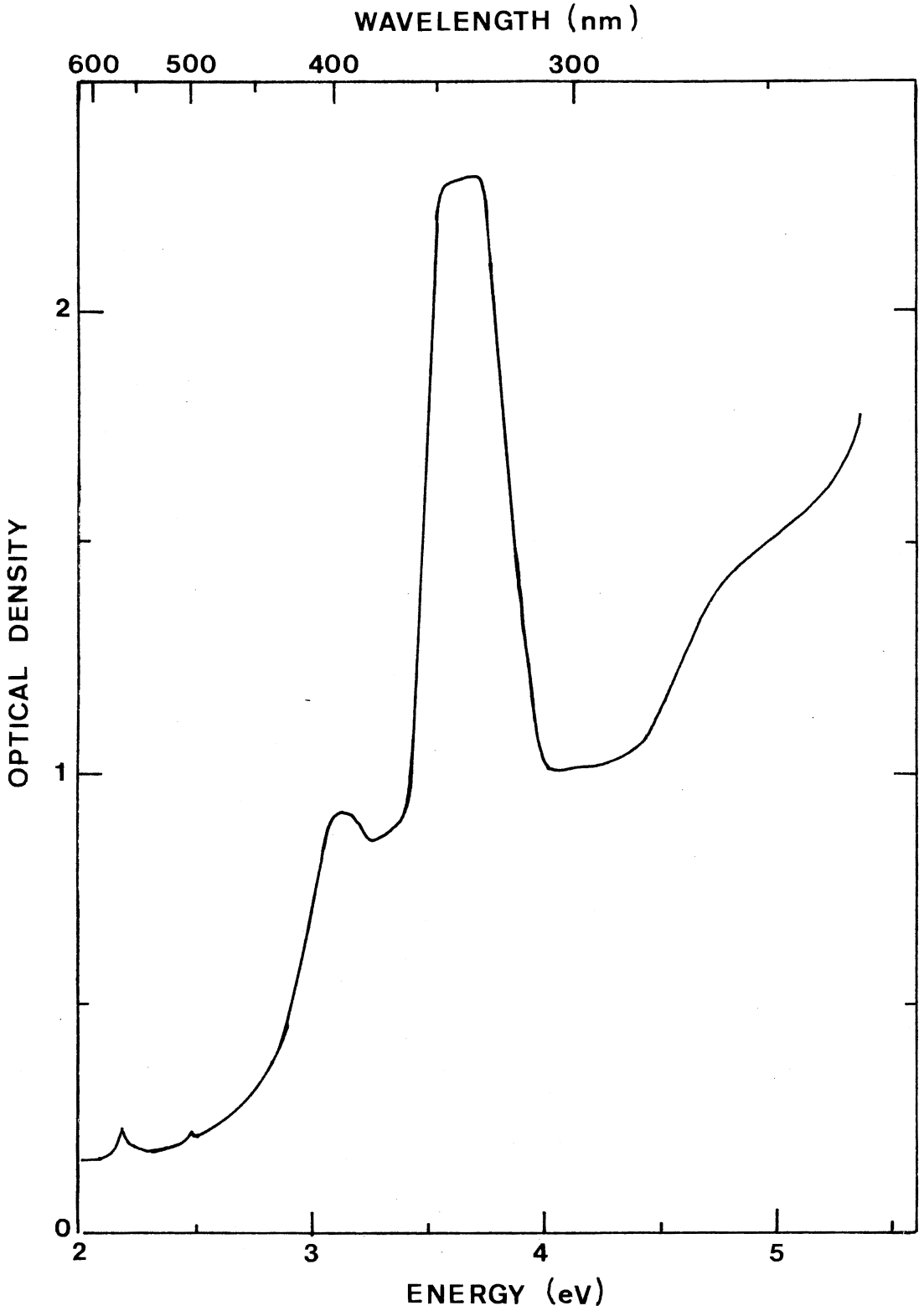

Figure 43. Optical Density Measured at 77 K for a CaO Sample Irradiated at 77 K With 1.5 MeV Protons to a Dose of About 5.6×10^{16} Protons/cm^2

195 K.

Although proton irradiation is more efficient than electron irradiation in producing F-type defects in CaO, the electron irradiated samples gave more satisfactory photoconductivity results since these samples have principally single defects throughout the bulk of the crystal. Electron irradiated samples were therefore used in the photoconductivity measurements reported here. Fluorescence measurements on the F^+-centers in CaO were made on electron irradiated samples and on the F-centers using additively colored samples from Oak Ridge National Laboratory.

III. Photoconductivity

The main part of the experimental results which remain to be described in this chapter concern the photoresponse of F-type centers in CaO. The temperature dependence of the luminescence intensity and the lifetime of the fluorescence from these centers as they relate to the photoconductivity were also investigated. The spectral dependence of the photoresponse will be described in this section and the temperature dependence of the photoresponse and fluorescence will be presented in the following section. The effects of gamma-irradiation and optical bleaching of the samples will be discussed in Section V.

Figure 44, curve a, illustrates the photoresponse, $\eta\omega_o$, of an untreated sample of CaO at 77 K over the spectral range from 2.5 to 4.5 eV. It can be seen that the photoresponse was immeasurably small until the incident photon energy was at least 3.4 eV and that there was, then, a photoresponse band located near 3.8 eV. Subsequent γ-irradiation of the sample at room temperature for several hours had little effect, except that the photoresponse below 3.0 eV was enhanced, although γ-irradiation

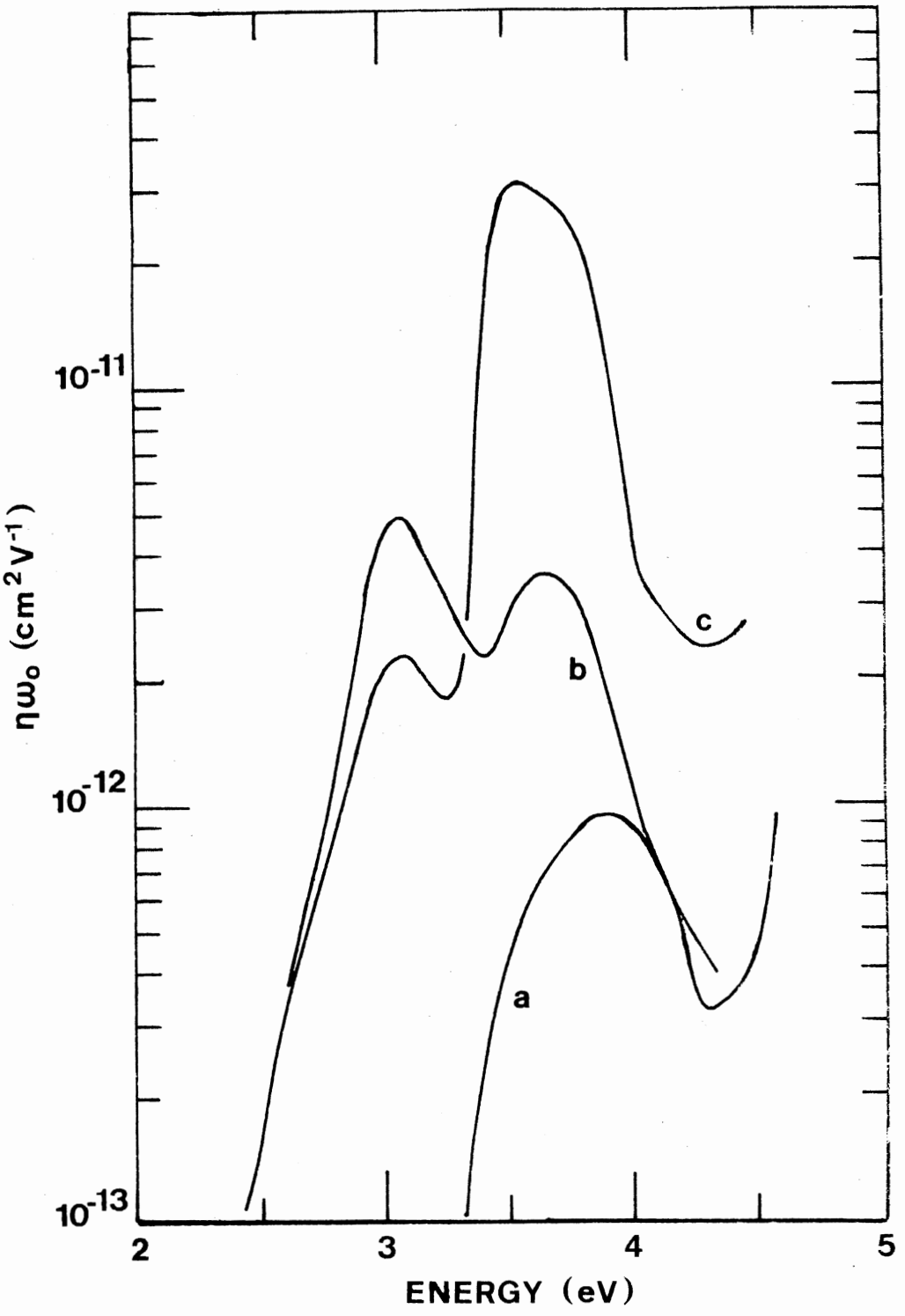

Figure 44. Spectral Dependence of the Photoresponse, $\eta\omega_o$, for CaO. An untreated sample measured at 77 K, curve a; a sample which had been irradiated at 77 K with 1.5 MeV electrons to a dose of about 5 x 10^{17} electrons/ cm^2 and measured at 77 K and 300 K, curves b and c, respectively

alone did not introduce any prominent photoresponse bands into the sample.

Figure 44, curves b and c, shows the photoresponse of a sample of CaO following irradiation at 77 K with 1.5 MeV electrons to a dose of approximately 5 x 10^{17} electrons/cm^2, and subsequent γ-irradiation at room temperature for about thirty minutes just prior to being mounted in the cryostat. The effect of γ-irradiation was to enhance the F-center photoresponse relative to the F^+-center photoresponse as shall be discussed in Section V. Curves b and c show the photoresponse of the same sample measured at 77 K and 300 K, respectively. The main features in the photoresponse were the nearly temperature independent band centered at 3.1 eV and the temperature dependent band near 3.65 eV. Electron irradiation is known to introduce both F^+- and F-centers in CaO (1) and by comparing the spectral dependence of the photoresponse to the optical absorption we shall show below that the photoresponse bands at 3.1 and 3.65 eV originate from F- and F^+-centers, respectively.

The photoresponse at 77 K of a CaO sample irradiated at 77 K to a dose of about 5 x 10^{16} electrons/cm^2 is shown in Figure 45, curve a. Figure 45, curve b, shows the photoresponse at 77 K of a sample which was irradiated at 77 K to a dose of about 3 x 10^{16} protons/cm^2. The samples used for the measurements shown in Figure 45 were γ-irradiated at room temperature just prior to mounting in the photoconductivity cryostat. It can be seen that the spectral dependence of the photoresponse is similar for both the electron and proton irradiated samples and that both exhibit bands located at 3.1 and 3.65 eV. Upon inspection of Figure 45, curves a and b, and Figure 44, curves b and c, in conjunction with Figure 41 or 43, one is immediately drawn to the tentative conclusion

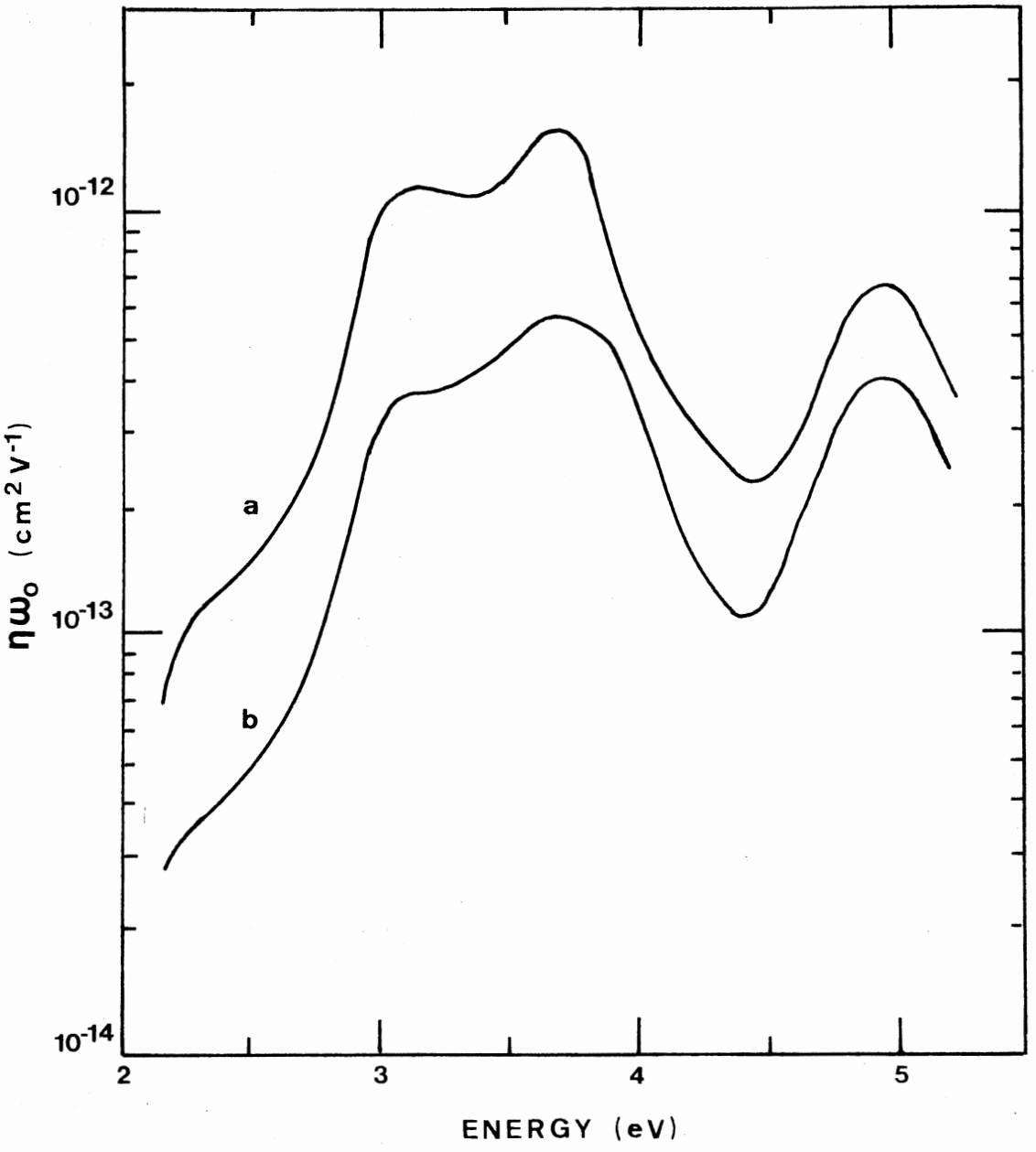

Figure 45. Spectral Dependence of the Photoresponse of CaO at 77 K: a Sample Irradiated at 77 K With 1.5 MeV Electrons to a Dose of About 5 x 10^{16} Electrons/cm^2, Curve a; and a Sample Irradiated at 77 K With 1.5 MeV Protons to a Dose of About 3 x 10^{16} Protons/cm^2, Curve b

that the photoresponse bands at 3.1 eV and 3.65 eV originate from F- and F^+-centers, respectively. However, because of some overlap of the absorption bands, a correlation between the photoresponse and absorption bands is more difficult for the F- and F^+-centers in CaO than for the F^+-center in SrO. In addition to these bands the absorption spectrum has a band at 4.8 eV which is also apparent in the photoresponse. This band may be associated with anion-cation vacancy pairs which have been observed optically in deformed CaO (85,94).

It can be seen in Figure 44, curve c, that the asymmetric and temperature dependent band located at 3.65 eV is by far the most prominent feature in the photoresponse of the electron irradiated sample at 300 K. This band can be shown to be due to F^+-centers by comparing it to the intensity of the light absorbed into the F^+ band by the same crystal. The continuous curve at the top of Figure 46 shows the photoresponse at 300 K of an electron irradiated sample in which the 3.1 eV band (F band) was further diminished by optical bleaching (see Section V). The broken curve at the top of Figure 46 shows the spectral dependence of the light absorbed in the same sample. The broken curve is, therefore, proportional to $[1-\exp(-\alpha d)]$ where α is the absorption coefficient of the F^+ band at 300 K. Assuming that the reflectivity of the sample and η_T remained constant over the F^+ band, the close agreement between the two curves, which were normalized at 3.7 eV, shows that the photoconductivity at 300 K originated from F^+-centers. However, the photoresponse of the sample and the spectral dependence of the absorption in the F^+ band at 77 K are not similar, as can be seen at the bottom of Figure 46. Since there is no reason to suppose that the temperature dependence of η_T was a function of wavelength across the F^+ band, we conclude that the

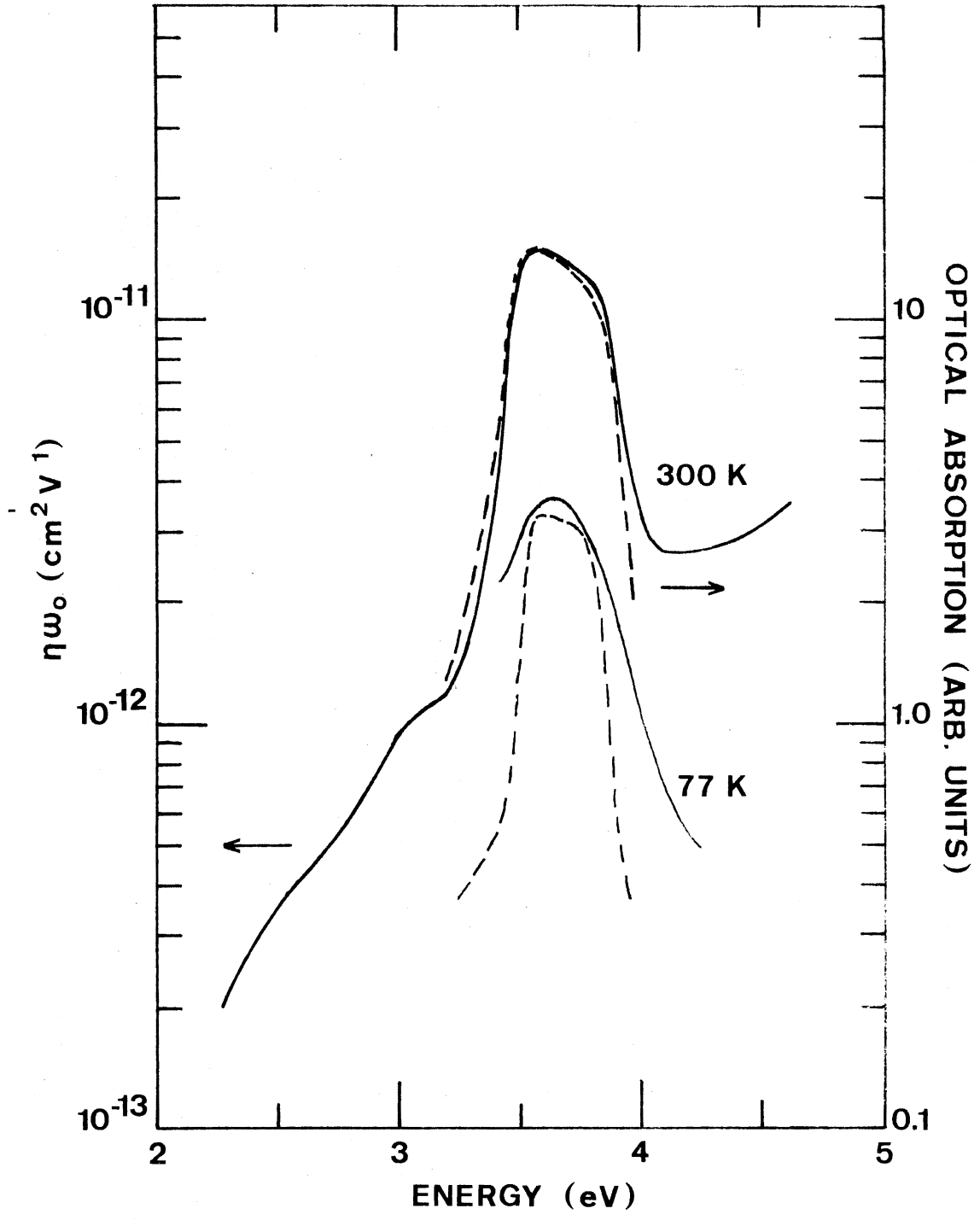

Figure 46. Comparison of the Spectral Dependence of the Photoresponse, $\eta\omega_o$, in Electron Irradiated CaO (Continuous Curves) and the Optical Absorption of the F^+ Band in the Same Crystal (Broken Curves) at 77 K and 300 K

photoconductivity of the sample at 77 K in the region of 3.7 eV originates mainly from an unidentified impurity.

A similar comparison cannot, however, be done for the F-center in CaO because although the photoresponse band centered at 3.1 eV in Figure 44, curve b, appears similar to the F band, it is partially masked by the presence of the 3.7 eV band and the background photoresponse. A more indirect method must therefore be used to verify that the photoresponse band located at 3.1 eV is due to the F-center in CaO. Using the fact that the F band photoresponse could be optically bleached at 77 K (see Section V), the photoresponse of the F band was obtained over a comparatively wide spectral range. In Figure 47, curve a, is shown the photoresponse at 77 K of a sample which had been irradiated to a dose of approximately 3×10^{17} electrons/cm^2. Figure 47, curve b, shows the photoresponse of the same sample after being bleached for 2 hours at 77 K with 3.1 eV light from a xenon lamp. As well as destroying the F band photoresponse, bleaching also reduced the photoresponse generally between 2.5 eV and 4.5 eV. In order to obtain the F band photoresponse, curves a and b were normalized at 4.5 eV and then subtracted to obtain the broken curve in Figure 47. The broken curve, which represents the spectral dependence of the F-center photoresponse, has a peak at 3.1 eV and a half-width of about 0.5 eV. This band was compared to and was found to be similar to the F band in additively colored CaO as reported by Modine (42).

The Spicer CaO crystals gave results which were basically similar to those obtained with the ORNL samples. A comparison of the photoresponse obtained on electron irradiated samples from W. & C. Spicer and Oak Ridge National Laboratory is illustrated in Figure 48. Curve a

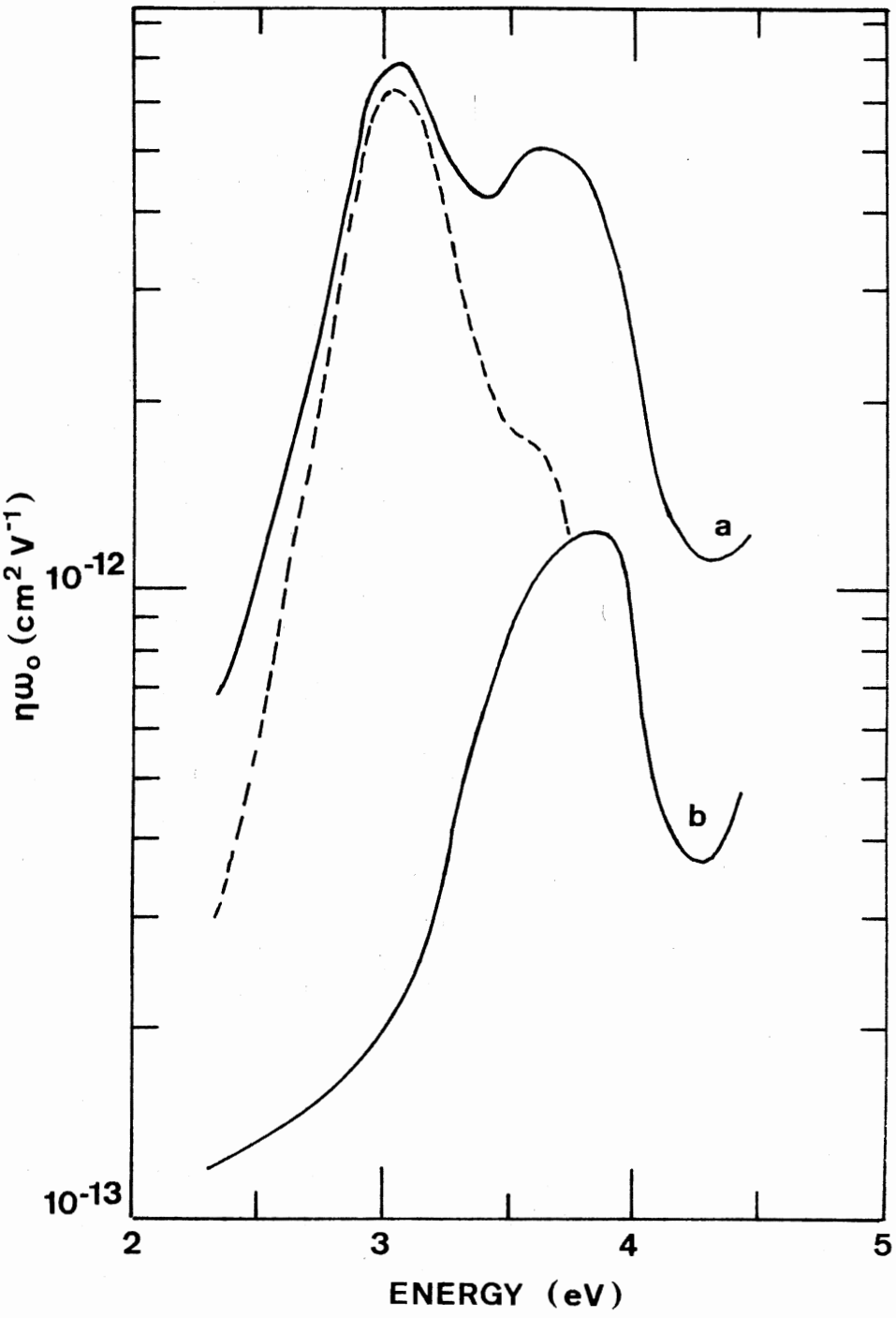

Figure 47. Comparison of the Spectral Dependence of the Photoresponse, $\eta\omega_o$, in Electron Irradiated CaO Before and After Illumination in the F Band for Two Hours at 77 K With 400 nm Light, Curves a and b, Respectively. All measurements were made at 77 K. The broken curve, obtained as described in the text, represents the spectral dependence of the F band photoresponse

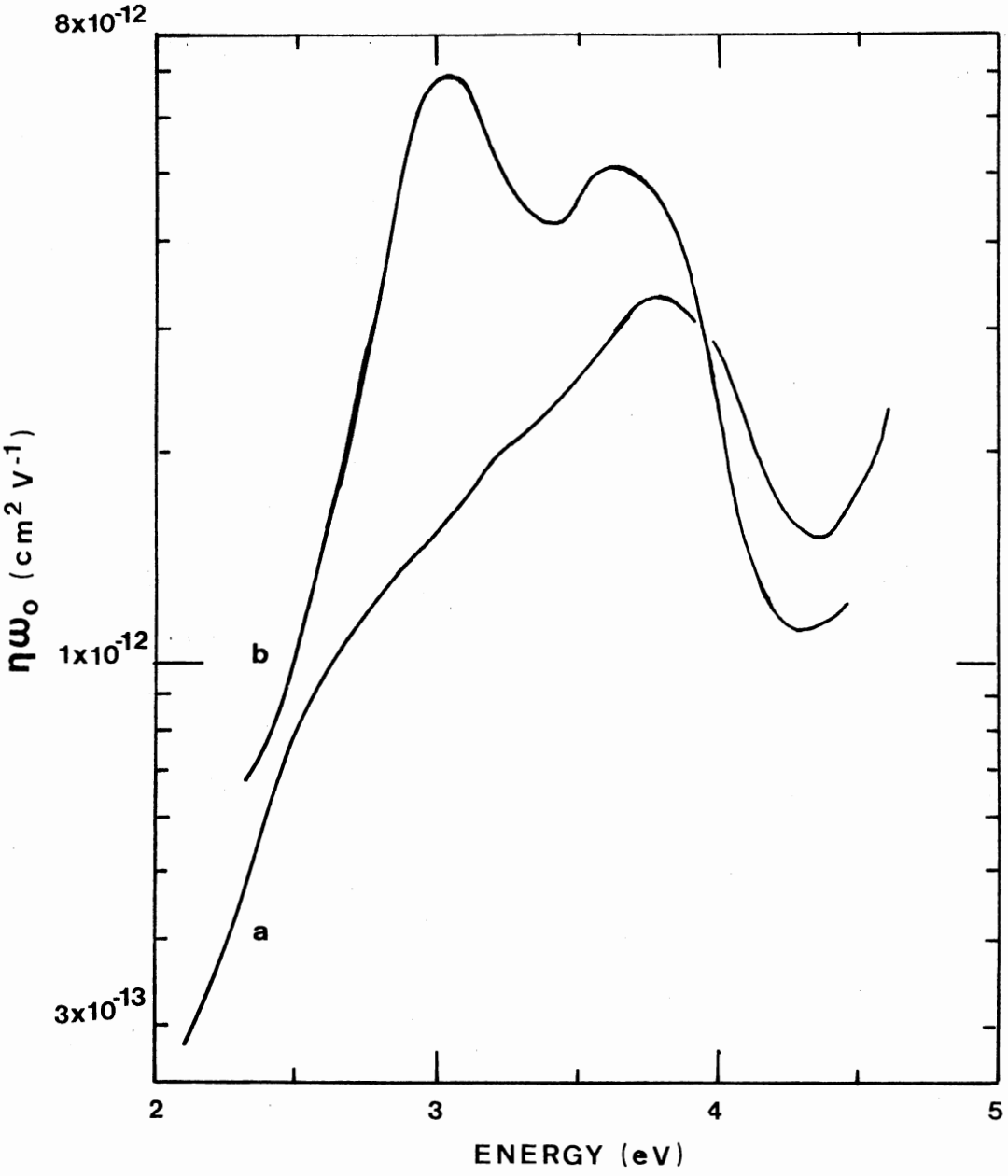

Figure 48. Spectral Dependence of the Photoresponse of CaO at 77 K Irradiated With 1.5 MeV Electrons: Curve a) Spicer Sample Irradiated at 195 K to a Dose of About 1 x 10^{18} Electrons/cm^2; Curve b) ORNL-sample Irradiated at 77 K to a Dose of About 3 x 10^{17} Electrons/cm^2

shows the photoresponse measured at 77 K on a Spicer CaO sample which had been irradiated at 195 K to a dose of about 1 x 10^{18} electrons/cm^2 and had an optical density of about 0.04. (This irradiation was performed with the sample in the optical cryostat in front of the Van de Graaff extension tube). Curve b is the photoresponse at 77 K on an ORNL sample which had been irradiated at 77 K to a dose of about 3 x 10^{17} electrons/cm^2 and had an optical density of about 0.1. Both crystals received an additional 30 minute γ-irradiation at room temperature immediately prior to photoconductivity measurements. One can readily see that the results for the Spicer and ORNL samples are similar but the background photoresponse produced by irradiation of the Spicer samples was relatively larger and tended to mask the F and F^+ bands which were more easily observed in the ORNL samples. Consequently, since this "masking" further complicated the analysis of data, the experiments reported here were performed on CaO samples from ORNL.

The photocurrent originating from the 3.1 eV and 3.65 eV bands reached its maximum value within a fraction of a second (the response time of the detection system) and was constant with constant illumination. The photocurrent from these bands also fell to zero equally fast upon removal of the incident light. The photocurrent at 3.1 eV and 3.65 eV was directly proportional to the applied electric field up to 1500 V/cm and also to the incident light intensity as the intensity was varied by a factor of 70. These measurements, accurate to within an experimental error of a few percent, are illustrated in Figure 49. An applied electric field of about 500 V/cm was usually used during the photoconductivity experiments.

Using the technique described in the previous chapter, due to Peria

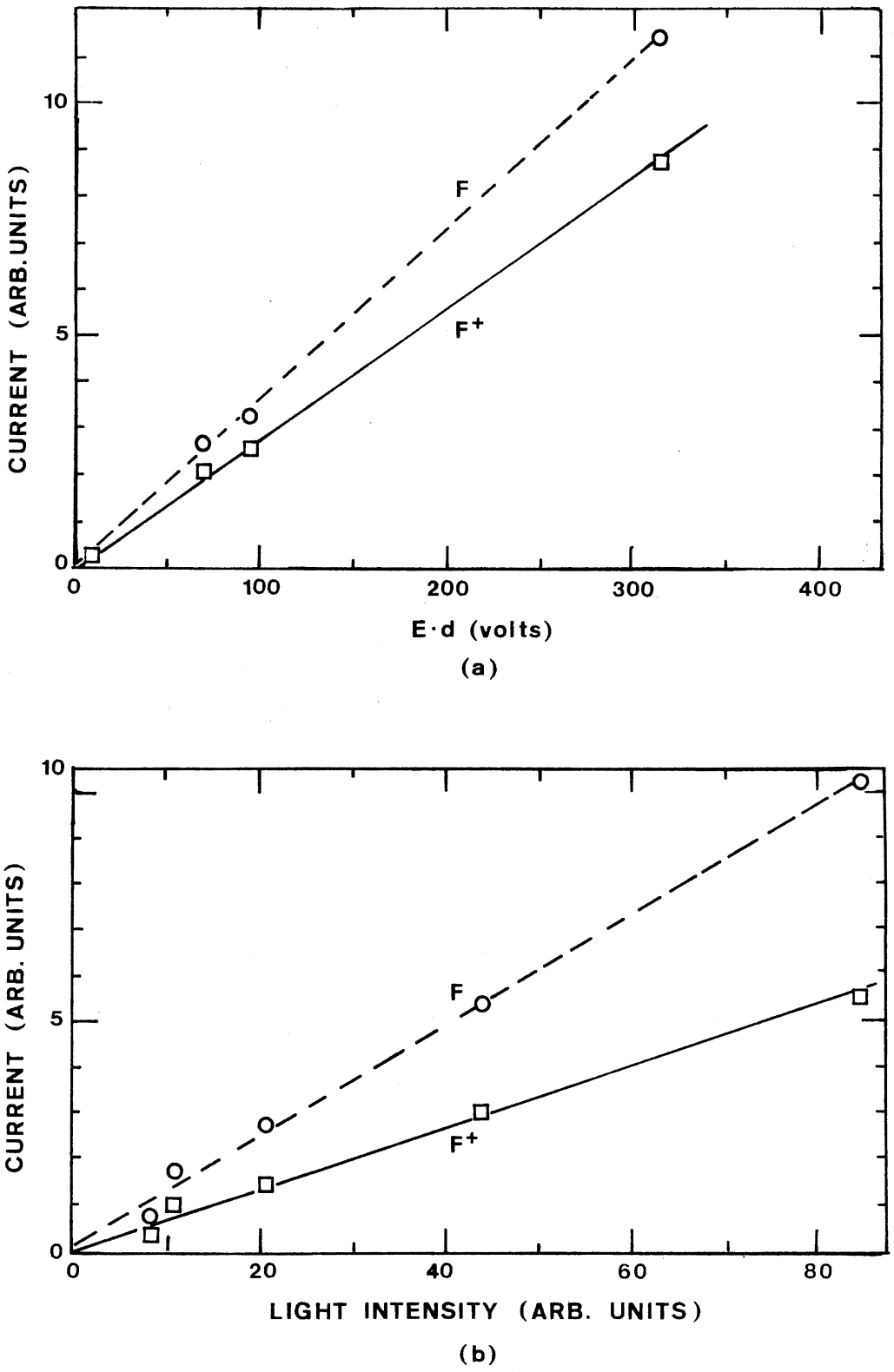

Figure 49. The Photocurrent at 3.1 eV (F-center) and 3.65 eV (F^+-center) was Directly Proportional to the Electric Field (a) and the Incident Light Intensity (b)

(87), our results indicate the sign of the charge carrier to be negative for the 400 nm F-band in CaO, as expected. We were unable, however, to determine satisfactorily the sign of the charge carrier for the 340 nm F^+ band in CaO using this technique. As will be seen in Section IV, the F^+-centers are not effectively fully ionized until a temperature of about 300 K is reached. At this temperature, however, the dark current is also large and accurate photocurrent measurements are comparatively difficult to make.

IV. Temperature Dependence of Photoconductivity and Fluorescence

It was seen in Figure 44 that the F band photoresponse was nearly independent of temperature between 77 K and 300 K, whereas the F^+ band photoresponse increased significantly over the same temperature range. The detailed temperature dependence of the F and F^+ band photoresponse between 65 K and 350 K is shown in Figure 50. The different symbols in Figure 50 indicate measurements made during different experiments, which were made necessary in part by the sensitivity of the F band photoresponse to bleaching. Between individual experiments the sample was γ-irradiated at room temperature for about thirty minutes in order to restore the F band photoresponse as we discuss below in Section V.

In a separate experiment, the thermally stimulated or dark current was also measured over the temperature range from 77 K to 250 K. Available traps had been filled by ultraviolet illumination of the sample at 77 K in the absence of an electric field. With an electric field across the crystal, the dark current was measured as the sample warmed. The small dark current rose sharply in the region of 230 K. In spite of

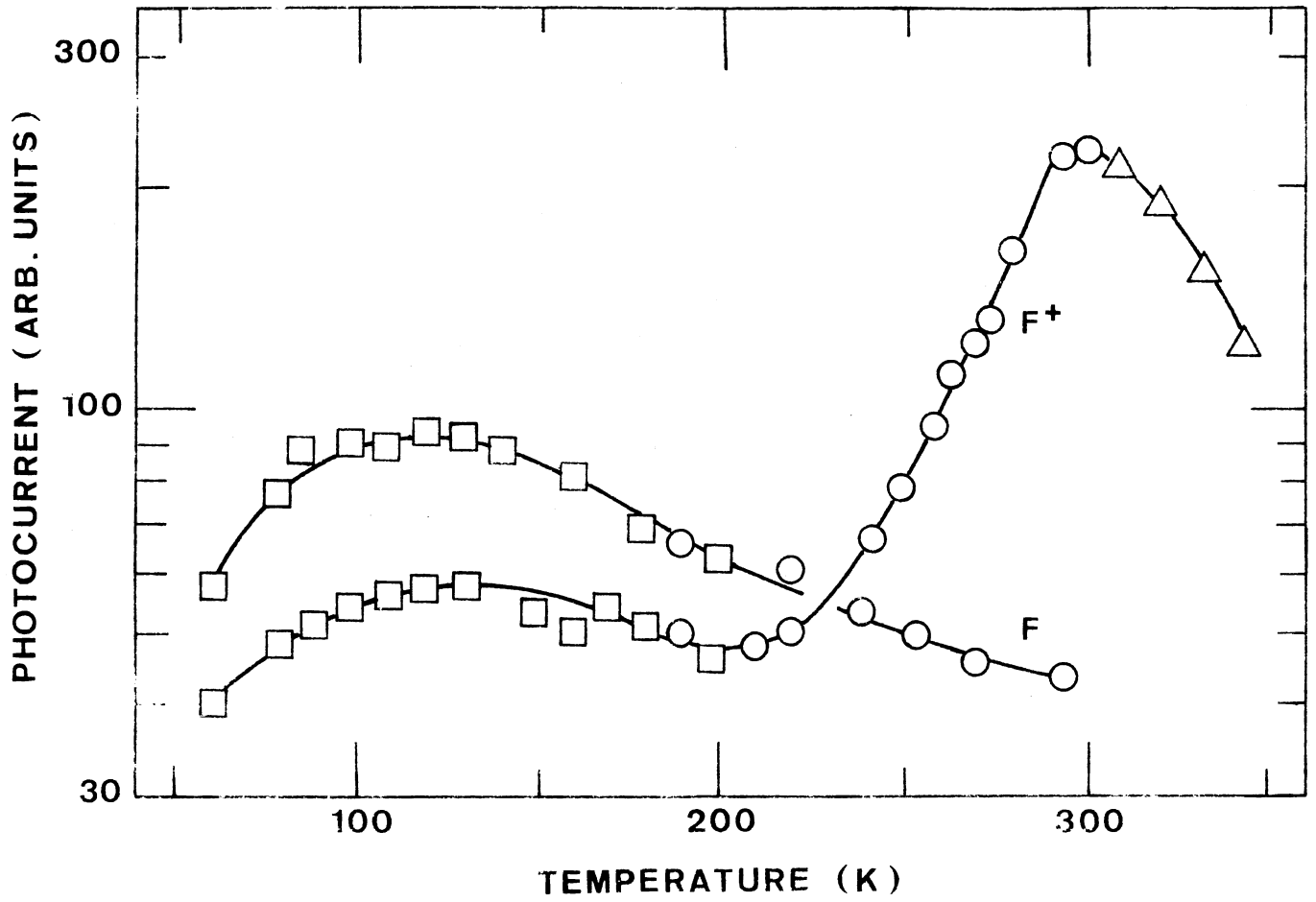

Figure 50. Temperature Dependence of the Photocurrent Produced by the F and F^+ Bands in CaO. The measurements were made with an incident photon energy of 3.1 eV and 3.65 eV, respectively. The various symbols indicate data collected in separate experiments

this large dark current, the increasing photocurrent from the F^+-center was markedly noticeable and was easily obtained as a function of increasing temperature.

Below about 210 K the photoresponse in the region of 3.7 eV originated mainly from an impurity band which was discussed in Section III, and it was only above 230 K that the F^+ band was recognizable. The sharp increase in F^+ band photoresponse with increasing temperature beginning at 210 K is indicative of a thermally assisted ionization. The possibility that this increase was due to a thermally extended range of the charge carriers (55) was ruled out because the photocurrent reached its maximum value within a fraction of a second (the response time of the detection system) and fell to zero equally fast upon removal of the incident light. If we assume that ω_o and the oscillator strength, f, remain independent of temperature over the interval of interest, the increase in the photoresponse between 230 K and 300 K is then due to an increasing quantum efficiency for thermal ionization.

In addition, the increase in F^+ photoresponse with increasing temperature was accompanied by a corresponding decrease in the fluorescence yield of the F^+ emission, as we will now show. The F^+ emission band shape was measured at various temperatures between 77 K and 350 K using the same sample that was used for the photoresponse measurements in Figure 50. The F^+ emission band measured at 77, 175, 243 and 346 K is illustrated in Figure 51. For these measurements the luminescence was excited with the 334.2 nm line from a mercury lamp. The F^+ emission band is centered at 3.35 eV (25) and M_o, which is proportional to the area under the emission curve, measures directly the number of centers involved in absorption and emission. M_o is expected to be temperature

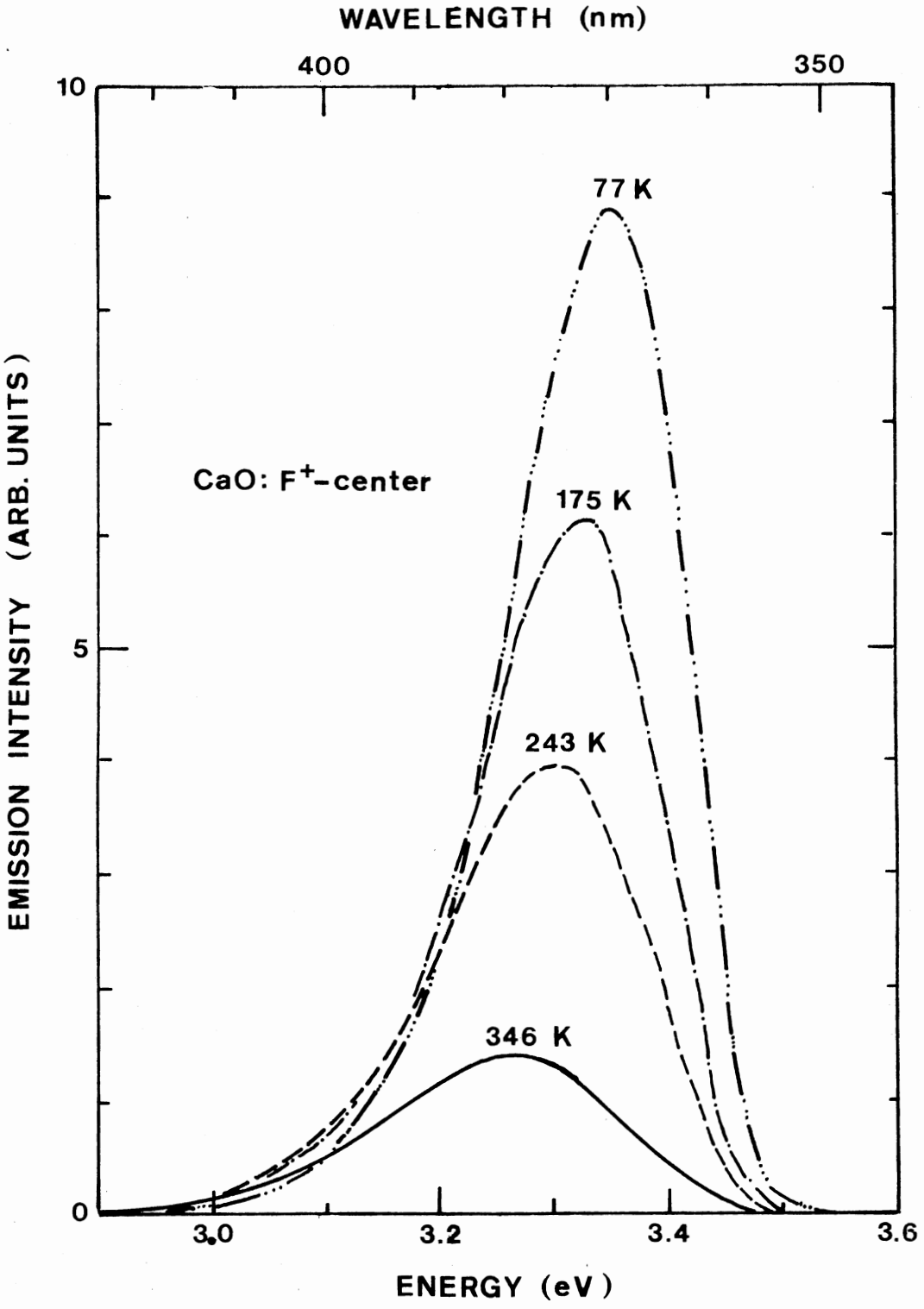

Figure 51. The F^+-emission Band in Electron Irradiated CaO Measured at Various Temperatures. The luminescence was excited with the 334.2 nm line from a mercury lamp

insensitive provided the quantum efficiency for fluorescence remains constant. The temperature dependence of the normalized zeroth moment, M_o, of the F^+ emission is shown in Figure 52. It can be seen that M_o remained constant at temperatures between 77 K and 120 K and then decreased continuously with increasing temperature up to 350 K, which was the maximum temperature obtained. The electron in the relaxed excited state of the center has two principle competing modes of escape: 1) radiative decay to the ground state (fluorescence) and 2) thermal ionization of the charge carrier (photoconductivity). For the simple two level model developed in Chapter II, the fraction of excited centers which decay by luminescence is given by η_R (Equation II-25) and the fraction which decay by thermal ionization is given by η_T (Equation II-24), such that $\eta_R + \eta_T = 1$. Only one excited state is considered and other modes of escape are neglected. When taken in conjunction with the photoresponse data, Figure 50, which represents an increase in the quantum efficiency for thermal ionization, we see that the decrease in M_o then represents a decrease in the quantum efficiency for the F^+ fluorescence. Notice that the increase in free electron yield from F^+-centers which should be apparent in Figure 50 between 120 K and 200 K was masked by the temperature independent photoresponse from the 3.7 eV impurity band. The results presented in Figure 52 are in substantial agreement with those of Evans et al. (46) which were obtained from neutron irradiated CaO. These samples contained a preponderance of F^+-centers. However, our results are somewhat different from those obtained by Henderson et al. (25) on heavily electron irradiated CaO. Henderson et al. found an increase in M_o of about 20% between 100 K and 230 K, followed at temperatures above 230 K by a decrease in M_o similar to that

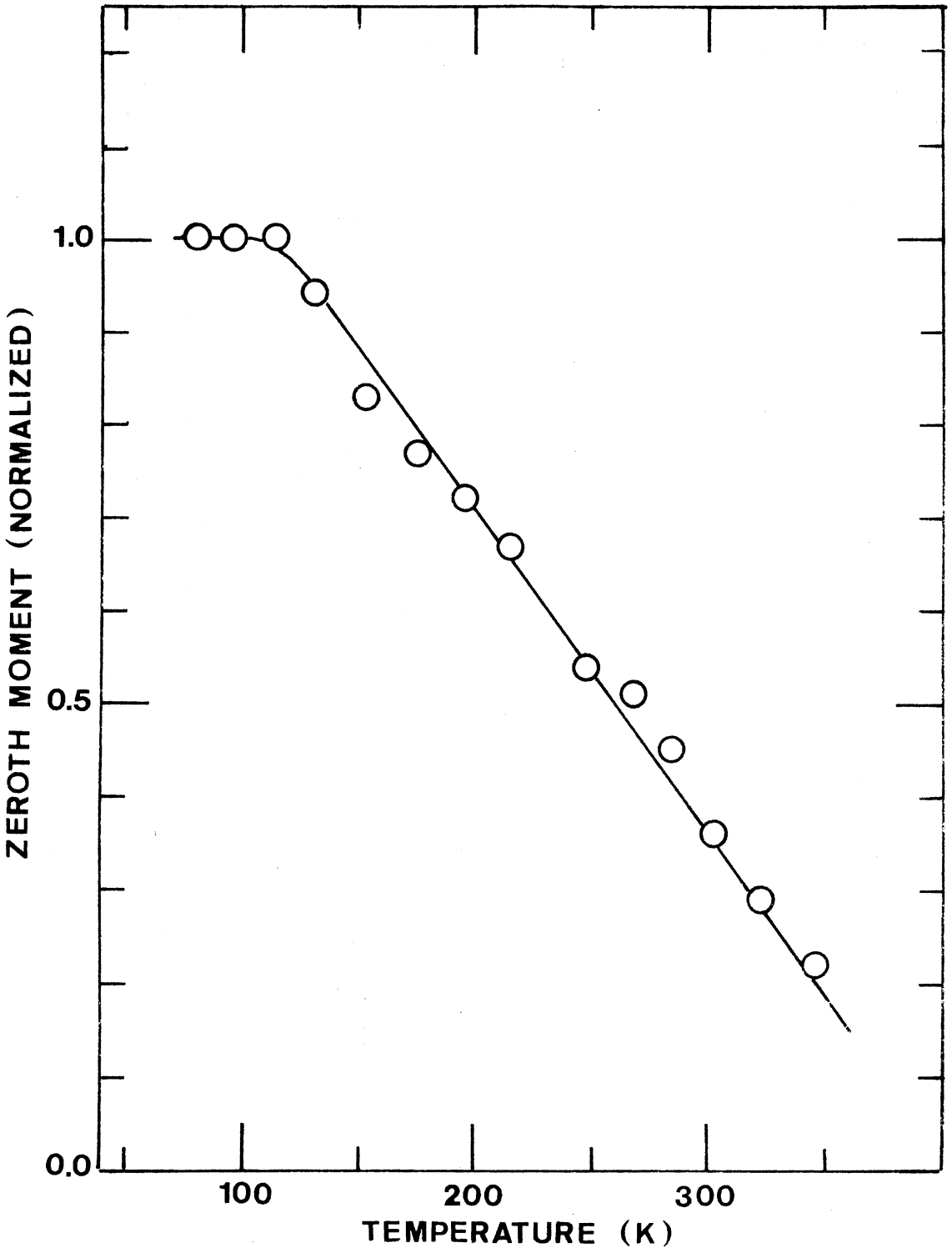

Figure 52. Temperature Dependence of the Zeroth Moment, M_o, of the F^+ Luminescence Band in Electron Irradiated CaO. The measurements were made on the same sample used in obtaining Figure 50

reported here. It is though that the increase in M_o with increasing temperature occurred because of conversion of F-centers to F^+-centers by the exciting light (25,95). A conversion of this kind has been observed by Kemp et al. (93) in additively colored CaO and by Chen et al. (35) in electron irradiated MgO. In our samples, however, the concentration of F-centers was small (see Section V) and any F to F^+ conversion which occurred would not significantly increase the concentration of F^+-centers.

Considering the results shown in Figure 50 for the F-center photoresponse, we see that as the temperature increases from 65 K to 300 K the photoresponse remains fairly insensitive to this temperature change except for a gradual decrease, due in part to bleaching of the F-centers. There is no indication of thermal ionization occurring in this temperature range. We may infer that if a sharp increase characteristic of thermally assisted ionization does occur, it does so at temperatures below 65 K which suggests that the relaxed excited state of the F-center lies very close to the bottom of the conduction band. These experimental results are consistent with the calculations of Wood and Wilson (58,59).

The F-center emission spectra was also measured over the temperature range from 77 K to 350 K. Several such curves are shown in Figure 53. The F-center luminescence was excited with the 365 nm line from a mercury lamp and the peak of the emisson occurred at about 2.05 eV (25, 41,47). The peak at about 2.15 eV which was also measured in our sample is thought to be associated with an impurity. These measurements, which were made on additively colored samples supplied to us by Dr. Y. Chen, were in close agreement with those obtained by Henderson et al. (25). M_o, for the F-emission, decreased from 1.0 at 77 K to about 0.1 at 250 K.

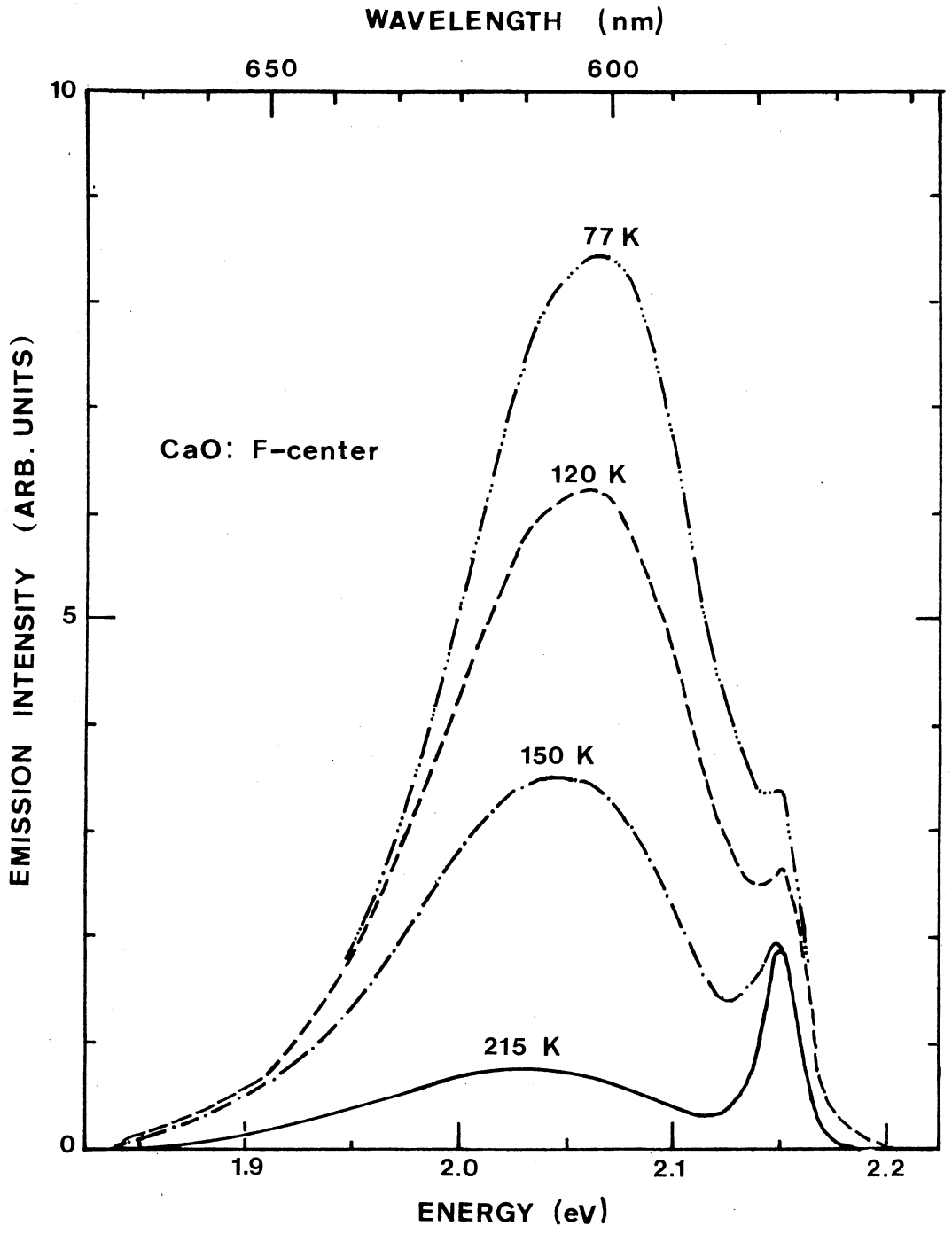

Figure 53. The F-emission Band in Additively Colored CaO Measured at Various Temperatures. The luminescence was excited with the 365 nm line from a mercury lamp

This decrease in M_o with increasing temperature was not matched by an increase in free electron yield (Figure 50) since the photoresponse remains essentially insensitive to temperature over the range reported here. This suggests that the luminescence from the F-band is quenched by a more indirect process. The data in Figure 50 will be further discussed in Section VI.

The fluorescence lifetime of the F^+ emission was measured on the same sample that was used for the photoresponse measurements, Figure 50, and the luminescence results, Figure 52. The emission decay curves were obtained in the temperature range from 77 K to 300 K. It was found that the fluorescence lifetime was at least as fast as the resolution of the apparatus, i.e., 30 nsec, over the whole temperature range from 77 K to 300 K, in a region where we have seen the fluorescence yield was decreasing and the free electron yield was increasing. A possible explanation of these results will be discussed in Section VI.

V. Irradiation Effects

We have described above how illumination into the F band tended to bleach the F-center photoresponse. The bleaching occurred with high efficiency at temperatures down to at least 77 K. It was also found that the spectral dependence of the photoresponse of a sample which had been electron irradiated several days before measurements were made, was similar to that of a bleached sample, which can be seen in Figure 47, curve b. The F-band photoresponse could be restored by γ-irradiating the sample at room temperature for about thirty minutes just before mounting it in the cryostat. The restoration of the F-center photoresponse by γ-irradiation was quite dramatic. For example the photore-

sponse curve, Figure 47, curve a, could be reproduced from the bleached or aged sample by γ-irradiation for only a few minutes. Results similar to ours on aged samples were obtained by Roberts and Crawford (80) in electron irradiated MgO, in which γ-irradiation was necessary prior to measurement in order to observe the F-center photoresponse.

In the preceding chapter it was shown that the F^+ photoresponse for SrO could be restored by illuminating the sample for a few seconds with light of energy greater than 3.7 eV. In contrast to this, it was found that illumination with light of energy greater than 4 eV did not restore the F or F^+ photoresponse in CaO. Neither did illumination at 77 K of the sample with light of energy greater than 2.5 eV enhance the photoresponse of the 3.7 eV band at the expense of the F band or bleaching with light of energy less than 2.5 eV have the opposite effect as was suggested by Kemp et al. (93). Kemp et al. showed that this interconversion process did occur in additively colored CaO crystals by comparing the optical absorption bands for the F-and F^+-centers.

In our samples the increase in F-center photoresponse was not accompanied by an increase in F-center concentration, as measured by the optical absorption of the sample. In Figure 54 the broken curve shows the optical absorption of a sample containing F-and F^+-centers produced by a previous electron irradiation. The sample had then been stored several days at room temperature before measurement. It can be seen that the sample contained mostly F^+-centers but that there is a small number of F-centers also present. After the sample had been γ-irradiated at room temperature for thirty minutes the absorption spectrum, shown as the continuous curve in Figure 54, was measured. It can be seen that the F^+ band was increased slightly by the irradiation while

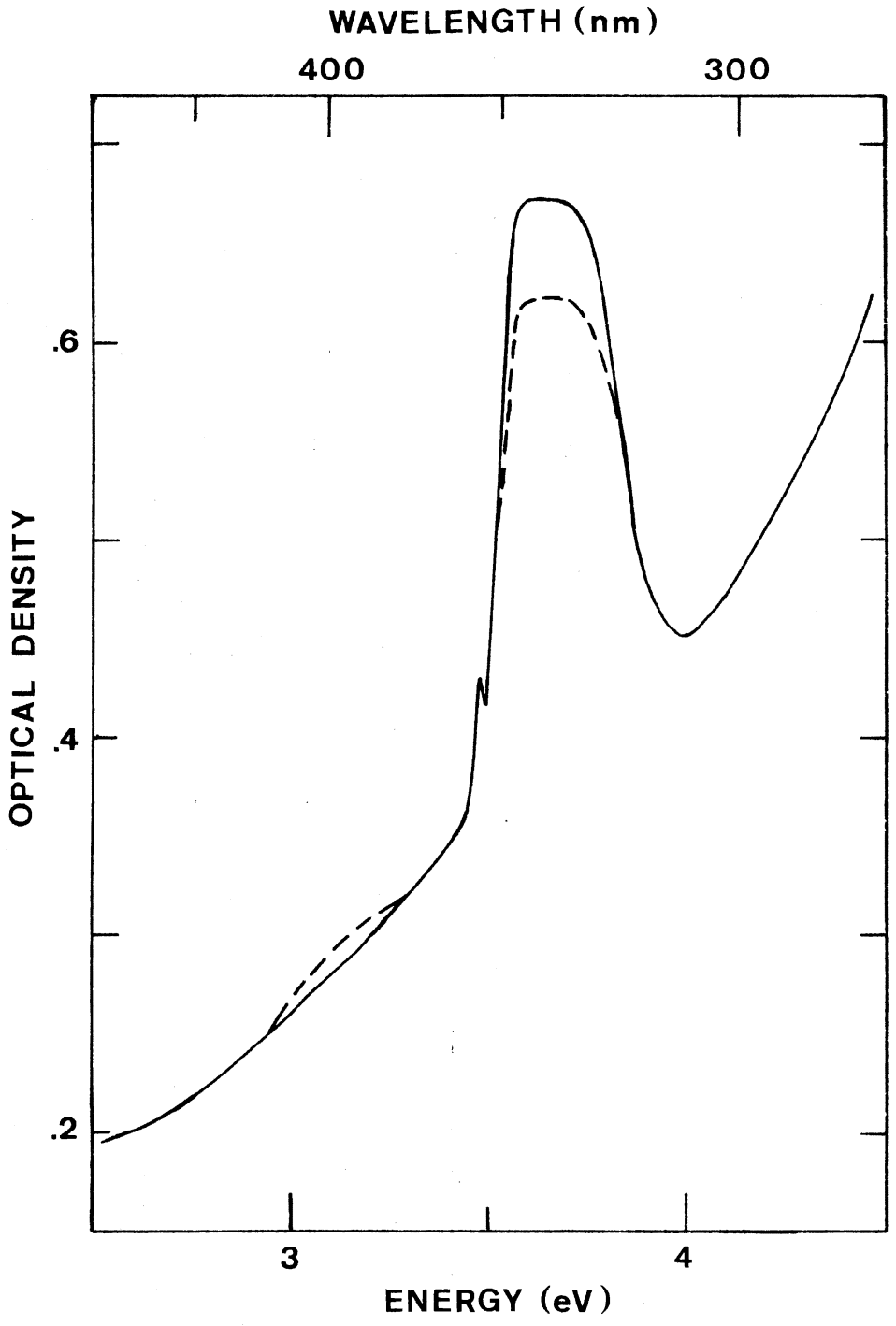

Figure 54. Comparison of the Intensity of the F^+ Band (3.65 eV) and the F Band (3.1 eV) in CaO at 77 K Before (Broken Curve) and After (Continuous Curve) γ-irradiation at Room Temperature for Thirty Minutes. The sample, which was 1.77 mm thick, had previously been electron irradiated at 77 K to a dose of about 5×10^{17} electrons/cm^2

the F-band was diminished. The effect of γ-irradiation on our electron irradiated samples was, therefore, similar to the effect of ultraviolet light on the additively colored CaO samples used by Kemp et al. (93).

The increase in F-center photoresponse following γ-irradiation of our sample was, therefore, not due to an increase in the number of centers. Recall that the photoresponse of the crystal for a given wavelength of incident light is expressed as the product, $\eta\omega_o$, where η is the free carrier yield and ω_o is the mean range of the carriers in the direction of a unit applied electric field. Frequently an increase in the photoresponse is attributed to the quantum efficiency, which in this case would imply an increase in the number of centers producing this photoresponse. But as has already been pointed out, the optical absorption measurements (Figure 54) show that this is not the case. Rather the increase in F-center photoresponse following γ-irradiation is due to an increase in the mean range, ω_o, of the electrons released by the incident light. We estimate that the mean range was increased in this way by a factor of at least thirty. The fact that the photoresponse in the spectral region of 3.7 eV was not increased by an equally large factor (see Figure 47) may suggest that the charge carriers released at 3.7 eV are positive holes rather than electrons. A variation in the sign of the charge carriers released by incident light of different wavelengths has been observed previously in MgO, for example (87).

The changes in photoresponse and optical absorption of our samples described above were only temporary. After several days the sample reverted to its equilibrium state. It is apparent that the trapping mechanisms operative in CaO samples containing F-type centers are quite complicated. However, one possible line of further investigation is

the dependence of the photoresponse of F^+- and F-centers on the absolute and relative number of centers present.

The F^+ band photoresponse could not be optically bleached even at room temperature. It is already well known that the F^+ absorption band cannot be bleached optically (7). Figure 50 shows that at 77 K illumination of the F^+ band does not produce free charge carriers so that no optical bleaching would be expected. Illumination at room temperature, which does produce free charge carriers, must produce a metastable state of the crystal which then returns to the initial state, i.e., F^+-centers, upon removal of the incident light. An alternative consideration is that the samples contain a significant concentration of oxygen vacancies, i.e., F^{2+}-centers. These would be expected to be strong electron traps and once having trapped an electron would become F^+-centers.

VI. Analysis and Discussion

The electronic structure of the F-center in CaO calculated by Wood and Wilson (57,59) is in substantial agreement with experimental results, including those reported here. The F band corresponds to an allowed transition from the $^1A_{1g}$ ground state to the $^1T_{1u}$ excited state. According to present theory (59) (Figure 55) absorption occurs into two $^1T_{1u}$ excited states, the second level, $^1T_{1u,2}$ lying roughly two tenths of an eV above the first in absorption. According to calculations the two absorption transitions contribute almost equally to the strength and half-width of the absorption band. The charge density in the $^1A_{1g}$ ground state is localized in the vacancy whereas in the $^1T_{1u,1}$ and higher states it is well outside of the vacancy. In emission the relaxed excited $^1T_{1u,2}$ state (not shown on the configuration coordinate diagram

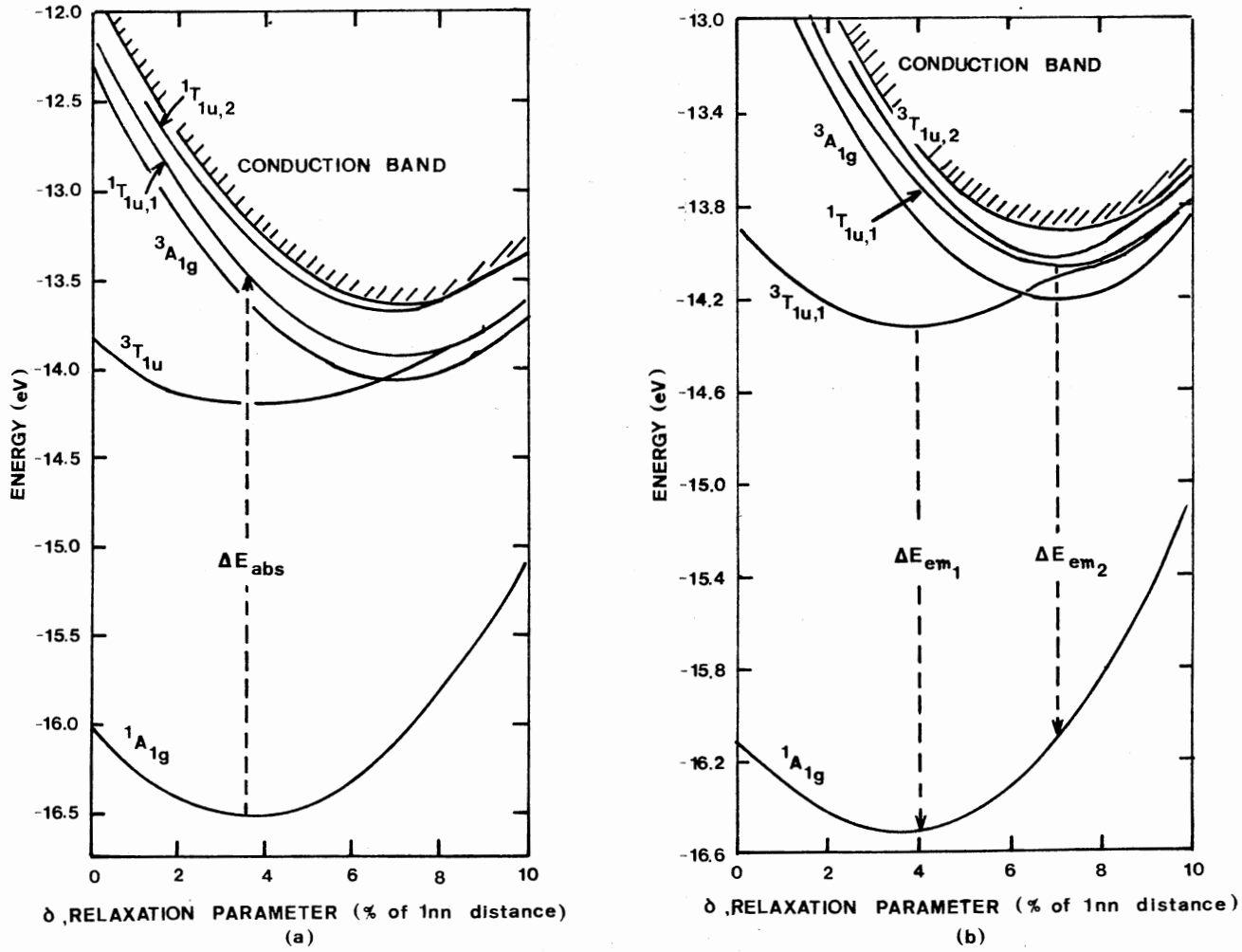

Source: Wood and Wilson (59)

Figure 55. Configuration Coordinate Diagram for CaO F-center in Absorption (a) and Emission (b). (1nn = first nearest neighbor distance)

for emission) was found within about 0.05 eV of the conduction band. It is highly probable that the release of electrons for photoconductivity occurs from the $^1T_{lu,2}$ state. Thermal ionization across such a small energy gap would be expected to occur below 65 K which explains why no significant temperature dependence in the F band photoresponse is observed above 65 K and also why the F-center could be optically bleached at 77 K.

Let us recall similar experimental measurements on the F-center in KCl (73) and the F^+-center in SrO (Chapter IV of this dissertation) for which a sharp increase in the free electron yield was accompanied by a corresponding decrease in the fluorescence yield over a given temperature range. In light of this, we might then expect that since there was no such increase in the free electron yield for the F-center in CaO with increasing temperature, the fluorescence yield (as measured by the Zeroth Moment) should also remain nearly constant over the same temperature range. This, however, is contrary to the results reported in Section IV. There is no simple explanation for this apparent conflict. Theoretical calculations suggest that there are many excited states and, in fact, curve crossing. The luminescence may be quenched by radiationless transitions between a given excited state and the other nearby excited states. This suggestion is further supported by experimental results for the emission from the CaO F-center (47). At temperatures below 25°C, Bates and Wood (47) report that the $^3T_{lu}$ level is predominantly populated, and therefore the $^3T_{lu} \rightarrow {}^1A_{lg}$ transition is dominant. As the temperature increases, the $^1T_{lu}$ level ($^1T_{lu,1}$ according to Wilson (91)) becomes populated at the expense of the $^3T_{lu}$ level and the $^1T_{lu} \rightarrow {}^1A_{lg}$ transition becomes dominant. The two transitions lie within about

0.05 eV of one another. These emission results are consistent with ours reported in Section V, which were obtained at temperatures less than 300 K.

At this point it is also worth reporting that the photoconductivity produced by illuminating additively colored samples (see Appendix B) containing a large number of F-centers (~ 10^{18} cm^{-3}) had some unusual features. The photocurrent decreased as the illumination continued and, in addition, a transient dark current was produced which took several minutes to decay at 77 K. The fluorescence of these samples also contained a component with a lifetime of the order of minutes which appears related to the transient dark current described above. A similar transient dark current is produced by illumination of the F-band in additively colored MgO (80).

It was shown in Chapter IV, Section V, that the temperature dependence of the F^+ band photoresponse in SrO could be analyzed quite well in terms of a two level model. A similar analysis for the temperature dependence of the F^+ band in CaO, though possible, is more difficult because the impurity photoresponse at 3.7 eV masks the F^+ band photoresponse below 210 K.

In order to make use of the relationship

$$\left(\frac{1}{\eta_T} - 1\right) = \left(\frac{\tau_o}{\tau_R}\right) e^{E_a/kT}$$

where η_T is the free carrier yield; E_a, the activation energy for thermal ionization; τ_R, the radiative lifetime; $1/\tau_o$, the pre-exponential frequency factor for thermal ionization; k, Boltzmann's constant; and T, the temperature, we assume that at 300 K (see Figure 50) an F^+-center which

had absorbed a photon was thermally ionized with unit probability, i.e., at this temperature η_T was equal to 1. In addition, we assume that the range, ω_o, did not change over the temperature range from 230 K to 280 K. This is not an unreasonable assumption over a small temperature range and has indeed been found to be the case in some alkali halides (73). With these approximations we can use the data in Figure 50 to obtain values for η_T as a function of temperature. The results are presented in Figure 56, from which we obtain a value for E_a of 0.24 eV and a value for τ_R/τ_o of 2×10^4. Within the model our estimate of E_a is to an accuracy of about 20% and the estimate of τ_R/τ_o is within a factor of about 5. In the alkali halides (73) τ_o was found to be within an order of magnitude of 10^{-12} sec. Assuming τ_o has a similar value in the alkaline earth oxides, our value of τ_R/τ_o suggests a value for τ_R of about 20 nsec. This is in good agreement with the radiative lifetime τ_R of at least 30 nsec obtained by fluorescence lifetime measurements and reported in Section IV.

In the two-level model a decrease in the quantum efficiency for fluorescence with increasing temperature (see Figure 52) is expected to be accompanied by a decrease in the effective lifetime of the excited state (Equations II-23, II-25). However, any change which occurred in the lifetime could not be detected by our apparatus because the radiative lifetime, τ_R, was apparently shorter than 30 nsec, the resolution of the apparatus.

One would like to be able to look at a curve such as that in Figure 41 or Figure 43 and be able to make some kind of quantitative statement as to the relative number of F- and F^+-centers contained in the sample. However, such a comparison cannot be made directly from the curves be-

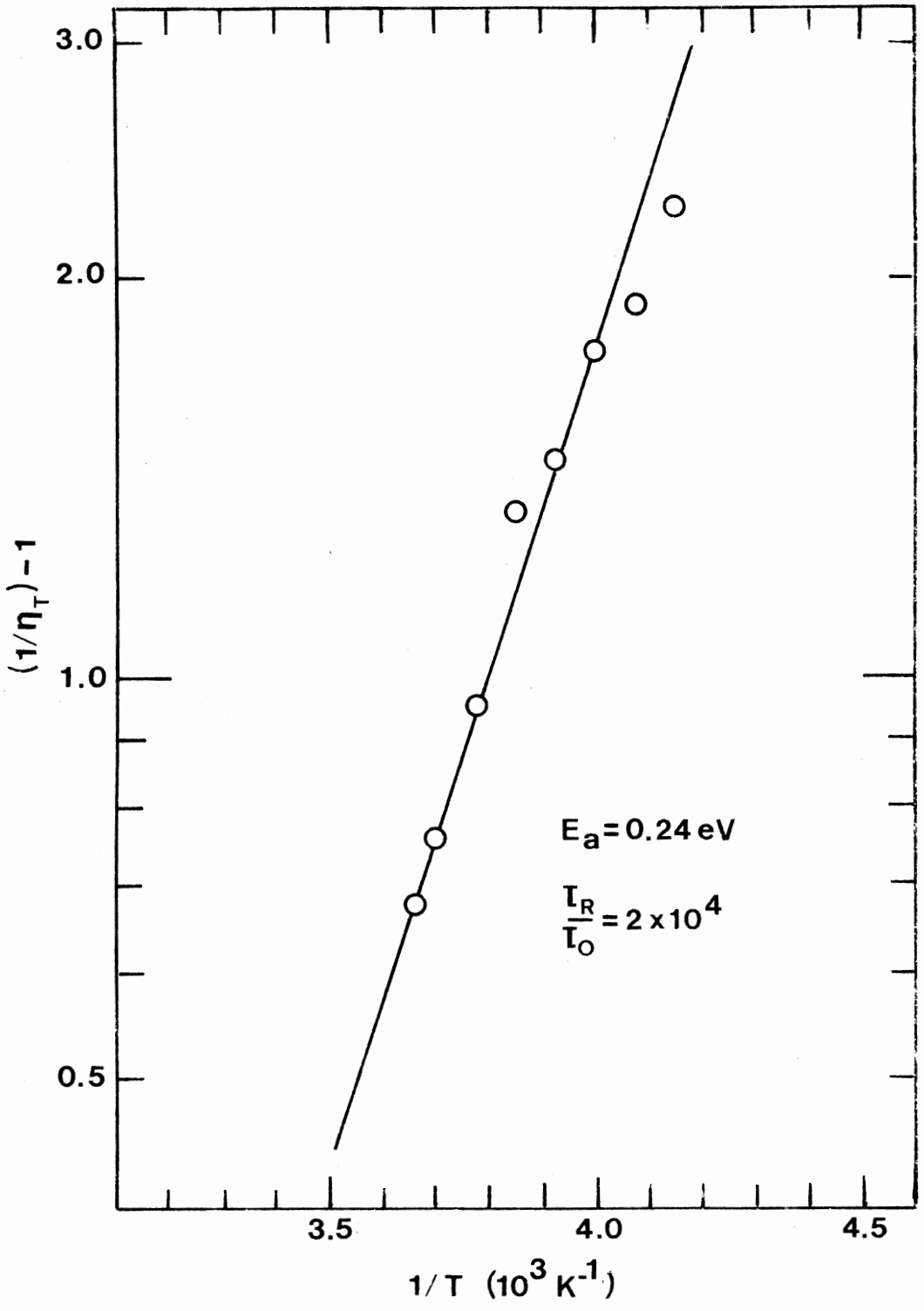

Figure 56. Semi-logarithmic Plot of $(1/\eta_T)-1$ Versus Inverse Temperature, 1/T. Data points were obtained from the experimental results shown in Figure 50 as described in the text

cause as we saw from Smakula's equation (Equation II-12) the intensity of the absorption depends on the product of two unknown quantities, the number of centers, N, and the oscillator strength, f, for the transition. The oscillator strength is generally not known and attempts to calculate it theoretically are highly suspect. Kemp et al. (96) have reported, as a result of ESR measurements, a value, f = 0.8, for the oscillator strength for the F^+ absorption in CaO. The oscillator strength for the CaO F-center $^1A_{1g} \rightarrow {}^1T_{1u,1}$ and $^1A_{1g} \rightarrow {}^1T_{1u,2}$ absorption transitions have been calculated by Wood and Wilson (59) as 0.1 and 0.08, respectively. (They also report that these values appear to be too small.)

If we assume that these values are correct for the oscillator strengths of the F- and F^+-center absorption in CaO, we can determine the approximate ratio N_{F^+}/N_F of F^+-centers to F-centers in a sample. For example, consider the data in Figure 43 in which the F^+ band has an optical density of about 1.7 and a half-width, W_{F^+}, of about 0.41 eV and the F band has an optical density of about 0.5 and a half-width, W_F, of about 0.4 eV. From Equation II-12 we have

$$\frac{N_{F^+} f_{F^+}}{N_F f_F} = \frac{\frac{n_1}{(n_1^2 + 2)^2} \alpha_1 W_{F^+}}{\frac{n_2}{(n_2^2 + 2)^2} \alpha_2 W_F}$$

where n_1, n_2 are the indices of refraction for the sample and α_1, α_2 the absorption coefficients measured at 3400 Å and 4000 Å, respectively. In the approximation that $n_1 \sim n_2$ and using the relation $\alpha = 2.303(OD)/d$ with the data in Figure 43 and $f_{F+} = 0.8$ and $f_F = 0.18$ ($f_{^1A_{1g} \rightarrow {}^1T_{1u,1}}$ +

$f_{^1A_{1g} \rightarrow {}^1T_{1u,2}}$) we have $N_{F+}/N_F \sim 0.8$. In other words, if we assume that the oscillator strength for the F-center is about 0.18, as calculated by Wood and Wilson, there are approximately equal numbers of F- and F^+-centers present. This is not what one would tend to think at a first glance of Figure 43. However, 0.18 is very likely too small for the F-center oscillator strength. Using the data in Figure 43, there is a whole range of values that the ratio N_{F+}/N_F can take on, depending on the value of the oscillator strength of the F-center. For example, $N_{F+}/N_F = 1$ for $f_F = 0.24$, $N_{f+}/N_F \sim 4$ for $f_F = 1$ and $N_{F+}/N_F \sim 8$ for $f_F = 2$ the maximum value possible. Without knowing f_F, we cannot make a definite quantitative statement about the ratio of N_{F+}/N_F of F^+- to F-centers in the sample. It is likely that these two excited states, $^1T_{1u,1}$ and $^1T_{1u,2}$, are the two most important ones and therefore contain most of the oscillator strength which sums to two. Consequently, it is probably correct that the sum of the oscillator strengths for these two transitions is much greater than 0.24, and probably even greater than 1 and the ratio $N_{F+}/N_F > 4$. Such an analysis is the basis for statements made earlier in this dissertation to this effect.

The temperature dependence of the emission band half-width can be used to determine the effective frequency, ω, of phonons interacting with the electronic states of the defect and the Huang-Rhys factor, S, for the CaO F^+-center as described in Chapter II, Section IV. Though the determination of the effective frequency and the Huang-Rhys factor was not among the original major objectives of this dissertation, it is instructive to use our data to compute this and compare it with other values. Figure 57 shows the temperature dependence of the emission half-width measured over the temperature range from 77 K to 350 K. The ex-

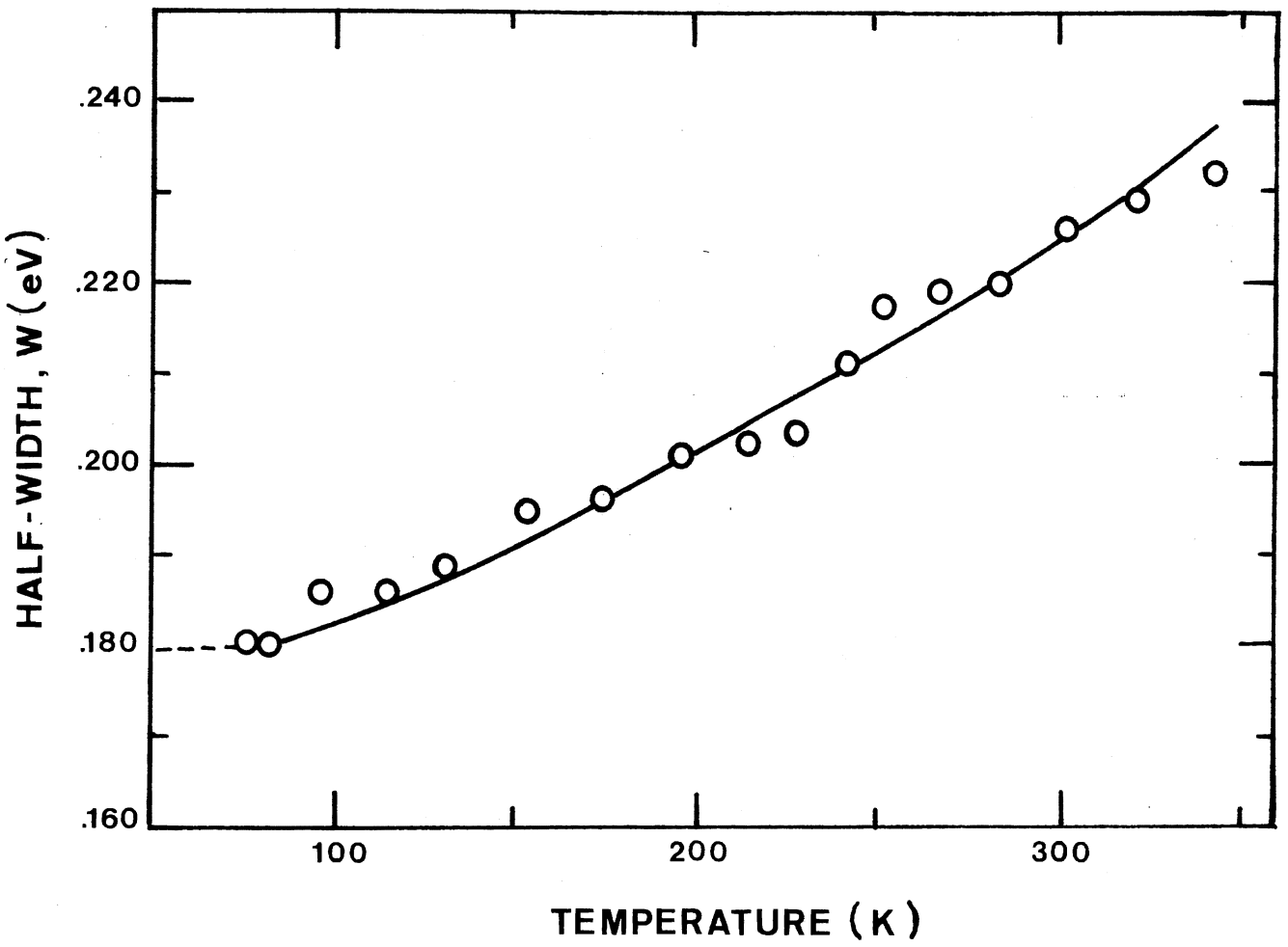

Figure 57. Temperature Dependence of the Width at Half-Maximum, W, for the CaO F^+-center Emission

trapolation is based on similar measurements reported by Escribe and Hughes (68), for absorption, and Henderson et al. (25,41) for emission, in which there is very little change in the half-width between 4 K and 77 K. Using the temperature dependent relationship for half-widths given in Equation II-19, we obtain the relation

$$\coth^{-1}\left[\frac{W^2(T)}{W^2(O)}\right] = \frac{\hbar\omega}{2k}\left(\frac{1}{T}\right)$$

which, when using the data in Figure 57 and assuming W(O) ~ W(77), yields the curve in Figure 58. From the slope of the straight line we obtain an effective frequency $\nu = 307\ cm^{-1}$. The Huang-Rhys factor can then be determined by several methods, including: 1) the band half-width relation from Equation II-16, 17, $[W(O)]^2 = 8 \ln 2\, S\hbar^2\omega^2$ and 2) the separation of the band centroid and the zero-phonon line ($\delta = S\hbar\omega$, see Chapter II, Section IV). Our results are shown in Table VI along with other reported results obtained by similar measurements. Our results are more or less in agreement with those reported earlier. The value, S', of the Huang-Rhys factor obtained above is that associated with either of the two non-cubic E_g or T_{2g} vibrational modes which are thought to couple equally (67,68) to the excited electronic state of the F^+-center in CaO. The effective Huang-Rhys factor (68) can then be approximated by $S = S_A + S_{E_g} + 3/2\ S_{T_{2g}}$ which for the equal coupling case, $S_{E_g} = S_{T_{2g}} = S'$, gives $S = \frac{5S'}{2} \sim 10$ if coupling to the A_{1_g} breathing modes is ignored. This result is in agreement with values reported by other authors (25, 68).

In conclusion we see that besides being in substantial agreement

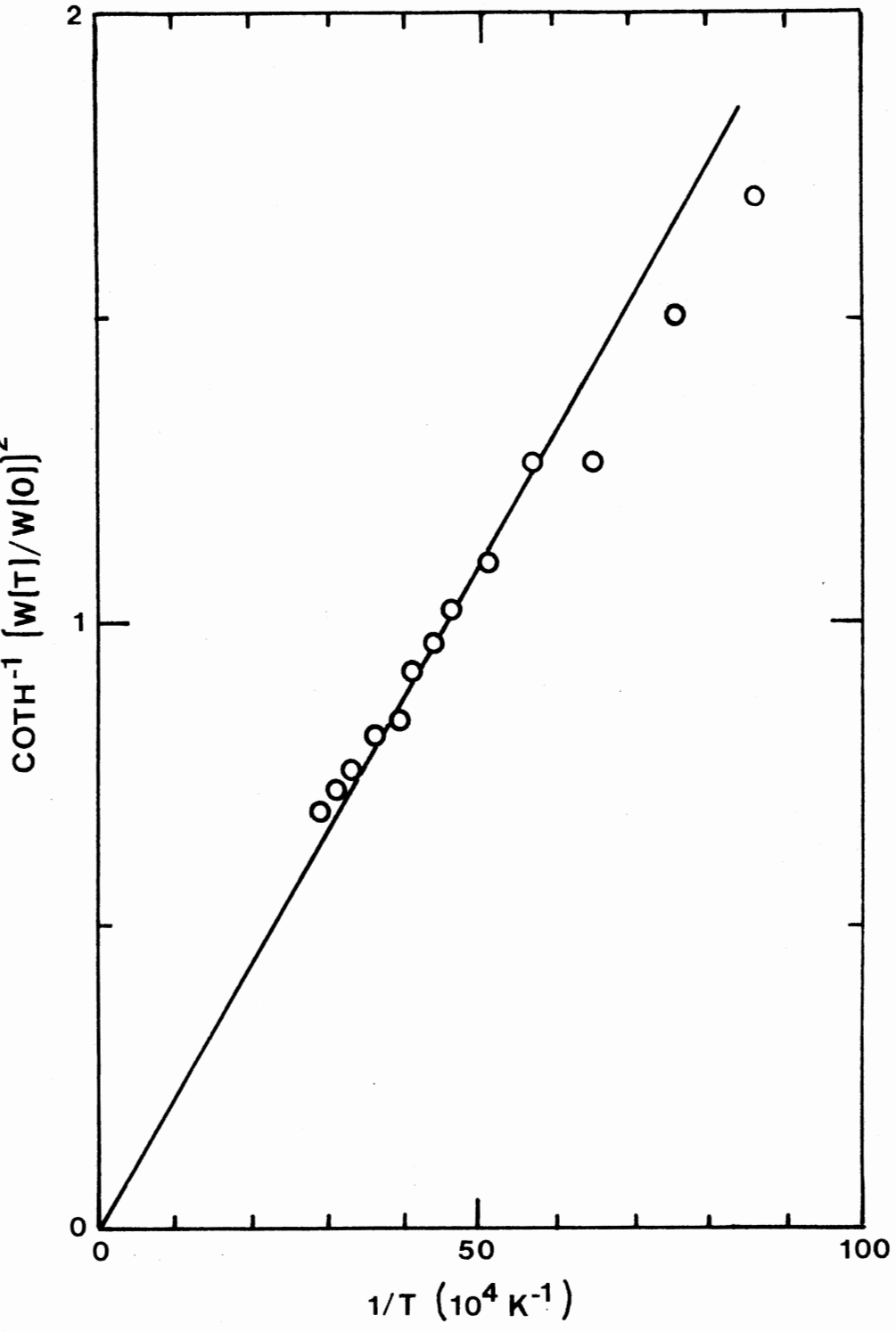

Figure 58. Plot of $Coth^{-1}[W(T)/W(O)]^2$ Versus Inverse Temperature, 1/T With W(O) ~ W(77). Data points were obtained from the experimental results shown in Figure 57 as described in the text

TABLE VI

MEASURED VALUES OF S, ν FOR THE CaO F^+-CENTER

Method	Our Results	Previous Results
Emission		
Zero-phonon-line centroid separation, δ $\delta = S\hbar\omega$	S' = 3.6; ν = 307/cm	S' = 3.5; ν = 250/cm (Ref. 46) S' = 3.2 ± 0.7; ν = 297/cm (Ref. 25)
Band half-width $W^2(0) = (8 \ln 2) S\hbar^2\omega^2$	S' = 4.18; ν = 307/cm	S' = 4; ν = 210/cm (Ref. 41)
Absorption		
Band half-width $W^2(0) = (8 \ln 2) S\hbar^2\omega^2$		S ~ 13-16 (R. G. Bessent in Ref. 7). S' = 3.3; ν = 302/cm S_A = 1.6; ν = 205/cm S = 9.84 ± 1.4 (Ref. 68)

with previous experimental and theoretical studies our results give further information about the electronic structure of the F- and F^+-centers in calcium oxide.

CHAPTER VI

SUMMARY AND PROBLEMS FOR FURTHER STUDY

I. Summary and Conclusions

We have reported here an experimental investigation of the electronic structure of the F^+-center in SrO and the F- and F^+-centers in CaO using the spectral response and temperature dependence of photoconductivity, with associated optical absorption, luminescence and fluorescence lifetime measurements. Measurements were made primarily on electron and proton irradiated samples with some measurements also being made on neutron irradiated and additively colored samples.

F^+-centers can be introduced into CaO by electron, proton, or neutron irradiation, as can also F-centers in CaO, but to a lesser extent. Additive coloration of CaO gives rise to both F- and F^+-centers with the formation of F-centers being dominant. The F^+-center can be introduced into SrO by proton or neutron irradiation. Electron irradiation, even at liquid nitrogen temperature, has so far been ineffective in producing F^+-centers in SrO, at least in so far as being able to produce a measurable optical absorption band is concerned. The two electron center, the F-center, cannot be introduced into currently available SrO by particle irradiation.

On the basis of charge consideration alone it might be expected that the F-centers in the alkaline earth oxides would produce photoconductivity in a manner similar to F-centers in the alkali halides, but

that F^+-centers, being positively charged, would not produce photoconductivity at ordinary room temperatures. The experimental results reported here indicate that the situation is not as straightforward as this viewpoint would predict. It was surprising that the results from the F^+-center in SrO and CaO most nearly resembled the F-center in the alkali halides. It was thus the F^+-center which proved to be the most interesting and from which we were able to gain the most new information. The F-center in CaO was less interesting due to, as our results indicated, the very close proximity of the excited electronic state to the bottom of the conduction band. SrO proved to be especially interesting and informative since we were able to focus our attention on the single band associated with the F^+-center, owing to the fact that the F-center could not be introduced into currently available SrO by particle irradiation. This is in contrast to the situation encountered with the other alkaline earth oxides where the presence of both an F and F^+ band usually complicate an analysis of the data.

The F^+-centers in SrO and CaO were shown to produce photoconductivity in a manner very similar to that of F-centers in alkali halides. Since photoconductivity originating from F^+-centers was unexpected, it is of interest to compare the magnitude of the photoresponse of the F^+-center in CaO and SrO to that measured from single electron F-centers in another material, such as MgF_2 (97). For a useful comparison it is necessary to compute the value $\eta_T\omega_o$ for the two centers, where η_T is the free electron yield or quantum efficiency per absorbed photon. The ratio of incident to absorbed photons striking the sample is given by $I_o/(I_o-I_o\ e^{-\alpha d})$, and hence $\eta_T\omega_o = \eta\omega_o/(1-e^{-\alpha d})$. If we estimate a maximum value of 0.002 for the optical density of the F^+-band for the SrO

sample used for Figure 29, we obtain a lower limit of 4×10^{-10} cm^2/V for $\eta_T\omega_o$ at 120 K. The F and F^+ optical densities of the CaO sample used in Figure 44, curves b and c, are 0.02 and 0.26, respectively. For the sample used in Figure 44 we then obtain $\eta_T\omega_o = 0.67 \times 10^{-10}$ cm^2/V for the F^+-center in CaO at room temperature and $\eta_T\omega_o = 1.1 \times 10^{-10}$ cm^2/V for the F-center in CaO at 77 K. For low concentration (α=9) F-centers in MgF_2, $\eta_T\omega_o$ is about 4×10^{-10} cm^2/V at room temperature. Therefore, the photoresponse per absorbed photon, $\eta_T\omega_o$, for all of these centers is the same order of magnitude.

The photoresponse of the F^+-center in SrO increased sharply as the temperature increased from 60 K to 110 K (Figure 29). Similarly the photoresponse of the F^+-center in CaO increased sharply as the temperature was varied from about 210 K to 300 K (Figure 50). The zeroth moment, M_o, of the F^+ emission in both SrO (Figure 39) and CaO (Figure 52) rapidly decreased as the temperature increased over these respective ranges. The temperature dependence of the F^+ photoresponse can be explained quite well in terms of a two level model (55). Using this model the thermal activation energy for the F^+-center photoconductivity in SrO was determined as 0.12 eV and in CaO as 0.24 eV. It is interesting that these values are close to those found for F-centers in alkali halides (73). For example, for KCl, E_a = 0.16 eV and for NaCl, E_a = 0.07 eV. If we take it that there is a trend in E_a for the alkaline earth oxides, we would expect the F^+ photoresponse in MgO to become observable only above room temperature and the F^+ photoresponse in BaO to be observable at or below liquid nitrogen temperature. The radiative lifetime, τ_R, could also be predicted from the temperature dependence of the photoresponse for the F^+-center in SrO and CaO. The radiative life-

time, τ_R, for the F^+-center in SrO was predicted to be on the order of a microsecond and for the F^+-center in CaO, τ_R was predicted to be about 20 nsec. Fluorescence lifetime measurements supported these predictions, yielding τ_R = 0.46 μsec and τ_R < 30 nsec for the radiative lifetime of the excited electronic state of the F^+-center in SrO and CaO, respectively. These values can be compared to the radiative lifetime of the excited state for the F-center in KCl which was determined to be on the order of 0.5 μsec (73).

The temperature dependence of the photoresponse originating from the F-center in CaO (Figure 50) showed no sharp increase in the photoresponse between 60 K and 300 K which would be characteristic of thermally assisted ionization. This implies that the relaxed excited state of the F-center lies very close to the bottom of the conduction band which is consistent with the theoretical calculations (0.05 eV) of Wood and Wilson (59). Since the F band is photoconducting throughout this temperature range, the curve shows principally the change of mobility and hence the mean range, ω, of the charge carriers (Equation II-28).

Although photoconductivity from F-centers in alkaline earth oxides is generally expected in analogy to F-centers in alkali halides, there is presently no satisfactory explanation of photoconductivity originating from F^+-centers. One possible explanation derives from a suggestion by Kemp and Neeley (86) that the A_{1g} ground state of the F^+-center might be several eV below the top of the valence band of the host crystal. If this suggestion is correct, once the F^+-center absorbed a photon it might, then, be energetically possible for an electron on one of the surrounding O^{2-} ions to jump into the vacancy. This process, which is a sort of charge transfer process, would leave a hole on the oxygen ion

and if this hole were released and sufficiently mobile, photoconductivity could occur. This explanation requires that the charge carriers be positive. From a somewhat involved experimental technique it appears, however, that the photocurrent excited by F^+-centers in SrO and by F-centers in CaO is carried by electrons. We were unable, however, to determine satisfactorily the sign of the charge carrier for the F^+-center in CaO.

The above results concerning the sign of the charge carriers in conjunction with the temperature dependence of the photoresponse can be interpreted as E_a, the thermal ionization energy, giving the relative separation in energy between the relaxed excited state of the center and the bottom of the conduction band. Thus according to this interpretation the relaxed excited electronic state from which photoconductivity originates is 0.12 eV below the bottom of the conduction band for the F^+-center in SrO, 0.24 eV below the bottom of the conduction band for the F^+-center in CaO and only about 0.05 eV below the bottom of the conduction band for the F-center in CaO.

It was found that prolonged illumination in the F^+ band of SrO at temperatures above about 90 K partially destroyed the photoresponse. However, the photoresponse could be restored by illuminating the sample with light of energy greater than 3.7 eV. The F-center photoresponse in CaO could also be optically bleached at all temperatures between 77 K and 300 K, but could then be fully restored by γ-irradiation at room temperature. The photoresponse of the F-center in CaO could also be "bleached" by storing the sample at room temperature for several days. The trapping mechanisms involved for either of these processes is not known. However, we determined that the increase in the F-center

photoresponse following γ-irradiation was due to an increase in the mean range, ω, of the electrons released by the incident light, rather than an increase in the number of F-centers.

For neither CaO or SrO did the F^+-center appear to be an efficient electron trap. This is supported by two observations: 1) the F^+-center in CaO or SrO cannot be optically bleached; and 2) there is no sign of F-centers being formed in SrO which has been heavily irradiated and which contains a comparatively large concentration of F^+-centers (Figure 23) and there are more F^+- than F-centers in similarly irradiated samples of CaO (Figures 41 and 43).

In addition we also recall the apparent conflict in Chapter V, Section VI, for the F-center in CaO in which a sharp decrease in M_o, and hence the quantum efficiency for luminescence, with increasing temperature was not accompanied by a corresponding increase in the photoresponse over the same temperature range (Figure 50). It was thus assumed that the luminescence was quenched by a more indirect process. This, in conjunction with the above information concerning the restoration of the F-center photoresponse and the F^+-center not being an efficient electron trap, indicates that the trapping mechanisms operative in CaO samples containing F-type centers are quite complicated.

The F^+-center in SrO and CaO are Jahn-Teller coupled systems in absorption (49,68) with the Jahn-Teller effect contributing significantly to the asymmetric shape of the absorption band. It appears that the F^+-centers in SrO and CaO are two different systems. The excited $^2T_{1u}$ electronic state of the F^+-center in CaO is nearly equally coupled to the T_{2g} and E_g non-cubic vibrational modes (67,68). It is not yet clear which vibrational modes are coupled to the excited $^2T_{1u}$ electronic state

of the F^+-center in SrO, though there are indications that nearly equal coupling to different vibrational modes than those above may be involved (60,91).

We have also seen that though certain aspects of the phenomena observed for these defects, such as the temperature dependence of the F^+-centers, can be explained quite well in terms of the two level model, there are also certain aspects in which the model is deficient. For example, the apparent sharp decrease in quantum efficiency for fluorescence from the F-center in CaO with increasing temperature without an accompanied increase in the free electron yield, the different components of the lifetime of the excited state of the F^+-center in SrO observed in fluorescence lifetime measurements, and trapping mechanisms involved in F-type centers in CaO, are but a few of the observed phenomena that cannot be explained in terms of a simple two-level model. It is thus apparent that there is a need for a more sophisticated model in terms of which the data may be analyzed and explained. One such model is that currently proposed by Wood and Wilson. Nevertheless, we have been able to gain significant insight and understanding concerning the electronic structure of these defects with the aid of this simple model. However, where it appears necessary for a more detailed model, the theoretical model being used by Wood and Wilson to calculate the electronic structure of these defects is a reasonable description of the system since their results are in basic agreement with our experimental results, as well as with the results of previous experimental studies. Besides being in substantial agreement with previous experimental and theoretical studies our results give further information about the electronic structure of the F-and F^+-centers in CaO and the F^+-center in SrO. With

the further development of theoretical models, such as that of Wood and Wilson, and collaboration with needed additional experimentation, hopefully the questions still unresolved at this point can be definitively answered.

II. Problems for Further Study

Several suggested future projects are listed below.

1. A study of the growth curves, as measured by optical absorption, for the F^+-center in SrO and the F- and F^+-centers in CaO as a function of irradiation dose using electron and proton irradiations at 77 K. Because of the necessity to prevent overheating of the sample, low current densities must be used during irradiation and consequently this study would be very time consuming. It would be interesting to see if the F^+ concentration saturates in either CaO or SrO and, if so, at what point the F-center concentration becomes more dominant than F^+-centers in CaO.

2. An isochronal anneal study for samples of CaO and SrO containing F and F^+-centers. Temperatures below, as well as above, room temperature should be considered. The purpose would be to determine at which temperature these defects become unstable. We know that the optical absorption of the F^+-center in CaO decreased over a period of several days while being stored at room temperature (Chapter V, Section V). Since these samples are hygroscopic, our irradiations, though done at 77 K, were done in the Van de Graaff extension tube, and consequently the sample had to be warmed to room temperature for removal and transferral to another cryostat. It is known that the thermal energy required to remove an electron from a trap is less than the energy $h\nu$ of a

photon which is just sufficient to eject the electron (55). Is it possible that F-centers produced by electron irradiation of CaO are unstable at or below room temperature thus making it appear that the creation of F^+-centers is more prevalent than that of F-centers during initial irradiations?

3. Investigate the dependence of the photoresponse, luminescence and $F \leftrightarrow F^+$ interconversion on the absolute and relative numbers of centers present, especially in CaO.

4. A more definitive determination of the sign of the charge carriers excited by F^+-centers in both SrO and CaO is needed, such as the more direct confirmation that would be provided by, for example, Hall effect experiments.

5. An investigation of the trapping mechanisms involved in SrO containing F^+-centers and in CaO containing F- and F^+-centers, especially as concerns the following: a) partial optical bleaching of the photoresponse from F^+-centers in SrO at temperatures greater than about 90 K which can be restored by short illumination of the sample with light of energy greater than 3.7 eV (one explanation could be that ultraviolet light releases charge carriers from comparatively deep traps and they repopulate F^+-centers); b) optical bleaching of CaO F-center photoresponse at temperatures greater than 77 K which can be restored by γ-irradiation at room temperature; c) a sharp decrease in the quantum efficiency for CaO F-center luminescence with increasing temperature while the photoresponse shows no temperature dependence over the same range.

6. Further experimentation is needed concerning luminescence from the F^+-center in SrO. One would like to be able to measure the 2.5 eV

emission band originating from the F^+-center alone, without the presence of and significant contribution from the overlapping 2.7 eV impurity band which was also obtained in our measurements. This would also permit a more accurate determination of the lifetime of the excited state of the F^+-center and determination of the role of the 0.46 μsec and 35 nsec lifetime components which we measured with regard to the F^+-center in SrO. If the emission from the F^+-center could be separated from that of the 2.7 eV impurity band, one would then also be able to study the temperature dependence of the emission band half-widths and gain information about the Huang-Rhys factor and the coupling of the electronic states to the lattice vibrations.

7. Determine the temperature dependence of the photoresponse from the F-center in CaO below 65 K to see if the photoresponse drops off sharply and obtain a value for E_a, the thermal activation energy.

8. Determine the radiative lifetime, τ_R, for the F^+-center in CaO by fluorescence lifetime measurements. Our measurements, $\tau_R < 30$ nsec, indicated that the fluorescence lifetime was at least as fast as the resolution of the apparatus, i.e., 30 nsec. Also investigate the lifetime component, which is on the order of minutes, which is associated with the F-center luminescence in CaO.

REFERENCES

1. Sonder, E. and W. A. Sibley, In Point Defects in Solids, edited by J. H. Crawford and L. M. Slifkin (Plenum, New York, 1972).

2. Markham, J. J., Solid State Physics, Suppl. 8 (Academic Press, New York, 1966).

3. Schulman, J. H. and W. D. Compton, Color Centers in Solids (Pergamon, New York, 1971).

4. Fowler, W. B., Physics of Color Centers (Academic Press, New York, 1968).

5. Crawford, J. H. and L. M. Slifkin, Point Defects in Solids (Plenum, New York, 1972).

6. Henderson, B. and J. E. Wertz, Advan. Phys. 17, 749 (1968).

7. Hughes, A. E. and B. Henderson, In Point Defects in Solids, edited by J. H. Crawford and L. M. Slifkin (Plenum, New York, 1972).

8. Goldstein, E., Sitz. Berliner Acad. Wiss. (1894), p. 937; Z. Instrumentkunde 16, 211 (1896).

9. Pohl, R. W., Proc. Phys. Soc. (London) (extra part) 49, 3 (1937).

10. Wyckoff, R. W. G., Crystal Structures, Vol. I, II (Interscience Publishers, New York, 1963).

11. Ander, P. and A. J. Sonnessa, Principles of Chemistry: An Introduction to Theoretical Concepts (Macmillan Co., New York, 1965).

12. Barrow, Gordon M., Physical Chemistry (McGraw-Hill Book Co., St. Louis, 1966).

13. Handbook of Chemistry and Physics (Chemical Rubber Publishing Co., Cleveland, 1963).

14. Cantor, S., Journal of Chem. Physics 59, 5189 (1973).

15. Ladd, M. F. C., Journal of Chem. Physics 62, 4583 (1975).

16. Roessler, D. M. and W. C. Walker, Phys. Rev. 159, 733 (1967).

17. Reiling, G. H. and E. B. Hensley, Phys. Rev. 112, 1106 (1958).

18. Whited, R. C. and W. C. Walker, Phys. Rev. 188, 1380 (1969).

19. Glascock, H. H. and E. B. Hensley, Phys. Rev. 131, 649 (1963).

20. American Institute of Physics Handbook (McGraw-Hill, New York, 1957).

21. Leighton, Robert B., Principles of Modern Physics (McGraw-Hill Book Co., New York, 1959).

22. Panofsky, W. K. H. and M. Phillips, Classical Electricity and Magnetism (Addison-Wesley Publishing Co., Reading, Mass., 1962).

23. Sibley, W. A. and D. Pooley, In Treatise on Materials Science, Vol. V, edited by H. Herman (Academic Press, New York, 1974).

24. Sibley, W. A. and Y. Chen, Phys. Rev. 160, 712 (1967).

25. Henderson, B., Y. Chen and W. A. Sibley, Phys. Rev. B 6, 4060 (1972).

26. Feldott, J. and G. P. Summers, Phys. Rev. B 15, (1977) (in press).

27. Feldott, J. and G. P. Summers, Phys. Rev. B 15, 2295 (1977).

28. Feldott, J., G. P. Summers, Y. Chen, M. M. Abraham and H. T. Tohver, Bull. Am. Phys. Soc. 22, 351 (1977).

29. Bessent, R. G., B. C. Cavenett and I. C. Hunter, J. Phys. Chem. Solids 29, 1523 (1968).

30. Hensley, E. B., W. C. Ward, B. P. Johnson and R. L. Kroes, Phys. Rev. 175, 1227 (1968).

31. Wertz, J. E., G. S. Saville, L. Hall, and P. Auzins, Proc. Brit. Ceram. Soc. 1, 59 (1964).

32. Henderson, B. and R. D. King, Phil. Mag. 13, 1149 (1966).

33. Chen, Y., W. A. Sibley, F. D. Srygley, R. A. Weeks, E. B. Hensley and R. L. Kroes, J. Phys. Chem. Solids 29, 863 (1968).

34. Chen, Y., R. T. Williams, W. A. Sibley, Phys. Rev. 182, 960 (1969).

35. Chen, Y., J. L. Kolopus and W. A. Sibley, Phys. Rev. 186, 865 (1969).

36. Kemp, J. C., J. C. Cheng, E. H. Izen and F. A. Modine, Phys. Rev. 179, 818 (1969).

37. Modine, F. A., Y. Chen, R. W. Major and T. M. Wilson, Phys. Rev. B 14, 1739 (1976).

38. Kemp, J. C., W. M. Ziniker, J. A. Glaze and J. C. Cheng, Phys. Rev. 171, 1024 (1968).

39. Merle d'Aubigńe, Y. and A. Roussel, Phys. Rev. B 3, 1421 (1971).

40. Ward, W. C. and E. B. Hensley, Phys. Rev. 175, 1230 (1968).

41. Henderson, B., S. E. Stokowski and T. C. Ensign, Phys. Rev. 183, 826 (1969).

42. Modine, F. A., Phys. Rev. B 7, 1574 (1973).

43. Johnson, B. P. and E. B. Hensley, Phys. Rev. 180, 931 (1969).

44. Rose, B. H. and E. B. Hensley, Phys. Rev. Letters 29, 861 (1972).

45. Kappers, L. A., R. L. Kroes and E. B. Hensley, Phys. Rev. B 1, 4151 (1970).

46. Evans, B. D., J. C. Cheng, J. C. Kemp, Phys. Letters 27A, 506 (1968).

47. Bates, J. B. and R. F. Wood, Solid State Commun. 17, 201 (1975).

48. Evans, B. D. and J. C. Kemp, Phys. Rev. B 2, 4179 (1970).

49. Hughes, A. E. and A. P. Webb, Solid State Comm. 13, 167 (1973).

50. Brown, F. C., The Physics of Solids (W. A. Benjamin, Inc., New York, 1967).

51. Edel, P., C. Hennies, Y. Merle D'Aubigńe, R. Romestain and Y. Twarowski, Phys. Rev. Letters 28, 1268 (1972).

52. Merle d'Aubigńe, Y., In Defects and Their Structure in Nonmetallic Solids, edited by B. Henderson and A. E. Hughes (Plenum, New York, 1976).

53. Sturge, M. D., Solid State Physics 20, 92 (1967) edited by F. Seitz, D. Turnbull and H. Ehrenreich (Academic Press, New York).

54. Kittel, C., Introduction to Solid State Physics, 4th ed. (John Wiley & Sons, Inc., New York, 1971).

55. Mott, N. F. and R. W. Gurney, Electronic Processes in Ionic Crystals (Oxford University Press, New York, 1940).

56. Mills, W. D., M. S. Thesis (Oklahoma State University, 1973).

57. Wood, R. F. and T. M. Wilson, Solid State Commun. 16, 545 (1975).

58. Wilson, T. M. and R. F. Wood, Journal de Physique 37, C7-190 (1977).

59. Wood, R. F. and T. M. Wilson, Phys. Rev. B 15, 3700 (1977).

60. Wilson, T. M., J. Feldott, G. P. Summers, and R. F. Wood, Bull. Am. Phys. Soc. 22, 351 (1977).

61. Schiff, L. I., Quantum Mechanics, 3rd Ed. (McGraw-Hill Book Co., St. Louis, 1968).

62. Herzberg, G., Molecular Spectra and Molecular Structure: I. Spectra of Diatomic Molecules (D. Van Nostrand Co., Inc., New York, 1950).

63. DiBartolo, B. and R. C. Powell, Phonons and Resonances in Solids (John Wiley & Sons, Inc., New York, 1976).

64. Klick, C. C., In Point Defects in Solids, edited by J. H. Crawford and L. M. Slifkin (Plenum, New York, 1972).

65. Estle, T. L., In Optical Properties of Ions in Solids, edited by B. DiBartolo (Plenum, New York, 1975).

66. Öpik, U. and M. H. L. Pryce, Proc. Roy. Soc. A 238, 425 (1957).

67. O'Brien, M. C. M., J. Phys. C 4, 2524 (1971).

68. Escribe, C. and A. E. Hughes, J. Phys. C 4, 2537 (1971).

69. Hughes, A. E., J. Phys. C 3, 627 (1970).

70. Schnatterly, S. E., Phys. Rev. A 140, 1364 (1965).

71. Fowler, W. B., Phys. Rev. A 135, 1725 (1964).

72. Swank, R. K. and F. C. Brown, Phys. Rev. Letters 8, 10 (1962).

73. Swank, R. K. and F. C. Brown, Phys. Rev. 130, 34 (1963).

74. Wild, R. L. and F. C. Brown, Phys. Rev. 121, 1296 (1961).

75. Hecht, K., Zeits. f. Physik 77, 235 (1932).

76. Van Heyningen, R. S. and F. C. Brown, Phys. Rev. 111, 462 (1958).

77. Brown, F. C. and N. Inchauspé, Phys. Rev. 121, 1303 (1961).

78. Welch, L. S., A. E. Hughes and G. P. Pells, "Properties of F_A Centers in CaO: Mg." (Paper presented at the Second Europhysical Topical Conference on "Lattice Defects in Ionic Crystals," West Berlin, Germany, August, 1976).

79. Hughes, A. E. "Proton Radiation Damage in MgO and CaO." (Paper presented at Workshop on Defects in Magnesium Oxide and Related Materials, Mount Pisgah, North Carolina, May 1975).

80. Roberts, R. W. and J. H. Crawford, N. Nonmetals 2, 133 (1974).

81. Dash, W. C., Phys. Rev. 92, 68 (1953).

82. Feldott, J. and G. P. Summers, Solid State Commun. 18, 347 (1976).

83. Feldott, J. and G. P. Summers, Bull. Am. Phys. Soc., 21, 345 (1976).

84. Zollweg, R. J., Phys. Rev. 111, 113 (1958).

85. Turner, T. J., N. N. Isenhower, and P. K. Tse, Solid State Commun. 7, 1661 (1969).

86. Kemp, J. C. and V. I. Neeley, Phys. Rev. 132, 215 (1963).

87. Peria, W. T., Phys. Rev. 112, 423 (1958).

88. Fedders, H., M. Hunger and F. Luty, J. Phys. Chem. Solids 22, 299 (1961).

89. Chiarotti, G., U. M. Grassano, G. Margaritondo and R. Rosei, Nuovo Cimento X 64B, 159 (1969).

90. Bogan, L. D. and B. D. Fitchen, Phys. Rev. B 1, 4122 (1970).

91. Wilson, T. M., private communication.

92. Nakai, Y. and K. Teegarden, J. Phys. Chem. Solids 22, 327 (1961).

93. Kemp, J. C., W. M. Ziniker and E. B. Hensley, Phys. Letters 25A, 43 (1967).

94. Chen, Y., M. M. Abraham, T. J. Turner and C. M. Nelson, Phil. Mag. 32, 99 (1975).

95. Chen, Y., Private communication. Dr. Chen has informed us that the CaO samples used in the experiments described in reference 25 were electron irradiated for many hours and certainly contained a significant concentration of F-centers. Because of a misprint, the light used to excited the F^+ luminescence in reference 25 is incorrectly stated to be the 3650 Å line from a mercury lamp. The light actually used was the 3342 Å line which was also used in the experiments described here.

96. Kemp, J. C., W. M. Ziniker and J. A. Glaze, Proc. Br. Ceram. Soc. 9, 109 (1967).

97. Summers, G. P., J. Phys. C 8, 3621 (1975).

98. Boas, J. F., T. P. P. Hall and A. E. Hughes, J. Phys. C. 6, 1639 (1973).

99. Hughes, A. E. and G. P. Pells, J. Phys. C 5, 2543 (1972).

APPENDIX A

ADDITIONAL EXPERIMENTAL RESULTS: SrO

APPENDIX A

ADDITIONAL EXPERIMENTAL RESULTS: SrO

We present here the results of experimental photoconductivity measurements on SrO which provided additional information. This information, though noteworthy, was not pursued in this study since it did not contribute directly to the other material presented in the body of this dissertation.

I. Proton Irradiated SrO

It is worth reporting that the photoconductivity produced by illuminating a proton irradiated sample of SrO had some unusual features. The Spicer sample had been proton irradiated at 77 K to a dose of about 8×10^{16} protons/cm^2 and had an optical density of about 0.2 at 3.1 eV. The photocurrent, measured at 77 K or 105 K, was the same for either direction of the applied electric field over the spectral region from 2 eV. The photocurrent, measured at 105 K, decreased as the illumination at a fixed wavelength continued in time (see Figure 59a) in the spectral region from 2.5 eV to 3.5 eV. The same effect was noted at 77 K although it was most pronounced in the region of the F^+ band (2.9 eV to 3.5 eV). In addition there was also a small transient dark current produced at 105 K and 77 K which took a couple of seconds to decay after removal of the incident light (2 eV to 3.5 eV) from the sample. Figure 59a shows the graph, proportional to the current, obtained with the

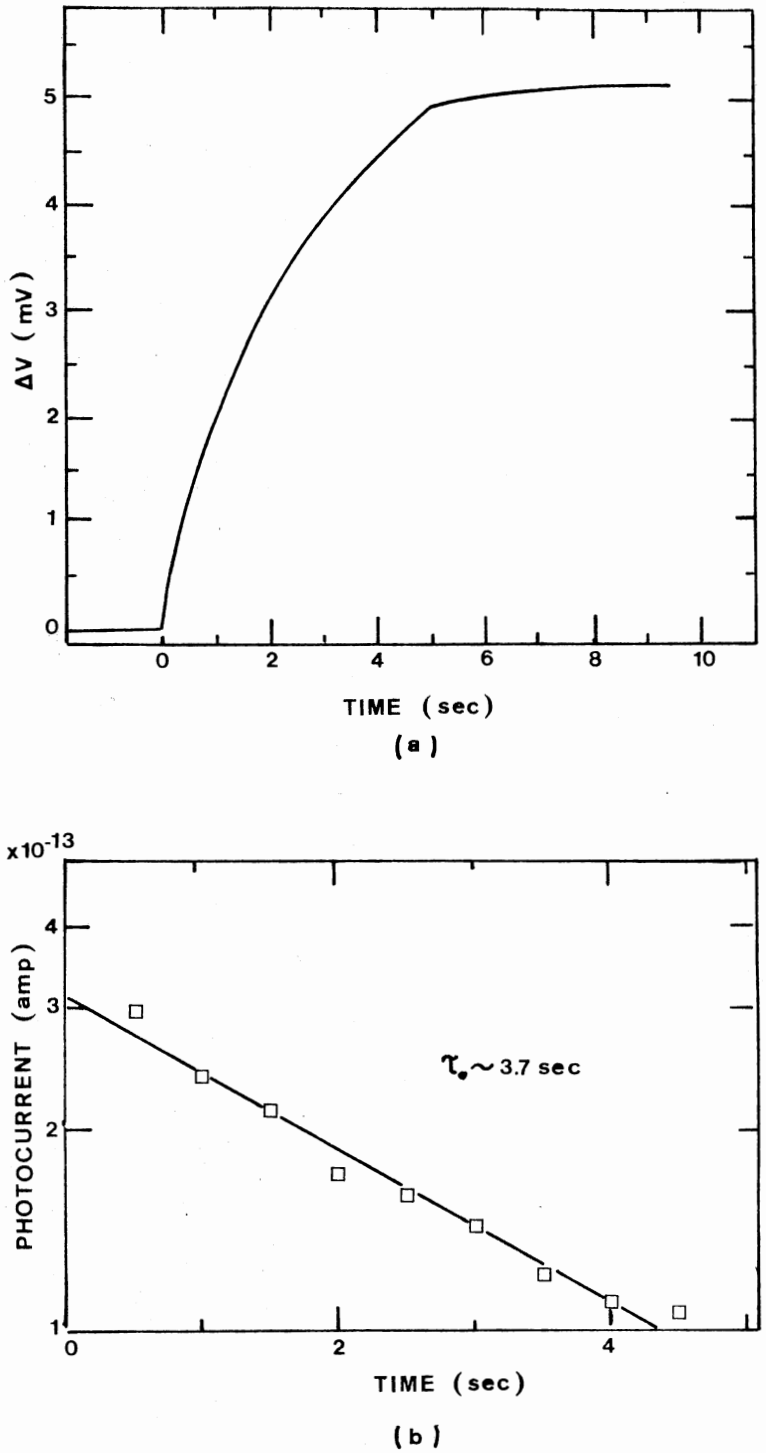

Figure 59. Photocurrent for 400 nm Light Incident on Proton Irradiated SrO at 105 K. Plot of ΔV as a Function of Time (a) and a Semilogarithmic Plot of Current Versus Time (b). Data points in (b) were obtained using the slope of the curve in (a) at various times

electrometer used in the "rate of charge" mode. This measurement was taken at 105 K for incident light of 4000 Å (3.1 eV). Figure 59b shows the semilogarithmic plot of the photocurrent, I ($\sim 10^{-13}$ amps), as a function of time. Using the relationship $I = I_o \exp(-t/t_o)$, we obtain a value of $t_o \sim 3.7$ seconds for the time required for the photocurrent to fall to 1/e of the initial value. Similar results were obtained at 77 K.

II. Neutron Irradiated SrO

The photoresponse measured at 77 K, 110 K and 145 K over the spectral range from 2 eV to 5 eV for an ORNL sample of SrO which had been neutron irradiated at room temperature is shown in Figure 60, curves a, b and c, respectively. The sample was placed in a ^{60}Co gamma source at room temperature for 30 minutes immediately prior to being cooled down in the photoconductivity cryostat. The photocurrent at 77 K and 110 K was constant in time with constant illumination. In comparing the two curves it can be seen that the temperature dependent band at 3.1 eV, corresponding to the F^+-center in SrO, is present, though hidden beneath the otherwise broad band. This indicates that the results obtained here are at least compatible with the results obtained on the electron irradiated samples. The other broad, unresolved photoresponse band is an indication of the massive damage done to the sample by neutron irradiation. It should also be noted that the photocurrent at temperatures above 200 K was negative, i.e., in the opposite direction to the applied field. We have presently no explanation for this effect.

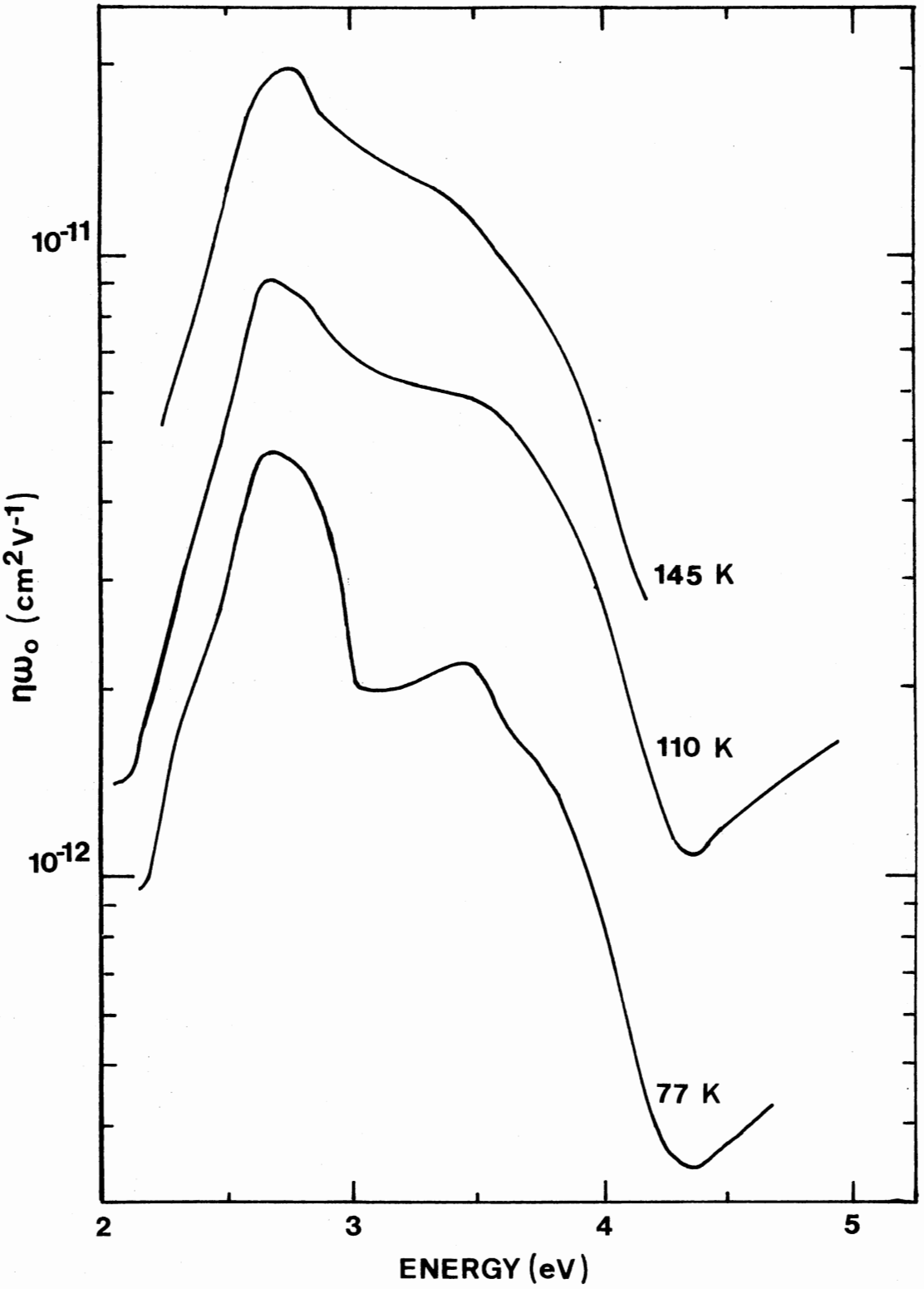

Figure 60. Spectral Dependence of the Photoresponse for ORNL-SrO Which Had Been Neutron Irradiated at Room Temperature, Measured at 77 K, 110 K and 145 K

APPENDIX B

ADDITIONAL EXPERIMENTAL RESULTS: CaO

APPENDIX B

ADDITIONAL EXPERIMENTAL RESULTS: CaO

We present here the results of additional experimental photoconductivity measurements on CaO. Though the information presented here is noteworthy, an analysis of these results was not pursued in this study since it did not contribute directly to the material in Chapter V.

I. Additively Colored CaO

Photoconductivity measurements were made on a Spicer sample of CaO grown with color centers. The sample contained a large number of F-centers and had an optical density greater than 6 at 430 nm. (The optical density was too large to be measured with the Cary 14 Spectrophotometer.) The photoconductivity produced by illuminating these samples had some unusual features. The photocurrent, rather than being constant in time with constant illumination, increased with continuing illumination with this effect being most pronounced in the spectral region between 2 eV and 3.1 eV. In addition a transient dark current was produced at 77 K which took several minutes to decay after the removal of the incident light. The dark current is an indication that shallow traps are being emptied. A similar transient dark current is obtained by illumination of the F-band in additively colored MgO (80).

Figure 61, curve a, shows the photoresponse measured at 77 K on a Spicer sample "as received" and curve b shows the photoresponse on the

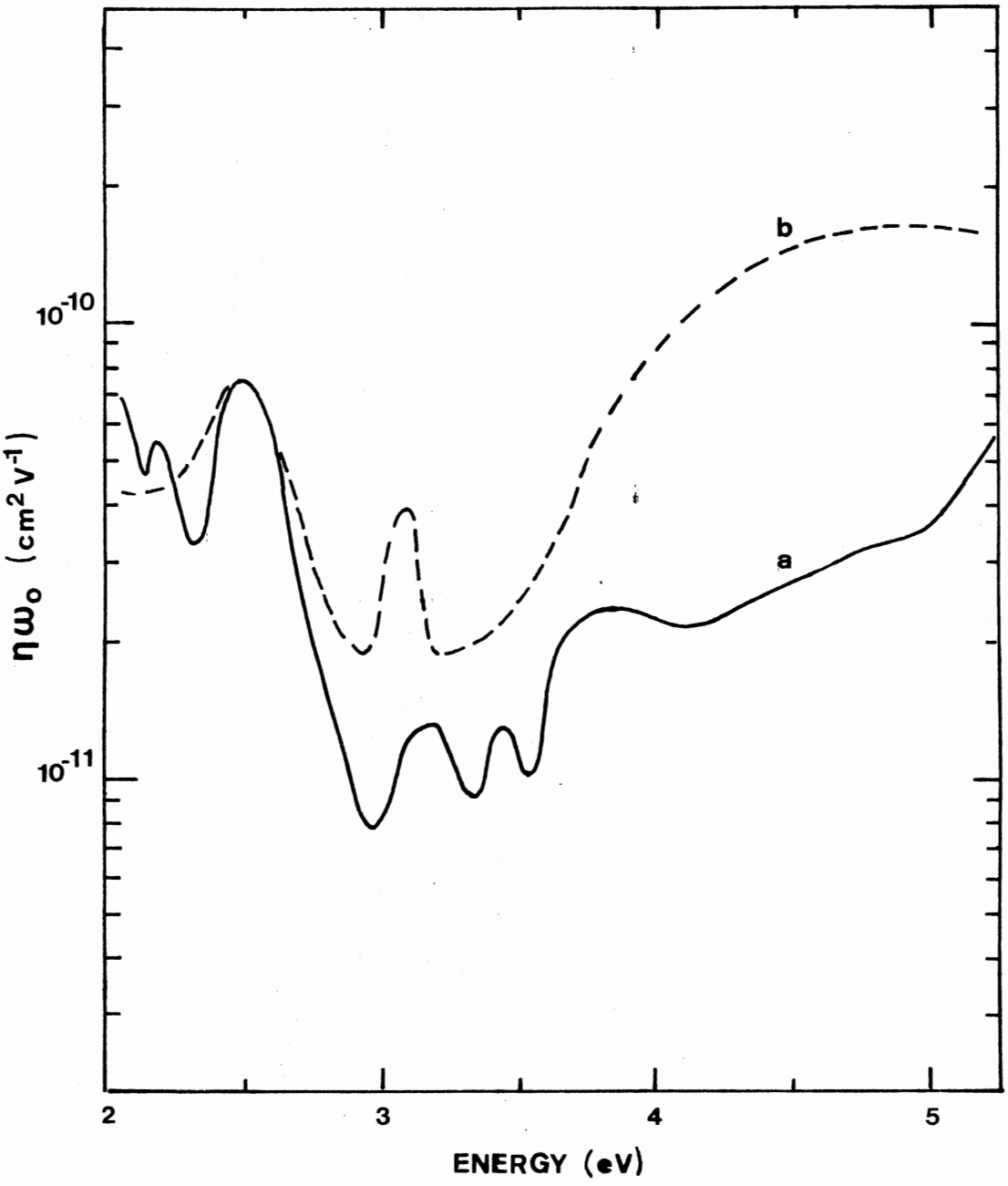

Figure 61. Spectral Dependence of the Photoresponse Measured at 77 K on Spicer CaO, Grown With Color Centers: as Received, Curve a; and Following γ-irradiation at Room Temperature, Curve b. The applied electric field was about 50 V/cm for both sets of measurements

same sample at 77 K following gamma-irradiation for 1 hour at room temperature. Both sets of measurements were made by reversing the direction of the applied electric field between individual measurements to prevent polarization effects in the sample. The applied electric field was about 50 V/cm. In addition both curves were obtained by alternating a measurement for 400 nm incident light between otherwise consecutive measurements throughout the spectral range from 2 eV to 6 eV. Gamma-irradiation enhanced the photoresponse in the spectral region between 3.5 eV and 5 eV.

The F band, 3.1 eV, photoresponse could be optically bleached at 77 K in a manner similar to the bleaching of the F band photoresponse discussed in Chapter V for electron irradiated CaO. There was also some evidence of $F \leftrightarrow F^{+}$ interconversion. The photoresponse at 3.1 eV (peak of F band) generally decreased as individual consecutive measurements were made for incident light of energy ranging from about 3.6 eV to 5.2 eV and generally increased for incident light of energy less than about 3 eV. A conversion of this kind has been observed by Kemp et al (93) in additively colored CaO.

Fluorescence lifetime measurements on Spicer samples of CaO grown with F-centers and ORNL additively colored samples of CaO showed that the fluorescence contained a component with a lifetime of the order of minutes which appears related to the transient dark current described above.

Based on the results reported here for photoconductivity and fluorescence measurements on additively colored CaO, it is obvious that complicated trapping mechanisms and energy transfer processes are involved.

II. Neutron Irradiated CaO

The optical density, measured at 77 K, on an ORNL-sample of CaO which had been neutron irradiated at room temperature is shown in Figure 62. The width of the F^+ absorption band is somewhat larger than that of the F^+ absorption band in the proton irradiated CaO sample shown in Chapter V, Figure 43. Similar results were noted in the comparison of the F^+ absorption band in neutron and proton irradiated SrO shown in Chapter IV, Figures 23 and 24, and is attributed to the massive damage done by neutron irradiation.

The photoresponse at 77 K, measured over the spectral range from 2 eV to 5 eV, is shown in Figure 63 for this same sample. The sample was placed in a ^{60}Co gamma source for 1 hour at room temperature immediately prior to mounting in the photoconductivity cryostat. The photocurrent was constant in time with constant illumination. The photocurrent reached its maximum value within a fraction of a second (the response time of the detection system) and fell to zero equally fast upon removal of the incident light. The photoresponse results are compatible with the results presented in Chapter V for electron and proton irradiated CaO, with the 3.1 eV and 3.65 eV bands being hidden in the broad unresolved photoresponse band between 2.5 eV and 4.3 eV, which is characteristic of the massive damage done to the sample by neutron irradiation.

The photocurrent at room temperature was masked by a large dark current and consequently accurate measurements could not be made. When detectable, at room temperature, the photocurrent was negative, i.e., in the opposite direction to the applied field. This result is similar to that reported in Appendix A for neutron irradiated SrO. At the present

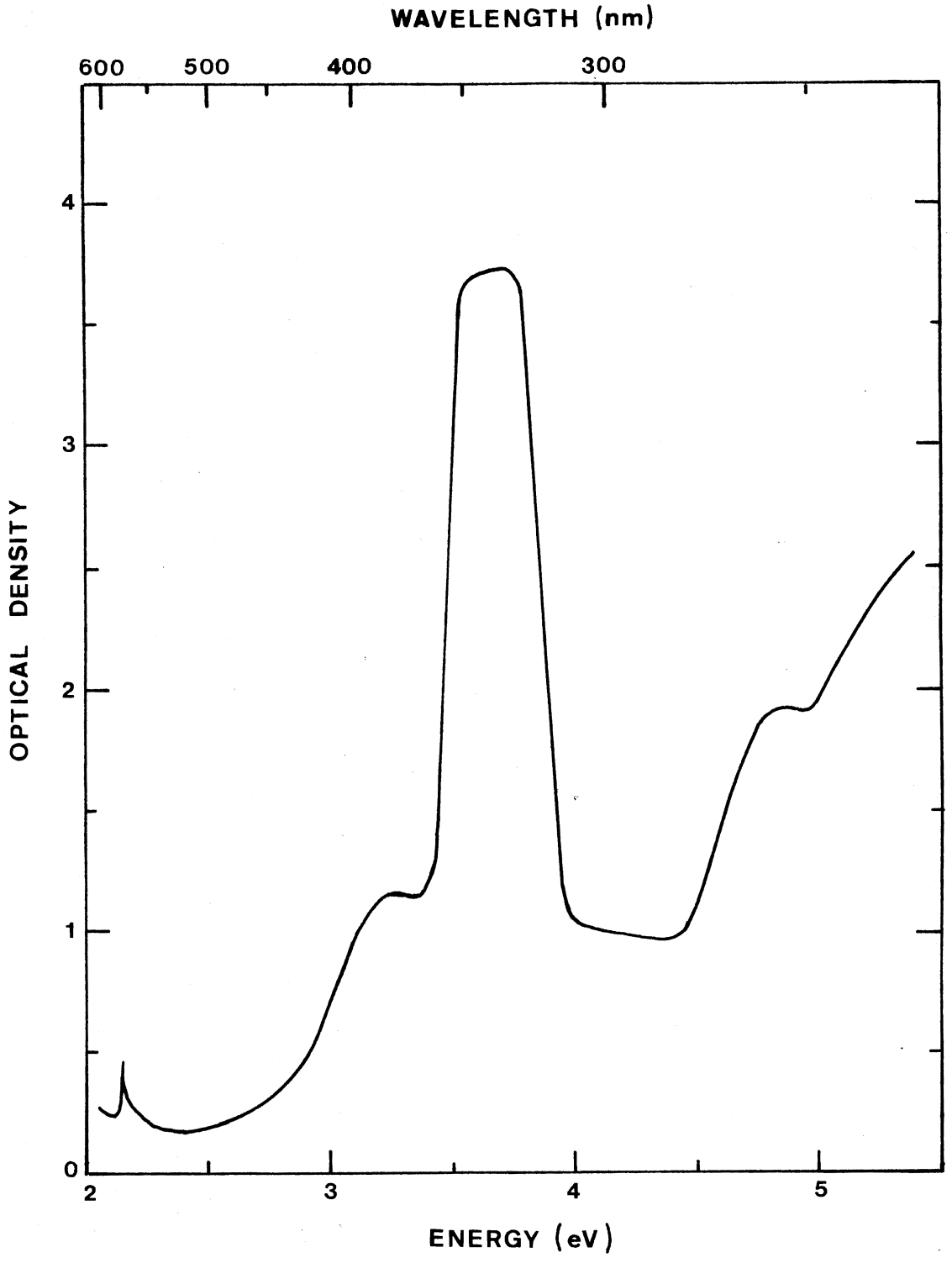

Figure 62. Optical Density, Measured at 77 K, of ORNL-CaO Which Had Been Neutron Irradiated at Room Temperature

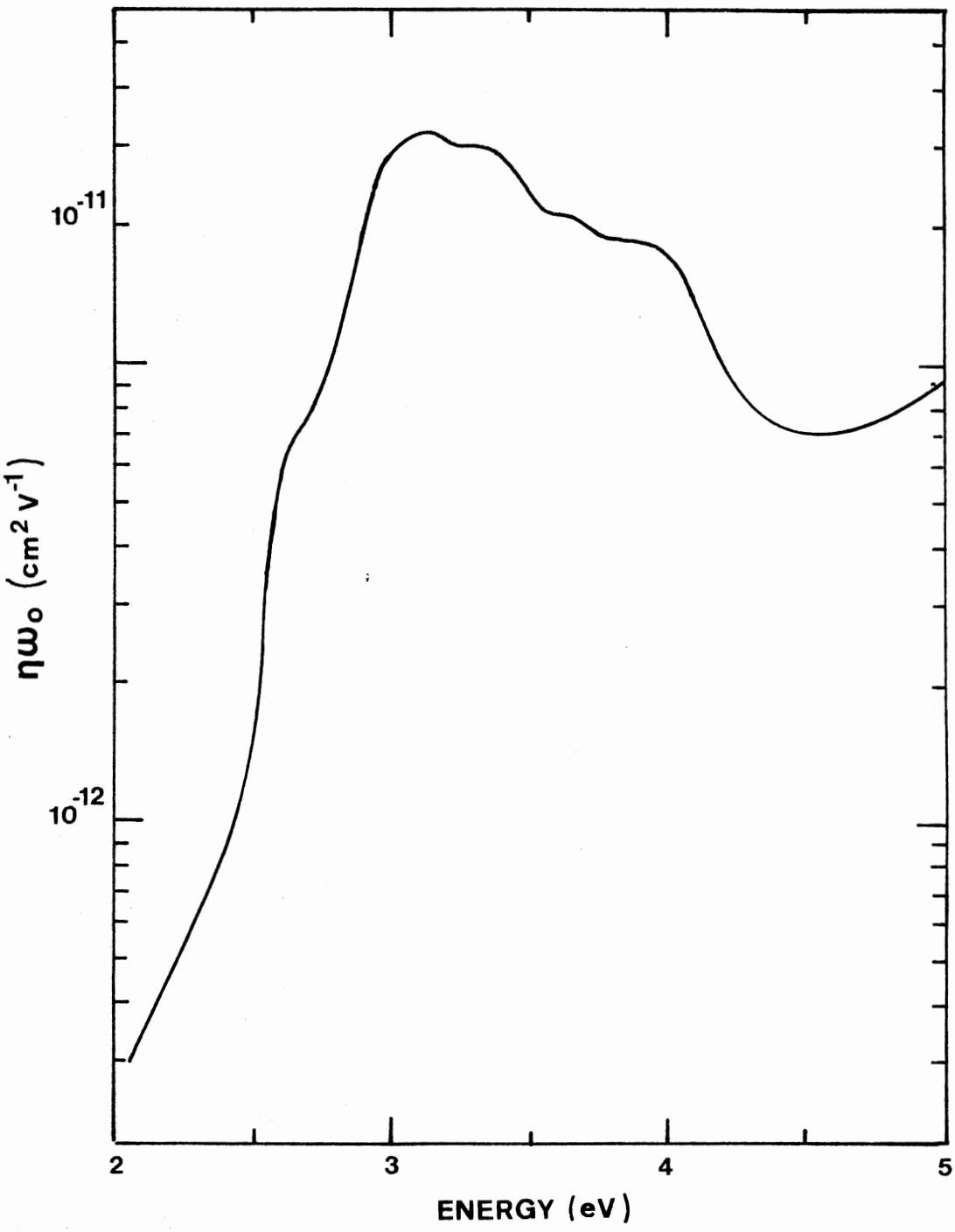

Figure 63. Spectral Dependence of the Photoresponse, at 77 K, of ORNL-CaO Which Had Been Neutron Irradiated at Room Temperature

time we have no explanation for this effect.

III. Magnesium-doped CaO

Samples of CaO doped with 1% Magnesium were received from A. E. Hughes of the Atomic Energy Research Establishment, Harwell. Just below a highly colored layer (region 1) at the surface of the melt is a region (region 2) in which new F^+-, F- and F_A^+-centers can be produced by ionizing radiation to a total concentration of about $10^{17}/cm^3$. Experiment (98) shows that, in this second region, a ratio of F_A^+:F^+ centers of about 2:1 can be produced by low energy electron, gamma or x-ray irradiation. These oxygen vacancy centers in magnesium-doped CaO have been studied by Hughes, et al. (78,99). It is thought that in this region of the melt, the F-type centers are produced by trapping electrons at pre-existing oxygen vacancies formed during cooling from the melting point rather than by knock-on particle collisions as in undoped CaO.

Some preliminary photoconductivity and associated optical absorption measurements were made on several samples of magnesium-doped CaO. These samples were chosen from region 2 of the melt which was described above.

Figure 64 shows the optical density on one such sample following electron irradiation at 77 K to a dose of about 2×10^{17} electrons/cm^2 (solid curve). The optical density measured on the untreated sample is indicated by the broken curve. Both curves were obtained at 77 K. The various color centers and the respective wavelength and incident photon energy at which peak absorption occurs are: F(400 nm, 3.1 eV); F^+ (340 nm, 3.65 eV); F_A (450 nm, 2.76 eV) (78); F_{Al}^+ (374 nm, 3.32 eV)

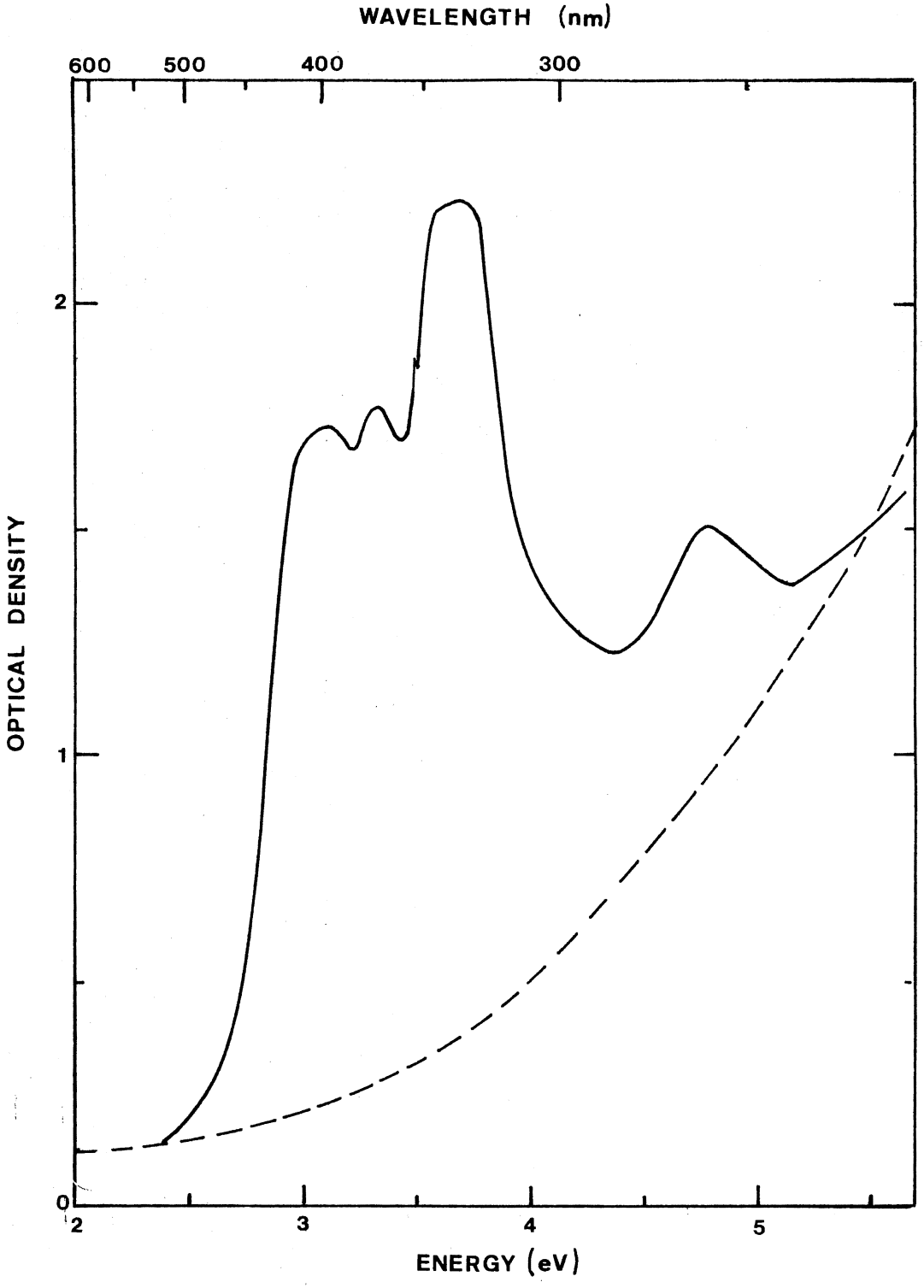

Figure 64. Optical Density of Magnesium-Doped CaO (Region 2): Untreated (Broken Curve) and Following Electron Irradiation at 77 K to a Dose of About 2 x 10^{17} Electrons/cm^2 (Continuous Curve)

(98); F^+_{A2} (340 nm, 3.65 eV) (98). The band at 260 nm, 4.8 eV, is due to anion-cation vacancy pairs which have been observed optically in deformed CaO (85,94).

The photoresponse measured on the same sample at 77 K is shown in Figure 65, curve a. The photocurrent was constant with constant illumination and rose to its maximum value within a fraction of a second and fell to zero equally fast upon removal of the incident light. The broad photoresponse band in the spectral region between 2.5 eV and 4.5 eV, a composite of the photoresponse from the various F- and F_A-type centers, hides the details of the structure of the individual bands. The photoresponse also bleached nearly uniformly throughout the spectral region between 2.5 eV and 4.5 eV as the energy of the incident photons scanned this same region. Figure 65, curve b, shows the photoresponse at 77 K on a similar sample of magnesium-doped CaO which had been subjected to nearly 60 hours of gamma-irradiation at room temperature. Again, the individual F- and F_A-type photoresponse bands are hidden beneath the broader unresolved band.

Complicated trapping mechanisms and energy transfer processes are involved in the absorption-emission-photoconductivity processes observed in these samples. An indication of this is given by an examinaton of the excitation spectrum for the 398 nm emission resulting from the 374 nm (F^+_A) band (99) which shows three bands peaking at 260 nm, 340 nm and 374 nm. Absorption at 260 nm excites luminescence at 347 nm, which will be strongly absorbed by the F^+ band. The F^+-center emits in a band peaking at 370 nm, which overlaps the 374 nm absorption band of the F^+_A-center. The F^+_A-center in turn emits in a band peaking at 398 nm (99). Excitation at 260 nm thus results in emission at 398 nm.

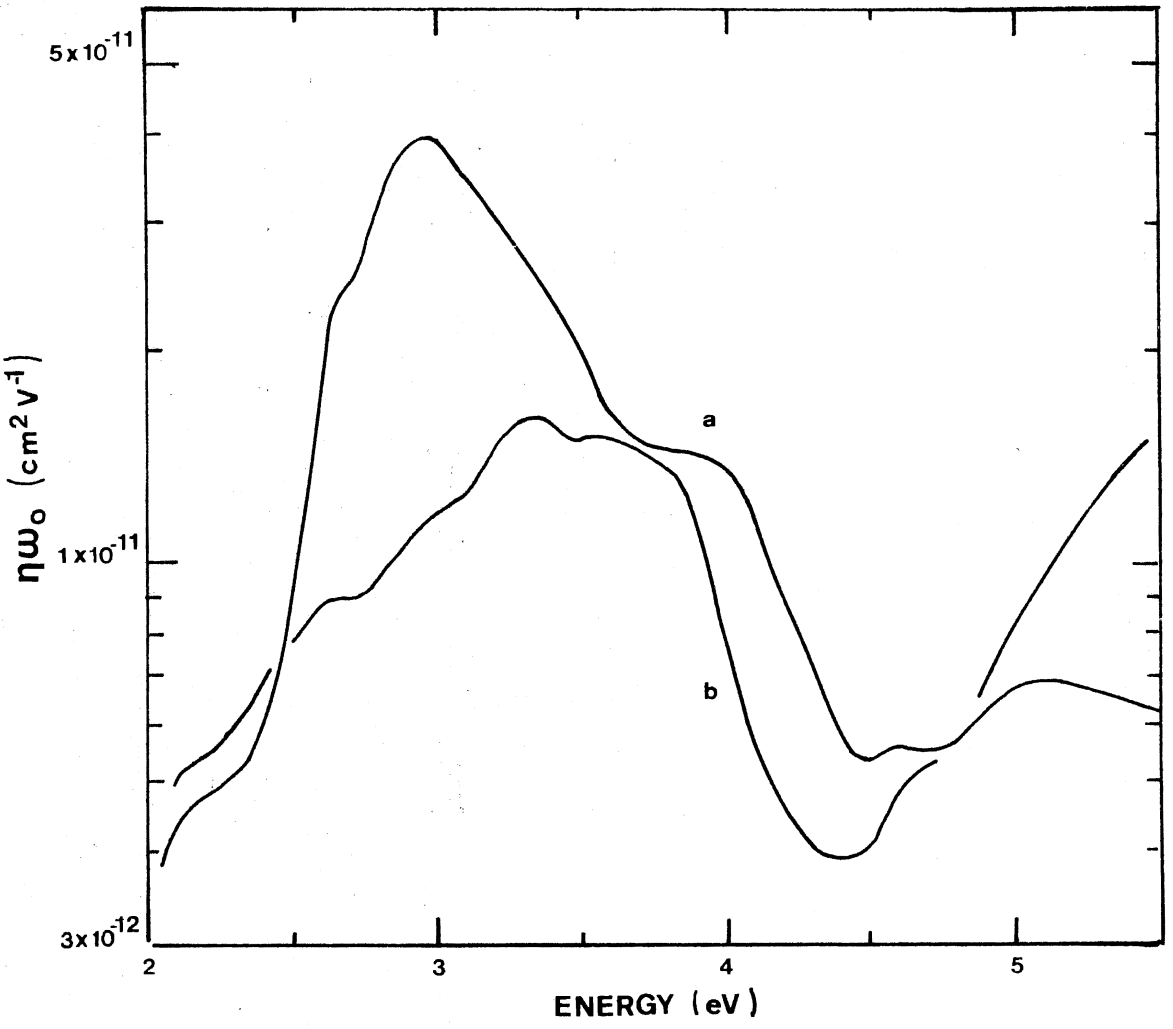

Figure 65. Spectral Dependence of the Photoresponse at 77 K of Magnesium-doped CaO (Region 2): a Sample Which Had Been Electron Irradiated at 77 K to a Dose of About 2 x 10^{17} Electrons/cm^2, Curve a; a Sample Which had Received Nearly 60 Hours of γ-Irradiation at Room Temperature, Curve b

VITA

Sister Jeanette M. Feldott

Candidate for the Degree of

Doctor of Philosophy

Thesis: ELECTRONIC STRUCTURE OF DEFECTS IN SOME OXIDES

Major Field: Physics

Biographical:

Personal Data: Born in Quincy, Illinois, February 23, 1942, the daughter of Mr. and Mrs. Albert J. Feldott; entered the Religious Congregation of the School Sisters of Notre Dame in St. Louis, Missouri, August, 1960.

Education: Graduated from Ewing Public High School, Ewing, Missouri, in May, 1960; received Bachelor of Science degree with a major in mathematics and a minor in chemistry from Notre Dame College, St. Louis, Missouri, in 1964; was named to Who's Who in American Colleges and Universities while attending Notre Dame College; received the Master of Science degree in physical science (physics and chemistry) from Emporia State University, Emporia, Kansas in August, 1972; was elected to Sigma Xi (Scientific Research Society of North America) while attending Oklahoma State University; completed requirements for the Doctor of Philosophy degree at Oklahoma State University in July, 1977.

Professional Experience: Math Teacher, Althoff High School, Belleville, Illinois, 1964-65; Physics, Chemistry and Math Teacher and Student Council Moderator, St. Francis Borgia High School, Washington, Missouri, 1965-73; Outstanding Young Teachers Award from the Jaycees, for the Washington, Missouri area and an award of Excellence in Chemistry Teaching in the greater St. Louis area from the Chemical Industry Council, 1971 and 1972 while teaching at St. Francis Borgia High School; Teaching and Research Assistant, Oklahoma State University, Stillwater, Oklahoma, 1973-77.